AD-A194 990

TGAL-87-3

MAXIMUM-LIKELIHOOD MULTICHANNEL DECONVOLUTION OF P WAVES AT SEISMIC ARRAYS

Z.A. Der, A.C. Lees, W.W. Chan, R.H. Shumway,
K.L. McLaughlin, E. Smart, T.W. McElfresh, and M.E. Marshall

Teledyne Geotech Alexandria Laboratories
314 Montgomery Street
Alexandria, Virginia 22314-1581

NOVEMBER 1987

FINAL REPORT
ARPA ORDER NO: 4511
PROJECT TITLE: Source Time Function Deconvolution
CONTRACT: F08606-86-C-0006

Approved for Public Release; Distribution Unlimited.

Prepared for:
DEFENSE ADVANCED RESEARCH PROJECTS AGENCY
1400 Wilson Boulevard
Arlington, VA 22209

Monitored by:
AFTAC/TGR
PATRICK AFB
FLORIDA 32925-6001

UNCLASSIFIED
SECURITY CLASSIFICATION OF THIS PAGE

ADA194990

REPORT DOCUMENTATION PAGE

Form Approved
OMB No. 0704-0188
Exp. Date: Jun 30, 1986

1a. REPORT SECURITY CLASSIFICATION: Unclassified	1b. RESTRICTIVE MARKINGS
2a. SECURITY CLASSIFICATION AUTHORITY	3. DISTRIBUTION/AVAILABILITY OF REPORT: Approved for Public Release; Distribution Unlimited.
2b. DECLASSIFICATION/DOWNGRADING SCHEDULE	
4. PERFORMING ORGANIZATION REPORT NUMBER(S): TGAL-87-3	5. MONITORING ORGANIZATION REPORT NUMBER(S)
6a. NAME OF PERFORMING ORGANIZATION: Teledyne Geotech Alexandria Laboratories; 6b. OFFICE SYMBOL (If applicable)	7a. NAME OF MONITORING ORGANIZATION: AFTAC/TGR
6c. ADDRESS (City, State, and ZIP Code): 314 Montgomery Street Alexandria, Virginia 22314-1581	7b. ADDRESS (City, State, and ZIP Code): Patrick Air Force Base Florida 32925-6001
8a. NAME OF FUNDING/SPONSORING ORGANIZATION: DARPA; 8b. OFFICE SYMBOL (If applicable): GSD	9. PROCUREMENT INSTRUMENT IDENTIFICATION NUMBER: F08606-86C-0006
8c. ADDRESS (City, State, and ZIP Code): 1400 Wilson Boulevard Arlington, Virginia 22209	10. SOURCE OF FUNDING NUMBERS: PROGRAM ELEMENT NO. 62714E; PROJECT NO. DT/6122; TASK NO.; WORK UNIT ACCESSION NO.

11. TITLE (Include Security Classification)
Maximum-Likelihood Multichannel Deconvolution of P Waves at Seismic Arrays

12. PERSONAL AUTHOR(S) Z.A. Der, A.C. Lees, W.W. Chan, R.H. Shumway, K.L. McLaughlin, E. Smart, T.W. McElfresh, M.E. Marshall

13a. TYPE OF REPORT	13b. TIME COVERED	14. DATE OF REPORT (Year, Month, Day)	15. PAGE COUNT
Final Report	FROM 10/1/85 TO 10/1/86	November 1987	183

16. SUPPLEMENTARY NOTATION

17. COSATI CODES			18. SUBJECT TERMS (Continue on reverse if necessary and identify by block number)	
FIELD	GROUP	SUB-GROUP		
08	11		Seismic source	Nevada Test Site
17	10		Seismic array	Novaya Zemlya
			Seismic moment	East Kazakh

19. ABSTRACT (Continue on reverse if necessary and identify by block number)

The results of maximum-likelihood multichannel deconvolution applied to array recordings and three component station networks for teleseismic P waves, are presented and interpreted in terms of possible surface reflections and other arrivals from explosions conducted at many of the world's major nuclear test sites. The deconvolution method utilizes the well known fact that P wave spectra can be decomposed into source and receiver spectral factors. The source functions obtained in the deconvolution process provide a better picture of the nature of explosion source time functions, and in particular of the presence or lack of secondary arrivals following the P wave such as pP or spall. The presence of such secondary arrivals and their effects on the first cycle of the P wave are very important in yield estimation. We find significant variations in the deconvolved source time function between test sites ~~which~~ may be associated with topography and testing practices. For instance, deconvolved source time functions for events at Shagan, Tuamotu, and Astrakhan show clear pP arrivals, while source time functions for events occurring in mountainous regions such as Degelen and the French Sahara test site at Ahaggar and geologically complex regions such

next page

20. DISTRIBUTION/AVAILABILITY OF ABSTRACT	21. ABSTRACT SECURITY CLASSIFICATION
☒ UNCLASSIFIED/UNLIMITED ☐ SAME AS RPT. ☐ DTIC USERS	UNCLASSIFIED
22a. NAME OF RESPONSIBLE INDIVIDUAL: Dr. Dean Clauter	22b. TELEPHONE (Include Area Code): (305) 494-5263; 22c. OFFICE SYMBOL: TGR

DD FORM 1473, 84 MAR — 83 APR edition may be used until exhausted. All other editions are obsolete.

SECURITY CLASSIFICATION OF THIS PAGE
UNCLASSIFIED

(19. Continued)

as Pahute Mesa and Yucca Flats often do not show pP arrivals. All of the source functions show complexity in addition to the initial P arrival and pP arrival, if present. There is also a great deal of variation between different source time functions for events at the same test site. Often, but by no means always, events occurring near each other look particularly similar. The site functions are also complex in most cases and azimuthal variations are significant in both source and receiver regions. Site and source effects contribute about equally to the energy observed in the P codas of the events analyzed.

Deconvolved source time functions should be especially useful for improving estimates of the m_b bias between test sites and to improve yield estimates since site as well at t^*, instrument, and any known source spectra are removed. Much of the observed m_b bias can be ascribed to the effects of pP interference, though some of the effects, especially at NTS, remain unexplained, and other physical processes must be involved. Estimation of the seismic moment from the area under the deconvolved source pulses of the French Sahara events resulted in moment estimates consistent with those obtained by other methods.

Accession For	
NTIS GRA&I	☑
DTIC TAB	☐
Unannounced	☐
Justification	
By	
Distribution/	
Availability Codes	
Dist	Avail and/or Special
A-1	

SUMMARY

The results of maximum-likelihood multichannel deconvolution applied to array recordings and three component station networks for teleseismic P waves, are presented and interpreted in terms of possible surface reflections and other arrivals from explosions conducted at many of the world's major nuclear test sites. The deconvolution method utilizes the well known fact that P wave spectra can be decomposed into source and receiver spectral factors. The source functions obtained in the deconvolution process provide a better picture of the nature of explosion source time functions, and in particular of the presence or lack of secondary arrivals following the P wave such as pP or spall. The presence of such secondary arrivals and their effects on the first cycle of the P wave are very important in yield estimation. We find significant variations in the deconvolved source time function between test sites which may be associated with topography and testing practices. For instance, deconvolved source time functions for events at Shagan, Tuamotu, and Astrakhan show clear pP arrivals, while source time functions for events occurring in mountainous regions such as Degelen and the French Sahara test site at Ahaggar and geologically complex regions such as Pahute Mesa and Yucca Flats often do not show pP arrivals. All of the source functions show complexity in addition to the initial P arrival and pP arrival, if present. There is also a great deal of variation between different source time functions for events at the same test site. Often, but by no means always, events occurring near each other look particularly similar. The site functions are also complex in most cases and azimuthal variations are significant in both source and receiver regions. Site and source effects contribute about equally to the energy observed in the P codas of the events analyzed.

Deconvolved source time functions should be especially useful for improving estimates of the m_b bias between test sites and to improve yield estimates since site as well at t*,

instrument, and any known source spectra are removed. Much of the observed m_b bias can be ascribed to the effects of pP interference, though some of the effects, especially at NTS, remain unexplained, and other physical processes must be involved. Estimation of the seismic moment from the area under the deconvolved source pulses of the French Sahara events resulted in moment estimates consistent with those obtained by other methods.

TABLE OF CONTENTS

LIST OF FIGURES

LIST OF TABLES

INTRODUCTION

The determination of the effect of surface reflection and other secondary arrivals on the estimated yields of nuclear explosions has been a major problem in nuclear monitoring work. The major philosophical issues in such work are the following:

a) Are the explosion source functions simple linear superpositions of P and pP pulses or are more complex source time histories such as those derived from nonlinear hydrodynamic code calculations appropriate?

b) Can we predict the effect of the secondary arrivals on the yields estimated from time domain measurements on the first cycle of the P wave signal or on m_b in particular? This depends on the resolvability of secondary arrivals and their physical interpretation.

c) What is the effect of these secondary arrivals on frequency domain measures of yield?

d) What are the limitations imposed by Q and the noise on the time resolution in separating multiple arrivals? Clearly, it is not possible to resolve pP delay times, even if pP is linear, of a few tenths of a second along low Q paths.

e) And, in general, what processes, e.g. Q, scattering, near source and receiver wave conversions, spall, Rayleigh-to-P conversions, etc., determine the waveforms and spectra of teleseismic P waves? Is the amplitude, or the area under it, associated with the first excursion of the trace on the deconvolved seismogram a better measure of yield than m_b?

In this report we present results of the application of a maximum-likelihood multichannel deconvolution technique which is designed to help resolve the above questions. The method is based on the factoring of P wave spectral matrices, consisting of recordings of multiple events at common test sites and using a common set of array sensors, into site and source related factors. The method has its roots in several previously proposed deconvolution techniques.

First, we shall discuss previous work in estimating pP times and amplitudes and previously developed deconvolution methods. Then we outline the maximum-likelihood multichan-

nel deconvolution algorithm and the caveats on its use. The bulk of this report is the results of deconvolutions of data from nuclear explosions at most of the major test sites: Degelen, Shagan, Novaya Zemlya, Astrakhan, Ahaggar, Tuamotu, Sinkiang, Pahute Mesa, and Yucca Flats. Deconvolutions have also been successfully performed on three-component regional and teleseismic data. The deconvolutions are interpreted in terms of the presence and characteristics of pP, the presence and complexity of other secondary arrivals and of the P wave coda, and azimuthal variations in the source-time function. We find that explosion source time functions, while they generally appear to contain a phase that is readily ascribable to pP, also contain a number of other arrivals. Both source and site terms appear to contribute about equally to the presence of P coda. Finally, we demonstrate that the deconvolved source-time functions can be used to improve estimates of m_b bias and yield.

BACKGROUND

One of the fundamental problems that motivates research on explosion source time functions is the possible effects of secondary arrivals such as pP on estimated yields. Assuming that m_b is used for deriving yields through some m_b-yield formula, a complex interaction of Q, source scaling, and pP interference will affect the measured m_b or other measures of source energy. To perform realistic synthetic simulations, we need reliable estimates of Q, source waveforms, and pP parameters derived from the data. Ultimately, we need a better understanding of the nature of the secondary arrivals under different source-receiver-testing conditions and their effect on m_b and yield estimates.

Previous Work on pP Estimation

In much of the early work it was assumed that P waves are composed of P and pP pulses possibly convolved with some site-related transfer function. Therefore, a variety of methods have been proposed for estimating pP times and amplitudes. Spectral methods (Cohen 1970, 1975; Shumway and Blandford 1978) attempt to make use of the spectral modulation due to pP. In the case of complex site related modulation of P wave spectra, the spectral minima due to any, even solitary, pP arrival besides the direct P, may be completely disguised, thus making the interpretation of spectral minima difficult. Interpretation of spectral minima in power spectra in terms of multiple arrivals is totally nonunique since the phase information is lost and an infinite number of pulse sequences, derivable from each other by dispersive, all-pass filters (Robinson and Treitel 1980), may yield identical spectra.

Direct modeling of narrow frequency band P waveforms was also frequently used for the determination of various source and path parameters in seismology (Burdick and Helmberger 1979, Bache 1982). In order to explain the variations in amplitude and waveform due to

attenuation, Burdick *et al.* (1984) suggest that t^*_P should be around 1.0 sec. However, evidence now indicates that t* may be much lower than this, as is pointed out by Douglas *et al.* (1974, 1987), Der *et al.* (1982), and Bache *et al.* (1985). Moreover, it has been shown by Cormier (1982) that in the case of explosion P waves, such waveform fits are highly nonunique because the attenuation parameter t*, pP times and amplitudes, and the various source related parameters strongly trade off against each other. Generally speaking, waveform fits are not satisfactory substitutes for deconvolutions which make more efficient use of the total information in seismic signals and take advantage of the high dynamic range and consequently, the broad signal bandwidth provided by modern digital recording systems.

Another approach that has been proposed involves cross-equalization (or as the authors call it, "intercorrelation") of narrow band short-period waveforms (Mellman and Kaufman 1981; Lay *et al.* 1984 a,b). This method produces "pseudo-pP" delay times and amplitudes, i.e. the best fits to simple P+pP models. Since the results are not deconvolutions in the true sense they do not prove the existence or correctness of such models (Lay *et al.* 1984 a,b; Mellman *et al.* 1984).

Assuming the validity of the P+pP model, inter-event spectral amplitude ratios should be of the form

$$\frac{1 - \alpha_1 e^{-i\omega\tau_1}}{1 - \alpha_2 e^{-i\omega\tau_2}} \qquad (1)$$

because the site factors should cancel; additional adjustments may also be made for the weak effects of source scaling. Observed spectral ratios of P waves, however, cannot be fitted by any reasonable values of α_1 α_2, τ_1, or τ_2, where the α's and τ's are the pP amplitudes and delay times, respectively. The forms of the spectral ratios computed from data are much more complex, indicating complex sequences of arrivals from the source regions (Der *et al.* 1985b).

Moreover, "intercorrelations" can be performed on some arbitrary, narrow-band transients generated by convolving bursts of Gaussian random noise with combinations of instrument-attenuation-explosion impulse responses. The resulting correlations are just as high as those derived from the real data (Der *et al.* 1985b) giving fictitious "pP" times and amplitudes. Such exercises vividly demonstrate the fallacies that underlie most waveform matching schemes as applied to undeconvolved, narrow band raw signals that typically make up most raw short-period P-wave recordings. This objection is especially applicable to the WWSSN data, extensively used in most "intercorrelation" studies, the bandwidth of which is severely limited by the sharp high frequency cutoffs built into the system. The degree of freedom (or alternatively the information content) in such narrow-band data is so diminished (Goldman 1953) that the four parameters in the "intercorrelation" process can always match the waveforms regardless whether "pP" pulses are present or not. Since the recording system is not digital, the WWSSN data cannot be deconvolved digitally, and in this respect this system must be considered obsolete from the point of view of modern signal processing.

As a general comment, it may be stated that all proposed techniques for finding pP seem to work quite well with synthetic data that conform to the proposed signal model. The problem is that attempts are rarely made to verify from the data that the underlying models are valid. Based on present knowledge, however, we cannot even be sure that pP arrivals exist in most P waves from nuclear explosions. For example, the spectral modulations introducing pP "nulls" in the spectra are very rarely observed and often the associated "pP" lag times are unreasonably long. Moreover, it seems certain that along some low Q paths, a short pP delay time is not resolvable, and thus no usable pP "correction" may be derivable from the data.

MAXIMUM-LIKELIHOOD MULTICHANNEL DECONVOLUTION

The Structure of Seismic Signals

A major advance in the understanding of the structure of teleseismic P waves was the finding by Filson and Frasier (1972) that P wave amplitude spectra from a set of events observed at a narrow range of azimuths at multiple array sites may be factored as

$$Y_{ij}(\omega) = R_i(\omega)\, S_j(\omega)\ , \tag{2}$$

where $Y_{ij}(\omega)$ are the P wave spectra, $S_j(\omega)$ are the source factors, $R_i(\omega)$ are the factors appropriate to the receiver sites, and i and j correspond to the individual receivers and sources, respectively. The validity of this equation has been verified for a number of seismic arrays as well as more widely separated receivers (Lundquist *et al.* 1980) and the idea was also exploited for deriving "relative receiver functions", which are time domain representations of intersite transfer functions (Lundquist *et al.* 1980) including Q effects. This model simply states the factorability of the spectral matrix without assuming any model such as P+pP as mentioned above.

In this paper we talk of "receiver factors" and "source factors" in order to make the distinction from the related concept, the "relative receiver functions", which also incorporate some additional assumptions (Hart *et al.* 1979), such as the maximum "spikiness" condition (Wiggins 1978), which is not required by the physics of the problem. We separate the Q operator, the instrument, and sometimes a source wavelet (such as the von Seggern and Blandford (1972) wavelet for explosions, to be called VSB) from the "source factor" and combine these in an assumed known source wavelet, A_j. Thus, $S_j(\omega) = A_j(\omega)X_j(\omega)$ where $A_j(\omega)$ is the spectrum of the combined source wavelet, instrument, and Q. This way the "source factor", $X_j(\omega)$, is a Fourier transform of a spike sequence associated with the radiation from a source and the

"receiver factor", $R_i(\omega)$, is the Fourier transform of the site transfer function. The source factors should include all features that associate with a given source, such as source pulse shape (if not factored out), the P, pP, and spall arrivals, and scattered P waves generated near the source, such as Rayleigh-to-P conversions (Greenfield 1971). The site factors include peculiarities due to the geology near the particular sensor in the array, such as P-to-Rayleigh conversions on local topography, i.e. anything that determines the features in P waveforms peculiar to a sensor location. The two factors together, as we shall show below, define most of the details in the observed P waveforms that can be associated with either the given source or recording site provided that the factorability condition as defined by equation (2) is satisfied for the given data set. Since the receiver factors strongly depend on the azimuths and distances of the sources, they may be assumed to be constant for a given sensor only for limited source regions.

If we have N receivers (sites) and M sources, we may describe (N x M) P wave spectra (or time series) in terms of N + M factors; there is thus a considerable degree of redundancy in the problems with N and M sufficiently large. This helps us to separate the $R_i(\omega)$ from the $X_j(\omega)$. This cannot be achieved uniquely, however, unless something is known *a priori* about the properties of each. Otherwise, common spectral factors can be assigned to either the source or receiver factors, or canceling, reciprocal factors may be assigned to both the receiver and source factors as indicated below:

$$Y_{ij}(\omega) = [R_i(\omega)\, F(\omega)]\, [F^{-1}(\omega)\, X_j(\omega)]\, A_j(\omega) \qquad (3)$$

This is the most dangerous aspect in any simultaneous determination of source and site factors. Fortunately, if we estimate the source factors first by averaging over receiver sites, we may expect that in the first step the various site effects will be approximately averaged out under the assumption that these site terms are random and dissimilar. This assumption is

necessary only to set up the initial conditions, and the site terms will later be refined in the simultaneous inversion. In the following steps, the factors are refined without too much change, and thus the chances of introducing major distortion into the estimated source and site spike sequences are minimized.

Since all P wave signals are embedded in the noise background, it is desirable that the deconvolution-factoring process is optimized in some sense with respect to the noise i.e., we are trying to find some compromise between the resolution and the S/N ratio. Thus, although the original derivation of Shumway (1984) includes weighting with respect to noise spectra, in this work we do not maximize the S/N ratio in order to increase the time resolution of the deconvolution.

The Deconvolution Algorithm

Previously developed deconvolution schemes include time domain methods for estimating pP times and amplitudes (Marshall 1972; Bakun and Johnson 1973; Kemerait and Sutton 1982; Israelson 1983) which generally preserve the phase information and do not depend on the simple P+pP model. Least squares (l_2 norm) deconvolution models work well, but those that use the l_1 norm (Levy and Fullagar 1981; Mellman *et al.* 1984) were shown by Jurkevics and Wiggins (1984) to result in erroneous deconvolutions as judged by synthetic simulations. Deconvolution methods belong to the general type of "appraisal" methods, borrowing the terminology of Oldenburg (1981), in which we attempt to establish, from the data, signal models and to measure their parameters, as contrasted to the "direct modeling" waveform methods that attempt to fit the data to some *a priori* model without any attempt to verify its validity.

This multichannel deconvolution approach for estimating source and site region characteristics has several advantages. First, the method utilizes both amplitude and phase information in the frequency domain calculations. Since this is a frequency domain calculation, the

maximum available bandwidth can be used, avoiding the ambiguities associated with time domain fitting of narrow band seismic signals. Second, the S/N can be optimized by the maximum-likelihood procedure (see Shumway and Der 1985). Finally, no *a priori* assumptions need to be made about the complexity of either the source or the site spike series, e.g. the presence of pP does not need to be presupposed by providing an initial guess of the pP delay time and amplitude.

The detailed derivation of the maximum-likelihood multichannel deconvolution method is given in Der *et al.* (1983) and Shumway and Der (1985). Only the key formulas are repeated here:

$$\hat{X}_j = \frac{\sum_i \overline{A_j}\,\overline{R_i}\,Y_{ij}}{\sum_i |A_j|^2 |R_i|^2 + \theta_j} \quad \text{where } \theta_j = \frac{P_n}{P_{x_j}}\,, \tag{4}$$

$$\hat{\sigma}_j^2 = P_n \left[\sum_i |A_j|^2 |R_i|^2 + \theta_j\right]^{-1}, \quad \text{and} \tag{5}$$

$$\hat{R}_i = \frac{\sum_j \overline{A_j}\,\overline{\hat{X}_j}\,Y_{ij}}{\sum_j |A_j|^2 \left[|\hat{X}_j|^2 + \hat{\sigma}_j^2\right]}\,, \tag{6}$$

where

Y_{ij} data

A_j source wavelet spectrum

R_i receiver spike response

X_j source spike sequence

θ adjustable N/S ratio

P_n noise power spectrum

P_z initial signal power

σ_j^2 effective noise power in second step

and an overbar denotes the complex conjugate. The i's correspond to the individual receiver sites and the j's to the individual sources. Equations 4 through 6 are very similar to those presented by Oldenburg (1981) and Oldenburg *et al.* (1981), and are essentially multichannel versions of the same. The term θ corresponding to the signal-to-noise ratio performs the same function as in Oldenburg's (1981) formulas. It is apparent from Equation (4) that the procedure is also similar, in computational approach, to the iterative beaming method (Blandford *et al.* 1973) in which the previous estimates of the two interfering signals are iteratively estimated in each step.

The deconvolution is done in the frequency domain. The first step is to factor out the "known" spectra, $A_j(\omega)$, consisting of t^*, the instrument response, and, optionally, a VSB source function. Since we are working with source regions and receiver arrays of limited spatial extent, we assume that the attenuation parameter t^*_P is the same for all source-receiver pairs and that all instruments have the same response. At the start of the iteration process, the source and site functions are each initialized to an impulse in the time domain. The flow diagram of the iterations is depicted in Figure 1. We have found that four iterations were sufficient to stabilize the shapes of the source and site related pulse sequences.

The deconvolution process starts with the estimation of the source factors by deconvolving the source pulse and stacking these deconvolutions over the available sites. This is intuitively the most reasonable first step because we expect the site-generated pulse sequences to be more random than the source-related ones and thus they may be easier to average out by stacking. In order to ensure the desired deconvolution effect, we do not divide by the noise spectra,

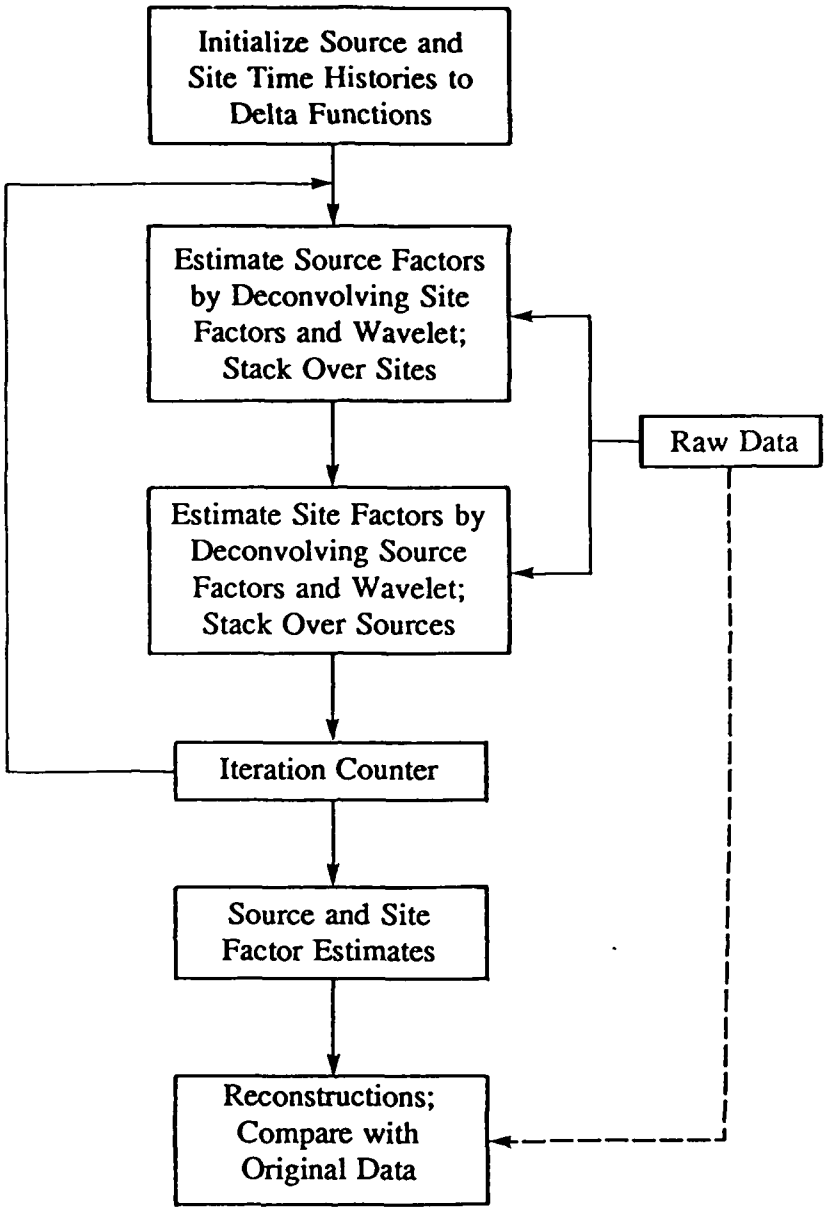

Figure 1. Flow diagram of the multichannel deconvolution process. In the center, the second and third boxes from the top correspond to Equations (4) and (6) in the text, respectively.

which would have resulted in no visible deconvolution, especially for events with the maxima in S/N ratio below 1 Hz. Instead, we have assigned a unit weight to all frequencies which had S/N ratios above 1 and excluded the frequency ranges with poor S/N ratios from the iterations. This conflicts with our objective of maximizing the S/N in the output, but allows increased resolution.

In all our deconvolution work we have used only complete matrices of event by site of P wave data, although the theory for doing deconvolutions with a sparse matrix has been worked out. For a given array, several data sets can often be found that have only a limited subset of common events and sensors sites. However, it is reassuring that for the common events, the source time function estimates are commonly quite similar regardless of the particular subdata set used from the given array demonstrating the robustness of the method.

Interpretation of the Results

The first estimates of source functions are similar to the stacked deconvolutions obtained by Marshall (1972) and Douglas *et al.* (1987). Instead of the frequency domain approach used here, they use Wiener filters designed in the time domain for removing t* effects and the instrument response. Despite these differences in the procedures, our results usually resemble theirs closely and in fact, if we do a "multichannel deconvolution" of one event at an array of sensors, we simply get a beam with the instrument, t*, and optionally VSB removed.

After several iterations, each source factor will contain the contribution appropriate to the particular source at all receivers including the source pulse, pP, and spall (in the case of explosion sources) arrivals, and any scattering contributions that may be associated with a particular source. The results require some interpretation: one must keep in mind that the deconvolution of the "known" source pulses (consisting of t*, instrument, and explosion scaling effects) will produce a one-sided pulse, ideally symmetric in time and having some side lobes because of

the limitations in the bandwidth of the deconvolution and the non-causal nature of the process. In any case, the results are easier to interpret than the original seismograms which are complex superpositions of complex wavelets.

Each site factor will contain the contribution of that site to the seismogram, mostly the random scattering effects attributable to near-receiver structure. The energy of the site factors is high frequency in character (Figure 2), and this accounts for the partial whitening of the spectra in the estimation of the source time functions. In order to see what effects this has on the coda one has to extract the low frequency part of them by band-pass filtering (Figure 2). The site time functions also appear "wrapped around" at time=0 sec because of the way the factoring was set up. Some precursors are visible because the process does not have a causality constraint, and partly because of the wrap-around effect.

Approximately sinc shaped resolution kernels characterizing the attainable resolution with the given bandwidth are also byproducts of the iterative process (Der *et al.* 1985b, Shumway and Der 1985). The resolution is typically more than 0.15 sec which is the width at half maximum of the resolution kernels. Ideally, the output source and site time functions will be sequences of delta functions since the attenuation operator, instrument, and, in some methods, the estimate of the source wavelet have been removed. However, in practice, it is impossible to obtain exact delta functions by deconvolution because of the bandwidth limitations in the signals and the ever present background noise. One must be satisfied with approximations to the delta function such as broader pulses resembling sinc functions. Figure 3 is an example of the obtainable resolution for a case when delta functions were the input to the deconvolution process and the output clearly mimics the input, though with broader pulses.

Since the deconvolved source pulse is often broader than one would desire, small pP delay times may not always be resolvable. If the pP delay time is smaller than the width of

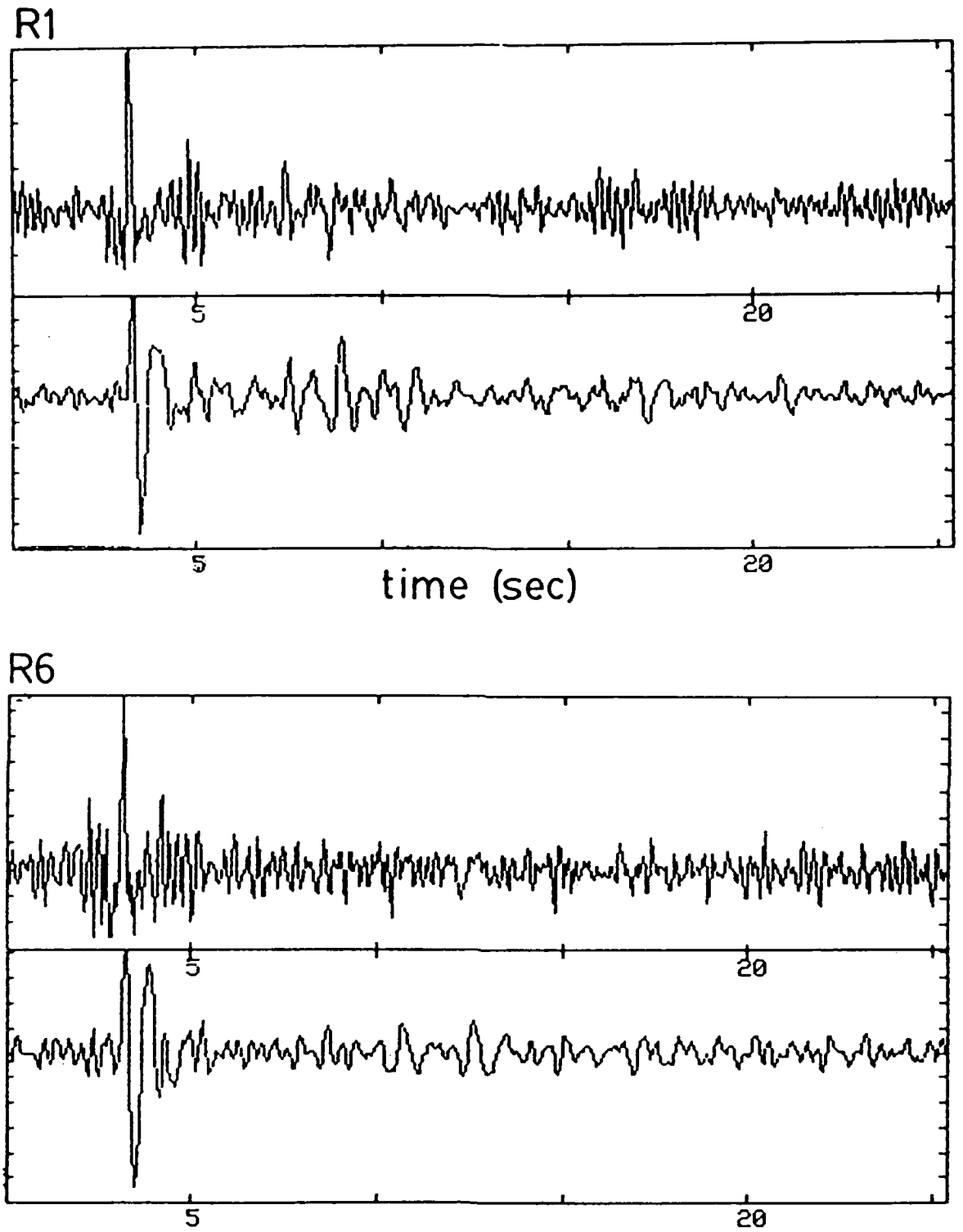

Figure 2. Examples of filtered site terms for a set of Kazakh data recorded at EKA. In each pair, the top trace is the deconvolved site term, which has been filtered in the bottom trace with a von Seggern and Blandford wavelet assuming a yield of 130 kt, t*=0.15 sec, and an EKA instrument response. The top sensor, R1, has a considerable amount of coda due to the site response.

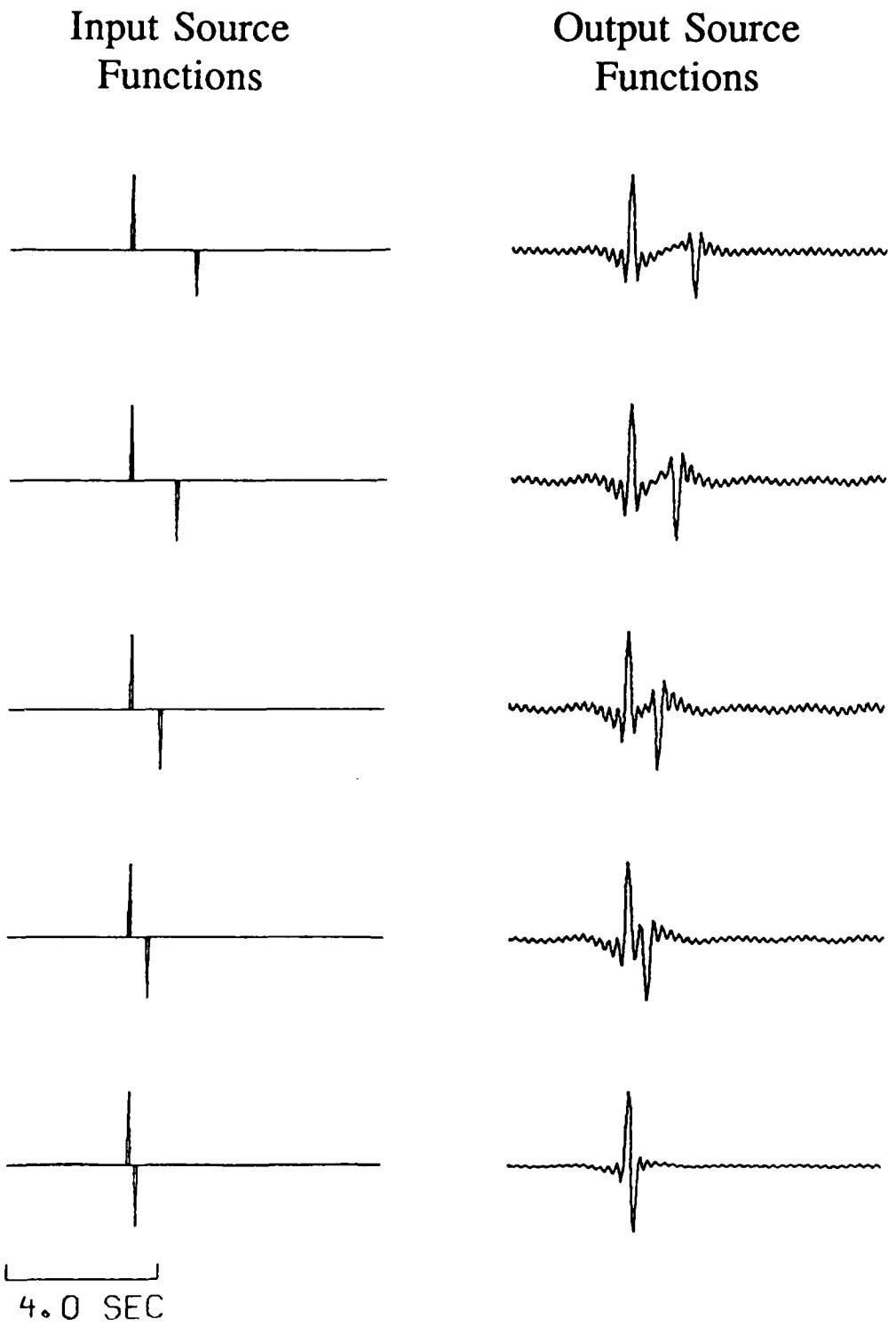

Figure 3. Band-limited deconvolution results for synthetic data. Input spike sequences for a range of pP times are shown on the left and the deconvolution output is shown on the right.

the resolution kernel, deconvolution will yield progressively smaller amplitudes in the deconvolved P+pP waveforms with decreasing true pP delay times without seeing any decrease in the observed delay time. This problem is illustrated in Figure 4, where the amplitudes from deconvolution decrease below 0.2 sec of true delay time while the observed delay time remains constant. Of course, for actual nuclear explosions, there is a lower limit to the pP delay time, assuming everything to be linear. This is imposed by the minimum depth of containment in the rocks in question. Moreover, at very shallow depth, the pP phase is expected to disappear, such as for cratering explosions.

As a final test, the results are checked by reconstructing each input trace from the convolution of the appropriate source and site terms and the wavelet consisting of t^*, instrument response, and VSB. In most cases the reconstructions and the original traces are very similar (Figure 5), including the details of the coda, and have high correlation coefficients. The excellent reconstructions of the original traces demonstrate, however, that the noncausality observed in the deconvolved source and site terms is not a major problem since most reconstructed traces do not have major precursors. The differences between the original and reconstructed seismograms can be inferred as a measure of the scattering unique to each individual path, i.e., energy unaccounted for by either site or source factors (which contain only the terms common to *all* of the seismograms from the respective source or site), and thus missing in the reconstructions.

Specific Data Processing Procedures

To prepare data for deconvolution, all traces are lined up in time on the first arrival. Since we are not interested in the absolute amplitudes in the context of estimating relative pP times and amplitudes, and because we want to give roughly equal weight to all the traces to ensure effective factoring, we multiplied each trace with two factors, one being appropriate to

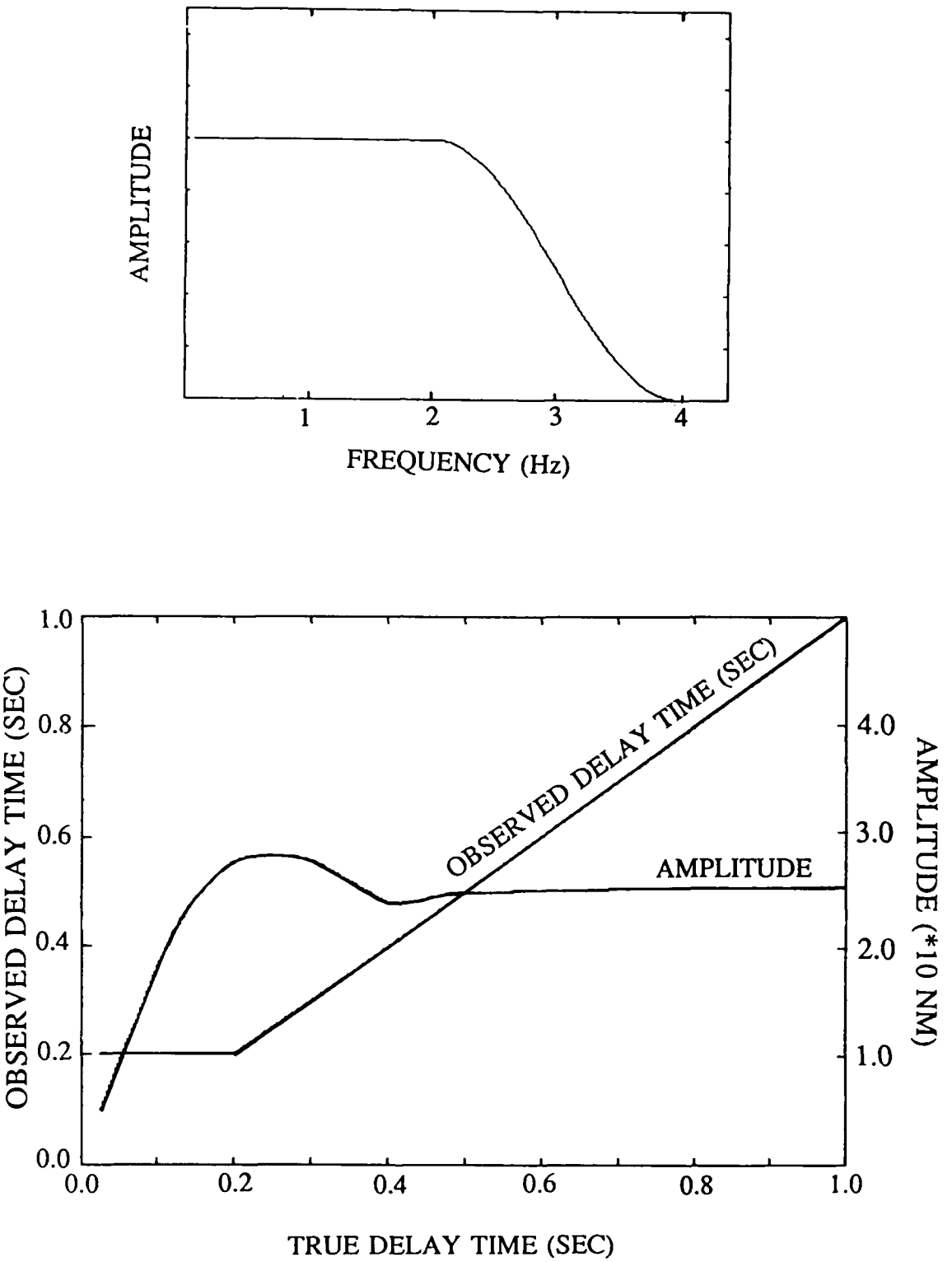

Figure 4. (Top) The spectral band of the P and pP wavelet used in the simulations. (Bottom) Estimated pP delay times and peak-to-peak waveform amplitudes for band limited deconvolutions as functions of true pP time delay (horizontal axis).

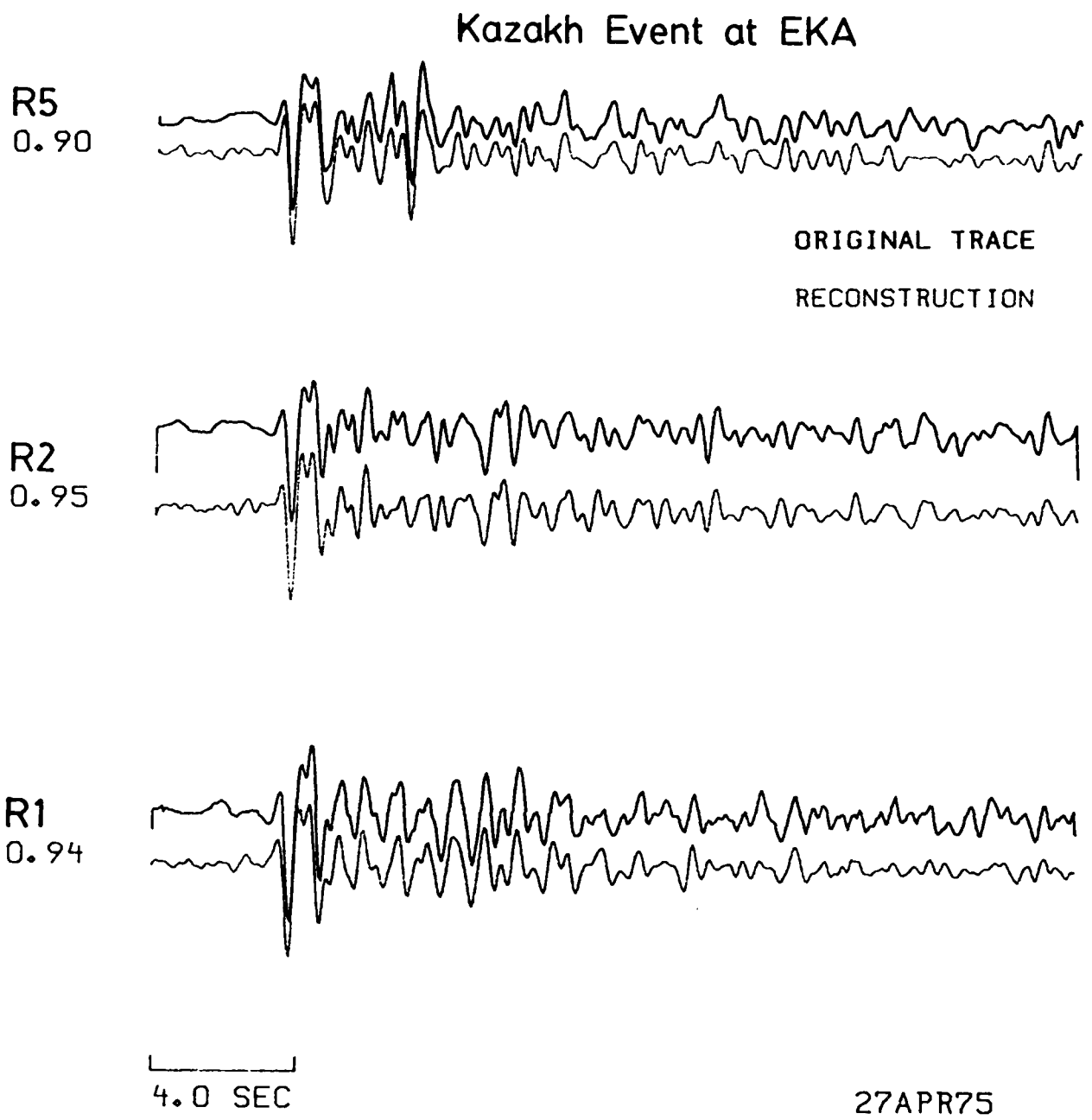

Figure 5. Examples of trace reconstructions (bottom) and original traces (top) for the 27 April, 1975, Shagan event at EKA for three sites. On the left side of each pair of traces is the name of the sensor and the correlation coefficient between the original and reconstructed traces.

the event, and the other to the site, which were designed to approximately equalize all peak amplitudes. This approach is consistent with the multiplicative structure of the spectra, and the exact values of the equalizing factors do not matter. After processing, the initial normalization factors can be divided out to estimate the proper relative amplitudes of the deconvolved traces. The deconvolution is more strongly dependent on the lining up of the first arrivals in order to gain maximum time resolution than it is on the S/N ratio, so it is acceptable that the process of equalizing the amplitudes results in a less than optimal S/N ratio in the output.

One option in the deconvolution procedure is to follow Douglas *et al.* (1987) and to include only the t* and the instrument response, and not the VSB source wavelet, into the "known" factor to be divided out in each step of the iteration. This way the source pulses may be directly observable in the source deconvolutions, together with the pulse width and the "overshoot". This approach has the advantage of allowing a direct look at the source pulse shape, but it is harder to estimate small closely spaced P and pP delay times from such results. This approach is also not subject to errors due to incorrect *a priori* assumptions about the shapes of the explosion time functions, as the explosion source parameters (k, B) are not very well known in advance (Mueller and Murphy 1970, von Seggern and Blandford 1972, Lay *et al.* 1984b); on the other hand, it appears that we know the shapes of the time domain attenuation and instrument response operators adequately enough to obtain reliable deconvolutions. An additional argument for the omission of the explosion source pulse from the deconvolution process is that inclusion of such a pulse makes sense only for finding the pP reflection (that has supposedly the same shape as the direct P); other arrivals (spall and arrivals in the coda) cannot be expected to have the same shape as the direct P pulse. If the deconvolution is done without removing the explosion time function, we essentially get a time history of teleseismic displacement smoothed by the approximately sin(x)/x shaped resolution kernel. If the results do not resemble the simple waveforms expected by a P+pP model (and they often do

not), then the conclusion is inescapable that such models are not valid. In our work we often performed the deconvolutions in both ways, and we shall identify results obtained by both approaches in this report. Figure 6 is an example of five Kazakh explosion source time functions deconvolved from NORSAR records, with and without removing the VSB. As expected, removing the VSB gives a more impulsive character to the source time function, and emphasizes the higher frequencies in the signal since some of the lower frequencies have been removed by the VSB.

Alternative models of explosion source time functions (Mueller and Murphy 1971) give results that are indistinguishable from those obtained from the von Seggern-Blandford model. Other time functions with ω^{-3} spectral falloff rates can be ruled out because they are in conflict with spectra of P waves from nuclear explosions along high Q paths (Bache 1982, Der *et al.* 1982). These remarks need not be considered when dealing with deconvolutions where the explosion source time function is not removed.

The deconvolutions presented in the following sections have all utilized the best constant t* operator for a given path as opposed to a frequency dependent t* operator, t*(f). This has been shown previously (i.e. Der and Lees 1985) to be a reasonable way to treat narrow band data when t*(f) is slowly varying. Refinement of the apparent t* in excess of 0.1 sec may require a reprocessing of the deconvolutions if the original value of this parameter is low (of the order of 0.2 sec). At higher values, even larger corrections produce only very small changes in the source time function. Extreme models of t*(f) may change the results, but only small variations in the source time functions are observed with reasonable t* models. Figure 7 is an example which demonstrates that for t* and t*(f) models that are appropriate for a given path, the deconvolved source time functions show only minor differences in waveform shape. The deconvolutions with t*(f) show slightly less high frequency energy than the deconvolutions

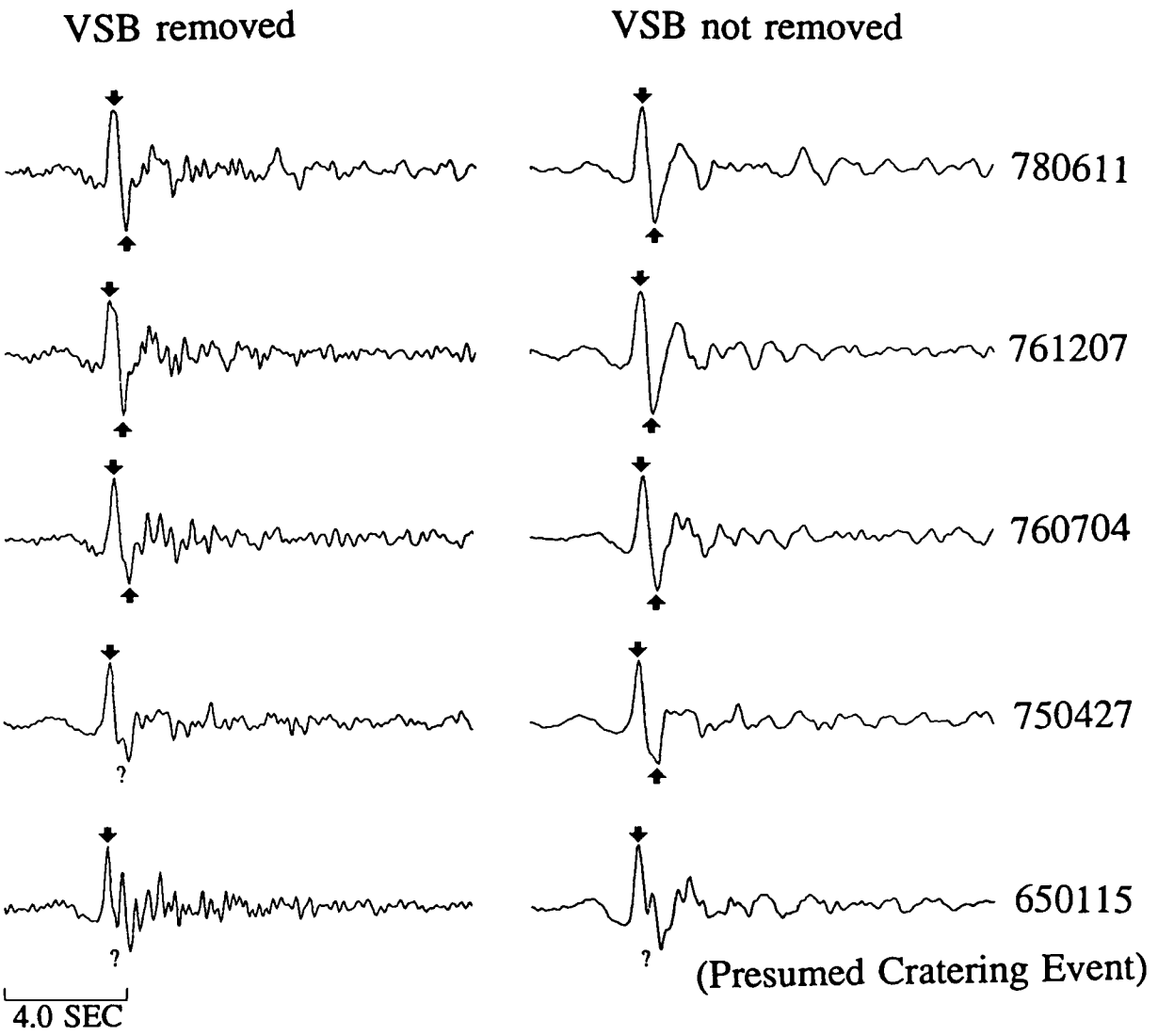

Figure 6. Deconvolved source time functions from Shagan data recorded at EKA. Source functions on the left have had a von Seggern and Blandford (VSB) wavelet removed in the deconvolution process while source functions on the right have not had the VSB removed. Note that removing the VSB results in a more impulsive looking source time function (theoretically, the initial P wave would be an impulse in this case, but the resolution is bandwidth limited).

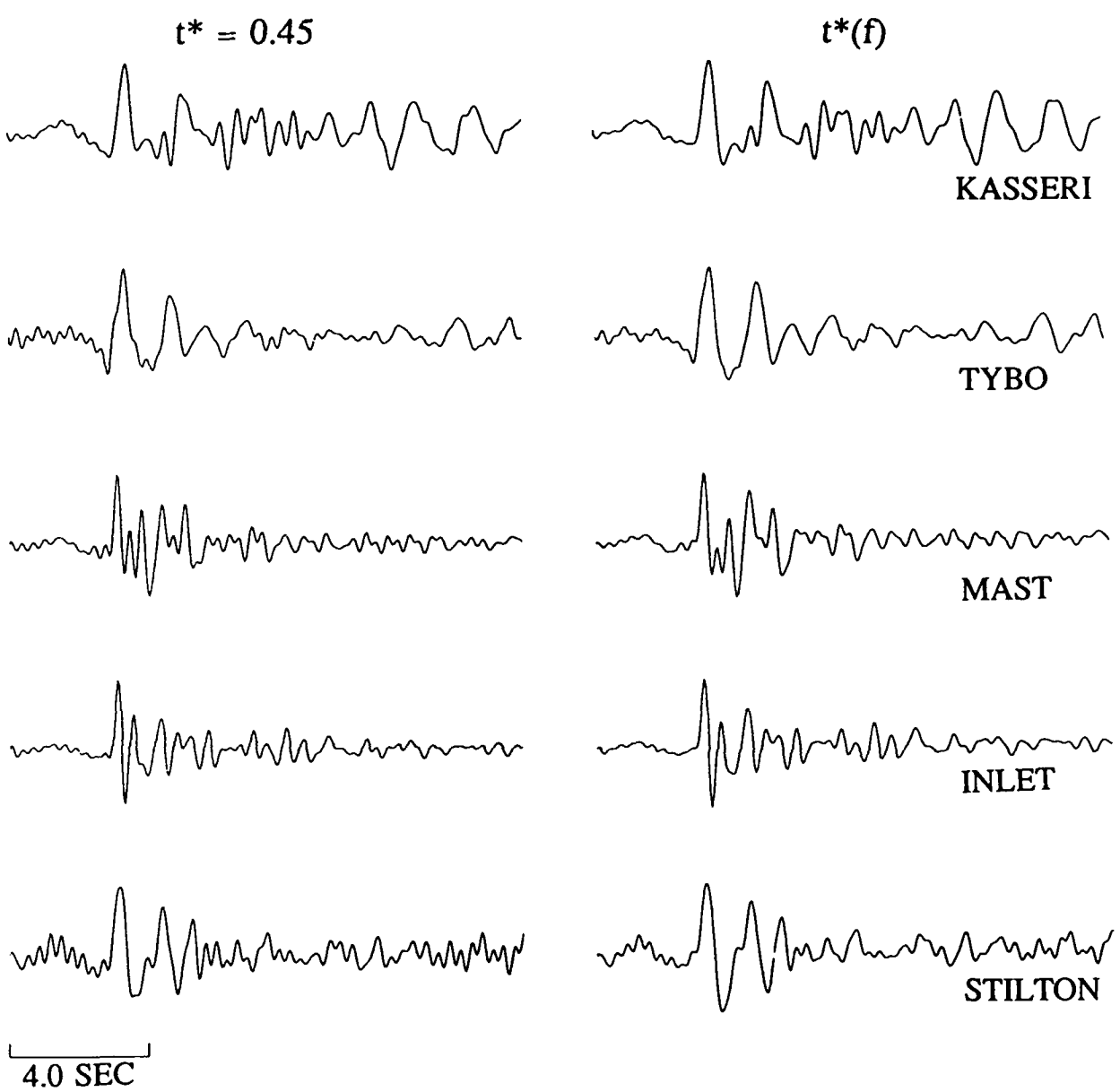

Figure 7. Deconvolved source time functions from NTS events recorded at NORSAR. Source functions on the left have had a constant t* of 0.45 sec removed in the deconvolution process while source functions on the right have had a frequency dependent t* (QP T-S from Der and Lees 1985) removed in the deconvolution process. There are only small differences in the deconvolved source terms which result from using the different t*s.

performed with constant t* since the attenuation decreases with frequency in the t*(f) model.

In the deconvolutions presented in the rest of this report, we have assumed that the same instrument and t* was appropriate in deconvolving the wavelet from each seismogram in a data set. This assumption is not always valid; for instance the t*'s for the different RSTN stations are not all the same and the same instrument response is not appropriate if, say, NORSAR and EKA data were combined to make a larger receiver array. Therefore, we have modified the deconvolution program to allow different t*'s and instrument responses to be deconvolved from each seismogram. However, in practice, this does not improve the resolution of the deconvolutions. The most important part of preparing the data for deconvolution is, like for beaming, carefully lining up the initial P wave arrival. It is important that the initial arrivals are still lined up after the wavelet consisting of the instrument, t*, and VSB has been removed. However, when the instrument and/or t* is different for the different seismograms, the wavelet being divided out has its maximum at different times for the different seismograms (for instance, larger values of t* delay the arrival of the peak of the wavelet), and the seismograms become misaligned when they are divided by their respective wavelets. This results in deconvolved source time functions where the arrivals are poorly resolved, as shown in Figure 8. Therefore, in cases where the instrument response and/or t* vary between the different seismograms, the instrument and t* should be removed before doing the deconvolution, either by single channel deconvolution, or by multichannel deconvolution of smaller data sets where all of the seismograms have a common instrument response and t*. In the latter case, when the final multichannel deconvolution of all of the data is done, the site terms will really be different with respect to the site terms removed during the deconvolutions of the smaller data sets.

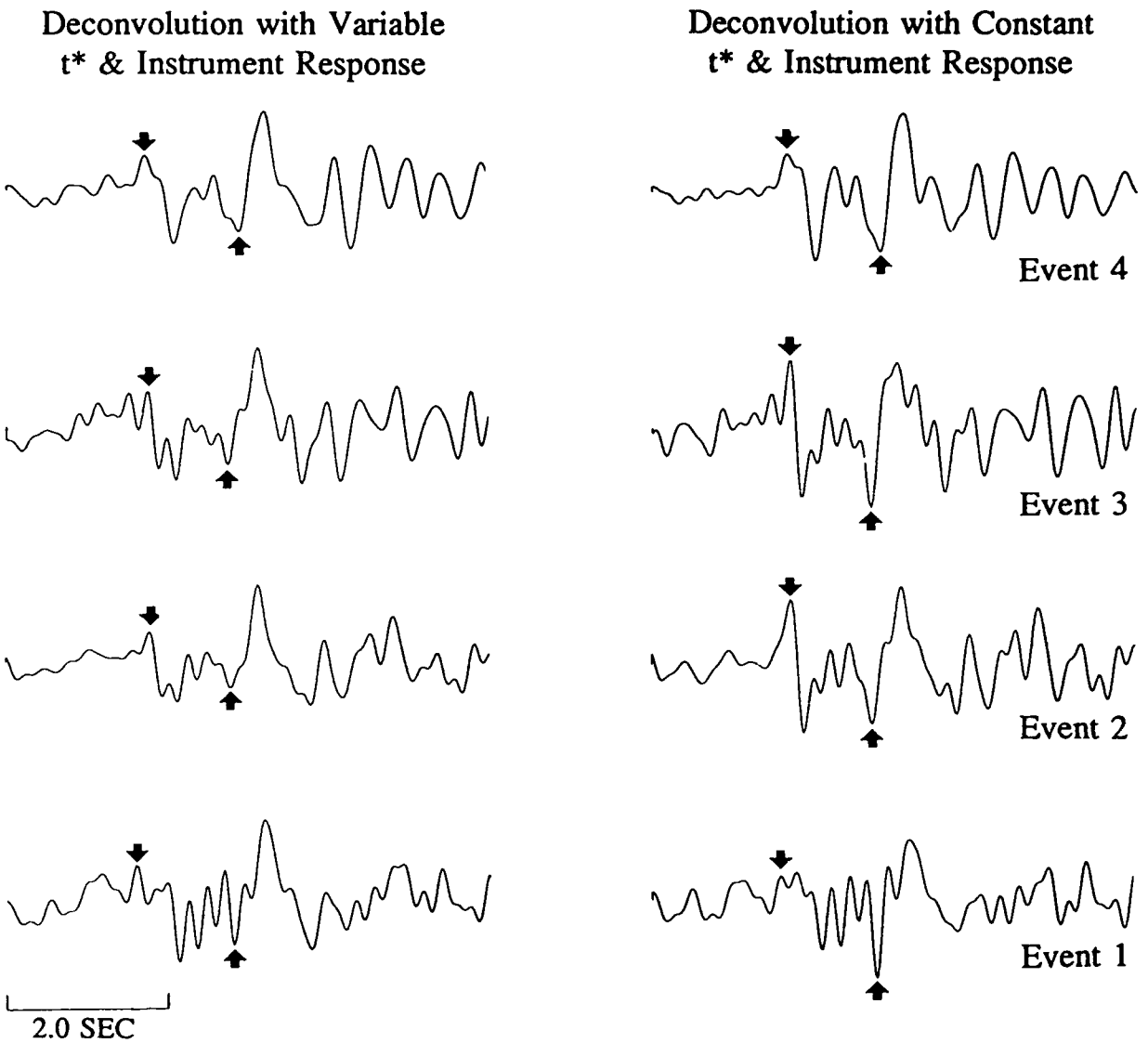

Figure 8. Deconvolved source time functions from Astrakhan data recorded at GBA and RSTN. Source functions on the left have had different t*s and instrument responses removed from each original input seismogram as appropriate for the different paths (i.e. instrument responses of GBA and the RSTN stations are different, and the RSTN stations have different t*s). Source functions on the right have had the same instrument and t* removed from every seismogram, and the P and pP arrivals are much better resolved in this case than with the variable t* and instrument response.

DECONVOLUTIONS FOR DIFFERENT TEST SITES

In the course of this project, we have deconvolved waveforms for some 245 different source-receiver array pairs. Table 1 summarizes the number of events deconvolved for each source region-receiver array pair. The events in each data set are described in Tables 2 to 13 and the source region to receiver array distances are given in Table 14.

For many of the deconvolutions we have used data recorded at the AWRE arrays EKA, GBA, WRA, and YKA. These arrays are described by Mowat and Burch (1977). Table 15, after Bache *et al.* (1985), lists some of the parameters of the arrays and layouts of the arrays are shown in Figures 9 a-d.

In the rest of this section, we will discuss the results of deconvolutions of data from the different nuclear test sites, Degelen, Shagan, Novaya Zemlya, Astrakhan, French Sahara, Tuamotu, Sinkiang, Yucca Flats, and Pahute Mesa, and of three-component regional and teleseismic data.

Degelen

A map of the locations of the Degelen explosions is shown in Figure 10. Figures 11 through 14 show the source functions at the various arrays with the estimated VSB removed in the deconvolution process. The P and pP phases are marked on each trace. It is apparent that only a few of the events show secondary arrivals, interpretable as pP, with negative amplitudes similar in size to the initial P wave pulse. Most events do not show a clear pP. It may be argued that many Degelen events were shallow enough for preventing the development of pP pulses, possibly by nonlinearity of deformation near the surface. An alternative explanation may be the complex topography above the explosions.

Table 1

Number of Events Deconvolved for Each Source Region-Receiver Array Combination						
Event Region	Receiver					
	EKA	YKA	WRA	GBA	RSTN	NORESS
Degelen	10	9	8	10		
Shagan	31	6	6	12	4	
NZ (P)	9	12	11	5		
NZ (PcP)	18					
Astrakhan				10	4	
French Sahara	4	3				
Tuamotu		11	5	2	3	
Sinkiang					3	
Yucca Flats	7	7		5		
Pahute Mesa	13		2	5		
Leningrad						4
SW Norway						6

Table 2

Degelen Events Used in Deconvolutions

Event	Array EKA	Location YKA	WRA	GBA	Origin Time	Lat(°N)	Lon(°E)	m_b
670226	X				03:57:57.4	49.750	78.125	6.0
711230	X				06:20:57.8	49.772	78.093	5.8
770329	X	X		X	03:56:57.6	49.790	78.086	5.4
770730	X	X	X	X	01:56:57.7	49.759	78.097	5.1
780326		X	X	X	03:56:57.6	49.768	78.044	5.6
780422	X	X	X	X	03:06:57.6	49.761	78.186	5.3
781031	X	X	X	X	04:16:57.8	49.806	78.143	5.2
790506	X	X	X	X	03:16:57.7	49.774	78.049	5.2
790531	X	X	X	X	05:54:57.7	49.835	78.127	5.2
791018			X	X	04:16:57.7	49.837	78.148	5.2
800522	X	X		X	03:56:57.7	49.784	78.082	5.5
800731	X	X	X	X	03:32:57.7	49.807	78.148	5.3

Location information from Marshall et al (1984).

Table 3

Shagan Events Used in Deconvolutions

Event	Array EKA	Location YKA	WRA	GBA	Origin Time	Lat(°N)	Lon(°E)	m_b
650115	X				05:59:58.4	49.940	79.010	5.8
720210	X				05:02:57.5	50.014	78.878	5.4
721210	X				04:27:07.3	50.001	78.973	6.0
731214		X			07:46:57.2	50.044	78.987	5.8
741016	X	X		X	06:32:57.6	49.979	78.898	5.5
750630		X			03:26:57.6	50.004	78.957	4.6
751029	X			X	04:46:57.3	49.946	78.878	5.7
751225	X		X	X	05:16:57.2	50.044	78.814	5.7
760421	X	X		X	05:02:57.2	49.890	78.827	5.3
760609		X		X	03:02:57.2	49.989	79.022	5.1
760704	X				02:56:57.5	49.909	78.911	5.8
761123				X	05:02:57.3	50.008	78.963	5.9
761207	X				04:56:57.4	49.922	78.846	5.9
770629	X	X		X	03:06:57.8	50.006	78.869	5.2
770905	X		X	X	03:02:57.3	50.035	78.921	5.7
771130	X				04:06:57.4	49.958	78.885	6.0
780611	X		X	X	02:56:57.6	49.898	78.797	5.9
780705	X			X	02:46:57.5	49.887	78.871	5.8
780829	X		X	X	02:37:06.3	50.000	78.978	5.9
780915	X		X		02:36:57.4	49.916	78.879	6.0
781104	X		X	X	05:05:57.3	50.034	78.943	5.6
781129	X				04:33:02.5	49.949	78.798	6.0
790623	X				02:56:57.5	49.903	78.855	6.2
790707	X				03:46:57.3	50.026	78.991	5.8
790804	X				03:56:57.1	49.894	78.904	6.2
791028	X				03:16:56.9	49.973	78.997	6.0
791202	X				04:36:57.5	49.891	78.796	6.0
791223	X				04:56:57.4	49.916	78.755	6.2
800629	X				02:32:57.7	49.939	78.815	5.7
801227	X				04:09:08.1	50.057	78.981	5.9
810422	X				01:17:11.3	49.885	78.810	6.1
811018	X				03:57:02.6	49.923	78.859	6.1
811129	X				03:35:08.6	49.887	78.860	5.7
820831	X				01:31:00.7	49.924	78.761	5.4
821226	X				03:35:14.2	50.071	78.988	5.7

Location information from Marshall et al (1984).

Table 4

Novaya Zemlya Events Used in Deconvolutions

Event	Array EKA	Location YKA	WRA	GBA	Origin Time	Lat(°N)	Lon(°E)	m_b
1966300	PcP		P_{diff}		05:57:58.1	73.388	54.845	6.47
1967294	PcP				04:59:58.5	73.385	54.826	5.99
1968312	PcP		P_{diff}		10:02:05.5	73.388	54.873	6.11
1969287	PcP				07:00:06.6	73.389	54.796	6.18
1970287	PcP		P_{diff}		05:59:57.6	73.301	55.044	6.77
1971270	PcP				05:59:55.8	73.393	54.923	6.63
1972241	PcP				05:59:56.9	73.386	54.859	6.46
1973255	PcP		P_{diff}		06:59:54.8	73.316	55.059	6.96
1973270(S)	P,PcP	P			06:59:58.5	70.756	53.754	5.84
1973300(S)	PcP		P_{diff}		06:59:58.0	70.801	53.958	6.90
1974306(S)	PcP				04:59:57.4	70.833	53.825	6.75
1975235	PcP				08:59:58.3	73.332	54.694	6.55
1975291(S,D)			P_{diff}		08:59:56.8	70.838	53.673	6.70
1975294	PcP		P_{diff}		11:59:58.0	73.308	55.012	6.59
1976273	PcP	P			02:59:57.7	73.360	54.880	5.77
1976294	P			P	07:59:58.1	73.399	54.835	4.89
1977244	P	P			02:59:58.0	73.339	54.626	5.71
1978222		P			07:59:58.0	73.293	54.885	6.04
1978270	P,PcP	P			02:04:58.6	73.350	54.677	5.68
1979267	P,PcP	P			03:29:58.8	73.346	54.679	5.80
1979291	P,PcP	P	P_{diff}		07:09:58.8	73.318	54.821	5.85
1980285(D)	P	P	P_{diff}	P	07:09:57.5	73.335	54.938	5.80
1981274		P	P_{diff}	P	12:14:57.3	73.308	54.817	5.91
1982284	P	P		P	07:14:58.7	73.348	54.601	5.52
1983230		P		P	16:09:58.9	73.358	54.974	5.84
1983268	P	P			13:09:58.2	73.326	54.564	5.71
1984299	PcP		P_{diff}		06:29:57.7	73.37	54.955	5.9

Location information from Lilwall and Marshall (1986) except for 1984299 where location information is from USGS.

(S) Southern Novaya Zemlya event.

(D) Double event per Lilwall and Marshall (1986).

Table 5

Astrakhan Events Recorded at GBA

Event	Location Origin Time	Lat(°N)	Lon(°E)	m_b
1982289a	05:59:57.4	46.77	48.22	5.2
1982289b	06:04:57.4	46.77	48.24	5.2
1982289c	06:09:57.4	46.77	48.22	5.2
1982289d	06:14:57.5	46.75	48.20	5.4
1983267a	04:59:57.2	46.81	48.29	5.2
1983267b	05:04:57.3	46.81	48.27	5.1
1983267c	05:09:57.4	46.84	48.33	5.0
1983267d	05:14:57.4	46.84	48.29	5.2
1983267e	05:19:57.4	46.88	48.30	5.4
1983267f	05:24:57.0	46.80	48.29	5.3

ISC location information.

Table 6

French Sahara Events Used in Deconvolutions				
Event	Array			
	EKA	YKA	WRA	GBA
Emeraude	X	X		
Grenat	X	X		
Rubis	X			
Saphir	X	X		

Table 7

Tuamotu (Mururoa) Events Used in Deconvolutions

Event	Array					Location		
	EKA	YKA	WRA	GBA	RSTN	Origin Time	Lat(°S)	Lon(°W)	m_b
1976193		X				00:29:59.05	21.859	138.768	5.01
1977050		X				23:29:58.94	21.834	138.846	5.00
1977187		X				22:59:58.52	21.780	138.954	4.92
1977328				X		16:59:58.37	21.896	138.884	5.80
1978081		X				17:29:58.95	21.714	138.926	4.77
1978334			X	X		17:31:58.48	21.866	138.949	5.80
1978353		X				16:56:59.98	21.769	138.945	4.97
1979083		X				16:27:58.79	21.830	138.909	4.89
1979180		X				23:26:58.02	22.140	138.456	4.81
1980083		X	X			19:36:58.49	21.864	138.928	5.62
1980092		X	X			19:30:58.68	21.854	138.763	5.10
1980168		X	X			18:26:58.56	21.864	138.904	5.29
1980188		X				17:26:58.96	21.845	138.861	4.67
1980201			X			23:46:58.51	21.855	138.949	5.71
1983109					X	18:52:57.8	21.81	138.95	5.6
1983145					X	17:30:58.6	21.85	138.94	5.9
1984133					X	17:30:58.6	21.83	138.97	5.7

Location information from Marshall et al (1985) except for 1983109, 1983145, and 1984133 where location information is from ISC.

Table 8

Sinkiang Events Used in Deconvolutions

Event	Location			
	Origin Time	Lat(°N)	Lon(°E)	m_b
1984277	05:59:57.82	41.602	88.730	5.24
1984354	06:00:04.26	41.680	88.443	4.72
1987156	05:00:03.1	41.67	88.82	6.30

Location information from NEIS except for m_b's which are from McLaughlin et al (1987c).

Table 9

Pahute Mesa Events Used in Deconvolutions

Event	Array EKA	Location YKA	WRA	GBA	Date	Origin Time	Lat(°N)	Lon(°W)
BOXCAR	X				680426	15:00:00.0	37.295	116.456
CAMEMBERT	X			X	750626	12:30:00.2	37.279	116.369
CHESHIRE	X				760214	11:30:00.2	37.243	116.420
ESTUARY	X			X	760309	14:00:00.1	37.310	116.364
FAULTLESS	X				680119	18:15:00.1	38.63	116.22
FONTINA	X				760212	14:45:00.2	37.271	116.488
HANDLEY	X				700326	19:00:00.2	37.300	116.534
INLET	X				751120	15:00:00.1	37.225	116.368
KASSERI	X		X	X	751028	14:30:00.2	37.290	116.412
MAST	X				750619	13:00:00.1	37.350	116.320
MUENSTER	X		X	X	760103	19:15:00.2	37.297	116.333
PURSE	X				690507	13:45:00.0	37.283	116.501
TYBO	X			X	750514	14:00:00.2	37.221	116.474

Locations were announced except for FAULTLESS, for which the location is from the ISC.

Table 10

Yucca Flats Events Used in Deconvolutions

Event	Array EKA	Location YKA	WRA	GBA	Date	Origin Time	Lat(°N)	Lon(°W
BULKHEAD		X		X	770427	15:00:00.1	37.095	116.028
CABRILLO		X			750307	15:00:00.2	37.134	116.084
CHIBERTA	X				751220	20:00:00.2	37.128	116.062
CREWLINE		X		X	770525	17:00:00.1	37.094	116.045
FARALLONES	X			X	771214	15:00:00.1	37.136	116.086
HEARTS	X				790906	15:00:00.1	37.088	116.053
LOWBALL	X	X			780712	17:00:00.1	37.079	116.044
QUARGEL		X		X	781118	19:00:00.2	37.127	116.084
SCANTLING		X			770819	17:55:00.1	37.110	116.055
STRAIT	X			X	760317	14:45:00.1	37.107	116.052
TOPGALLANT	X	X			750228	15:15:00.1	37.106	116.056
PILEDRIVER	X				660602	15:30:00.1	37.227	116.056

Locations were announced.

Table 11

East Kazakh Events Used in Deconvolutions of Three-Component RSTN Data

Event	Location Origin Time	Lat(°N)	Lon(°E)	m_b
1982339	03:37:12.6	49.91	78.84	6.1
1983279	01:47:06.5	49.93	78.84	6.0
1984050	03:57:03.4	49.91	78.81	5.8
1984116	01:09:03.5	49.95	78.94	5.9

ISC location information.

Table 12

Regional Events Used in Deconvolutions of NORESS Data
Leningrad Region Mine Blasts ($\Delta \sim 9°$)

Event	Location Origin Time	Lat(°N)	Lon(°E)	M_L
1985193	11:05:21.6	59.1	28.2	3.3
1985199	21:16:08.0	64.4	28.8	4.6
1985262	14:33:21.6	59.5	29.3	3.9
1986155	09:06:31.1	62.3	29.8	3.9
1986163	09:30:55.1	60.2	29.9	3.7
1986195	14:30:25.7	58.7	29.0	3.2

Location information from NORESS.

Table 13

Regional Events Used in Deconvolutions of NORESS Data
($\Delta \sim 4°$)

Event	Location			Type
	Origin Time	Lat(°N)	Lon(°E)	M_L
1985317	16:32:20.8	59.2	7.5	- explosion
1985324a	22:57:08.2	58.5	4.9	2.1 earthquake
1985324b	23:23:08.0	57.5	6.9	2.1 earthquake
1985324c	23:28:18.7	57.5	6.3	2.0 earthquake
1986017	14:10:58.0	59.1	4.9	2.3 explosion
1986045	14:13:19.3	58.1	6.2	2.4 explosion

Location and type information from Dysart (1986).

Table 14

Approximate Distances Between Source Regions and Receiver Arrays						
Event Region	Receiver					
	EKA	YKA	WRA	GBA	RSTN	NORESS
Degelen	47°	67°	85°	36°		
Shagan	47°	67°	85°	36°	67-94°	
NZ (P)	29°	44°	106°	61°		
NZ (PcP)	29°					
Astrakhan				41°	70-88°	
French Sahara	32°	81°				
Tuamotu		86°	79°	144°	73-89°	
Sinkiang					75-94°	
Yucca Flats	71°	26°		128°		
Pahute Mesa	71°		117°	128°		
Leningrad						9°
SW Norway						4°

Table 15

United Kingdom Sponsored Arrays						
Station	Code	Location	Element Spacing (km)	Maximum Element Spacing (km)	Date Operational	Date of Digital
Eskdalemuir Scotland	EKA	55°19'59"N 3°09'33"W	0.9	9.8	17 May 1962	14 Nov 1983
Yellowknife Canada	YKA	62°29'34"N 114°36'17"W	2.5	22.5	26 Nov 1962	-
Gauribidanur India	GBA	13°36'15"N 77°26'10"E	2.5	32.0	1 Feb 1966	4 Mar 1979
Warramunga Australia	WRA	19°56'39"S 134°20'27"E	2.5	26.3	1 Mar 1966	7 Jun 1977

From Bache et al (1985).

Eskdalemuir Array (EKA)

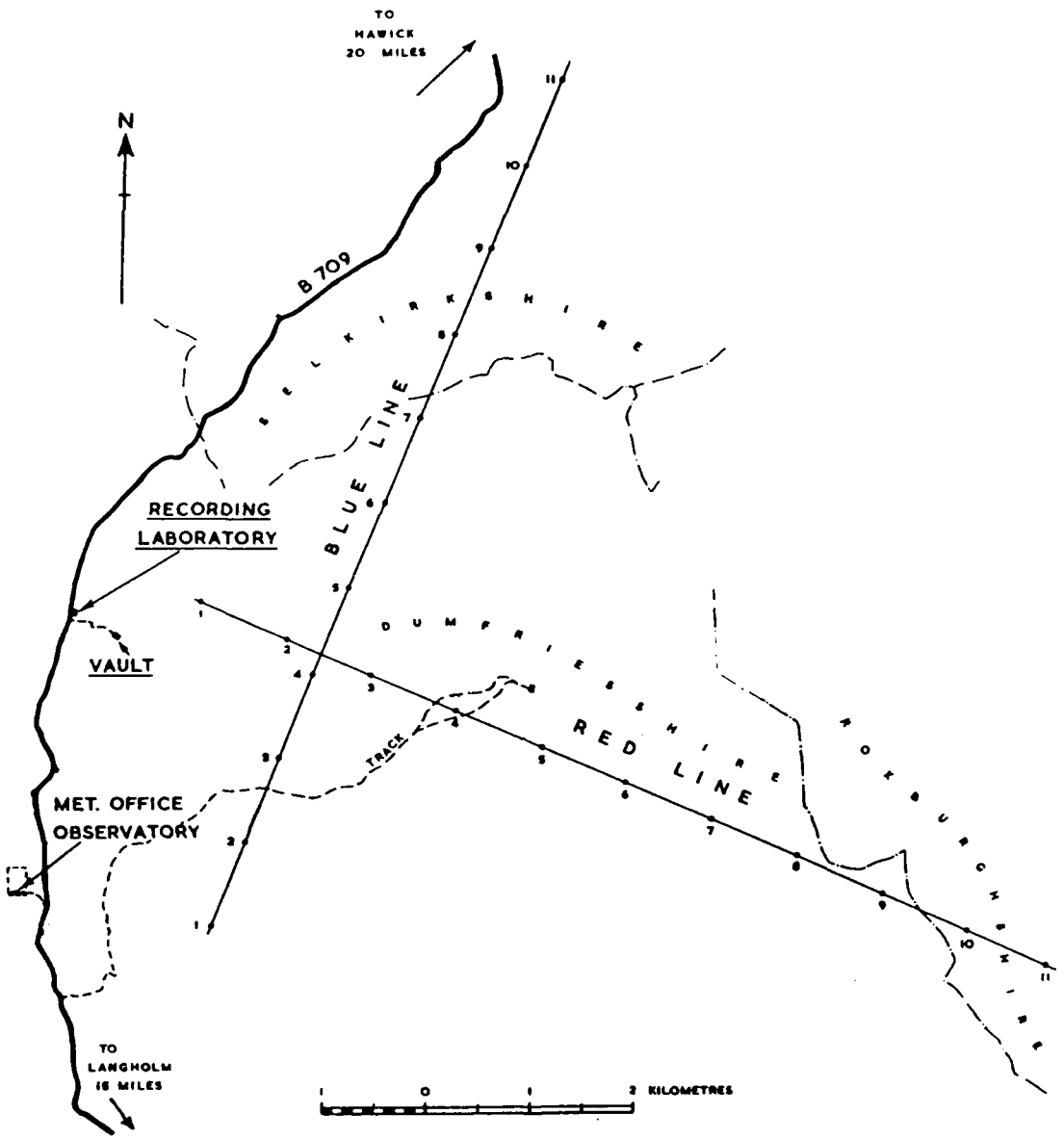

Figure 9(a). Layouts of the AWRE arrays EKA (from Mowat and Burch, 1977).

Gauribidanur Array (GBA)

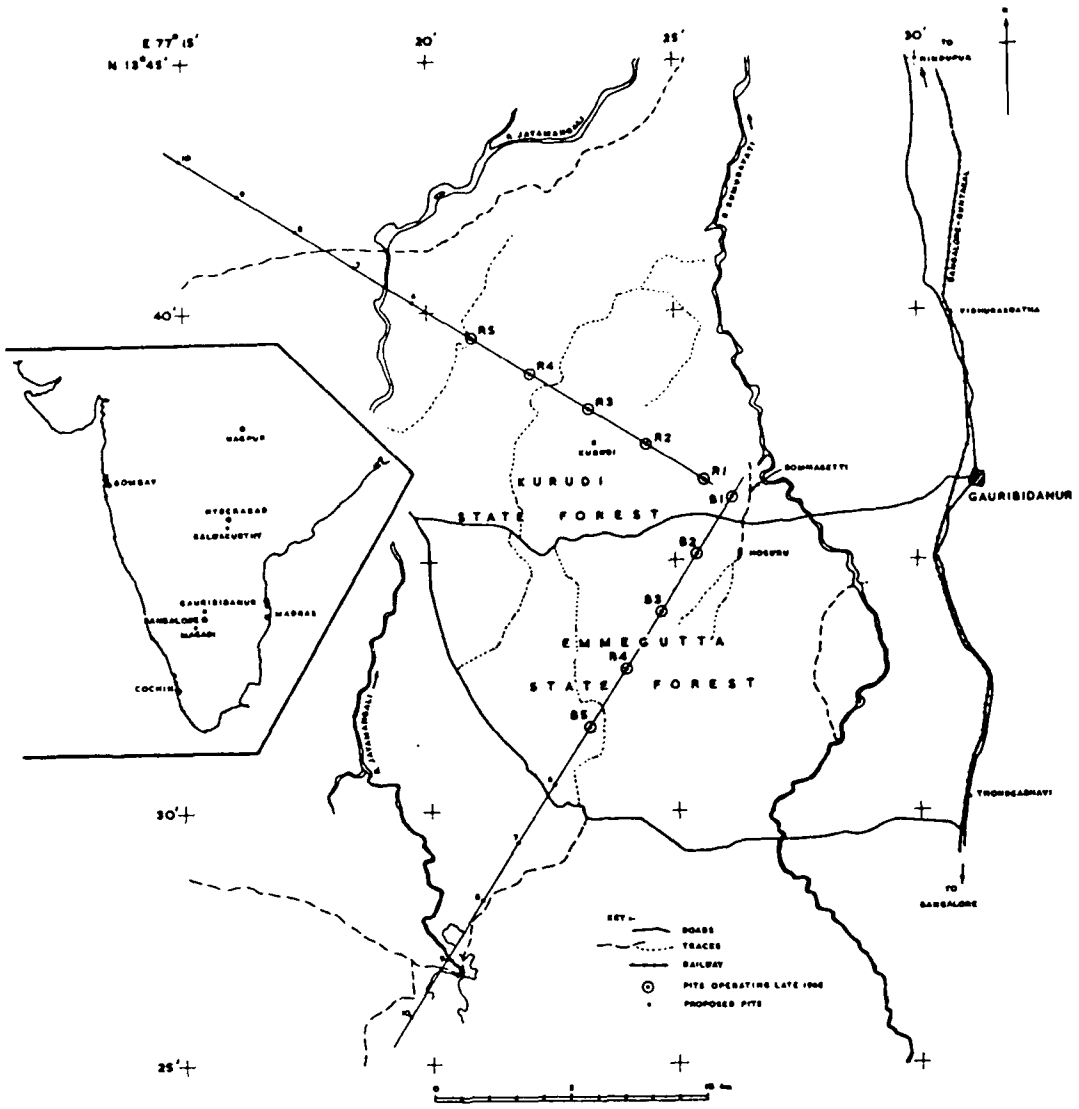

Figure 9(b). Layouts of the AWRE arrays GBA (from Mowat and Burch, 1977).

Warramunga Array (WRA)

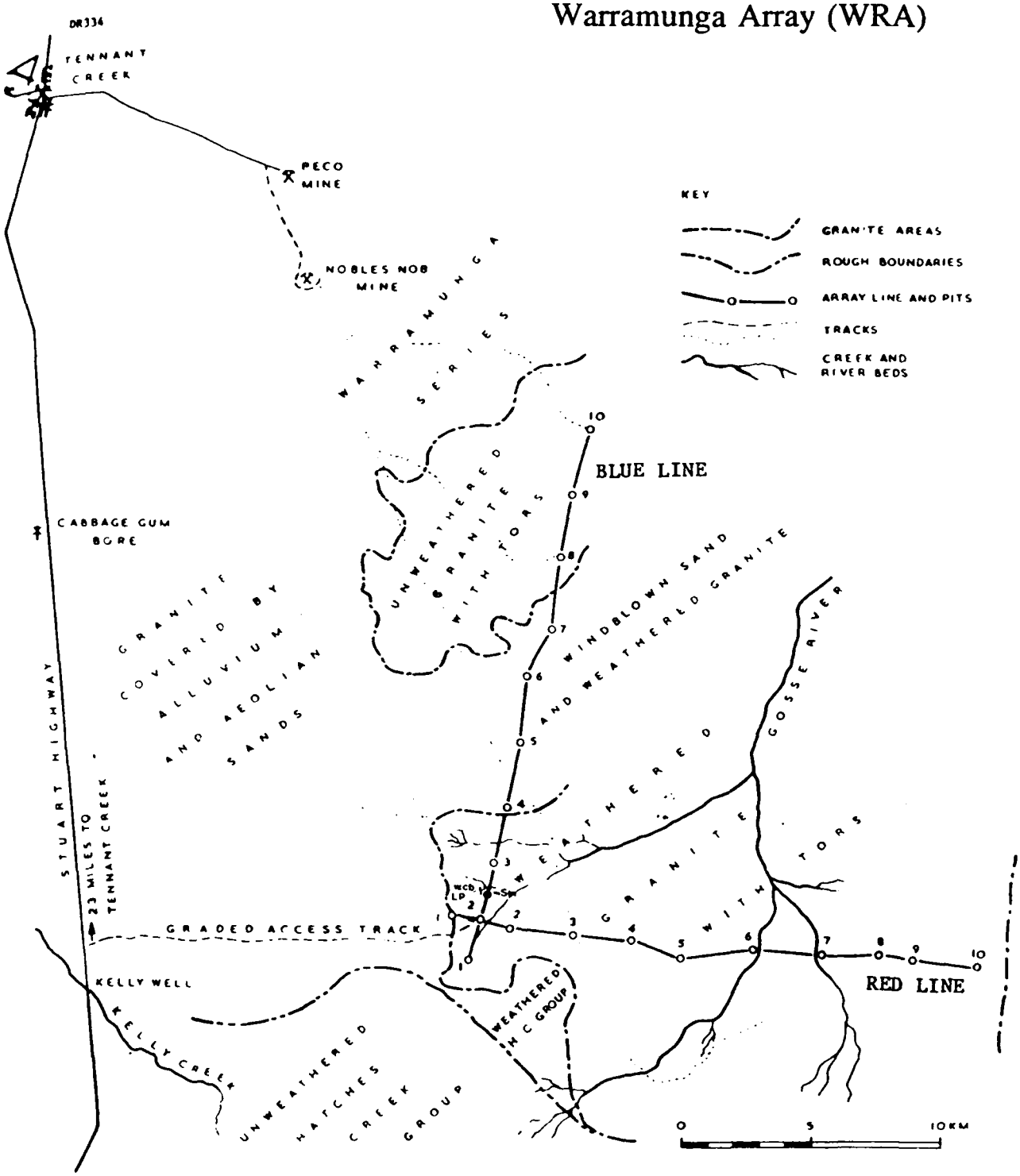

Figure 9(c). Layouts of the AWRE arrays WRA (from Mowat and Burch, 1977).

Yellowknife Array (YKA)

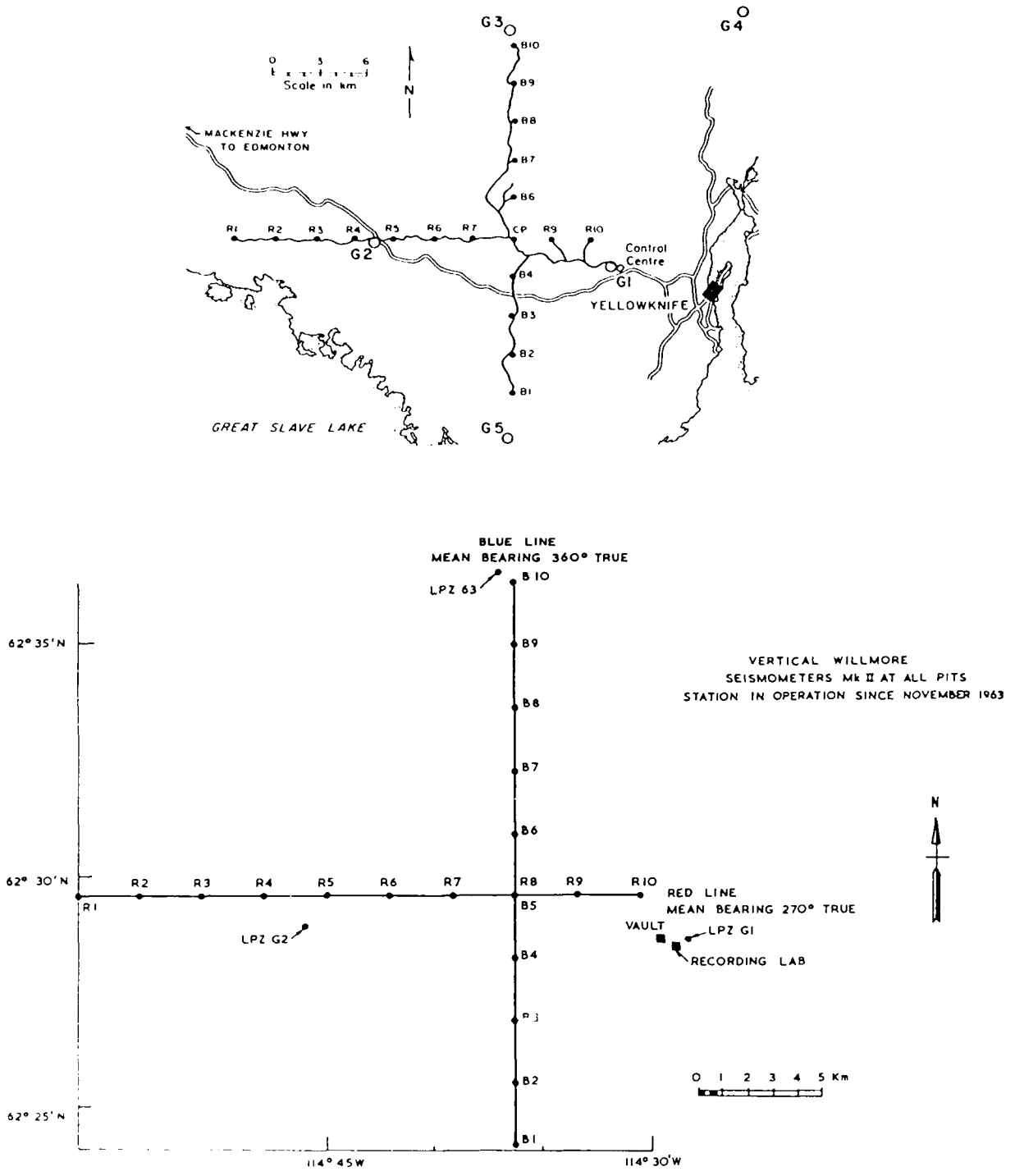

Figure 9(d). Layouts of the AWRE arrays YKA (from Mowat and Burch, 1977).

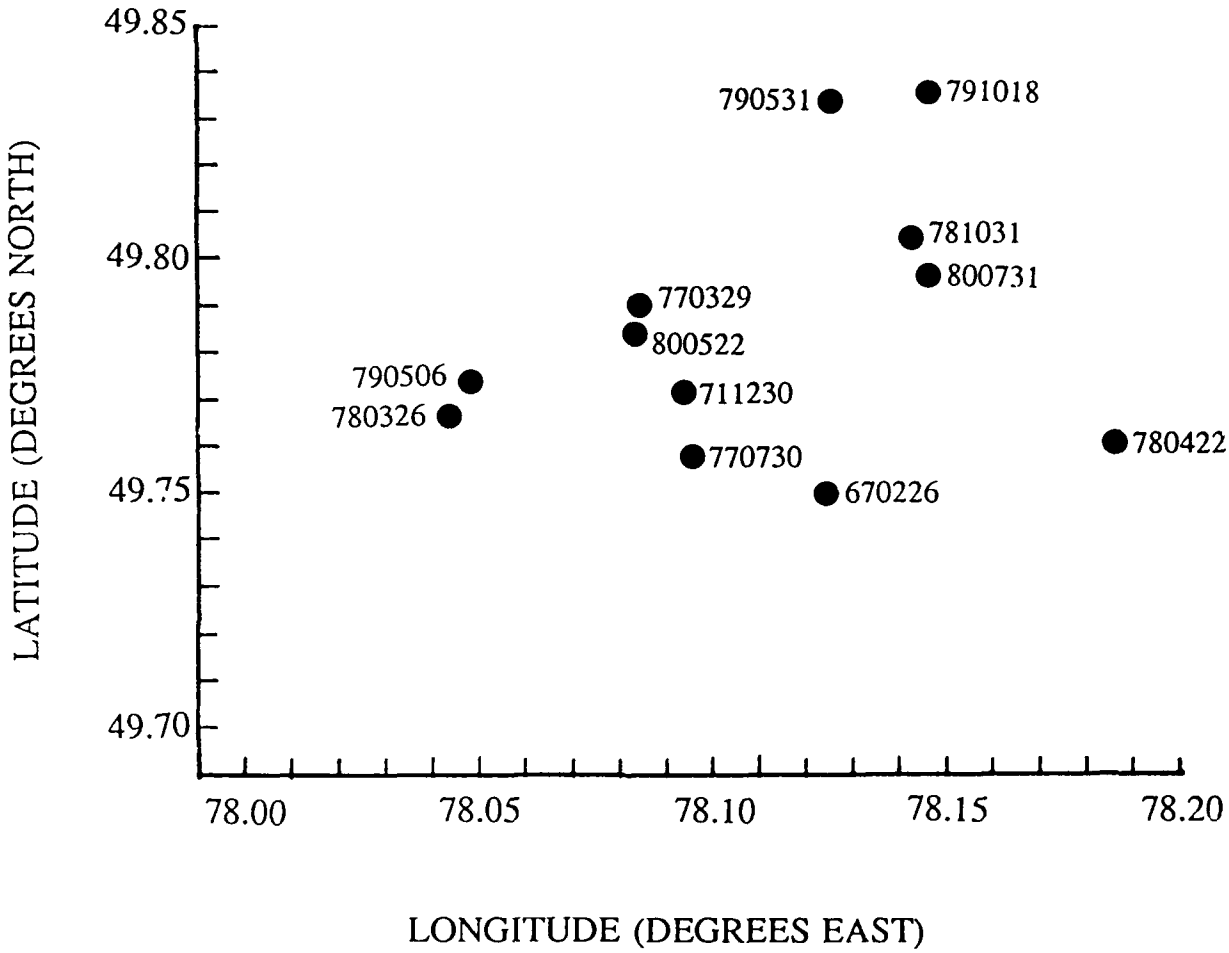

Figure 10. Locations (Marshall *et al.* 1984) of the Degelen events analyzed in this study.

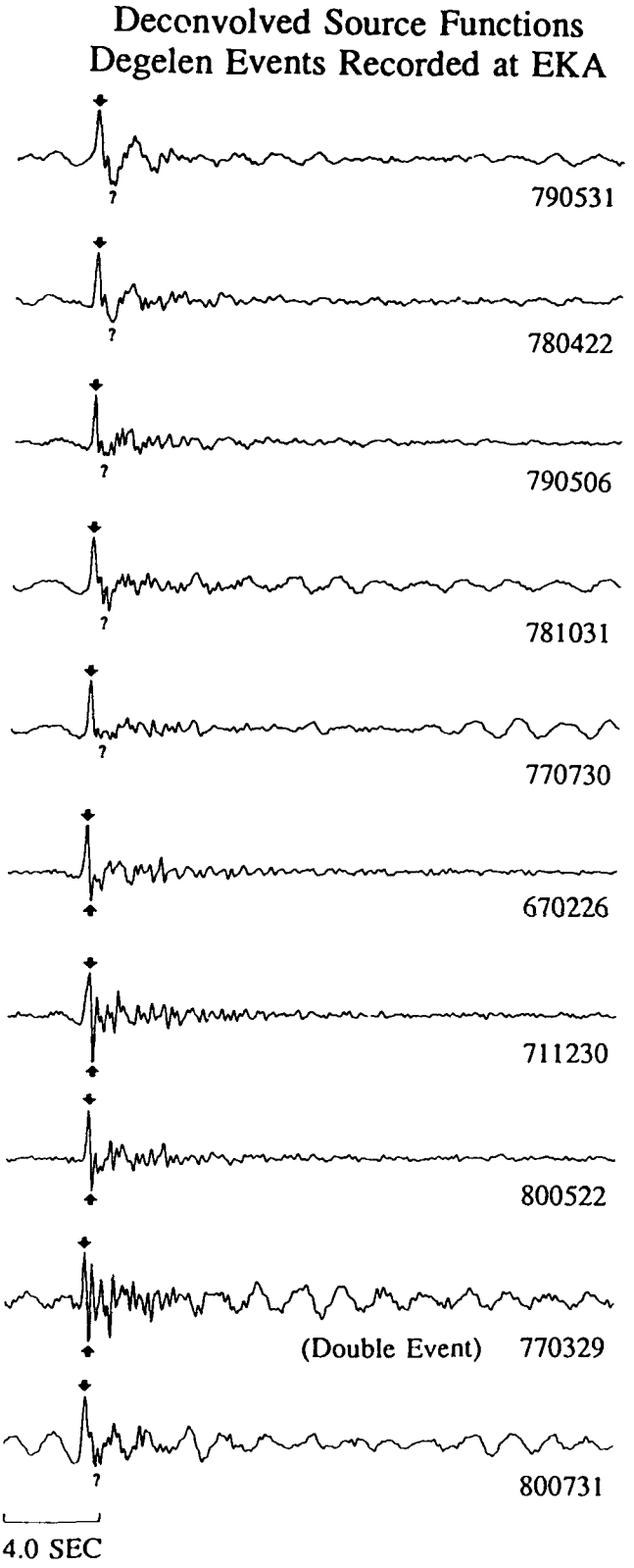

Figure 11. Deconvolved source functions for Degelen events at EKA. The estimated VSB wavelet has been removed in the deconvolutions. The P and pP, if present, arrivals are marked on each trace.

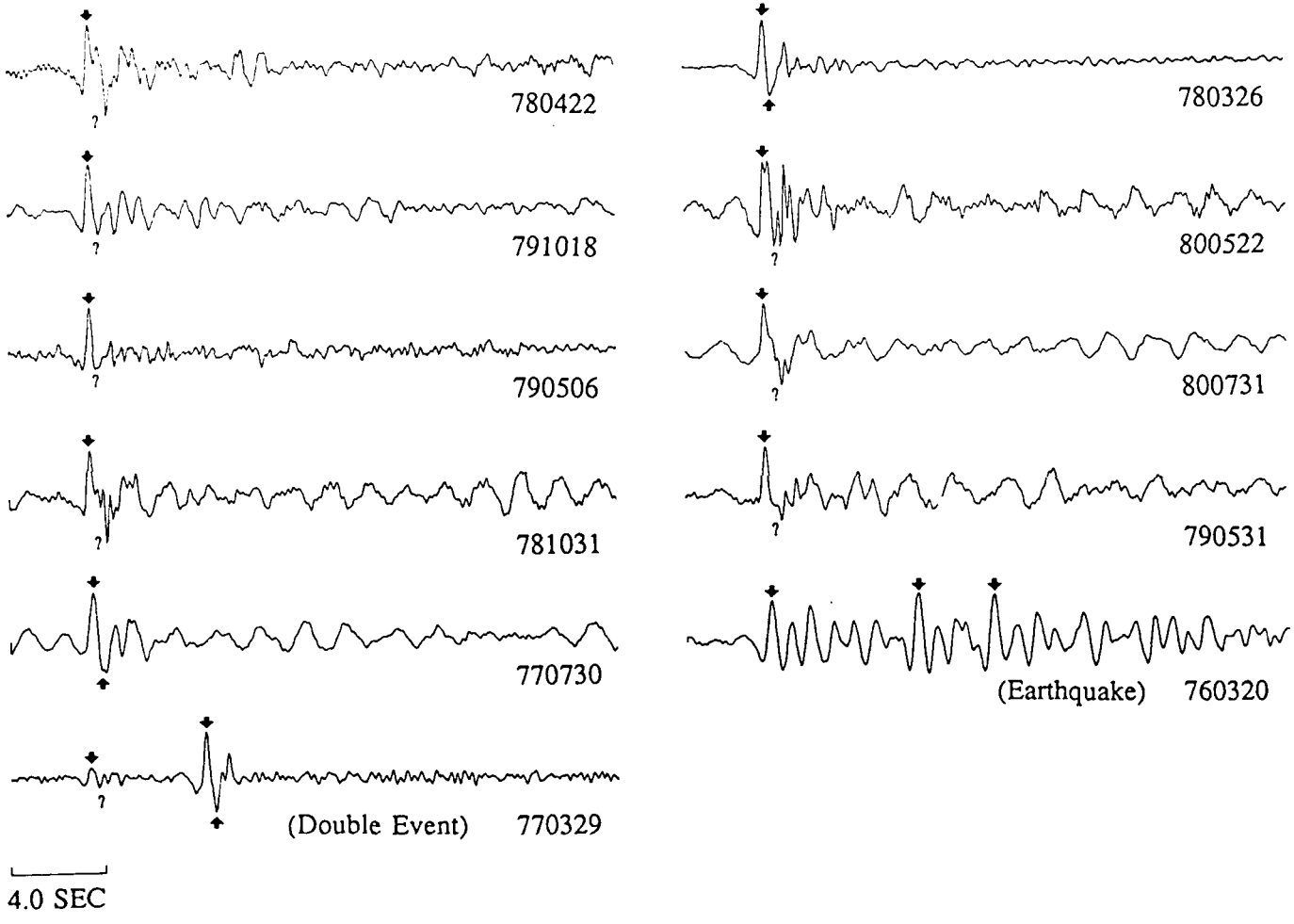

Figure 12. Deconvolved source functions for Degelen events at GBA. The estimated VSB wavelet has been removed in the deconvolutions. The P and pP, if present, arrivals are marked on each trace.

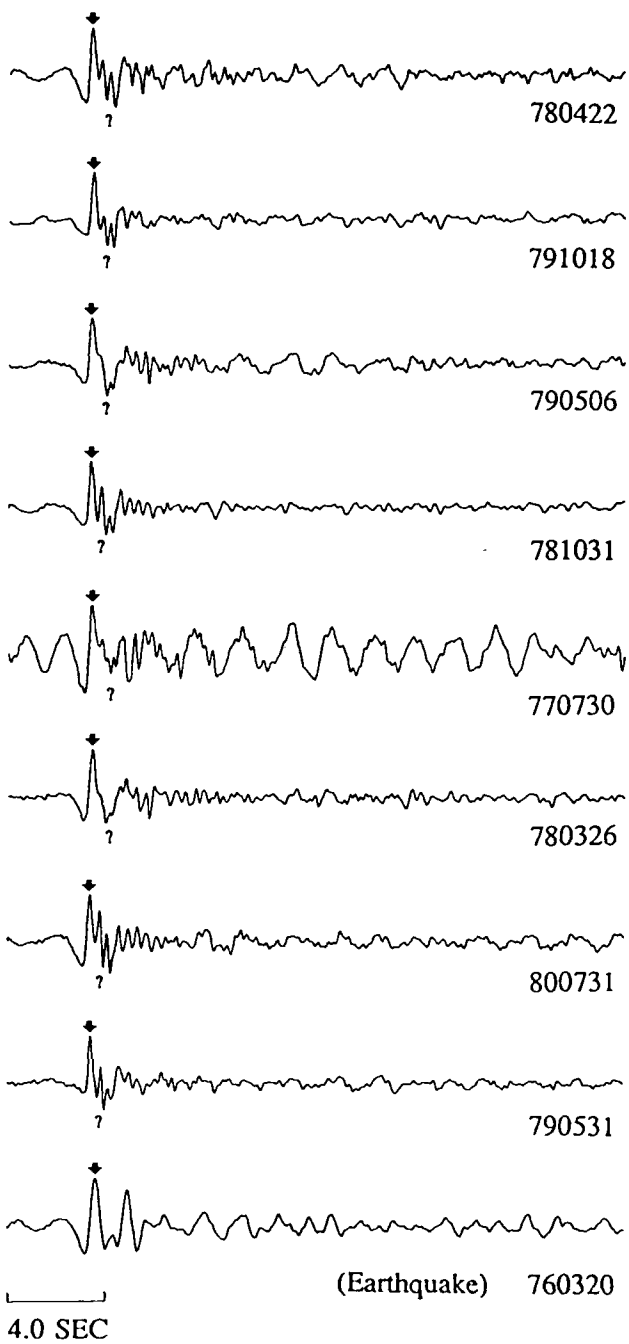

Figure 13. Deconvolved source functions for Degelen events at WRA. The estimated VSB wavelet has been removed in the deconvolutions. The P and pP, if present, arrivals are marked on each trace.

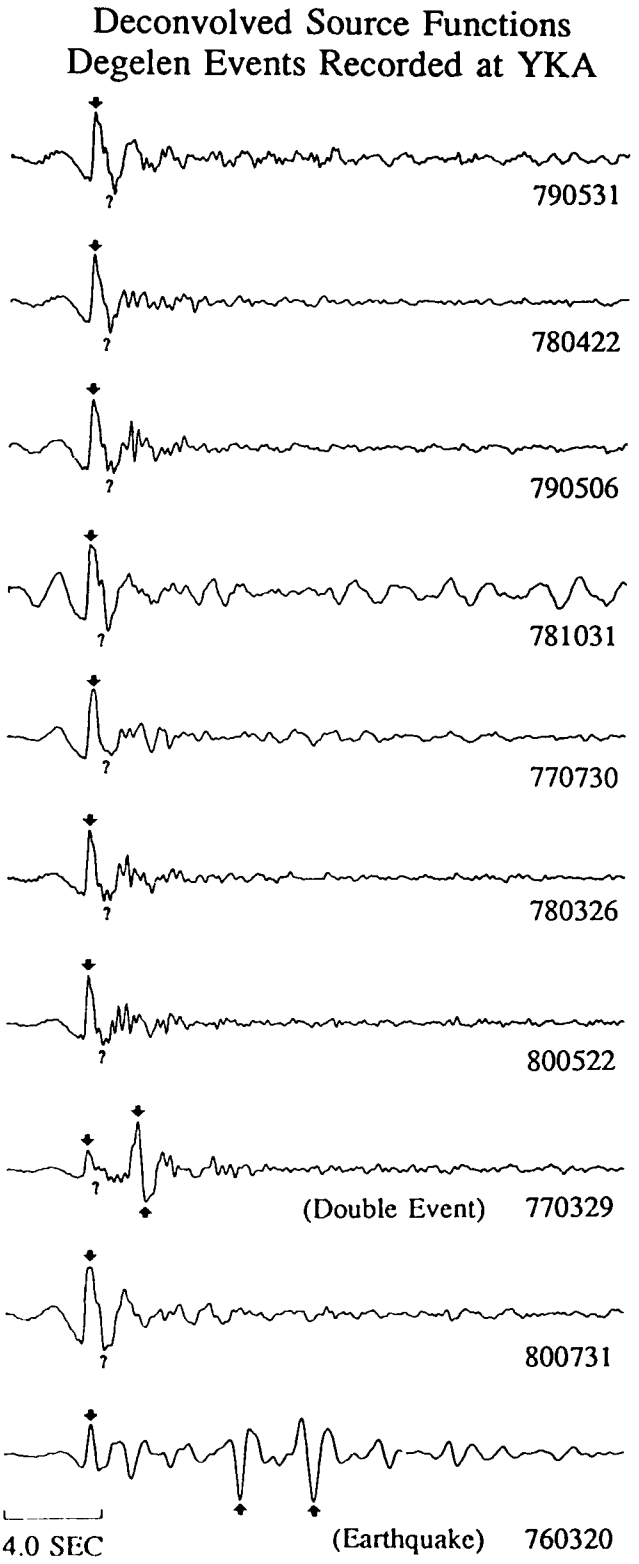

Figure 14. Deconvolved source functions for Degelen events at YKA. The estimated VSB wavelet has been removed in the deconvolutions. The P and pP, if present, arrivals are marked on each trace.

There are significant variations in the deconvolved source time functions across the Degelen test site as shown in Figures 15 to 18. The deconvolved source time functions, with the VSB removed, are plotted in their relative locations for deconvolutions at each of the AWRE arrays. In each figure there are cases where events near each other have very similar source time functions such as 781031 and 800731 at all 4 arrays. Often the waveforms can be matched for several seconds into the coda. Event 790531 is a little farther from 781031 and 800731 but is fairly similar to them, though not as similar as 781031 and 800731 are to each other. 790506 and 780326, two other events very close to each other have similar source time functions from recordings at YKA and WRA, but look quite different at GBA.

Another interesting feature is the differences in the deconvolved waveforms at the different arrays. In Figure 19 we show the results obtained for common events at the four AWRE arrays, this time without removing the VSB source pulse. The events are loosely arranged by the locations in Figure 10. For events recorded at a given array, there often appear to be more similarities between the source functions of events that were spacially close to each other, though we have not studied this in a quantitative manner.

The event of March 20, 1976 (760320) is an earthquake which occurred in the vicinity of Degelen (see, for example, Rodean 1979). Variations in pP and sP amplitude and polarity are clearly seen at the different azimuths for this event. Figures 20 and 21 show individual seismograms of the earthquake data as well as the deconvolved source time function at GBA and YKA, respectively. Especially at GBA, this is another good example of how the deconvolution process brings out the later arrivals in seismic records and makes it easier to determine the polarities.

Another interesting event (770329) has been identified as a double event (McLaughlin *et al.* 1986b) with time shifts appropriate to different distances relative to the various arrays.

Deconvolved Source Functions
Degelen Events Recorded at EKA

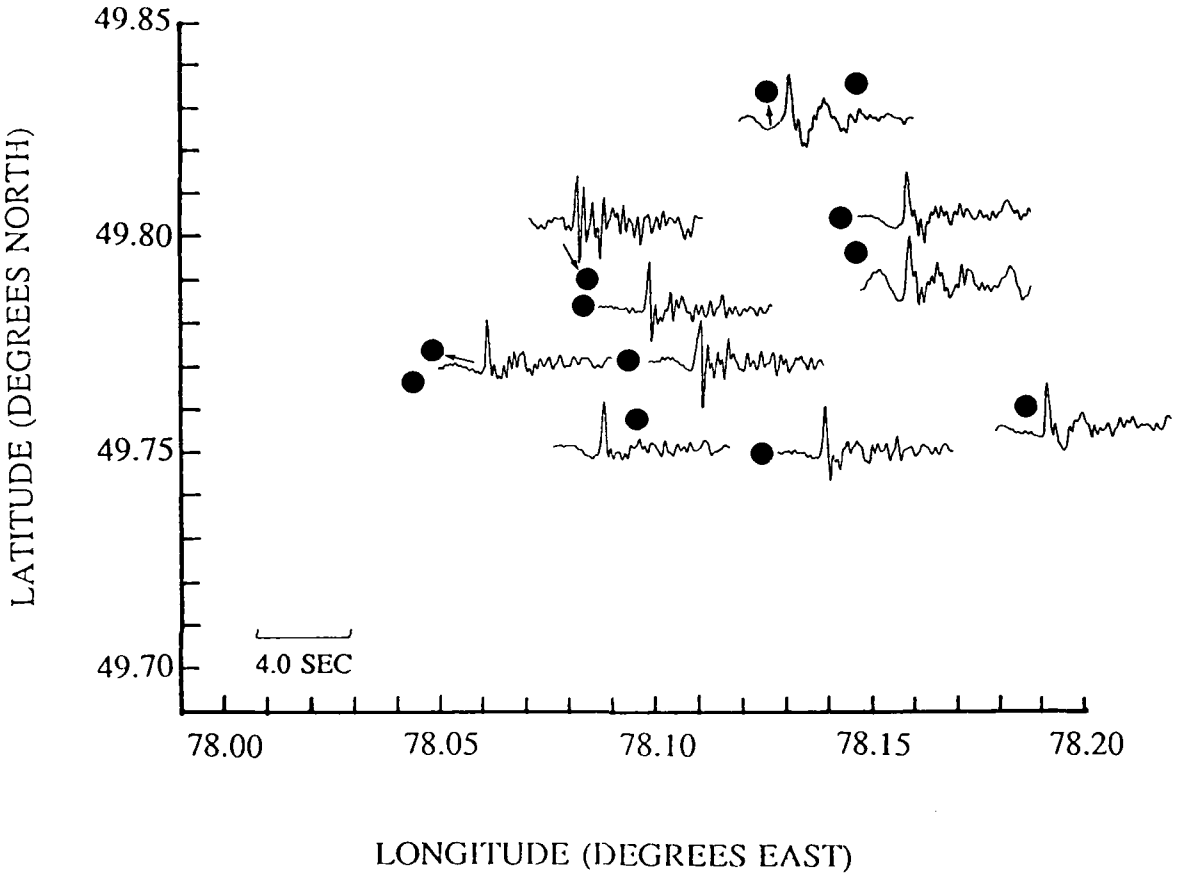

Figure 15. Deconvolved source functions for Degelen events recorded at EKA plotted on the map in Figure 10. The estimated VSB wavelet has been removed in the deconvolutions.

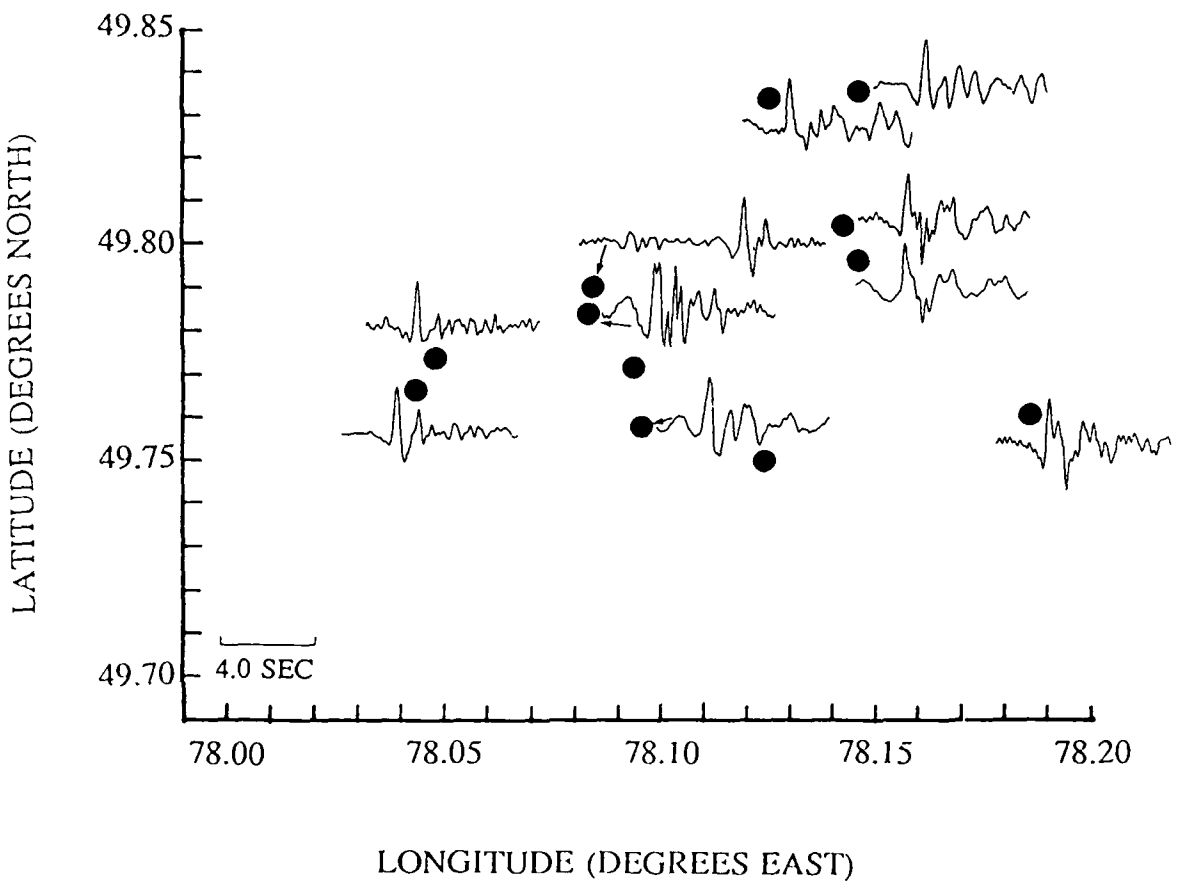

Figure 16. Deconvolved source functions for Degelen events recorded at GBA plotted on the map in Figure 10. The estimated VSB wavelet has been removed in the deconvolutions.

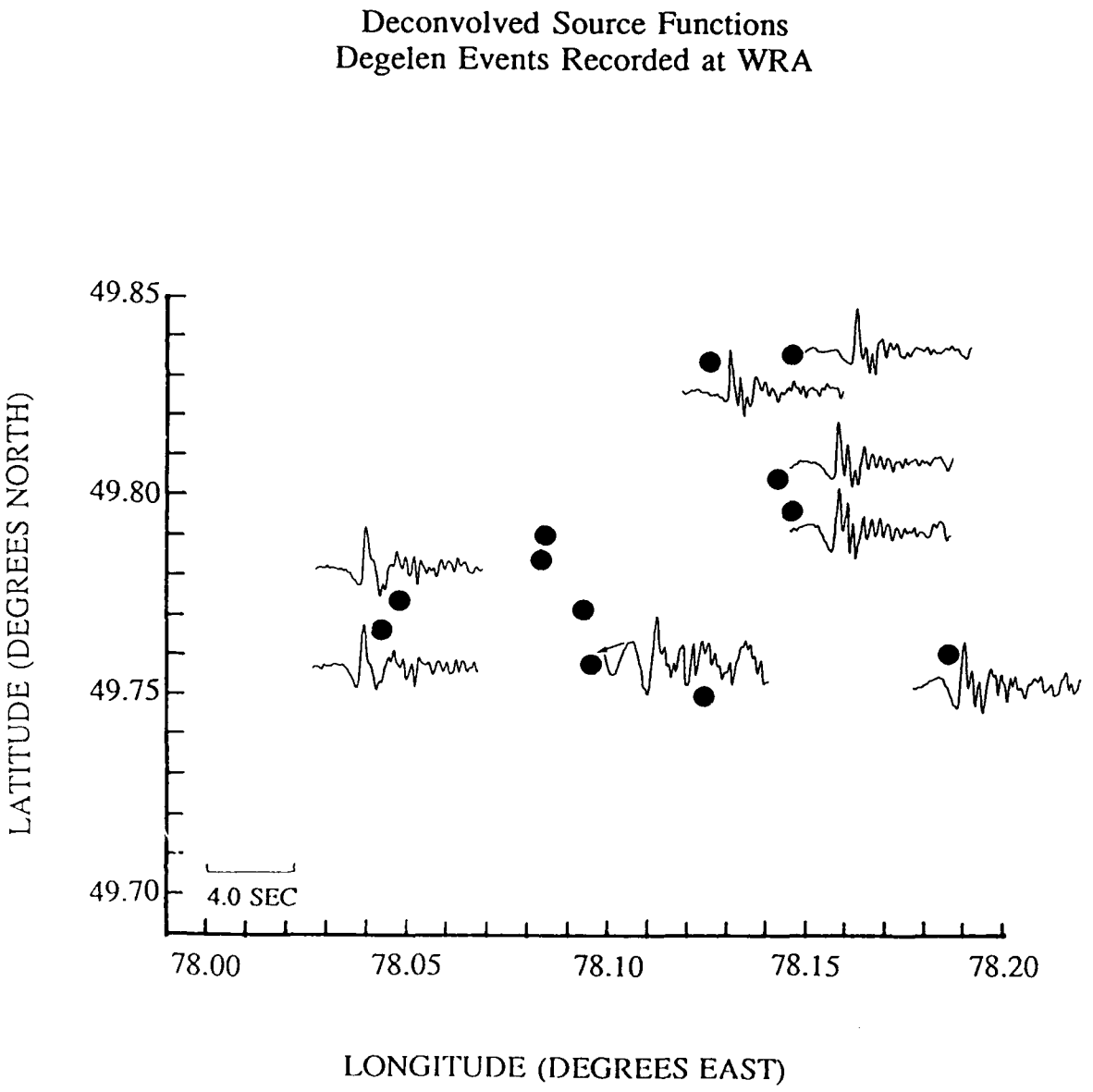

Figure 17. Deconvolved source functions for Degelen events recorded at WRA plotted on the map in Figure 10. The estimated VSB wavelet has been removed in the deconvolutions.

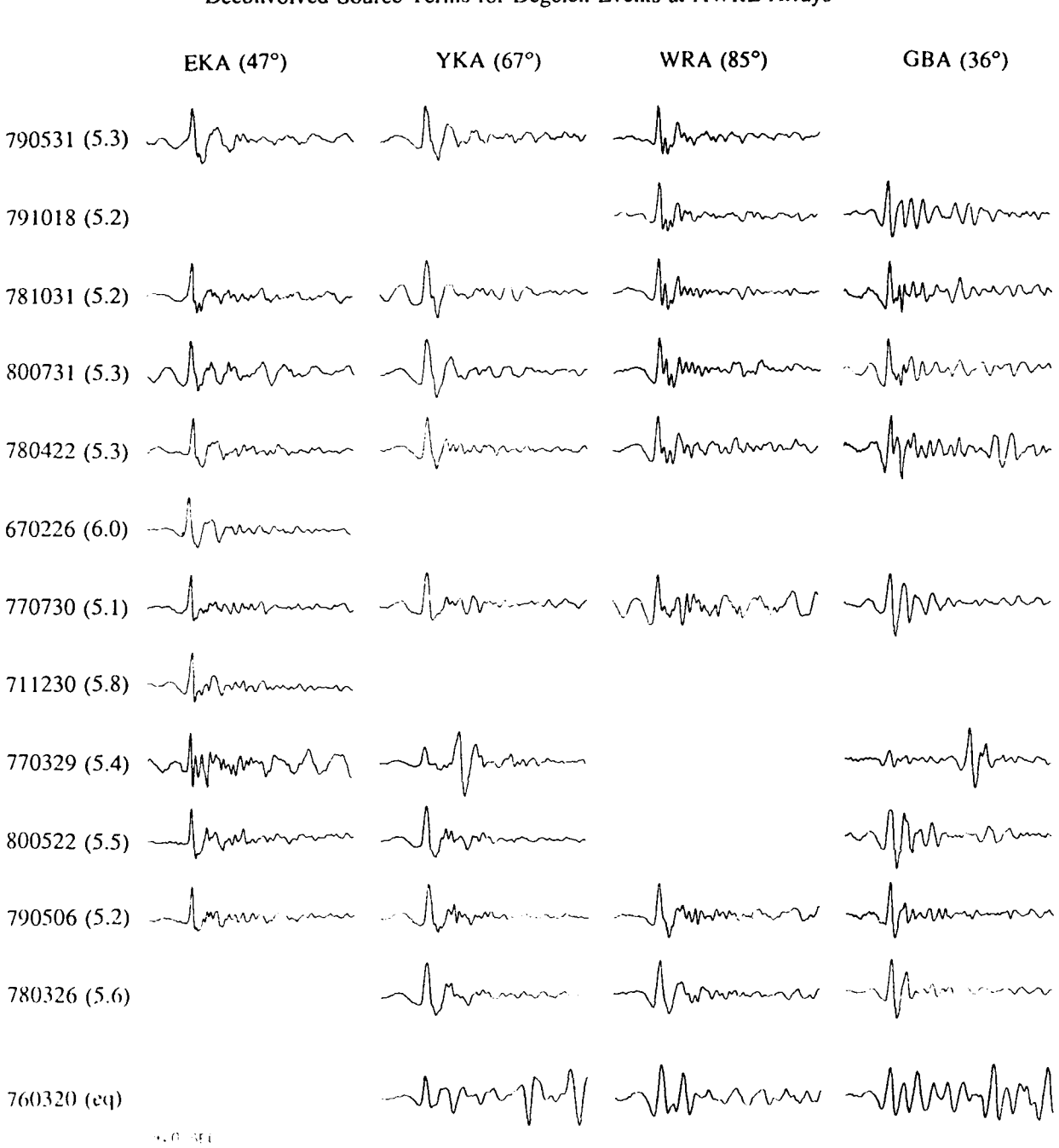

Figure 18. Deconvolved source functions for Degelen events recorded at YKA plotted on the map in Figure 10. The estimated VSB wavelet has been removed in the deconvolutions.

Deconvolved Source Functions
Degelen Events Recorded at YKA

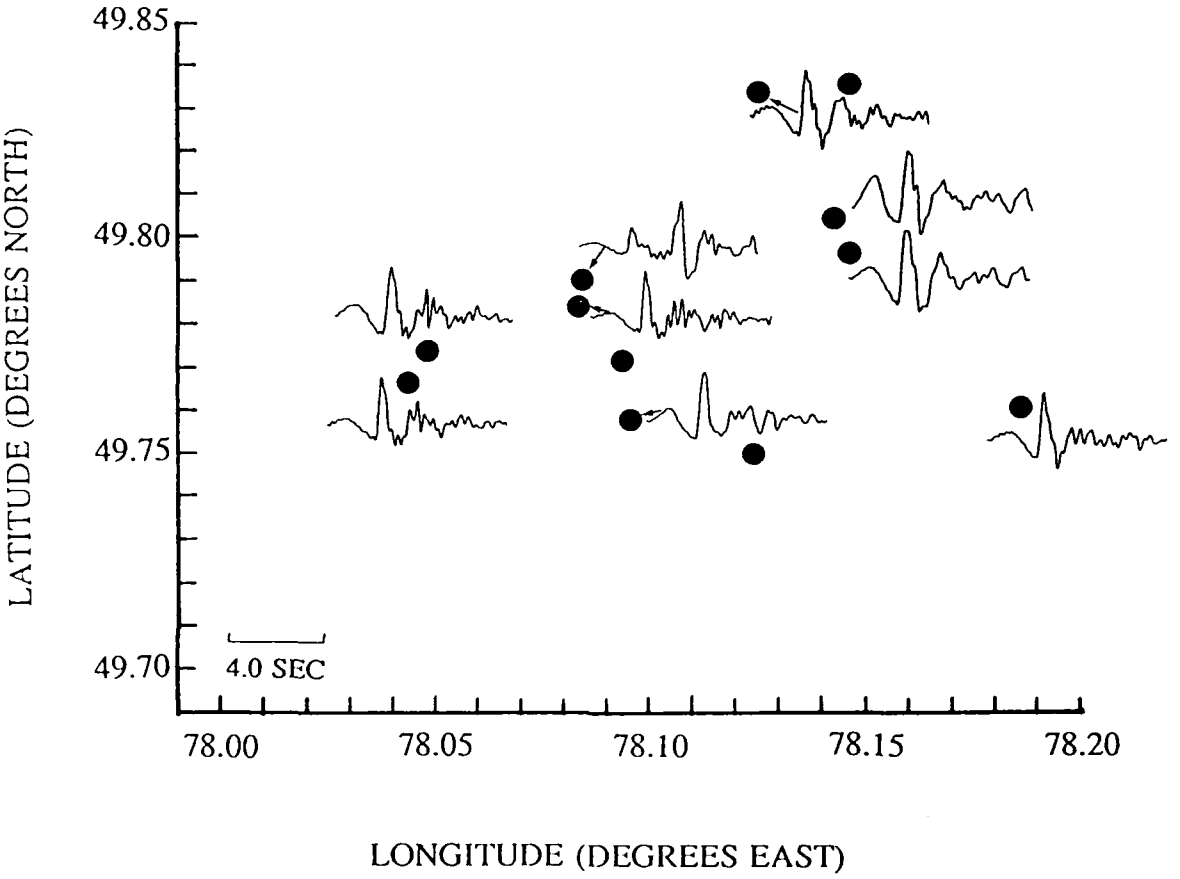

Figure 19. A set of source time functions for the Degelen test site and an earthquake (bottom) obtained at AWRE arrays. VSB wavelets have not been removed in these deconvolutions. Most of the traces do not show a clearly identifiable pP. The 770329 event consists of two nearly coincident events at two test sites (Degelen and Konystan) and shows variable time delays at the various arrays.

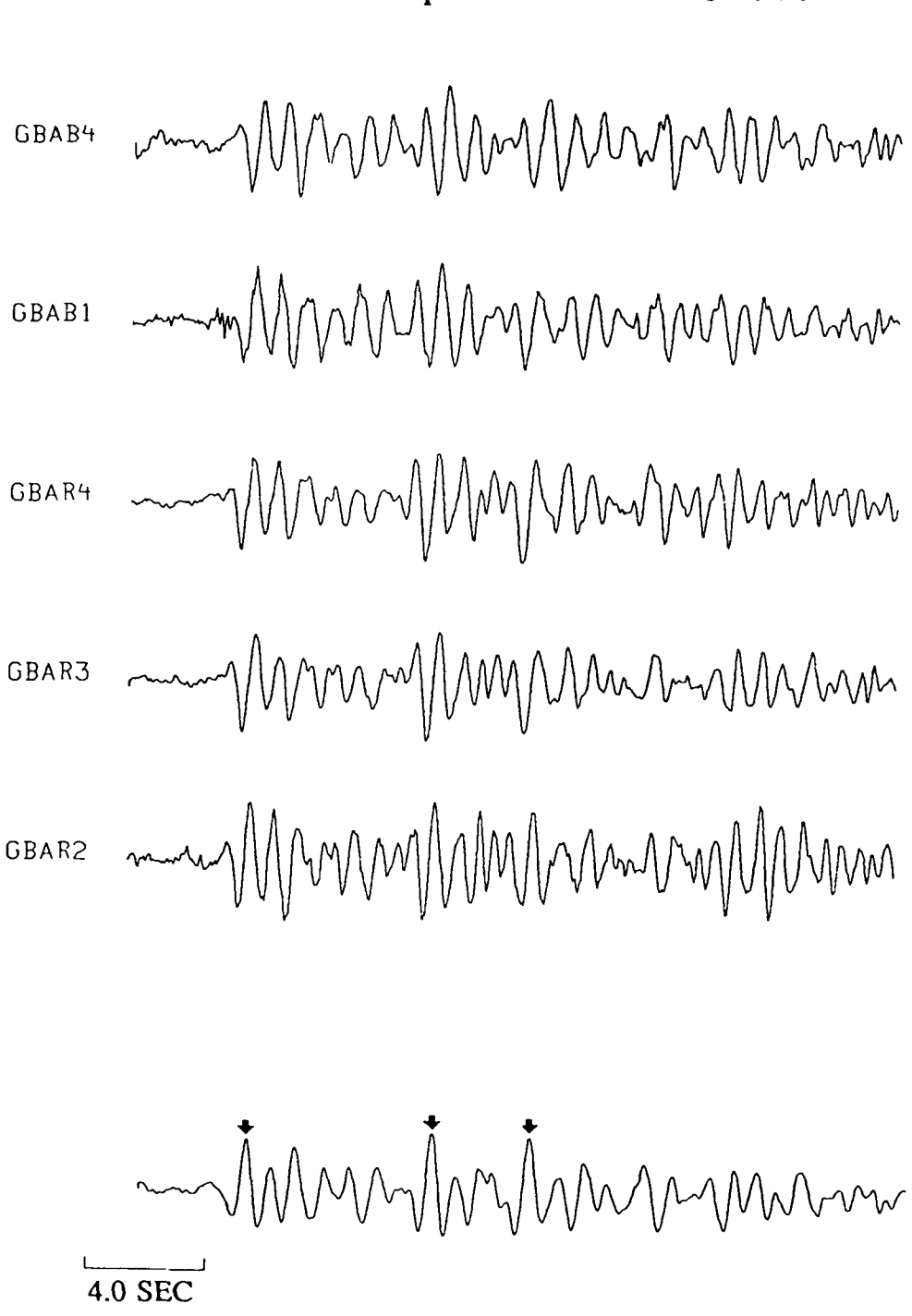

Figure 20. Original traces at GBA and the deconvolved source function for the Kazakh earthquake of March 20, 1976. Identification of pP and sP phases is simpler on the deconvolved source function than on the original traces, and it is easier to pick a polarity for all three phases on the deconvolved record.

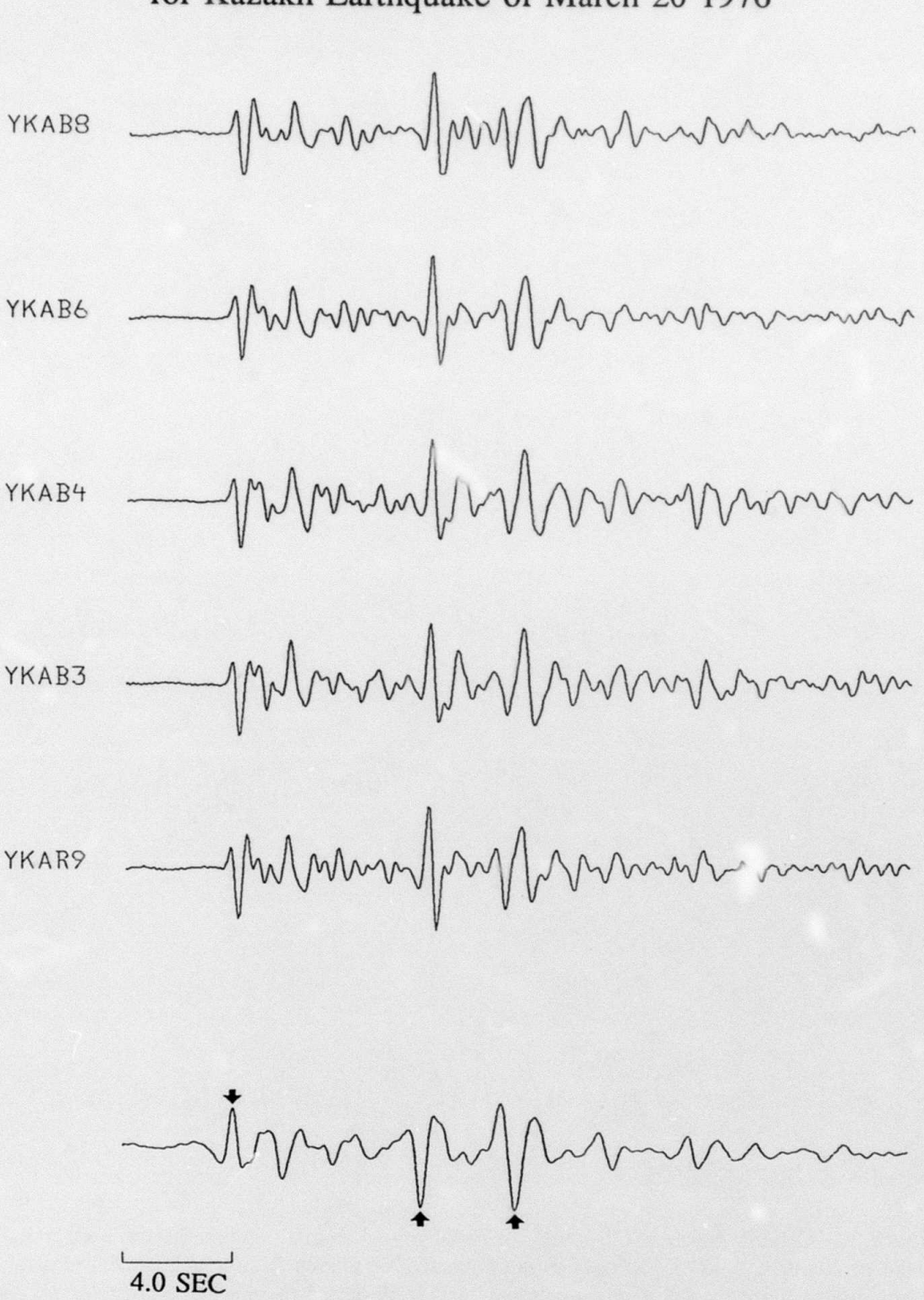

Figure 21. Original traces at YKA and the deconvolved source function for the Kazakh earthquake of March 20, 1976. It is easier to pick a polarity for all three phases on the deconvolved record than on the original traces.

For this event, note that the second event has a clear pP arrival, unlike most of the Degelen events. The second event is an explosion which occurred at the Konystan test site to the northwest of Degelen, which is a relatively flat and homogeneous geologic region.

With these events aside, there is still a large difference among the deconvolved waveforms at the different arrays, WRA and GBA show more of a high frequency coda than the other two arrays. (Some of the complexity at WRA may be due to its distance of ~85° from Degelen. At this distance, the Jeffreys-Bullen travel time curves predict that PcP will arrive ~3.8 sec after the P, and perhaps even sooner in this case since both the source and receiver regions are on shields which tend to have faster than average velocities.) There are two working hypotheses to explain this phenomenon. The first is that there are components in the site responses at each array (multiplicative factors in the frequency domain) that need to be removed in order to equalize the results. The other is that the time functions radiated by the various events are not the same in all directions, i.e. the source radiation is azimuthally asymmetric.

To decide which of these hypotheses is true, we have selected a set of events recorded at all four arrays and a set of sensors at each array and jointly deconvolved the data. Table 16 lists the events and sensors used in the joint deconvolution and Figure 22 shows the source functions from the joint deconvolutions as well as from deconvolution of the same set of events separately at each array. The source functions derived from the joint deconvolutions are much simpler than the source functions from the deconvolutions at the separate arrays. However, the source and site factors obtained from the joint deconvolution result in a noticeable degradation of the reconstructions of the original data indicating that the differences cannot be attributed to those in the site functions. This is shown in Figure 23 where reconstructions using the source and site factors from the joint deconvolution give correlation coefficients of

Table 16

Events and Receivers used in Joint Deconvolution of Degelen Events at AWRE Arrays				
Events	Sensors Used at Each Array			
	EKA	GBA	WRA	YKA
770730	R1	R2	R1	R1
781031	R4	R4	R2	R5
790506	R5	B1	R5	R7
780422	R8	B2	R8	R9
790531	B1	B7	B1	B3
800731	B4	B9	B4	B8

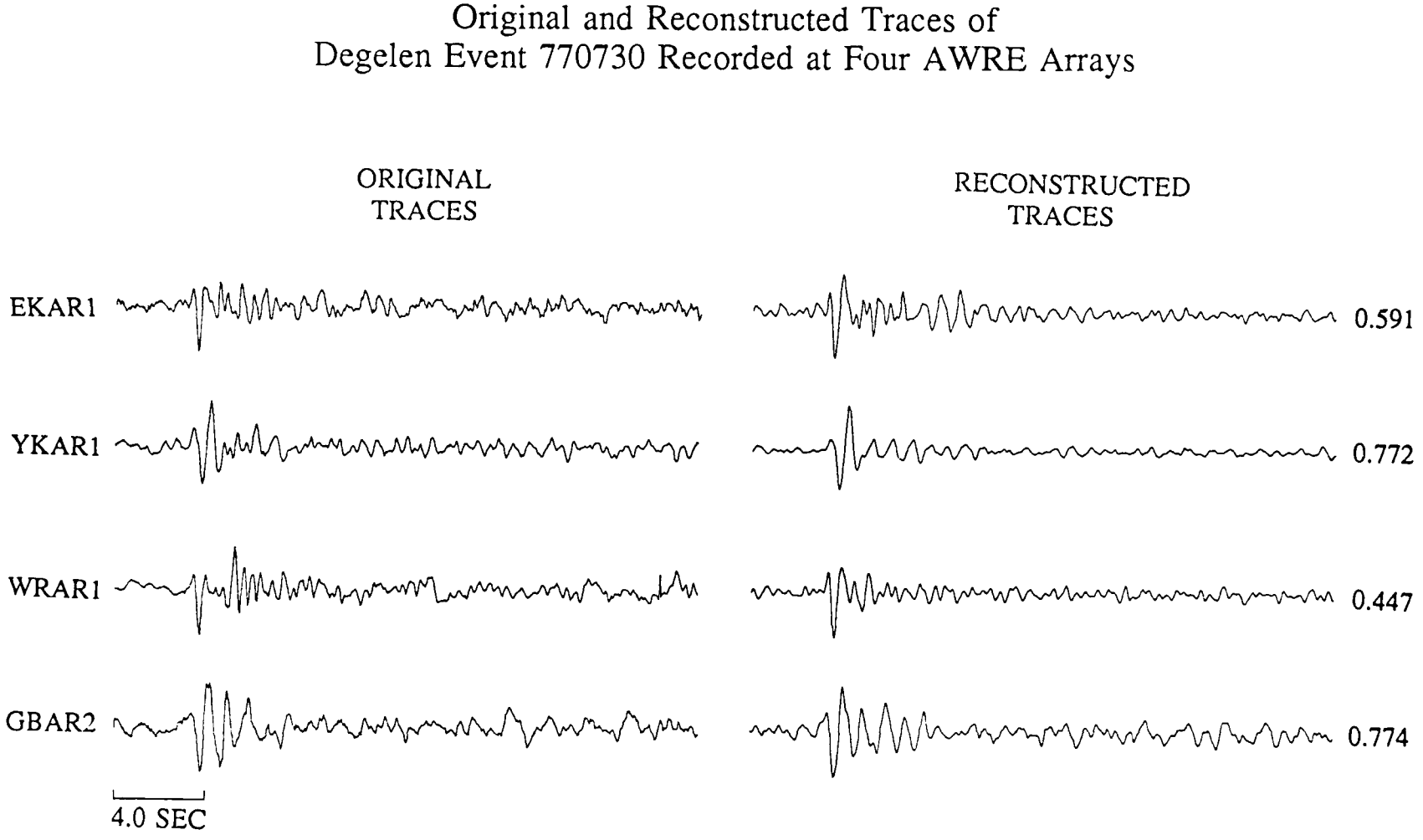

Figure 22. Comparison of source deconvolutions (VSB not removed) for a set of common events at each of the AWRE arrays and a joint deconvolution using six sensors at each array.

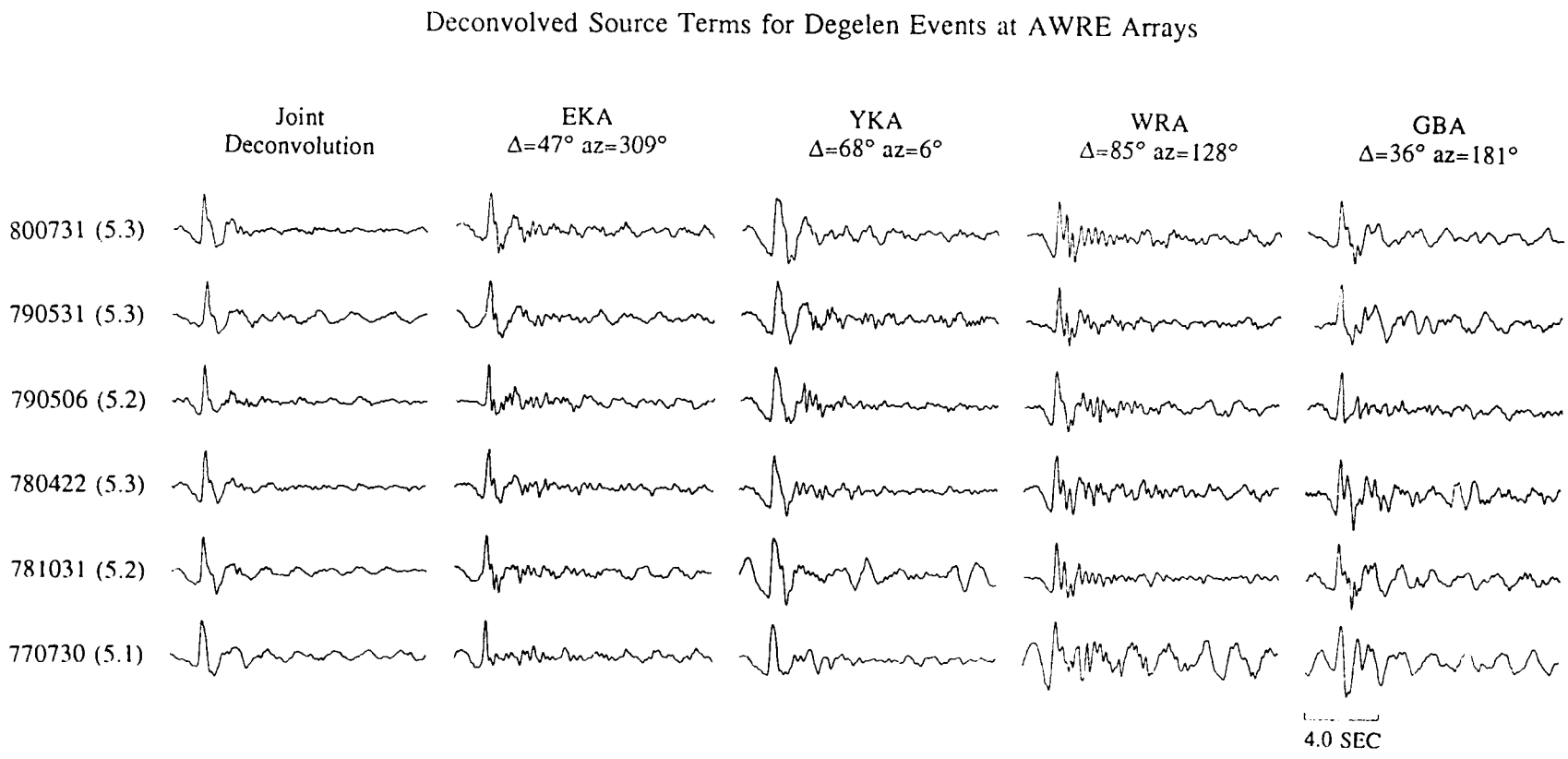

Figure 23. Comparison of some original traces and reconstructions obtained from the joint deconvolution of common events at the four AWRE arrays. The poor quality of reconstructions (unlike those at individual arrays) indicates a considerable asymmetry in the source radiation from Degelen.

only 0.4 to 0.8 when compared with the original traces while reconstructions using source and site factors from deconvolution of the same events at a single array give correlation coefficients of greater that 0.9. This leads to the conclusion that for the Degelen events, the differences of the deconvolution results at the various arrays must be attributed to azimuthal asymmetries in the source radiation of the individual events and the wide range of take-off angles for all ray-paths contributing to various degrees of triplication effects.

Shagan

Various subsets of the Shagan explosion data were deconvolved at EKA, GBA, WRA, and YKA. Marshall *et al.* (1984) classified the waveforms from Shagan events into types 1 (simpler) and 2 (more complex), the origin locations of which are shown on the map in Figure 24. Figure 25 is a map of the locations of the Shagan events deconvolved in this study, and Figures 26 to 29 show the source functions from deconvolutions with the VSB source pulse *removed. Most events show strong secondary arrivals of negative* polarity which may be interpreted as pP following the initial P wave arrival. In this respect, the Shagan results are noticeably different from those obtained for the Degelen test site. One exception is the cratering explosion (event 650115) which does not have a clear pP arrival. This event was also shown to have a magnitude bias of approximately 0.15 magnitude units relative to other (Shagan) events used for comparison (Der *et al.* 1985b, 1987).

The waveform classification of Marshall *et al.* (1984) for Shagan events are shown accordingly as "1" or "2" to the right of each trace in Figures 26 to 29. Class "1" events show simpler P + pP waveforms than do Class "2" events, and the results of the deconvolutions are generally consistent with the classifications of Marshall *et al.*. This can also be seen in Figures 30 and 31 where the deconvolved source time wavelets from recordings at EKA, with and without removal of the VSB, respectively, have been plotted on a map of the Shagan test site.

Waveform Classification of Shagan Events

Marshall, Bache, and Lilwall (1984)

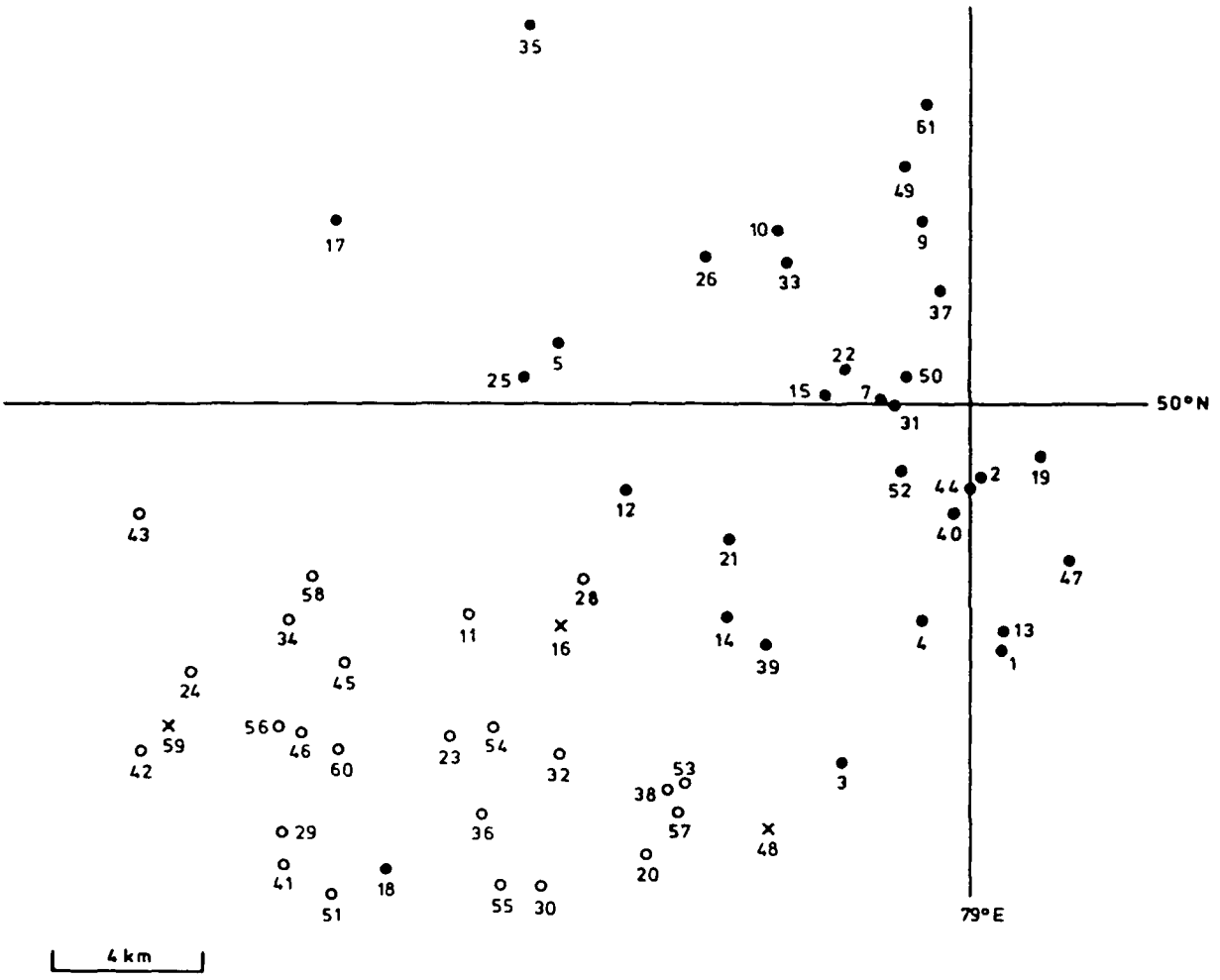

Figure 24. Location of Shagan events plotted with symbols representing explosion waveform classification. Open and solid circles represent class 1 and class 2 events, respectively, while an X represents an explosion of ambiguous classification. (from Marshall *et al.* 1984).

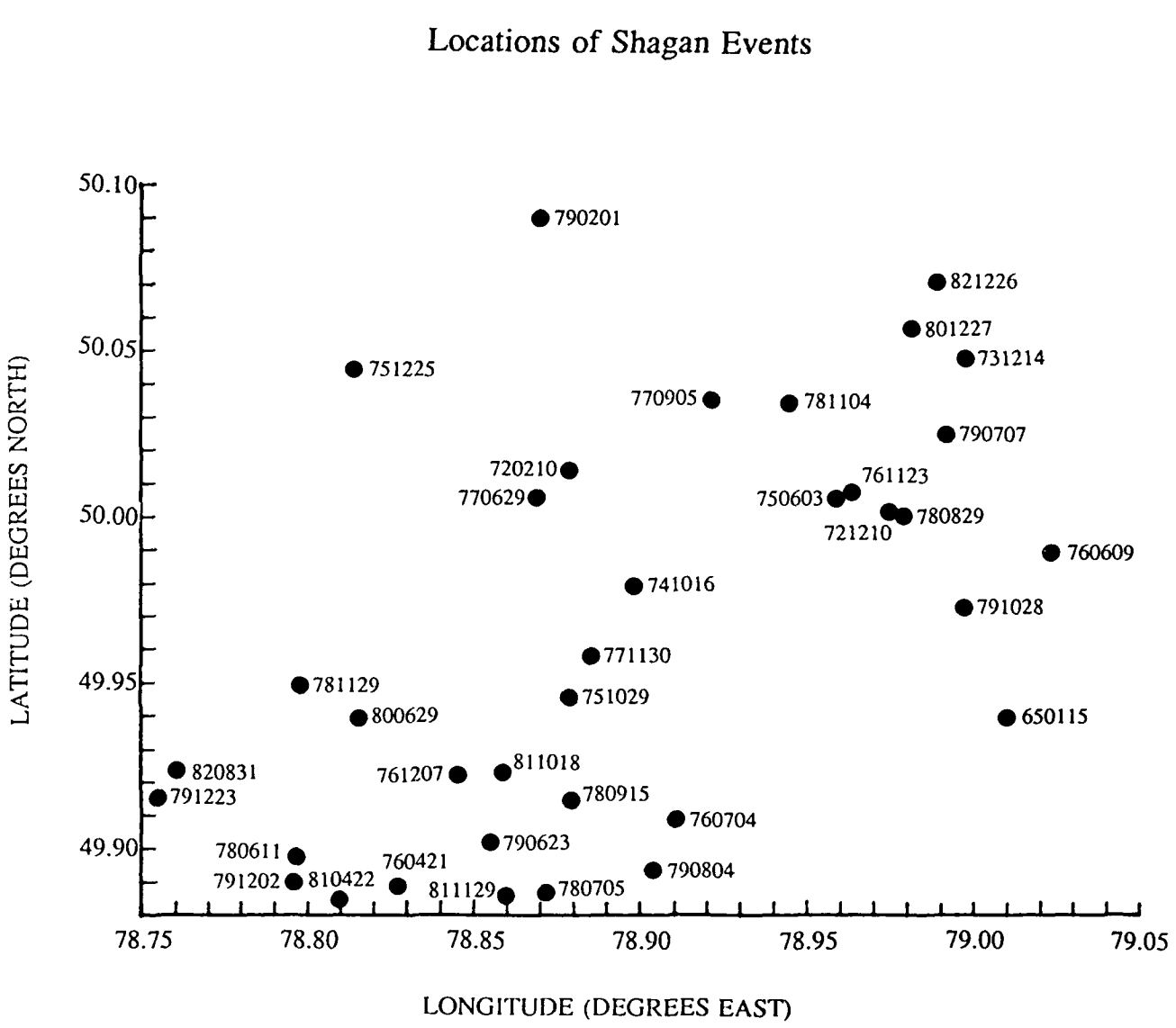

Figure 25. Locations (Marshall *et al.* 1984) of Shagan events analyzed during this study.

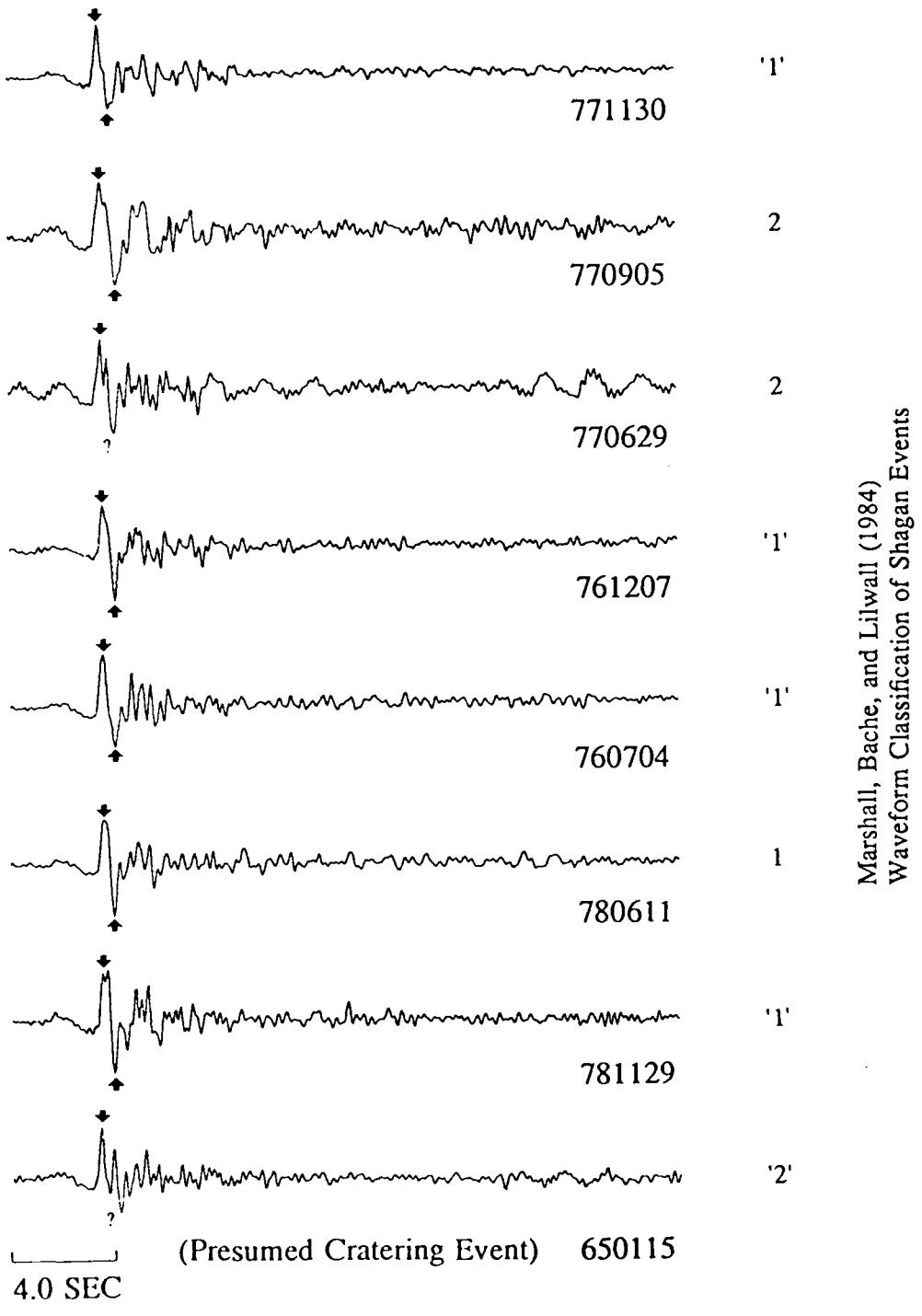

Figure 26. Source time function estimates obtained for Shagan explosions at EKA. A VSB wavelet has been removed in these deconvolutions. The waveform classification assigned by Marshall *et al.* (1984) is noted to the right of each trace. Note that the pP is missing for the cratering event (650115) and that the source function for this event is more complex than that for the buried explosions.

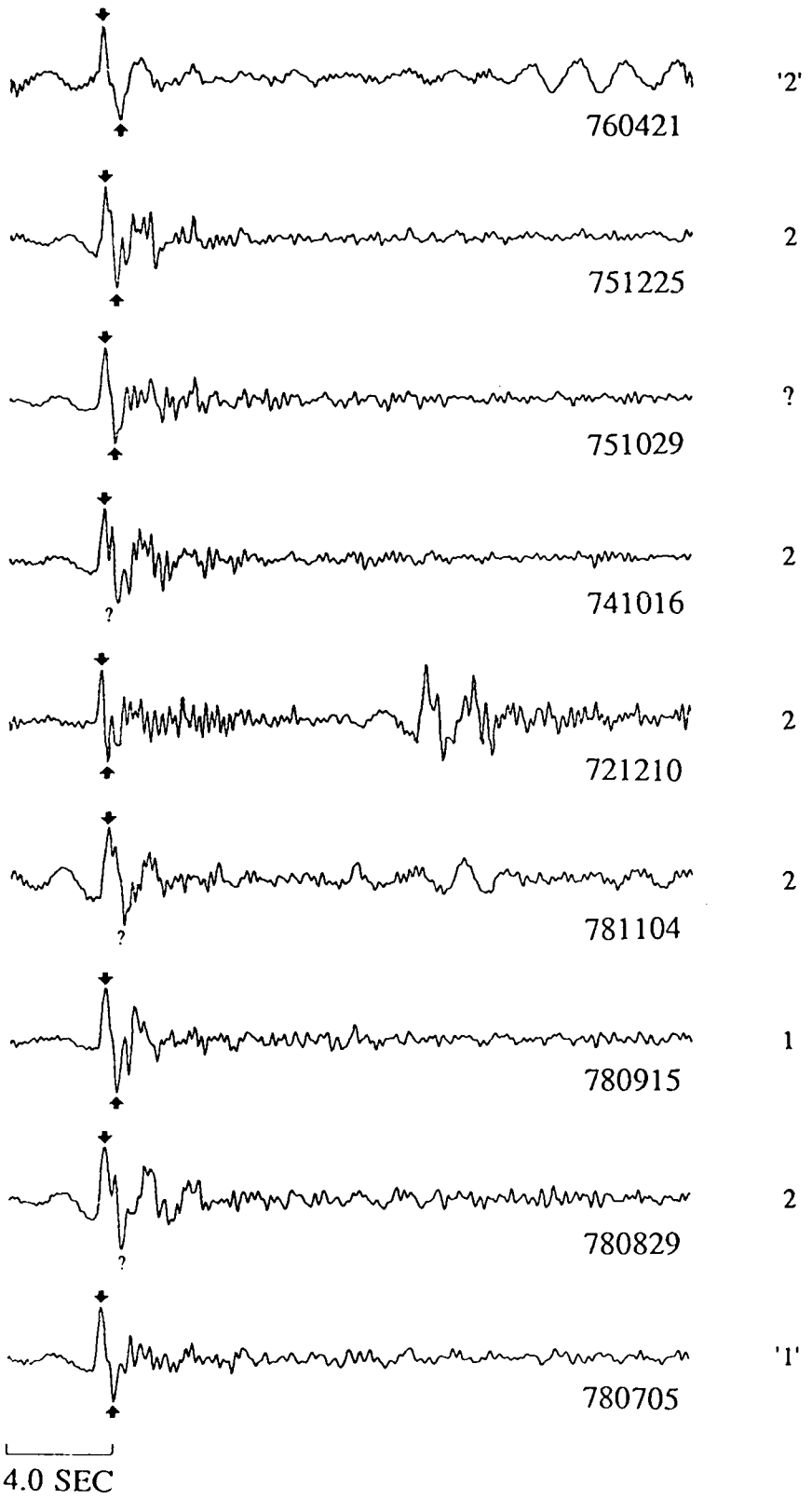

Marshall, Bache, and Lilwall (1984)
Waveform Classification of Shagan Events

Figure 26 (cont'd)

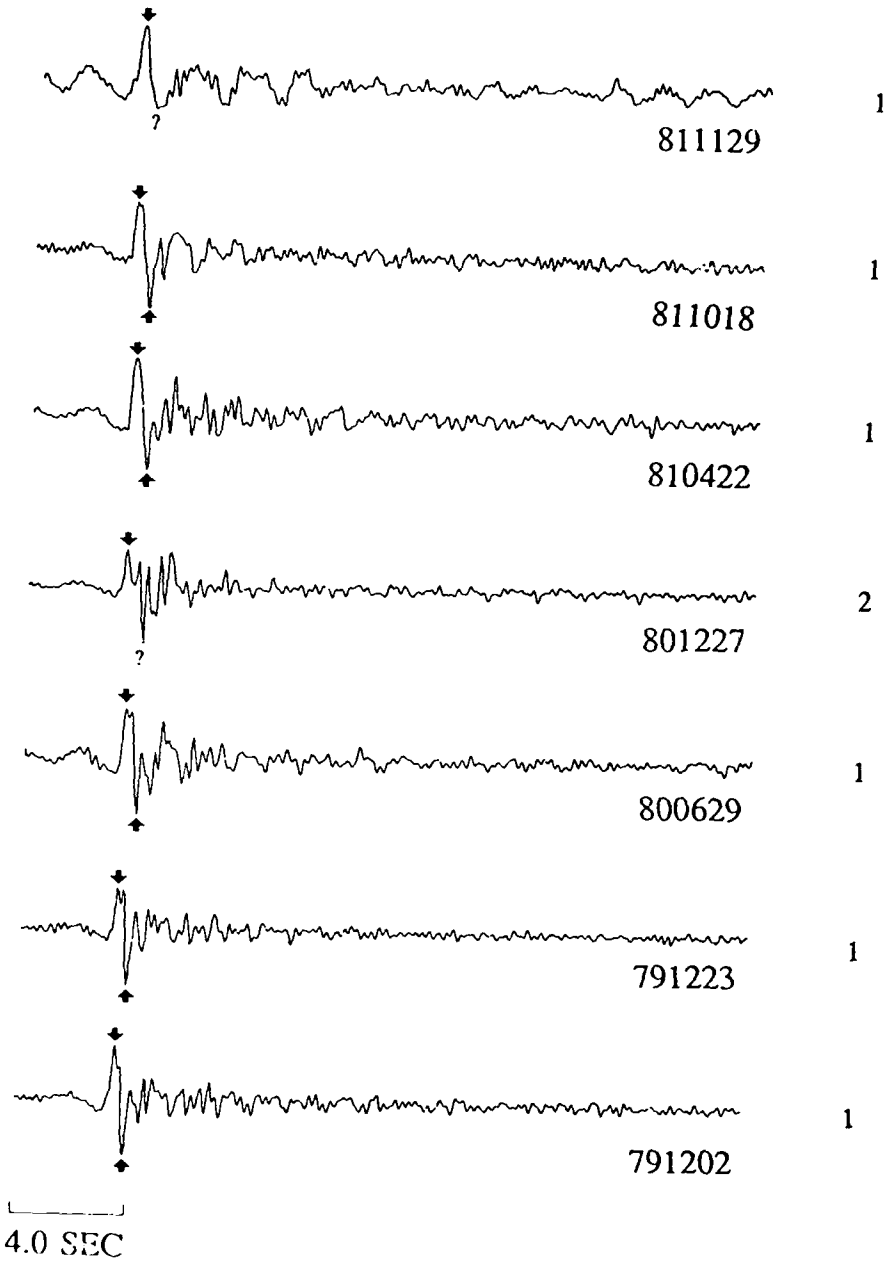

Marshall, Bache, and Lilwall (1984)
Waveform Classification of Shagan Events

Figure 26 (cont'd)

Deconvolved Source Functions
Shagan Events Recorded at EKA

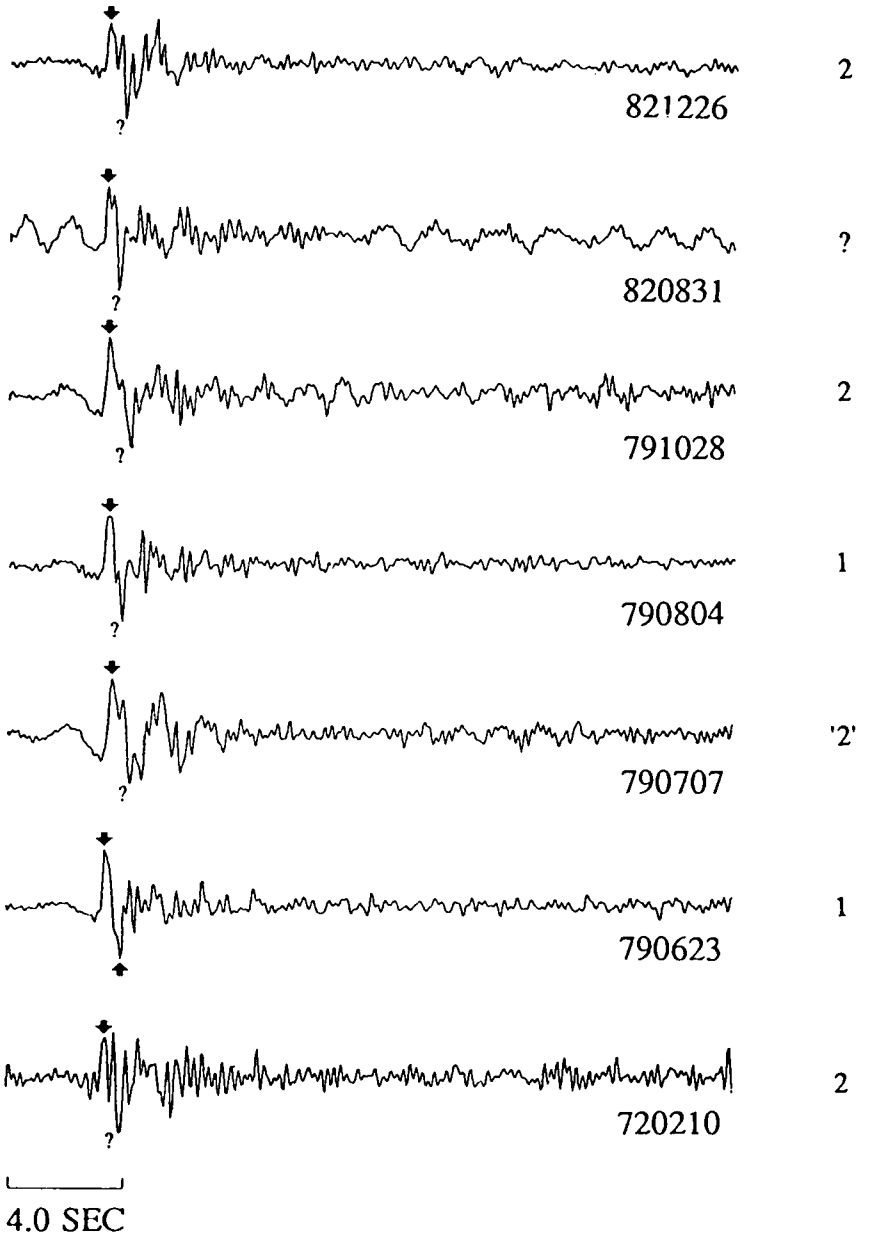

Marshall, Bache, and Lilwall (1984)
Waveform Classification of Shagan Events

Figure 26 (cont'd)

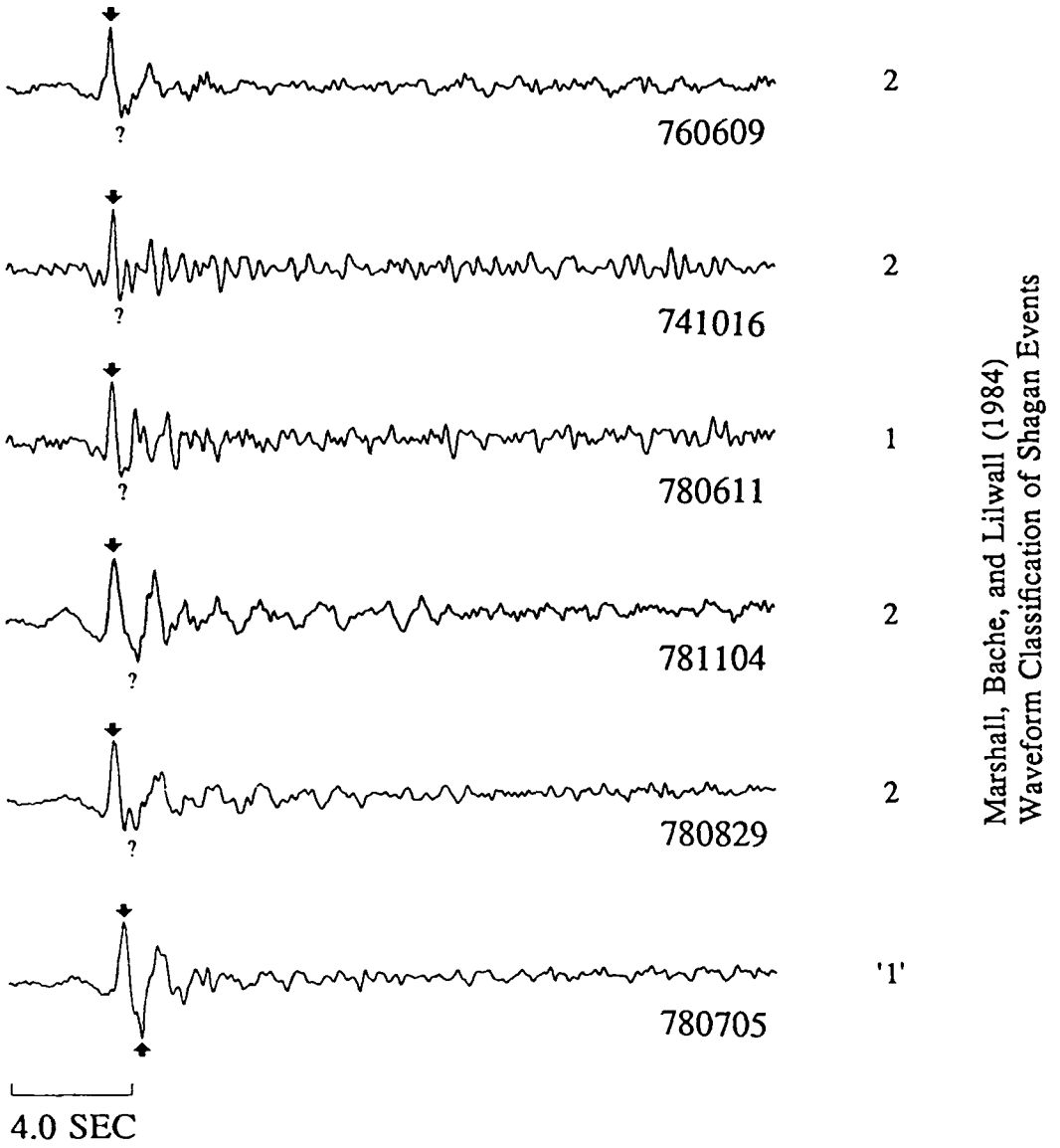

Figure 27. Source time function estimates obtained for Shagan explosions at GBA. A VSB wavelet has been removed in these deconvolutions. The waveform classification assigned by Marshall *et al.* (1984) is noted to the right of each trace.

Deconvolved Source Functions
Shagan Events Recorded at GBA

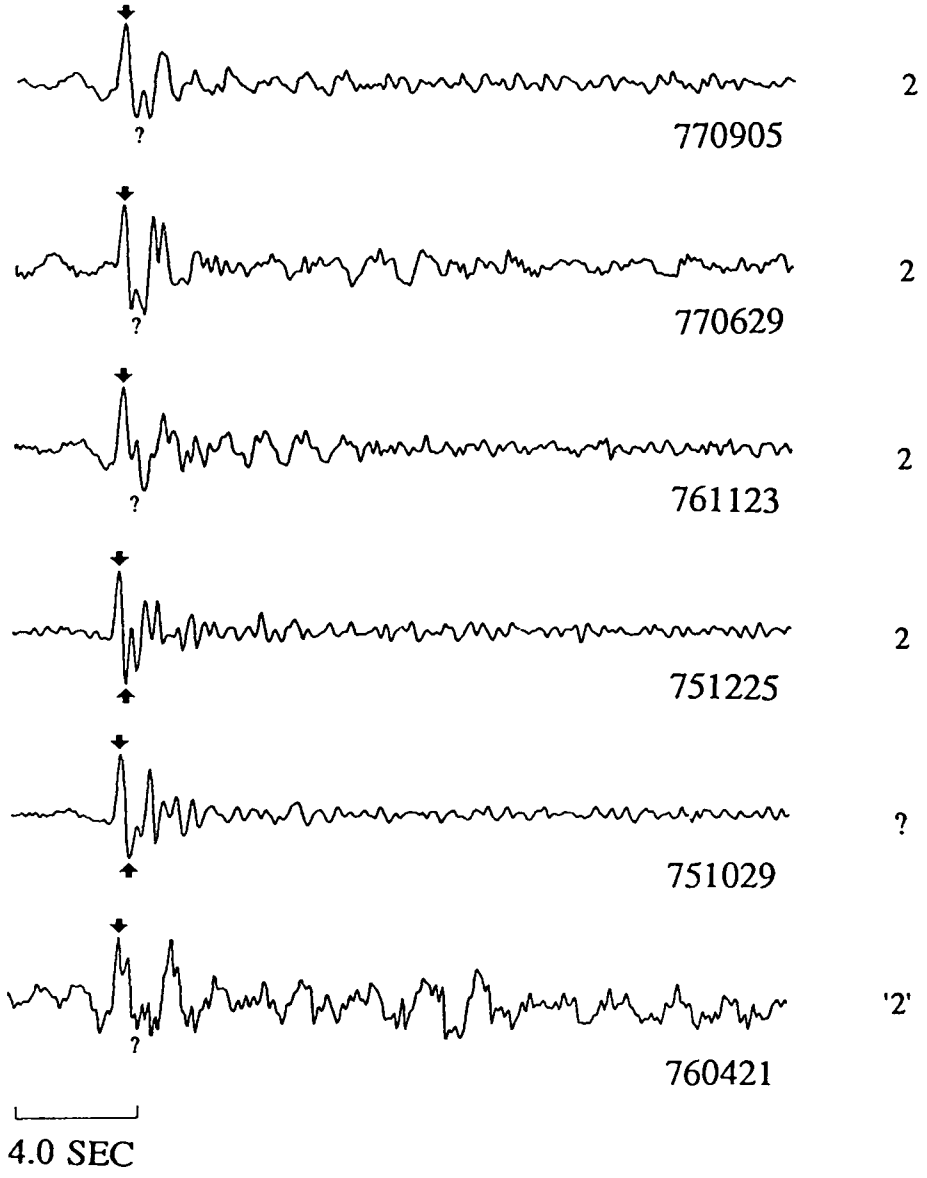

Marshall, Bache, and Lilwall (1984)
Waveform Classification of Shagan Events

Figure 27 (cont'd)

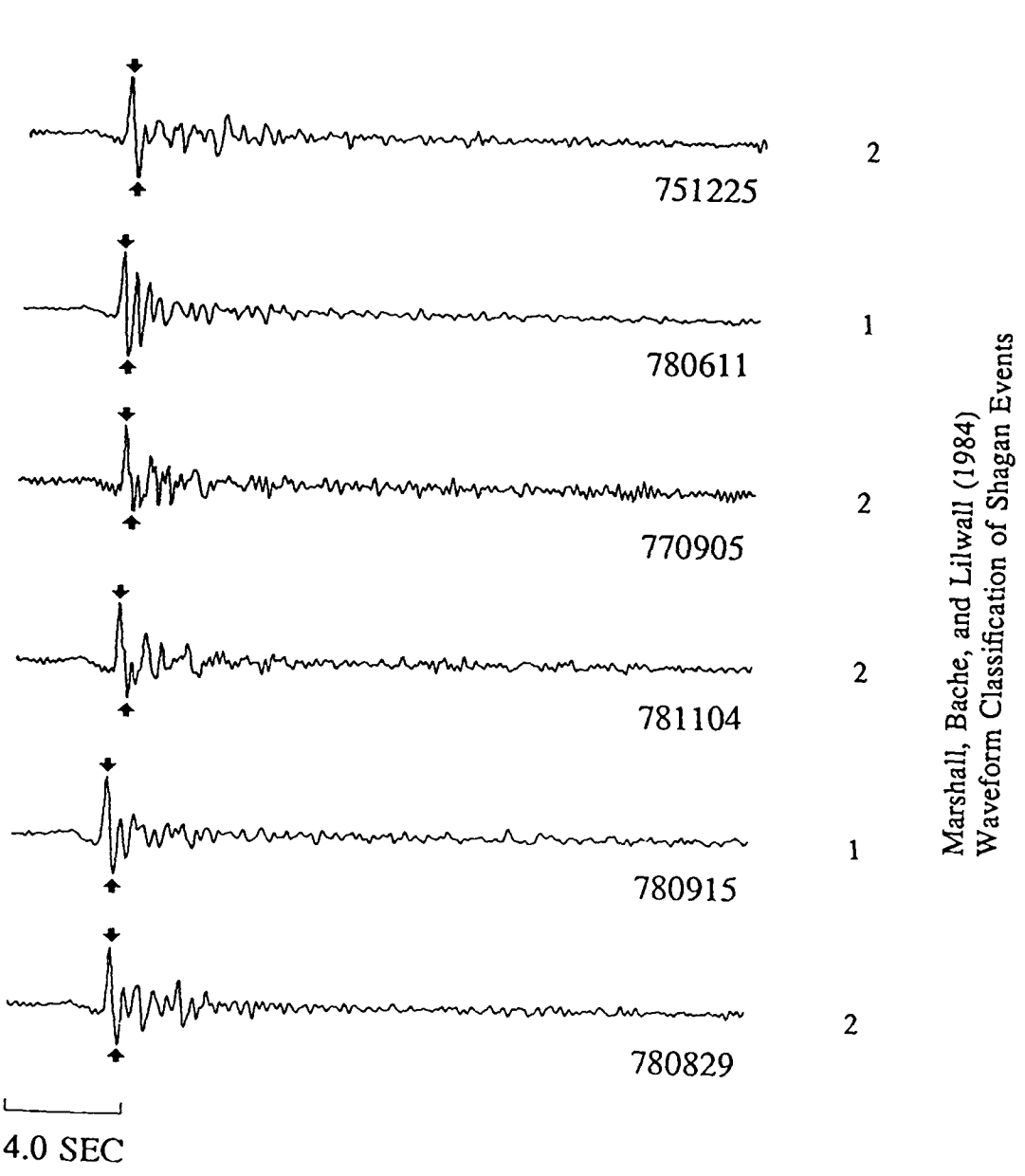

Figure 28. Source time function estimates obtained for Shagan explosions at WRA. A VSB wavelet has been removed in these deconvolutions. The waveform classification assigned by Marshall *et al.* (1984) is noted to the right of each trace.

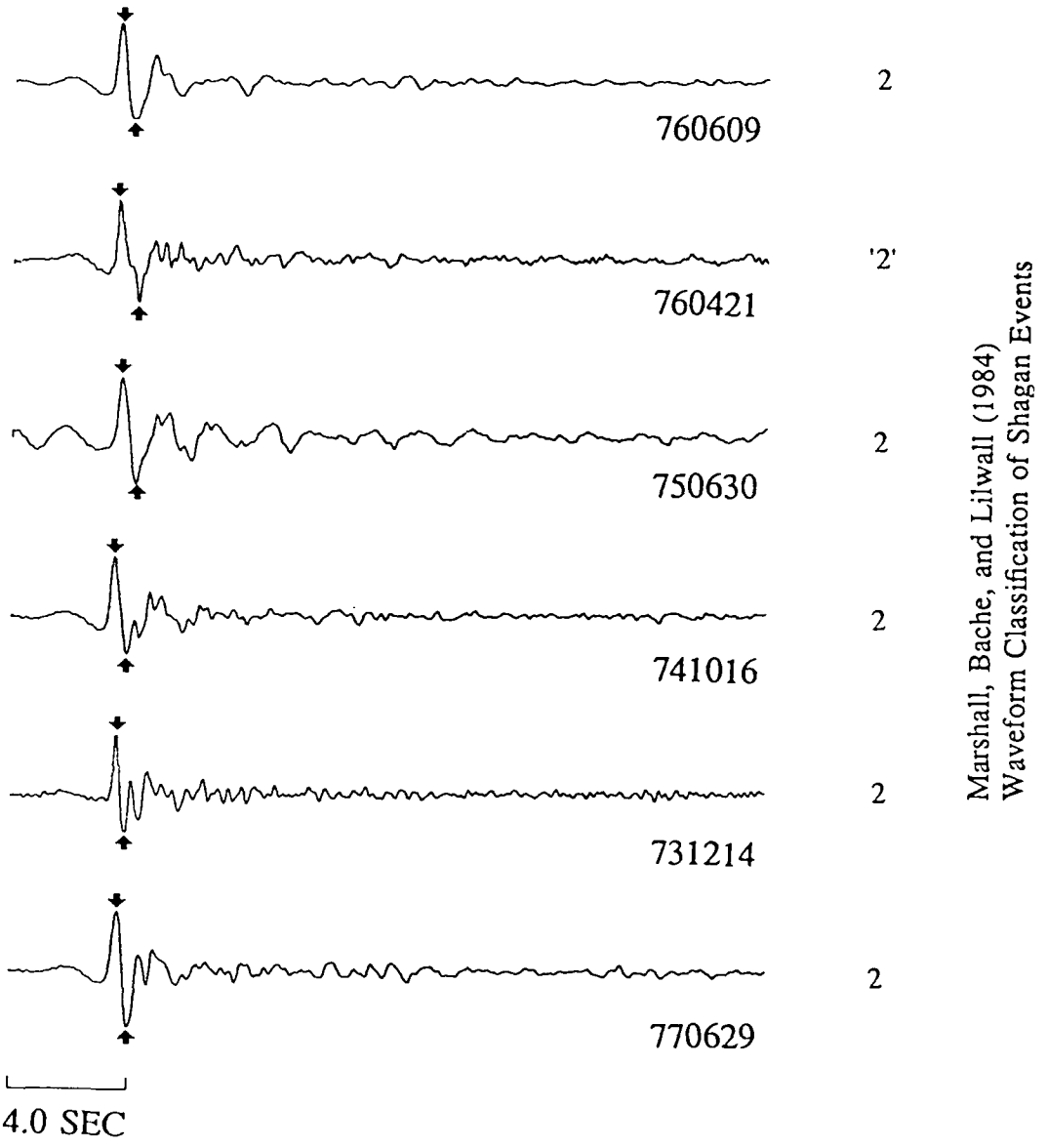

Figure 29. Source time function estimates obtained for Shagan explosions at YKA. A VSB wavelet has been removed in these deconvolutions. The waveform classification assigned by Marshall *et al.* (1984) is noted to the right of each trace.

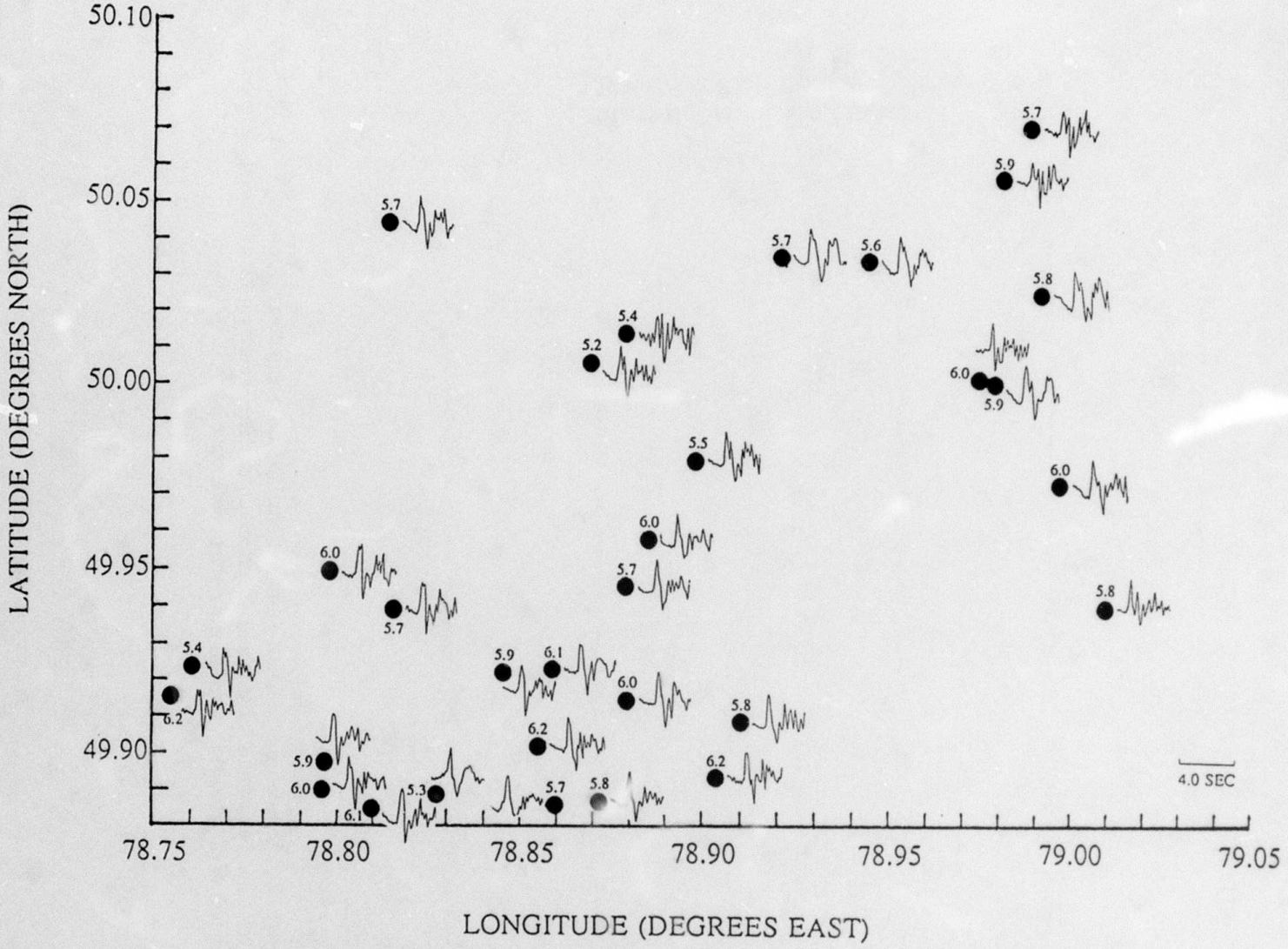

Figure 30. Deconvolved source time functions of Shagan events recorded at EKA plotted on the map in Figure 25. A VSB wavelet has been removed in these deconvolutions. The Marshall *et al.* (1984) m_b is noted next to each waveform.

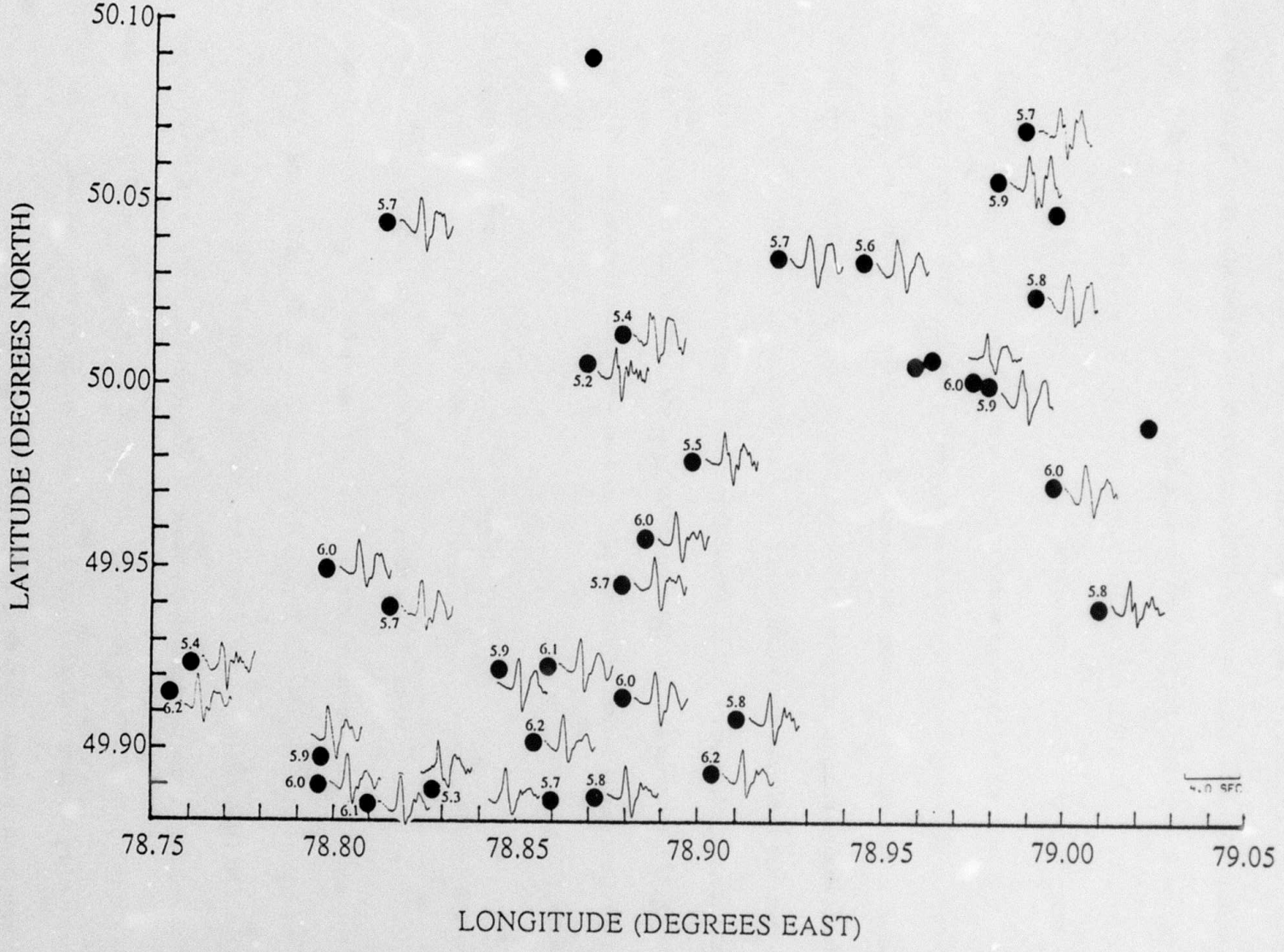

Figure 31. Deconvolved source time functions of Shagan events recorded at EKA plotted on the map in Figure 25. A VSB wavelet has *not* been removed in these deconvolutions.

Again, source functions from events in the northeastern portion of the test site are more complex than those from events in the southwestern portion of the test site. Here again, events very near to each other often have very similar source time functions. This is especially striking for 820831 and 791223 near the western edge of the test site since they have very different m_b magnitudes of 5.4 and 6.2, respectively.

One may ask the question whether the differences between the Degelen and Shagan source functions may be due to differences between the site responses for the two test sites. Based on past results the answer must be negative. The Shagan and Degelen test sites are not distant enough to cause appreciable differences in the site responses at common arrays, and it is even less likely that this would happen for three arrays at the same time. Moreover, we have been successful in the past in deconvolving a *mix* of Degelen and Shagan events recorded at NORSAR using the same site functions for both test sites, and the trace reconstructions were of excellent quality indicating that the site functions were practically the same (Der *et al.* 1985b, 1987).

Novaya Zemlya

The estimated locations of 23 northern Novaya Zemlya events, analyzed at EKA, GBA, YKA, and WRA, are shown in Figure 32. We have also studied 4 events from the southern Novaya Zemlya test site. Figures 33 to 35 show source time functions of P waves at the EKA, YKA, and GBA arrays with the VSB source pulse removed and Figure 36 is a composite of deconvolutions at the separate arrays, without the VSB removed. In Figure 36, the events are loosely arranged by location according to the map in Figure 32. Event 801011 has been identified by Marshall *et al.* (1986) as a double event and in our deconvolutions this can best be seen on the source function for 801011 as deconvolved at EKA.

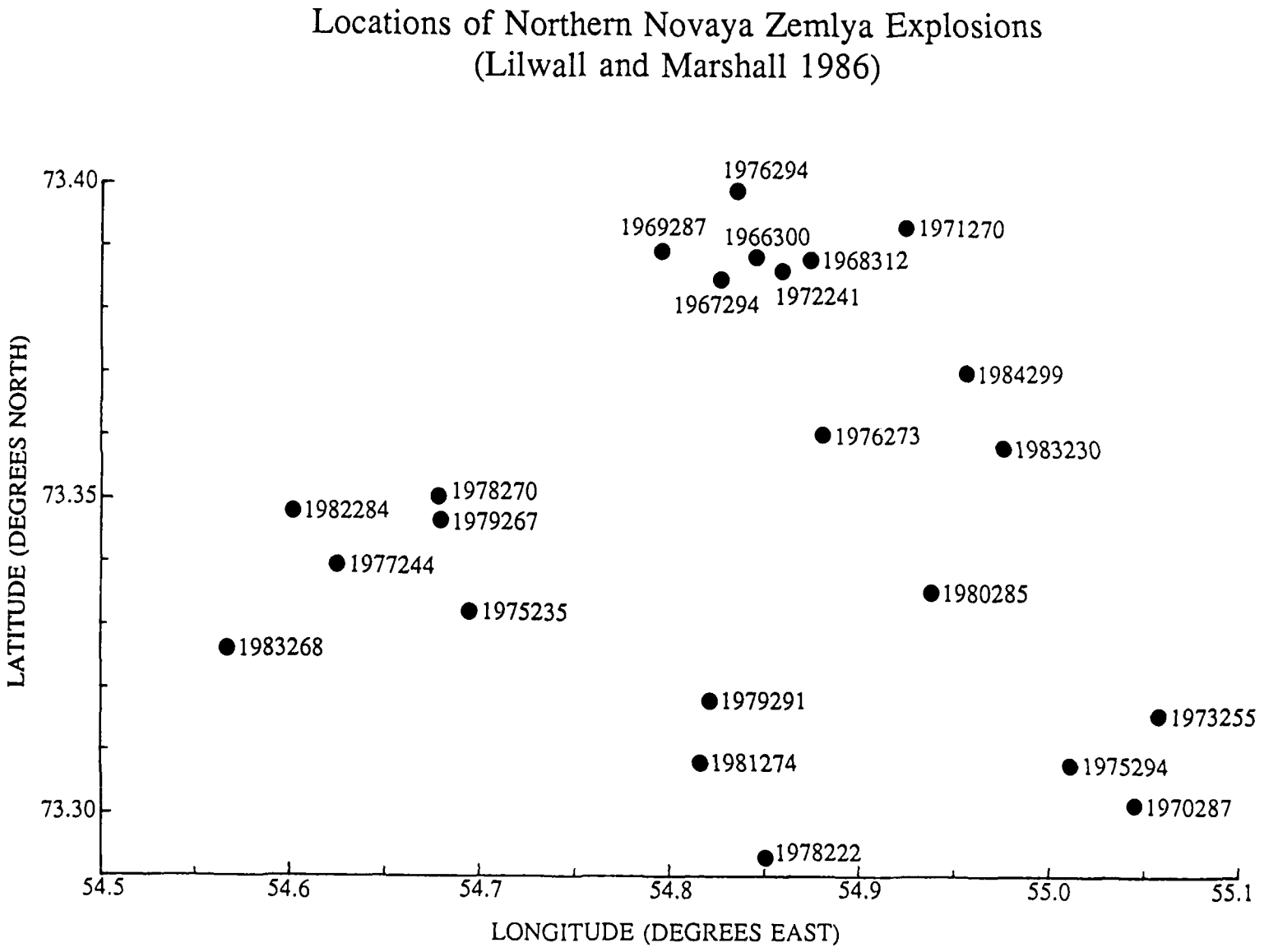

Figure 32. Locations (Lilwall and Marshall 1986) of northern Novaya Zemlya events analyzed in this report.

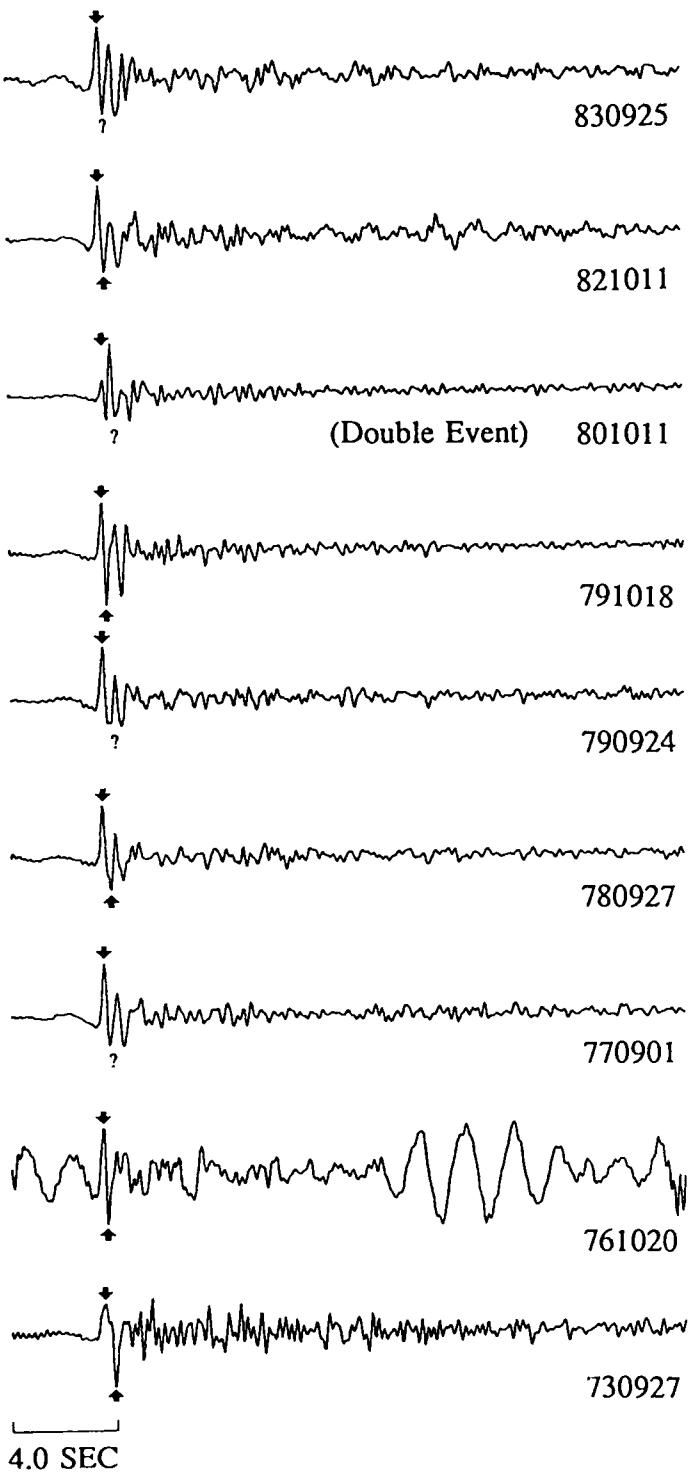

Figure 33. Source time function estimates obtained for Novaya Zemlya events at EKA. A VSB wavelet has been removed in these deconvolutions.

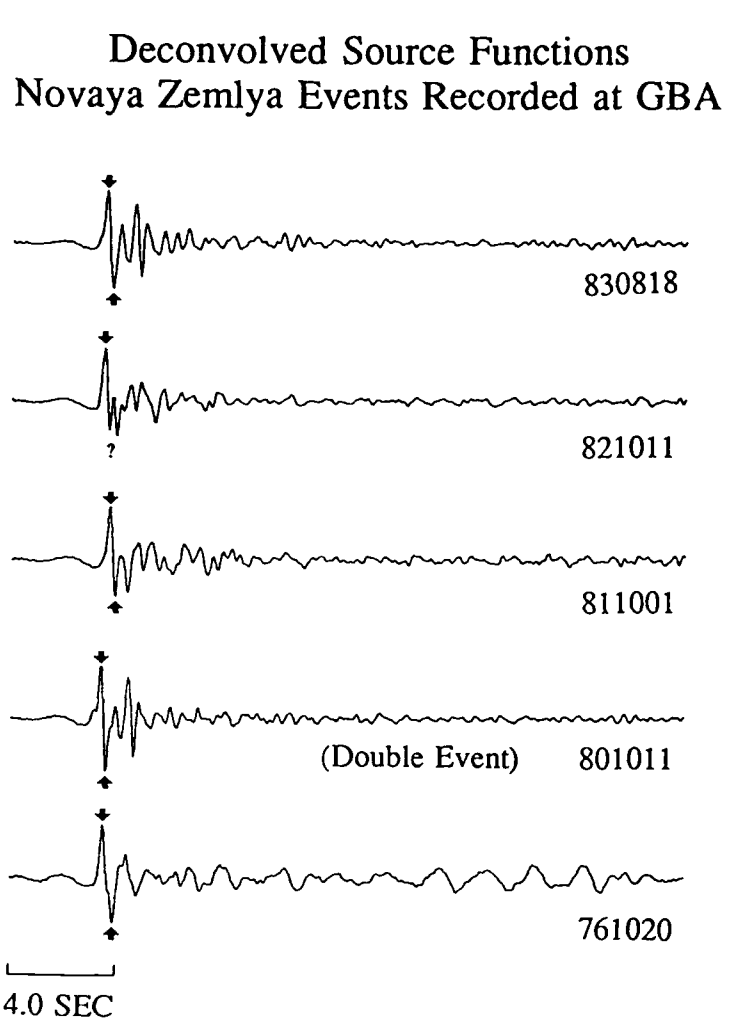

Figure 34. Source time function estimates obtained for Novaya Zemlya events at GBA. A VSB wavelet has been removed in these deconvolutions.

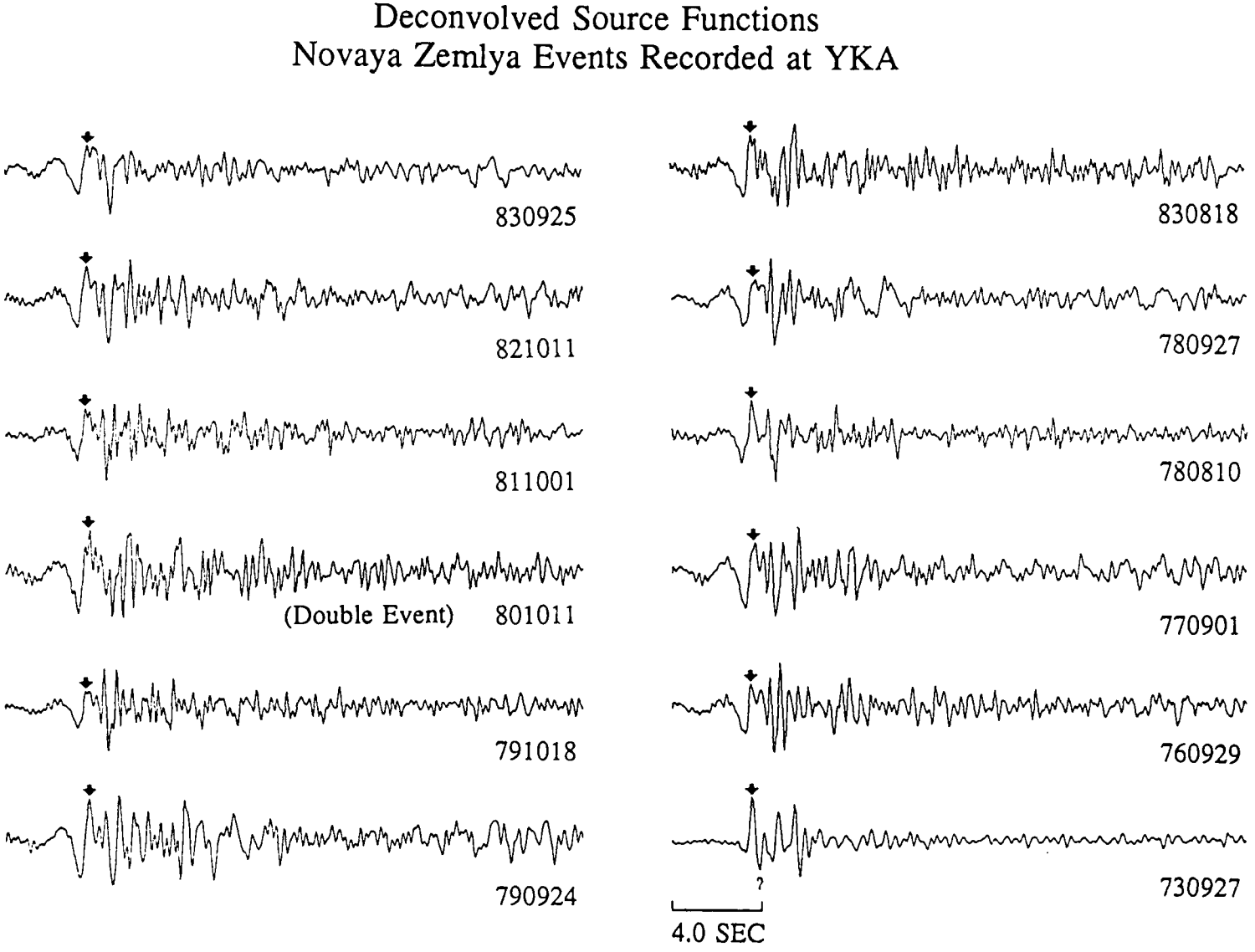

Figure 35. Source time function estimates obtained for Novaya Zemlya events at YKA. A VSB wavelet has been removed in these deconvolutions.

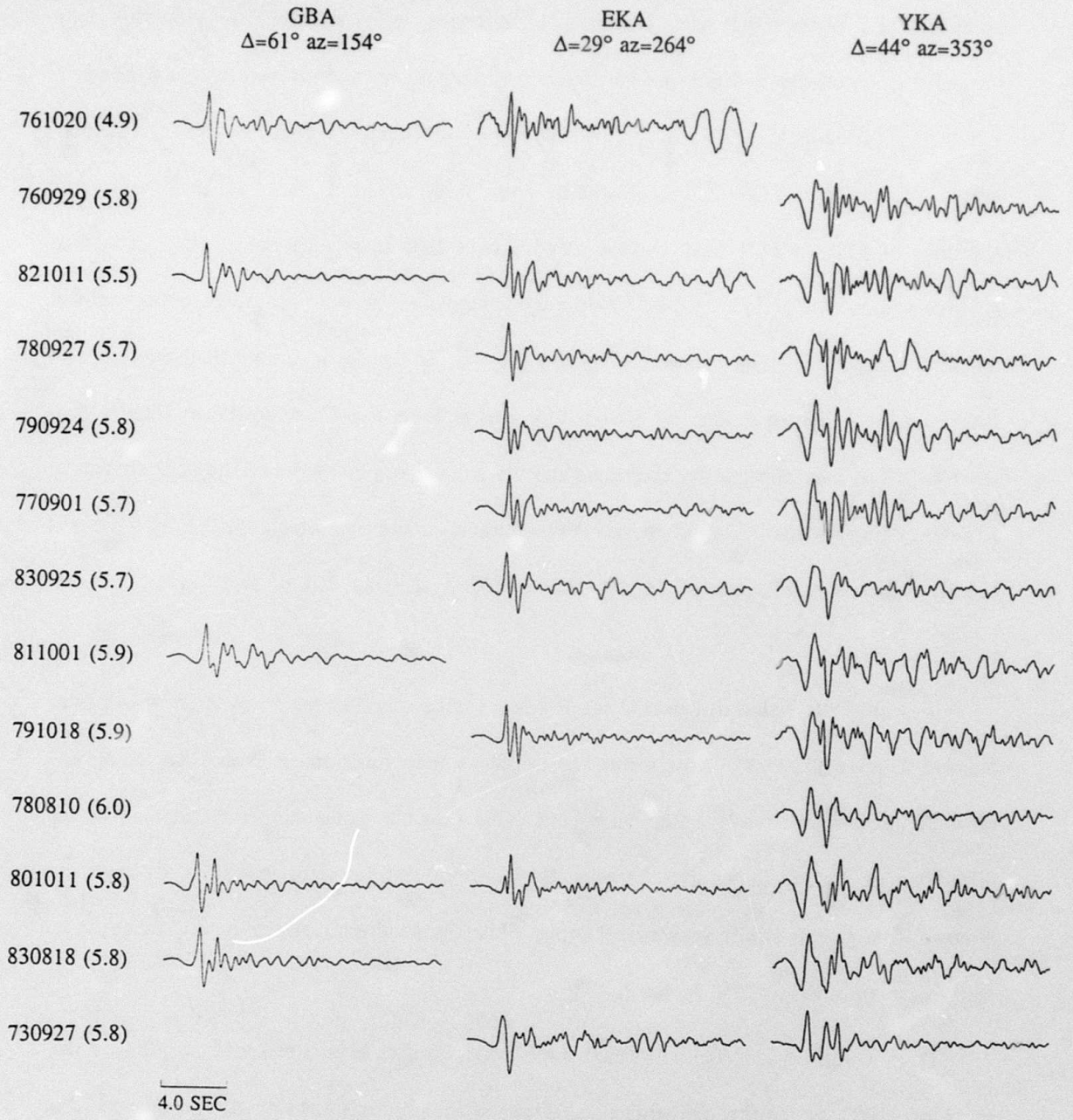

Figure 36. Source time function estimates for Novaya Zemlya events at three AWRE arrays. A VSB wavelet has not been removed in these deconvolutions. The source time functions (as well as the original seismograms) are quite complex at YKA in comparison with the other arrays.

The most striking observation about the waveforms in Figure 36 is how much more complex the P wave and P wave coda are at YKA than at EKA and GBA. However, even though the waveforms at YKA are very complex, they do reconstruct very well as shown in Figure 37. Greenfield (1971) has previously noted the complex coda for Novaya Zemlya events recorded at YKA and McLaughlin *et al.* (1986a) have observed that stations at azimuths of 352° to 111° from Novaya Zemlya have significantly shorter P wave coda than stations at azimuths of 150° to 349°. While the deconvolved sources at YKA are too complex to identify a pP arrival, it can be recognized on most of the deconvolutions of recordings at EKA and GBA. Even though the source functions at EKA and GBA are much simpler than those at YKA, they consistently show late arrivals other than pP. Some of the later arrivals at EKA may be due to triplications in the P wave travel time curve which still has two observable branches at a distance of 29° for shield models such as that of King and Calcagnile (1976).

It is also interesting to examine the P wave source function for an event from southern Novaya Zemlya (730927). This event has simpler source functions at both EKA and YKA than do the northern Novaya Zemlya events. One possible explanation for this may be the difference in surface topography between the northern and southern test sites; the northern Novaya Zemlya test site is very mountainous while the southern test site is in a much flatter area (per map in Lilwall and Marshall 1986).

Deconvolutions are also performed for Novaya Zemlya events recorded at WRA, a distance of ~105°, so the first arrival is P_{diff}. These deconvolutions are shown in Figure 38. For these deconvolutions, we estimated a t* of 0.45 sec from the slope of the P wave spectra after correction for yield and instrument response. This is much higher that the t* of around 0.2 sec used for all of the other Novaya Zemlya to shield station deconvolutions, but the added

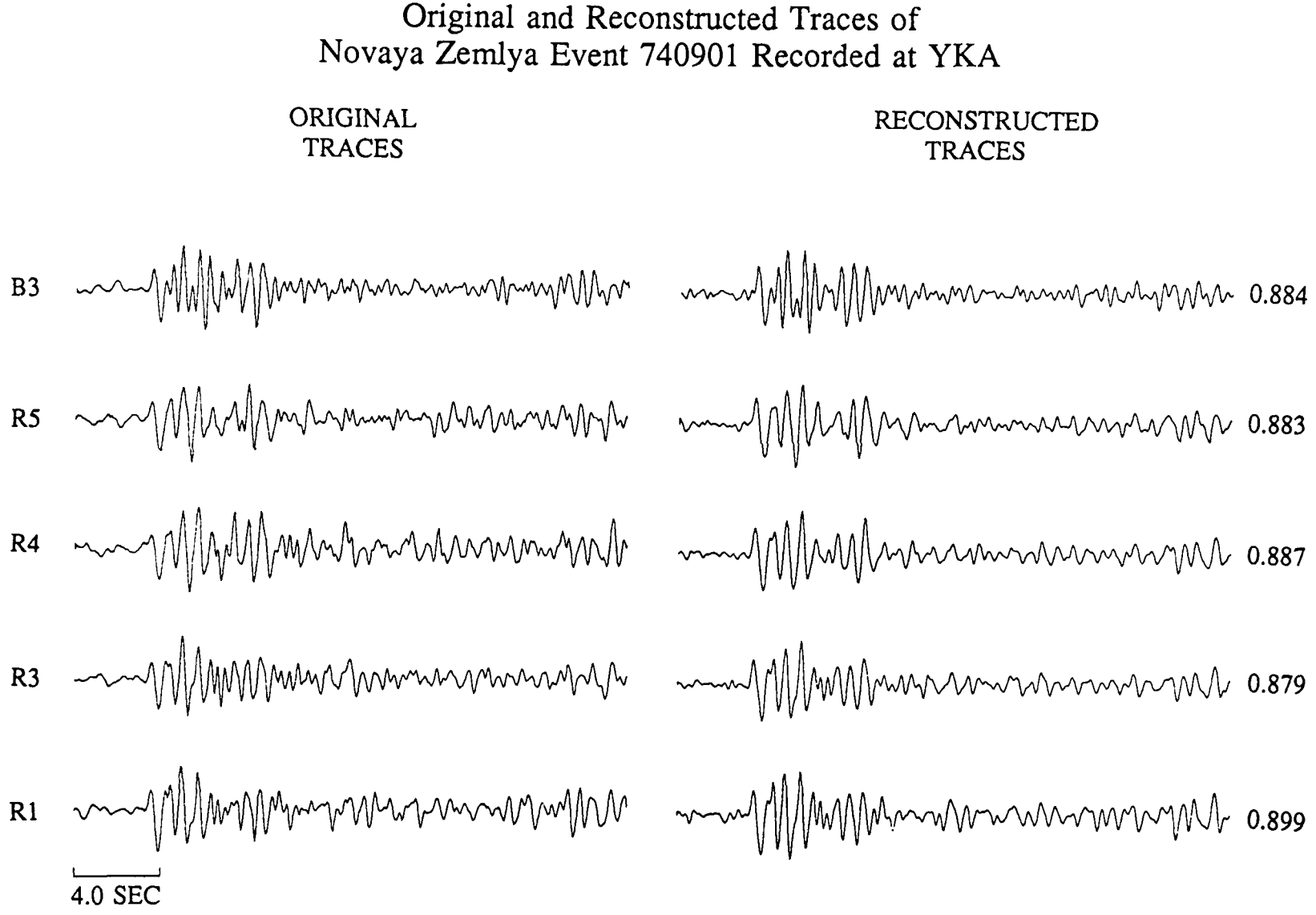

Figure 37. Examples of trace reconstructions compared to original traces at selected sites of YKA. The quality of reconstruction is quite good.

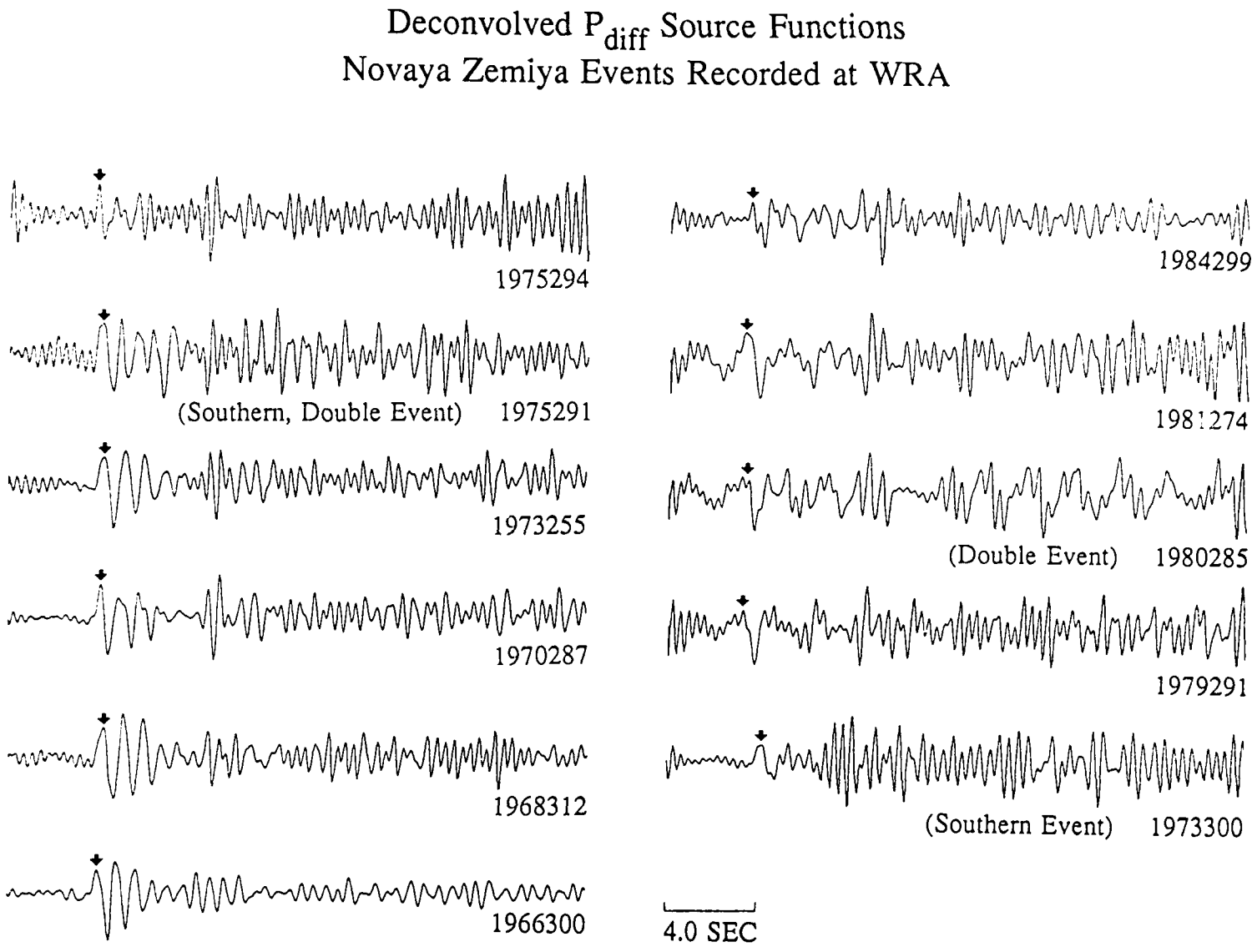

Figure 38. P_{diff} source time function estimates obtained for Novaya Zemlya events at WRA. A VSB wavelet has been removed in these deconvolutions.

attenuation may be due to diffraction or other interactions at the core mantle boundary. The deconvolved source time functions are relatively long period and ringing, with a second higher frequency arrival about 5 sec after the P arrival.

For the larger Novaya Zemlya events, the P waves clipped at the AWRE arrays (except for some of the P_{diff} observed at WRA), so deconvolutions were done of the PcP. A t* around 0.2 sec was measured from spectra as described in McLaughlin *et al.* (1987b), about the same t* as observed for the direct P wave, and used in the deconvolutions. The deconvolved source time functions of PcP from Novaya Zemlya, recorded at EKA are shown in Figure 39. Generally, the PcP show very clean, simple source time functions with a clear pPcP arrival. The pPcP and pP delays, relative to the respective PcP and P waves, are shown in Figure 40. There is a trend to a slight increase in depth phase delay time with increasing magnitude. For three events with magnitudes just under 6, both P and PcP were on scale and available in our data set. The deconvolutions of the respective P and PcP arrivals are shown in Figure 41. These were used by McLaughlin *et al.* (1987c) to scale the PcP to the P for yield estimates.

Figures 42 to 46 show the northern Novaya Zemlya deconvolved source time functions plotted on a map of the test site for the different receiver arrays. As with the other test sites, nearby events often have similar source time functions, while there are variations in source time function across the test site. Smaller variations between events might be expected for PcP and P_{diff} relative to P because the former two phases have more nearly vertical take-off angles. Figure 47 shows the deconvolved PcP phases for three of the southern Novaya Zemlya events. In comparing Figures 47 and 43, it seems that the PcP and pPcP pulses from the southern events are more complex than those of the northern events, though the coda is not any more complex. This is a sample of only three events, but maybe the VSB does not model the source functions of the southern events as well as the northern events, since the deconvolved

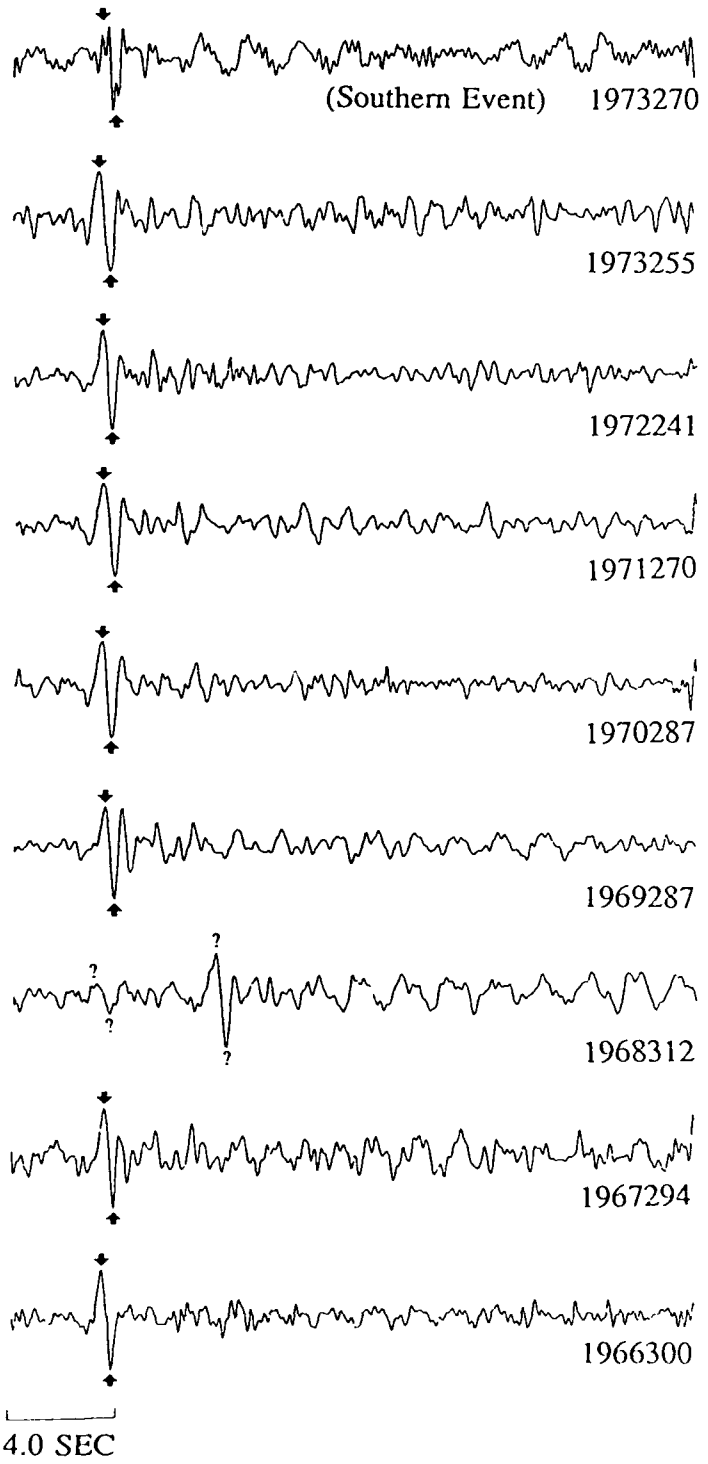

Figure 39. PcP source time function estimates obtained for Novaya Zemlya events at EKA. A VSB wavelet has been removed in these deconvolutions.

Deconvolved PcP Source Functions
Novaya Zemlya Events Recorded at EKA

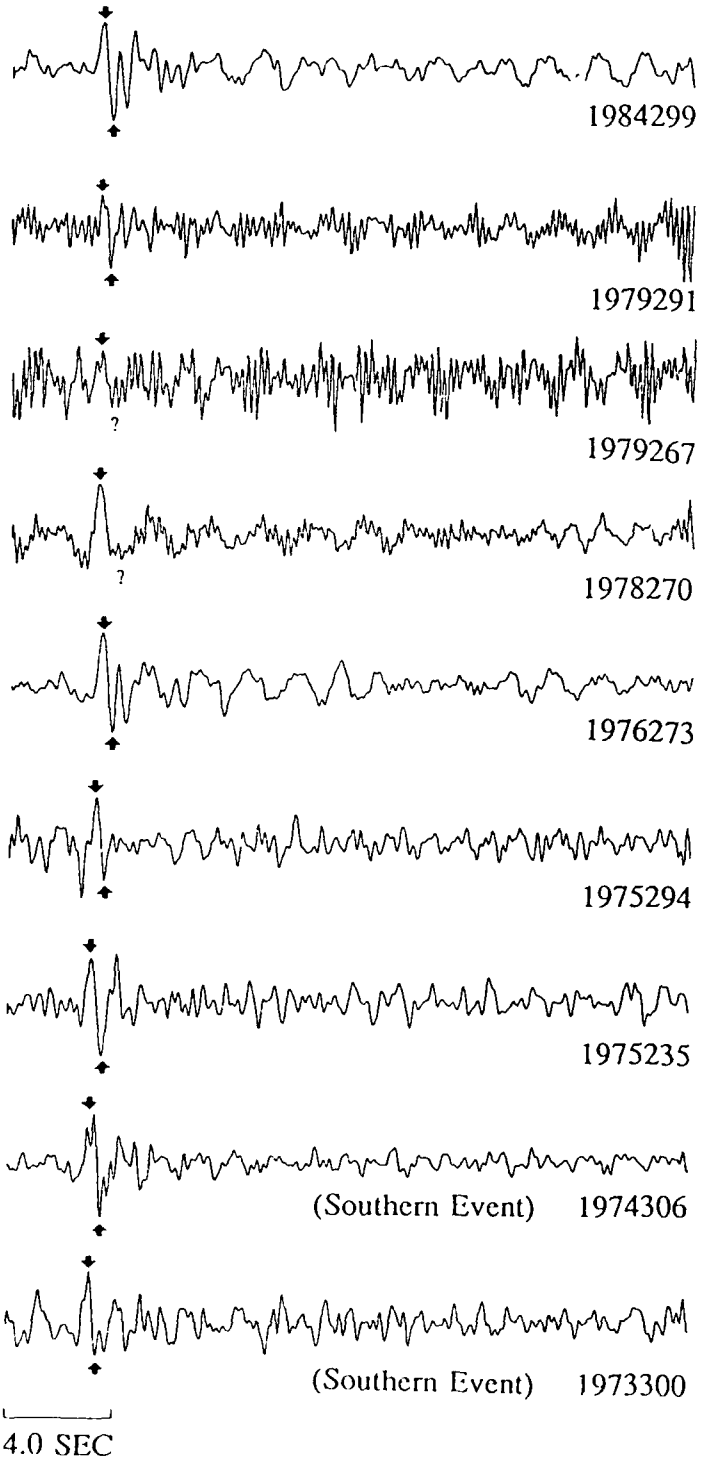

Figure 39 (cont'd)

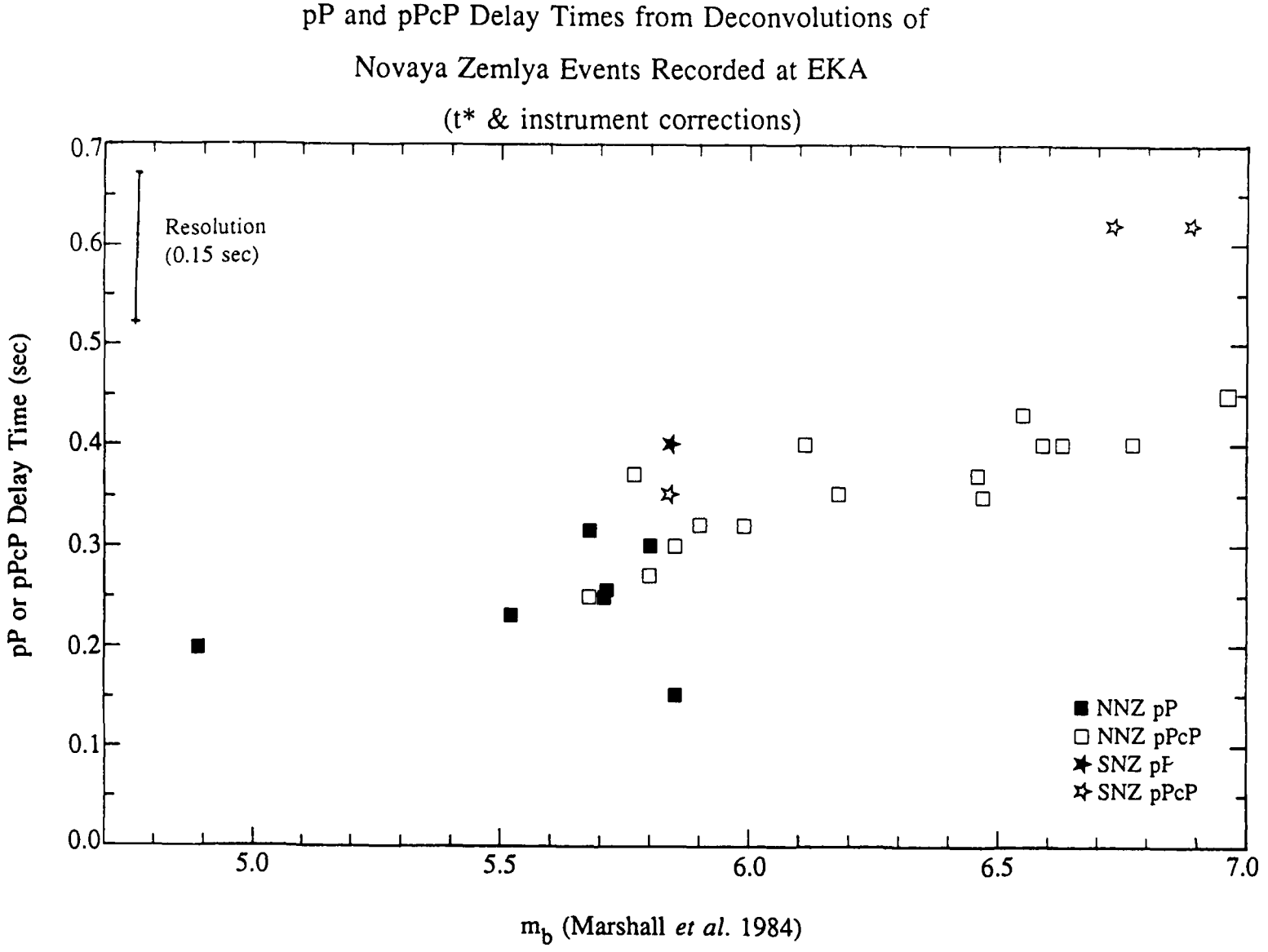

Figure 40. pP and pPcP delay times from deconvolutions of Novaya Zemlya events recorded at EKA. A VSB wavelet has not been removed in the deconvolutions from which the delay measurements were made.

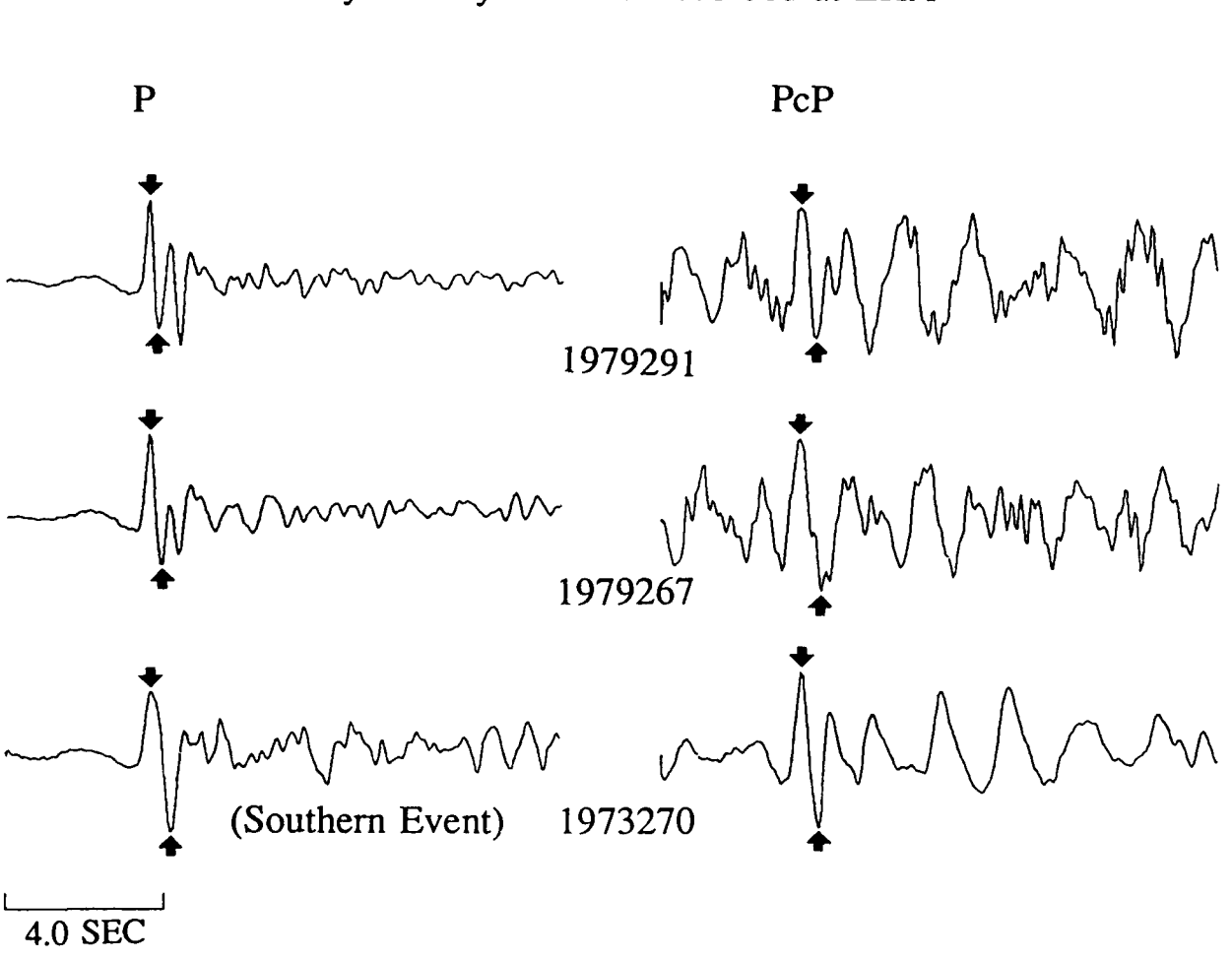

Figure 41. Deconvolved source time functions for P and PcP for three Novaya Zemlya events. A VSB wavelet has not been removed in these deconvolutions.

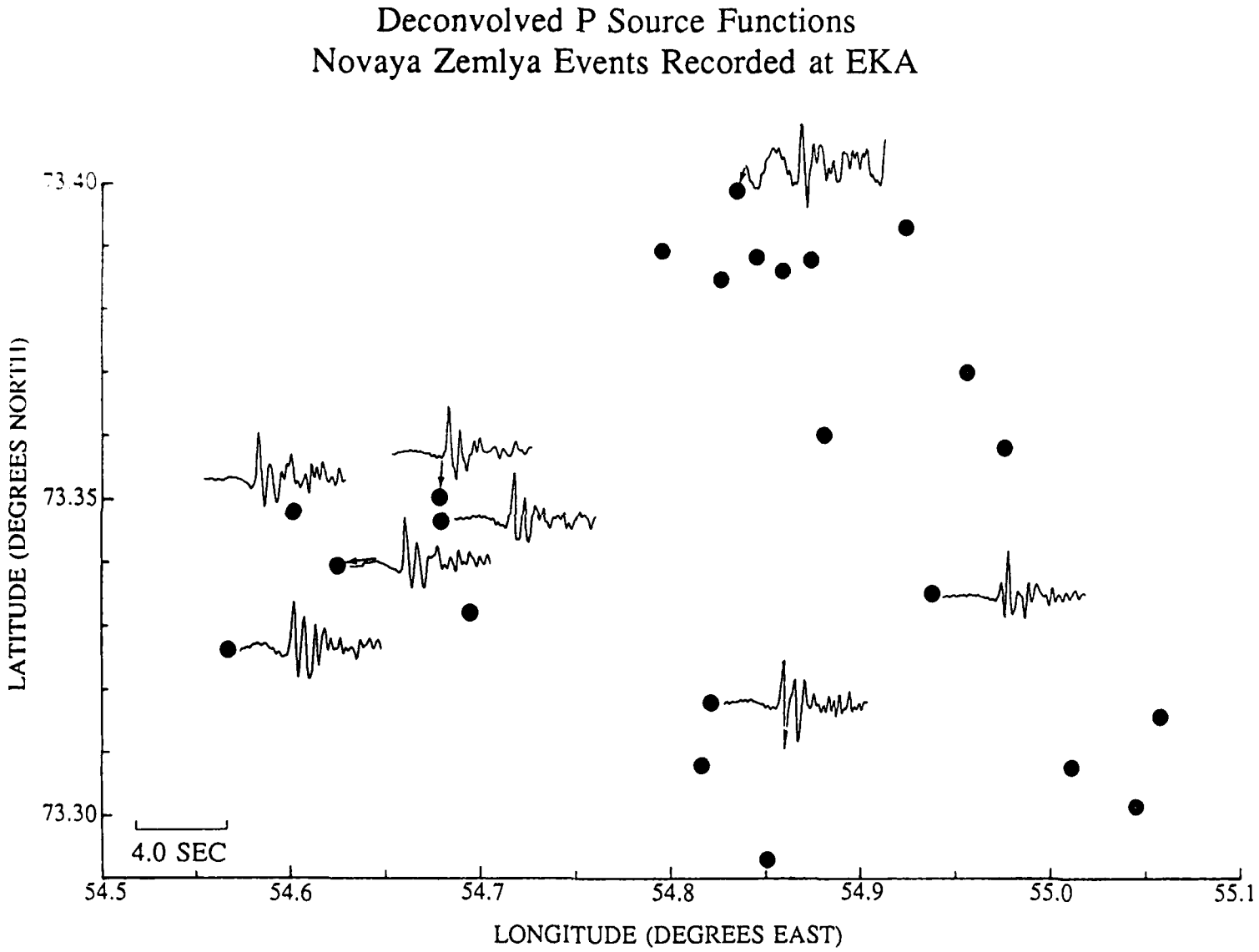

Figure 42. Deconvolved P wave source functions for Novaya Zemlya events recorded at EKA plotted on the map in Figure 32. The estimated VSB wavelet has been removed in the deconvolutions.

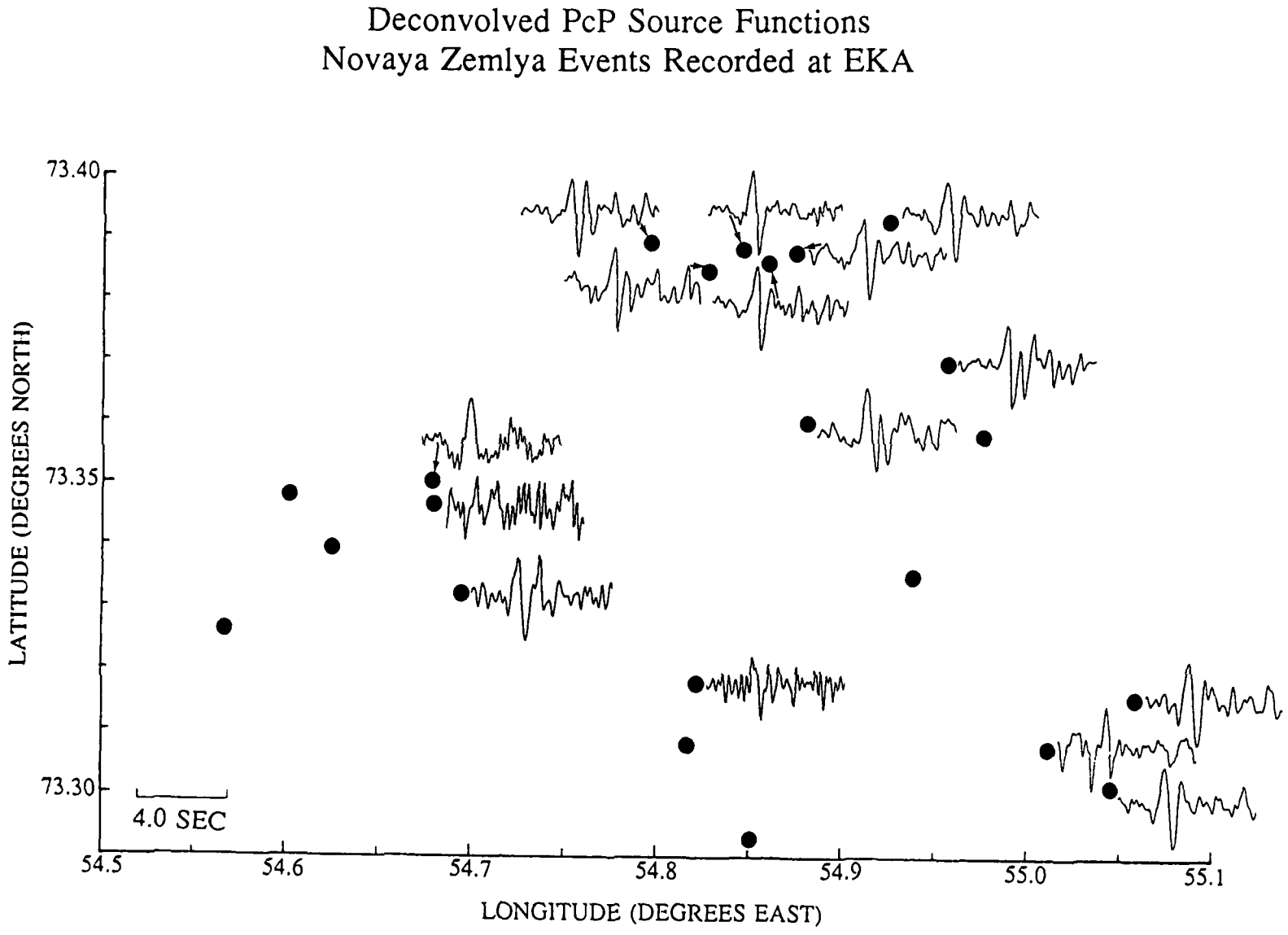

Figure 43. Deconvolved PcP source functions for Novaya Zemlya events recorded at EKA plotted on the map in Figure 32. The estimated VSB wavelet has been removed in the deconvolutions.

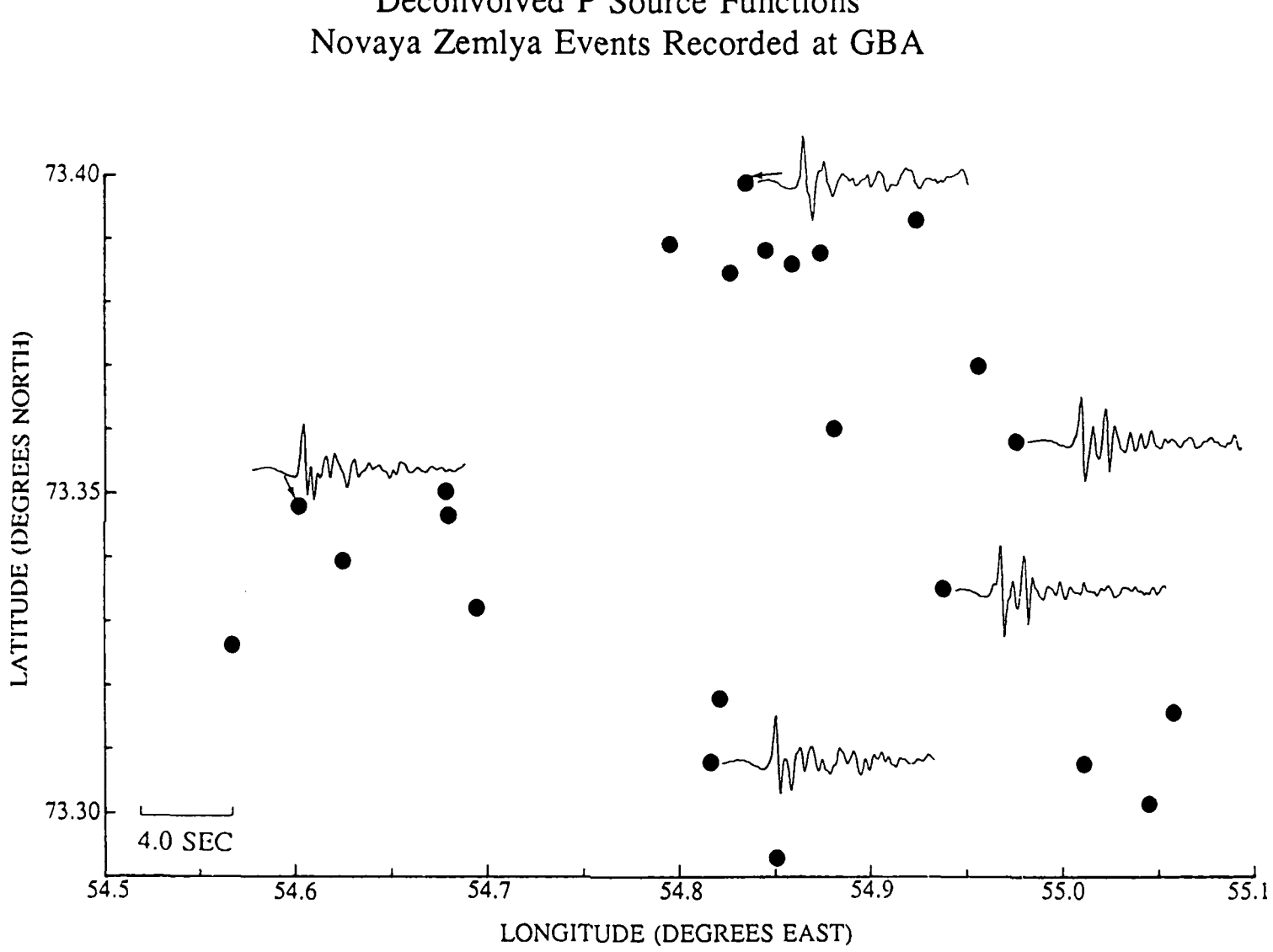

Figure 44. Deconvolved P wave source functions for Novaya Zemlya events recorded at GBA plotted on the map in Figure 32. The estimated VSB wavelet has been removed in the deconvolutions.

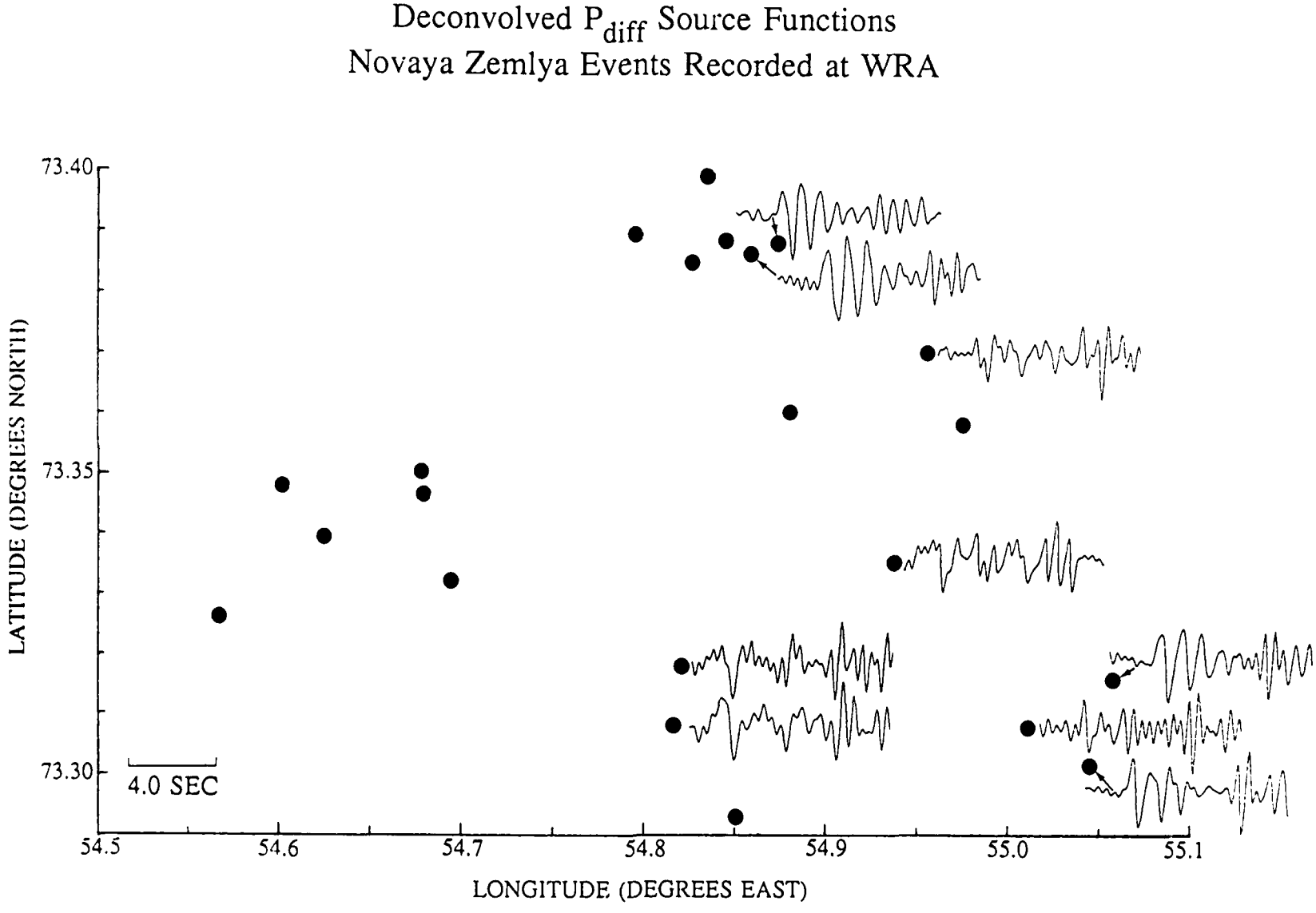

Figure 45. Deconvolved P_{diff} source functions for Novaya Zemlya events recorded at WRA plotted on the map in Figure 32. The estimated VSB wavelet has been removed in the deconvolutions.

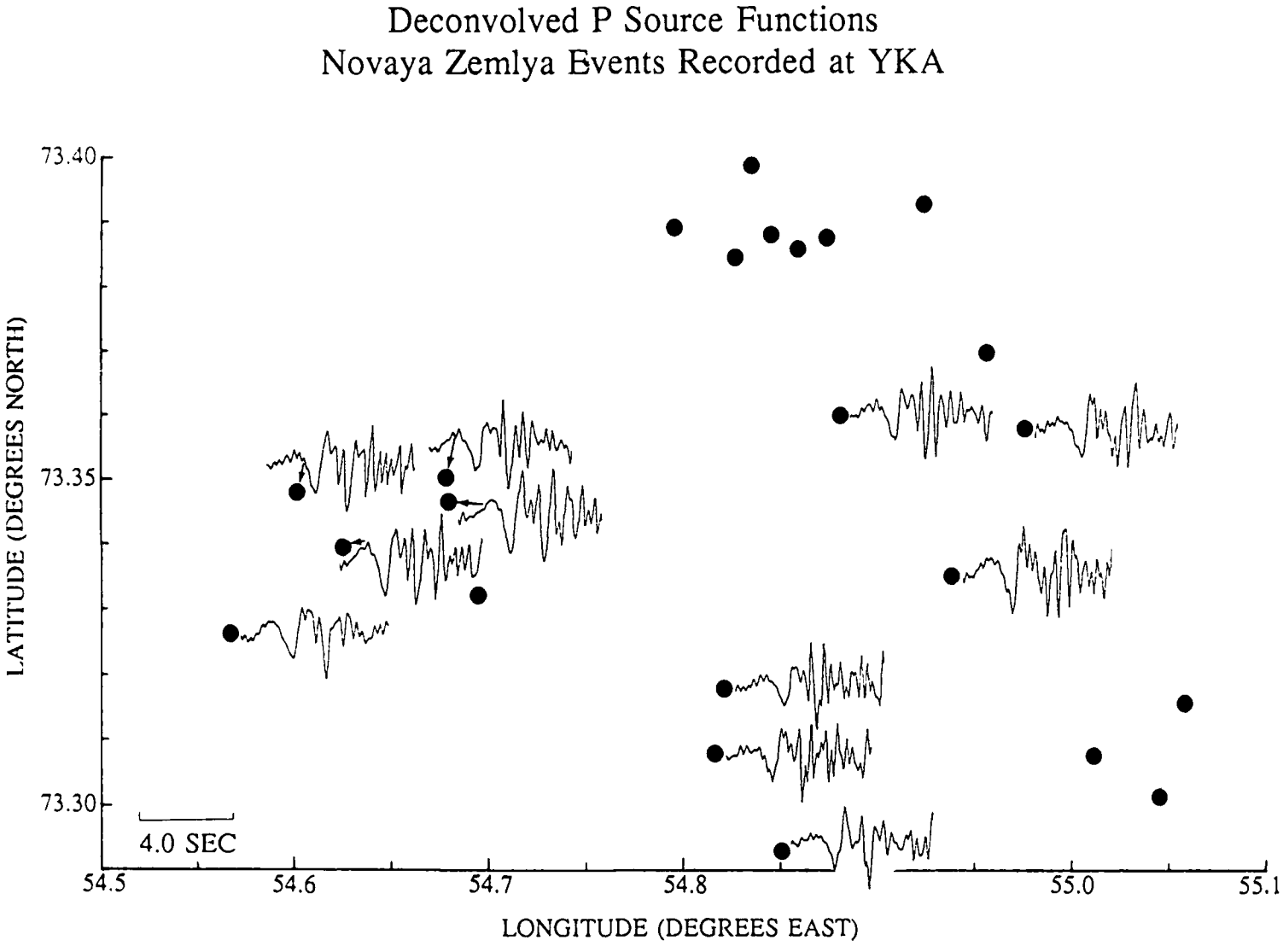

Figure 46. Deconvolved P wave source functions for Novaya Zemlya events recorded at YKA plotted on the map in Figure 32. The estimated VSB wavelet has been removed in the deconvolutions.

Deconvolved PcP Source Functions
Novaya Zemlya Events Recorded at EKA

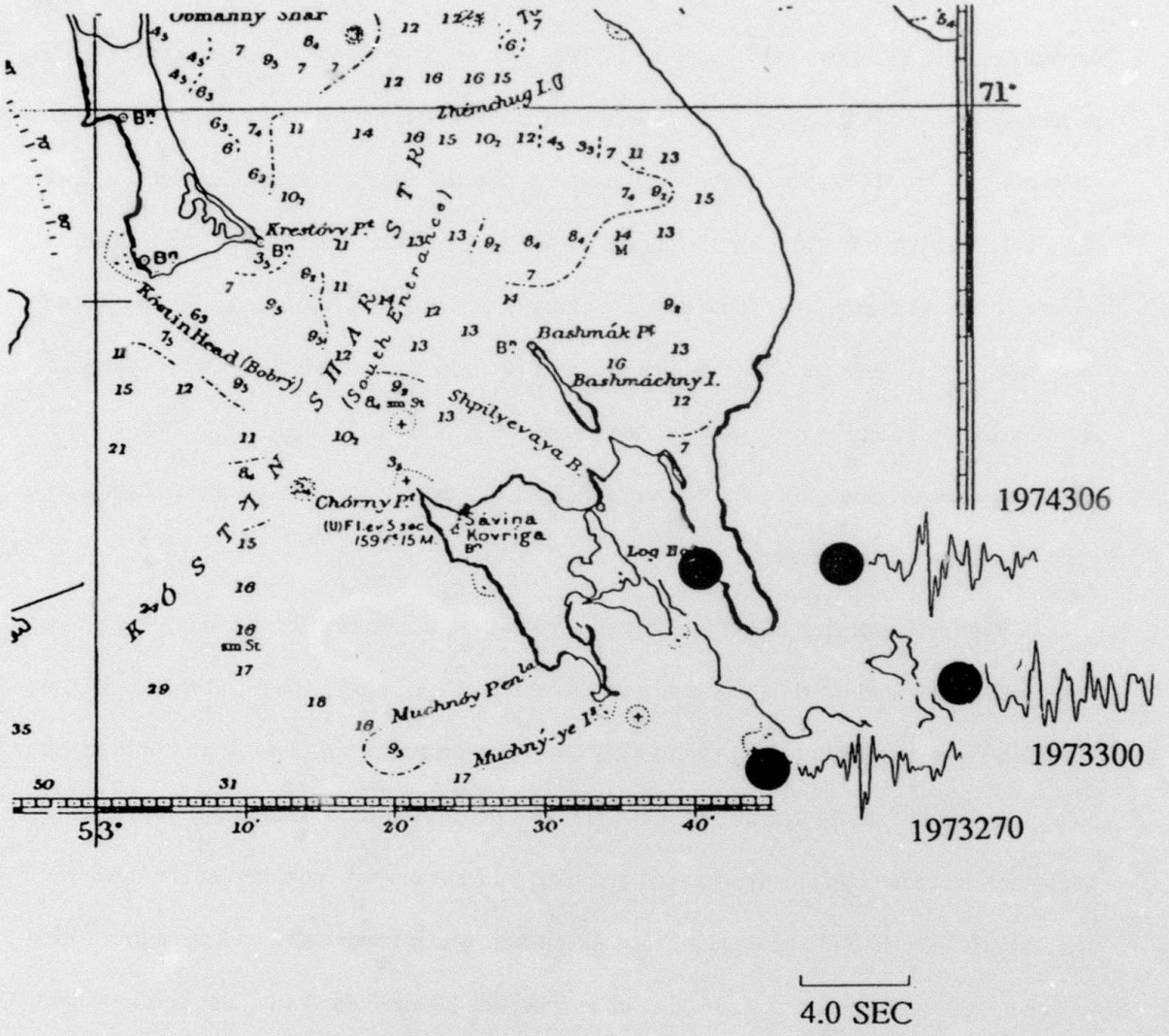

Figure 47. Deconvolved PcP source functions for southern Novaya Zemlya events recorded at EKA plotted on a map from Lilwall and Marshall (1986). The estimated VSB wavelet has been removed in the deconvolutions.

waveforms without removing the VSB do not show added complexity for the southern events.

Astrakhan

Two sequences of Astrakhan events containing 4 and 6 events, respectively, were deconvolved from observations at GBA and the RSTN. This work was done by Gupta *et al.* (1987) as part of a decoupling project, but the deconvolutions are included here for the sake of completeness. Figure 48 shows source time functions for the four events of October 16 1982 deconvolved separately from data recorded at GBA (left) and four of the RSTN stations (center). The relatively great depth of these shots can be inferred from the pP delay time of over 1 sec for all four shots. There are also two or three arrivals which consistently appear between the P and pP; perhaps these are earlier reflections from high impedance contrast layers between the shot point and the surface. This is a possibility because these shots were done in an area with salt layers.

A joint deconvolution of the two sets of deconvolved waveforms for the four events from GBA and RSTN stations (left and center traces of Figure 48) is performed and the results are shown in Figure 48 (right traces). In this case, a t* and instrument response were not removed since they had already been removed in the previous deconvolutions. The joint deconvolutions are somewhat more azimuthally averaged and they are less complex looking than the other two sets, though they do still show clear P and pP phases, which incidentally look very much like mirror images of each other. The source-time functions obtained from the joint deconvolution of the four events have a closer resemblance to those for RSTN than for GBA. Although no weighing function is imposed on the deconvolution process, the RSTN data have better S/N ratios probably contributing to their dominance in the deconvolved source-time functions.

Figure 49 shows the deconvolved source time functions for the six events of September 24, 1983 as recorded at GBA. As with the previous set of events, the pP delay time is over 1

Deconvolved Source-Time Functions of Astrakhan Events
Recorded at GBA, RSTN, and GBA & RSTN

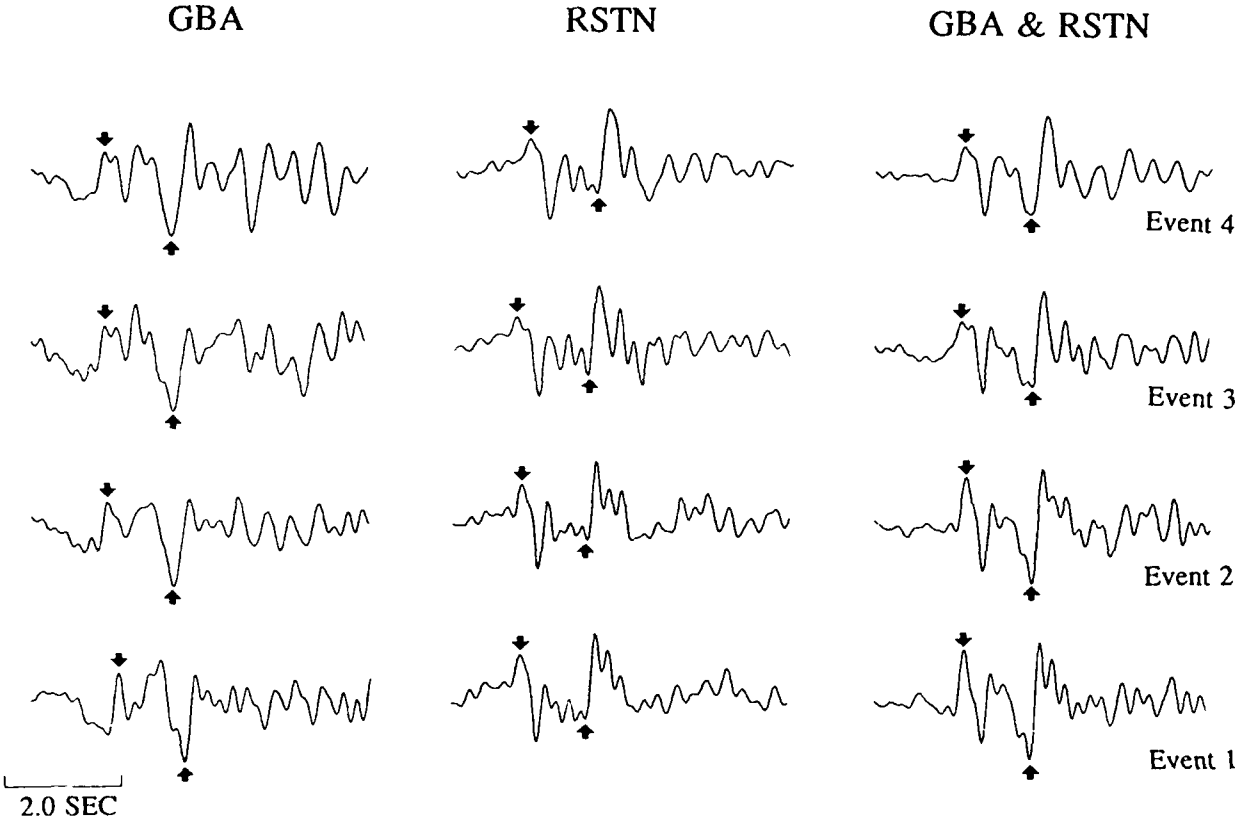

Figure 48. Deconvolved source time functions for the Astrakhan events of October 16, 1982, recorded at GBA and RSTN. The earliest event is "Event 1" and the latest event is "Event 4". The VSB wavelet has been removed in the deconvolutions. The source time functions at the left and center are from data recorded at GBA and four of the RSTN stations, respectively. The source time functions on the right are the result of deconvolving the two separate sets of deconvolutions at the left and center. This "joint" deconvolution contains the parts of the source time functions that are common to observations at both arrays.

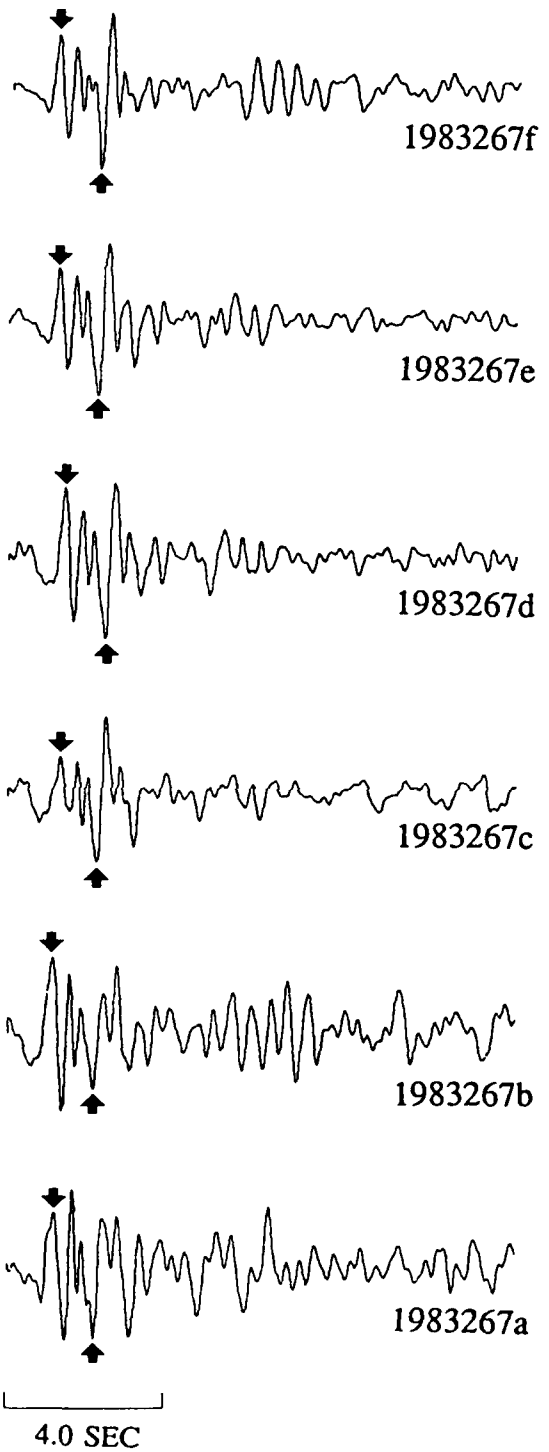

Figure 49. Deconvolved source time functions for the Astrakhan events of September 24, 1983, recorded at GBA. The VSB wavelet has been removed in the deconvolutions.

sec, and the multiple arrivals between the P and pP have larger amplitudes than those for the other four events. The six events are very closely co-located in space and time, so it is probably not surprising that their source functions look so similar.

Figure 50 shows the deconvolved source time functions for all ten Astrakhan events recorded at GBA. Again, the depth and other secondary arrivals are very similar for all ten events. The amplitudes of the multiple arrivals for events 1-4 are enhanced in this case whereby improving the S/N ratio to allow a better identification of the individual phases.

French Sahara (Ahaggar)

A map of the locations of the main events at this test site is shown in Figure 51. Only a few nuclear explosions in the French Sahara were available with acceptable S/N ratios at the AWRE arrays. The Sahara test site is another low Q area (Der *et al.* 1985a), thus making deconvolutions difficult. The deconvolutions yielded fairly complex time functions for the sources which vary considerably between EKA and YKA (Figure 52) though the difference in azimuth is only ~ 50°. We interpret this as azimuthal asymmetries in the radiation which, in the view of the complex topography of the test site is to be expected (McLaughlin *et al.* 1987b). Possible pP phases are observed less than 0.7 seconds after the direct P arrival for Saphir and Rubis at EKA and Grenat and Emeraude at YKA. The fact that good pP phases are observed for two events at EKA and for the other two at YKA provides support for the azimuthal asymmetries in the source radiation. Due to the limited bandwidth of the records we did not attempt to factor out the VSB source wavelet.

Tuamotu (Mururoa)

Seventeen events from the French south Pacific test site, Tuamotu, were also deconvolved. The locations of the events are plotted in Figure 53. Prior to performing the

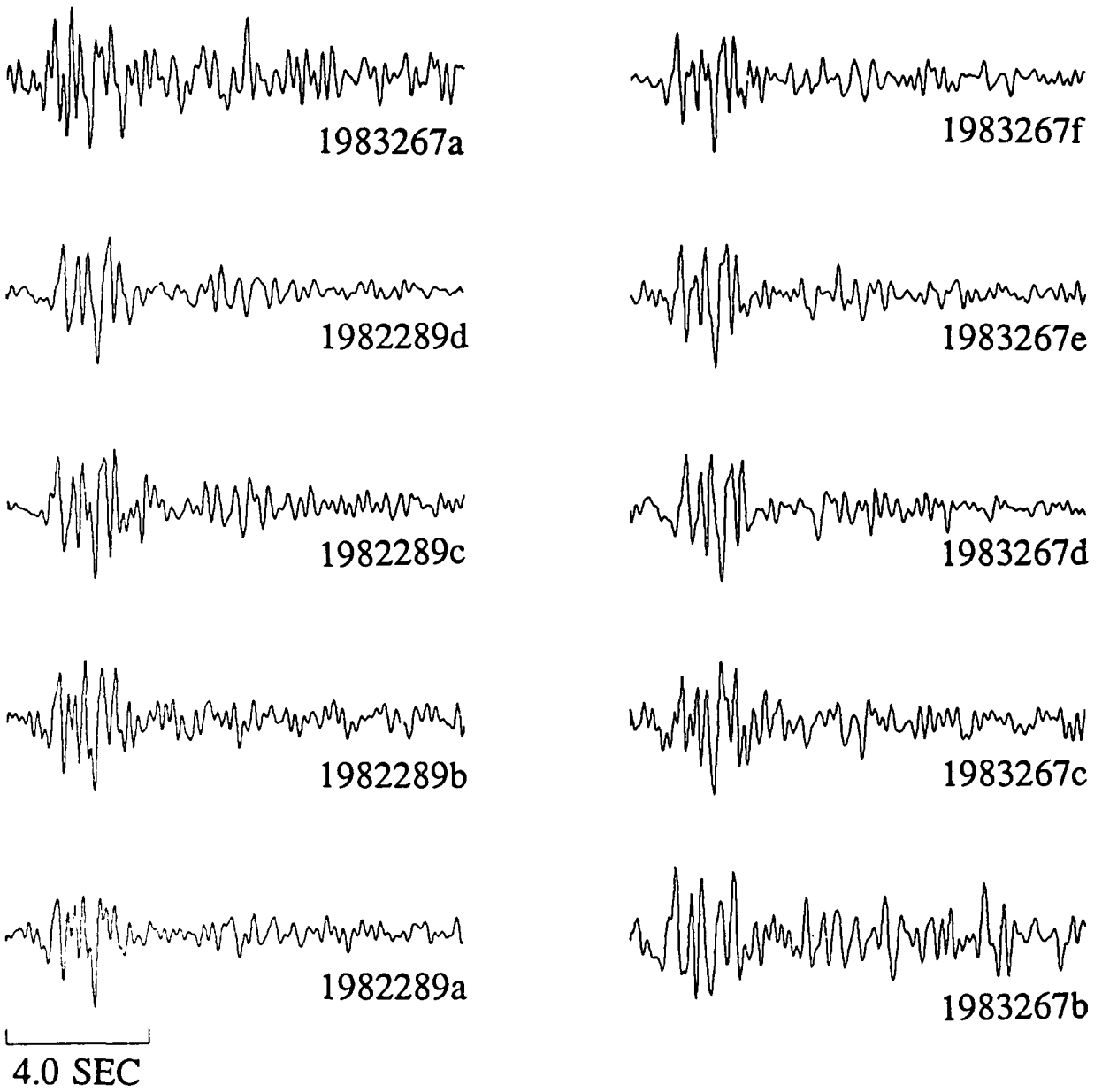

Figure 50. Deconvolved source time functions for the Astrakhan events of October 16, 1982, and September 24, 1983, recorded at GBA. The VSB wavelet has been removed in the deconvolutions.

Locations of French Sahara Events at the Taourirt Tan Afella Massif

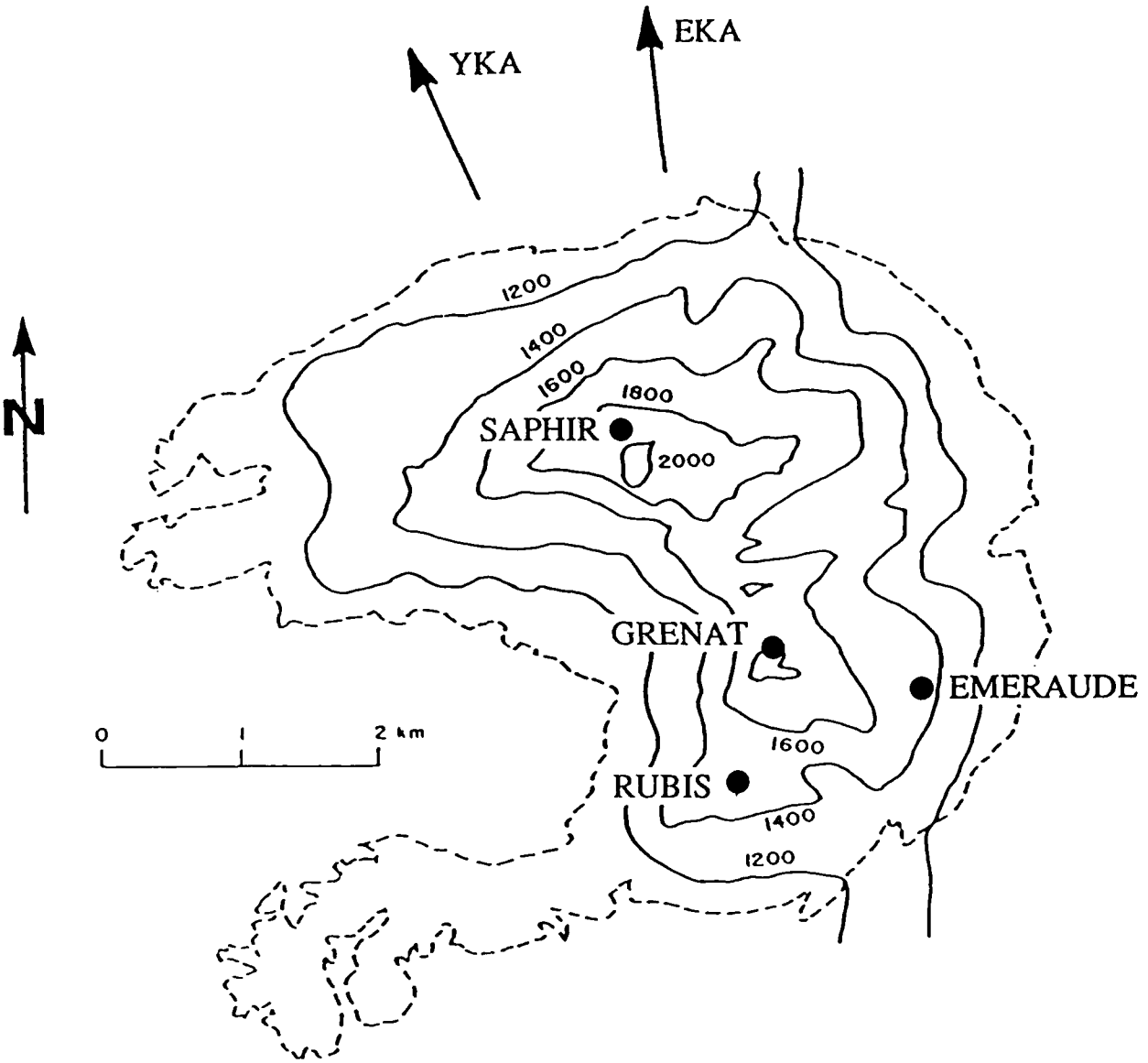

Figure 51. Locations of tests at the French Sahara test area (from McLaughlin *et al.* 1987b).

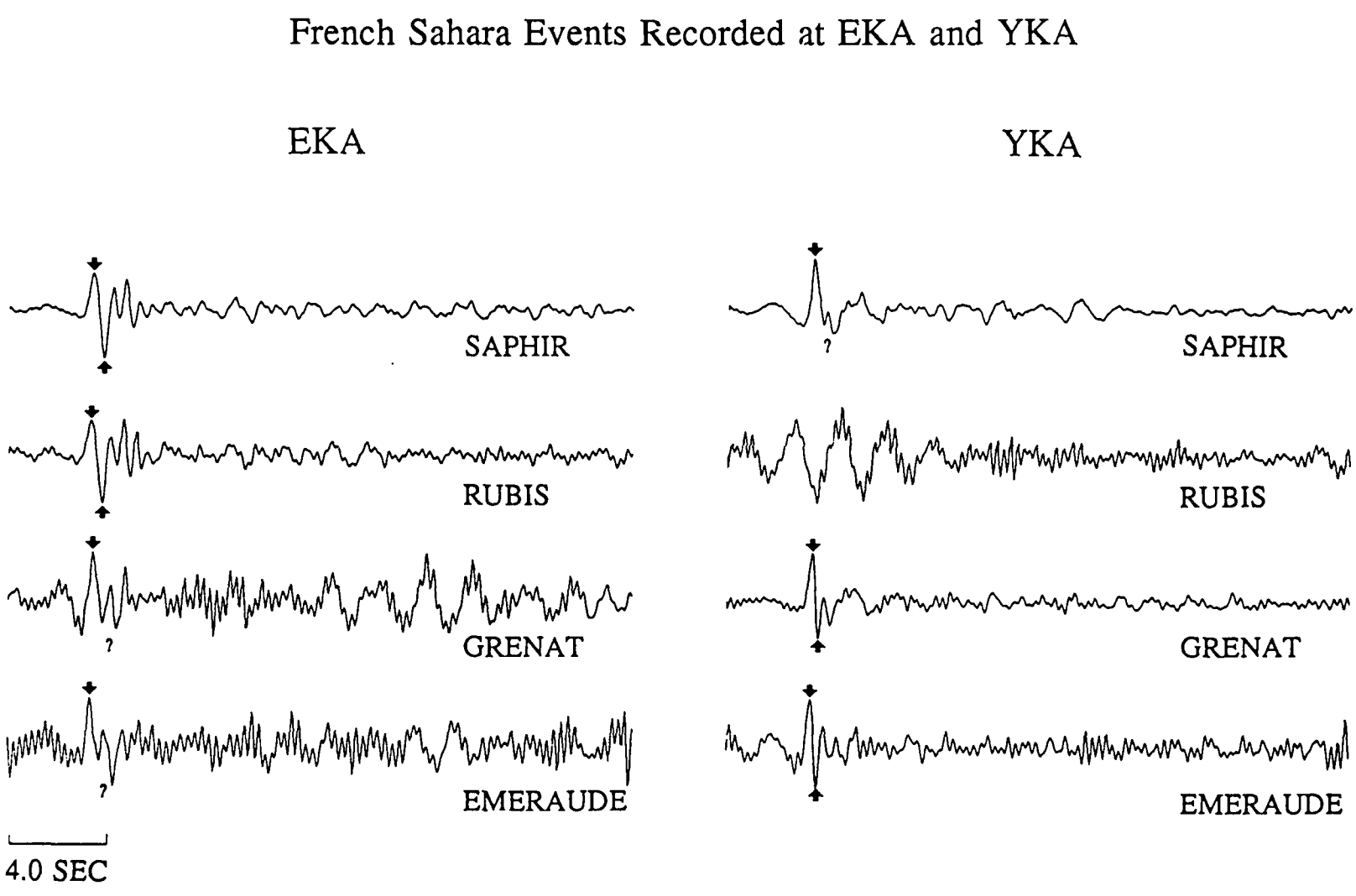

Figure 52. Deconvolution results for source time estimates for French Sahara events recorded at EKA and YKA. VSB wavelets have not been removed in these deconvolutions.

Locations of Tuamotu Explosions
(Marshall et al 1985)

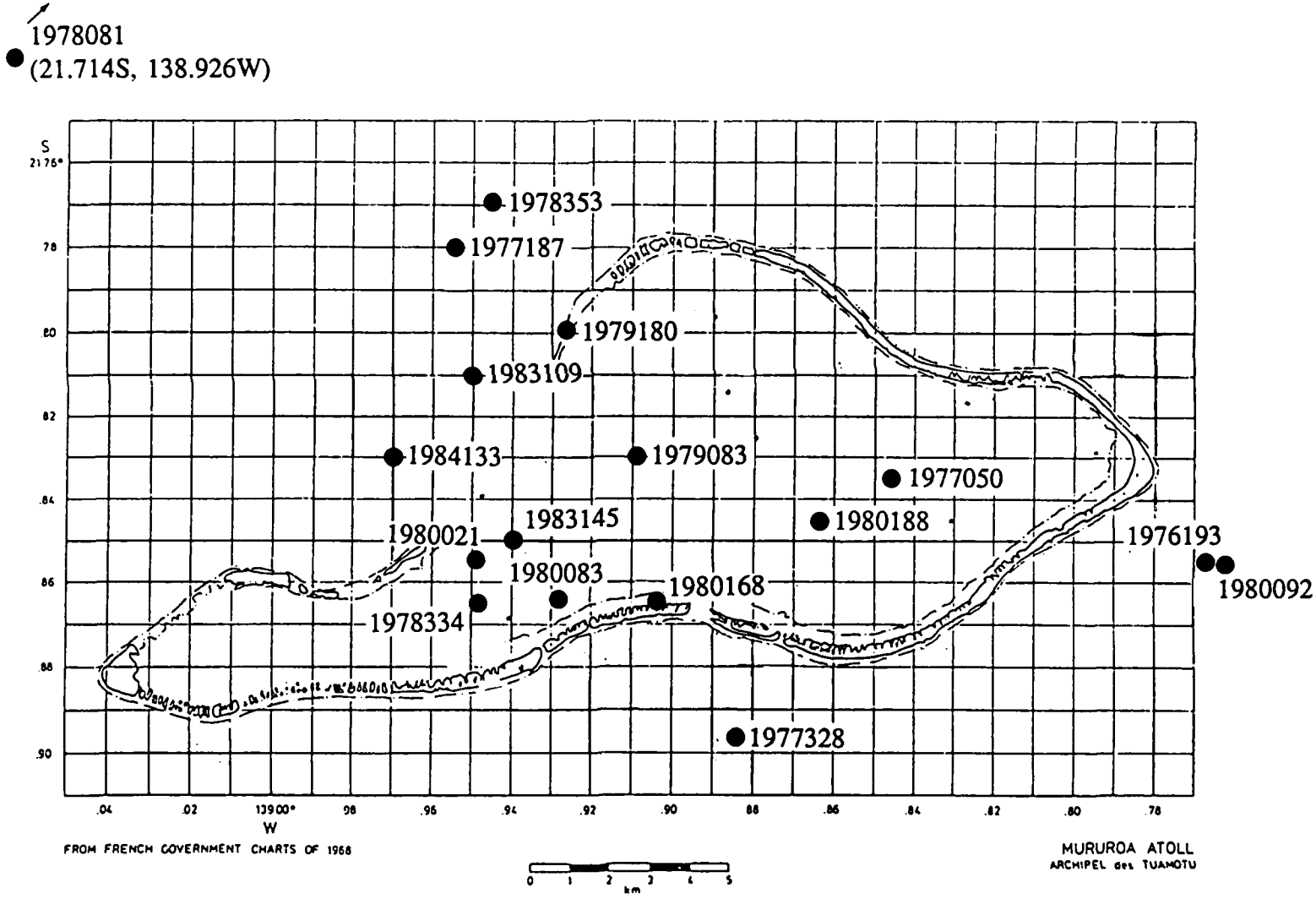

Figure 53. Locations (Lilwall and Marshall 1986) of the Tuamotu events analyzed in this study.

deconvolutions, it was necessary to estimate the t* to be used in the deconvolutions. The t* was estimated from a least squares fit of a line through the spectrum of a number of event-receiver pairs, where each spectrum was corrected for the instrument response and a VSB source time function with the appropriate yield. This is the same procedure as described by McLaughlin *et al.* (1986b, 1987b). We find an average t* of 0.45 (±0.05) sec. This is in reasonable agreement with other estimates of 0.35 by Der *et al.* (1985a) and McLaughlin et al (1986b). The results are tabulated in Table 17.

The deconvolved source time functions are shown in Figures 54 to 57. Figure 58 shows the deconvolved source time functions for Tuamotu events recorded at YKA plotted on the map of the event locations. The source functions at GBA are interesting mostly because three of the branches of PKP are clearly visible on the deconvolutions. At WRA, no prominent pP arrival can be observed from the deconvolutions, but the source-time functions show strong resemblance among the different events with the P phase and the possibly multiple reflections being particularly similar for events 80201, 80083 and 78334. Deconvolution of the YKA data shows very consistent pP with a delay of about 0.5 to 0.6 sec after the P phase in the source-time functions. The deconvolved source time functions for three events recorded at the RSTN also show a prominent pP arrival of about 0.5 sec with and without the VSB wavelet removed. Display of the source-time functions with respect to the event location in Figure 58 shows rather strong azimuthal source effects as seen from YKA.

Sinkiang

Deconvolutions were performed for three Chinese Sinkiang-region events recorded at the RSTN stations. Figures 59 and 60 show the source time functions with and without the VSB removed for 3 events recorded at 2 stations and 2 events recorded at 3 stations, respectively. Even though both cases are just barely overdetermined (6 seismograms with 5 parameters to

Table 17

t* Estimates for Tuamotu		
Path	t* (whole path) (sec)	t* (under Tuamotu) (sec)
Tuamotu→GBA	0.51 ± 0.06	0.43 ± 0.06
Tuamotu→WRA	0.57 ± 0.11	0.49 ± 0.11
Tuamotu→YKA	0.60 ± 0.15	0.53 ± 0.15
weighted average		0.45 ± 0.05

Deconvolved Source Functions
Tuamotu Events Recorded GBA

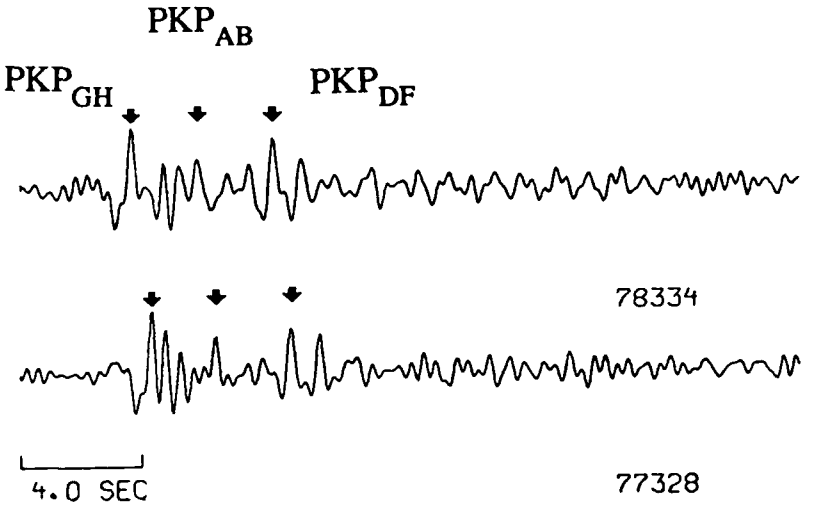

Figure 54. Deconvolved source functions for Tuamotu events recorded at GBA. The estimated VSB wavelet has been removed in the deconvolutions. Several arrivals of PKP can be seen in the source functions.

Deconvolved Source Functions
Tuamotu Events Recorded WRA

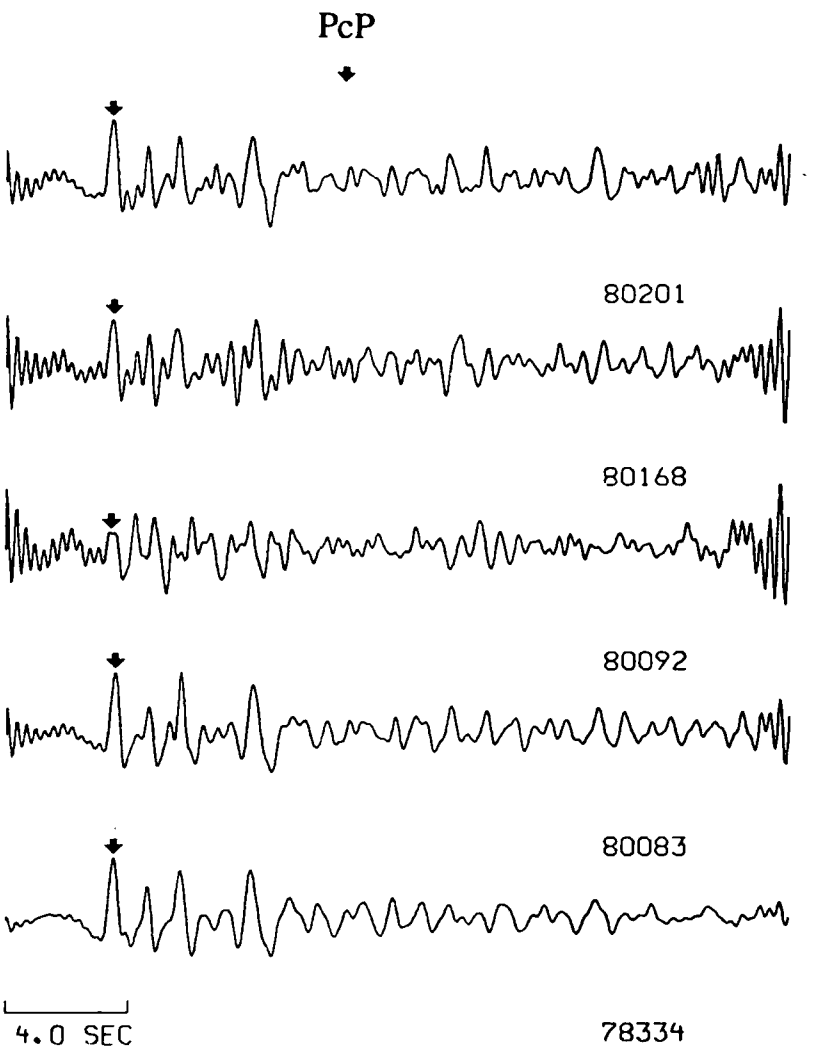

Figure 55. Deconvolved source functions for Tuamotu events recorded at WRA. The estimated VSB wavelet has not been removed in the deconvolutions. The predicted PcP arrival time is also shown.

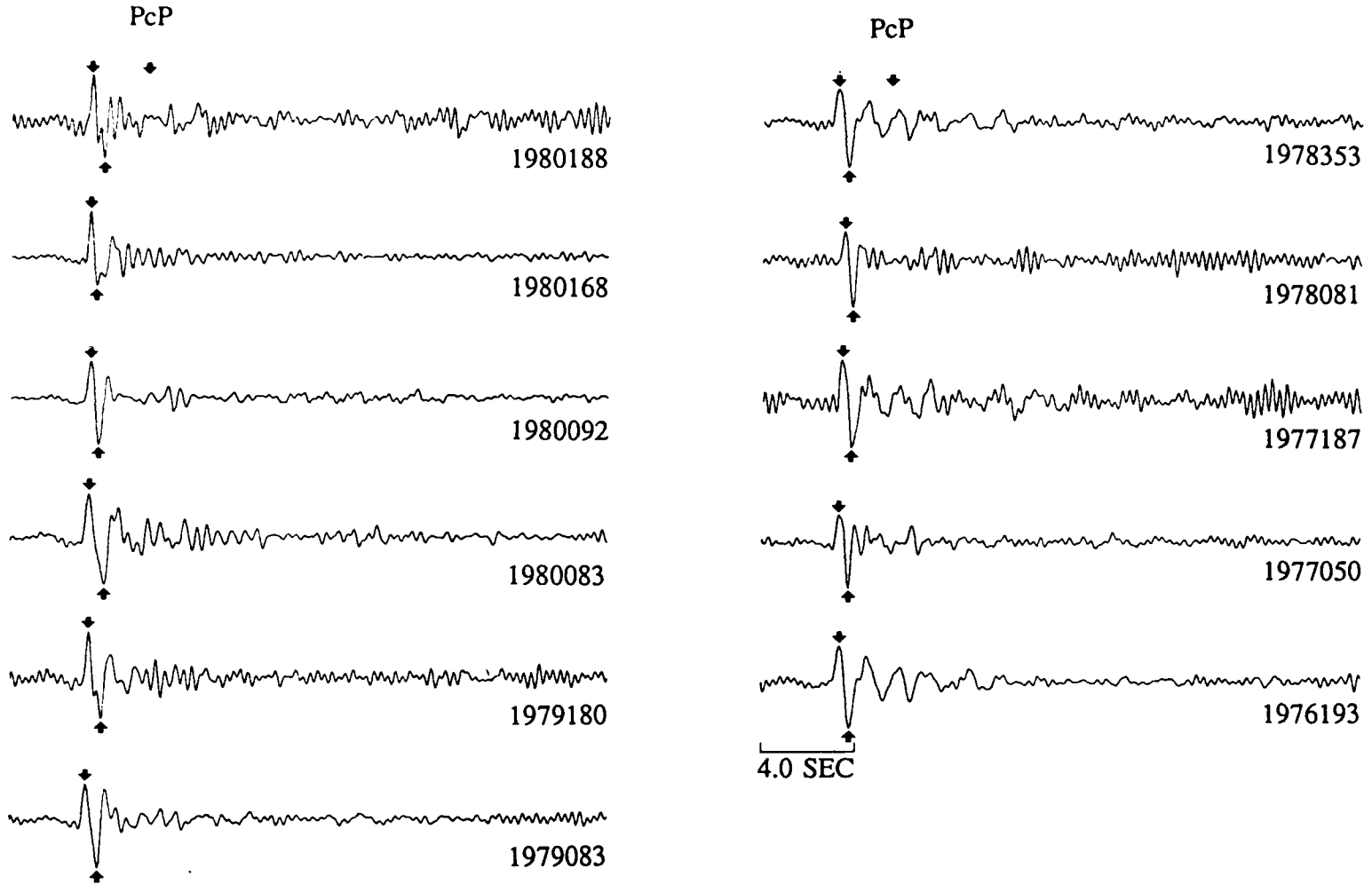

Figure 56. Deconvolved source functions for Tuamotu events recorded at YKA. The estimated VSB wavelet has been removed in the deconvolutions. The predicted PcP arrival time is also shown.

Deconvolved Source Functions
Tuamotu Events Recorded RSTN

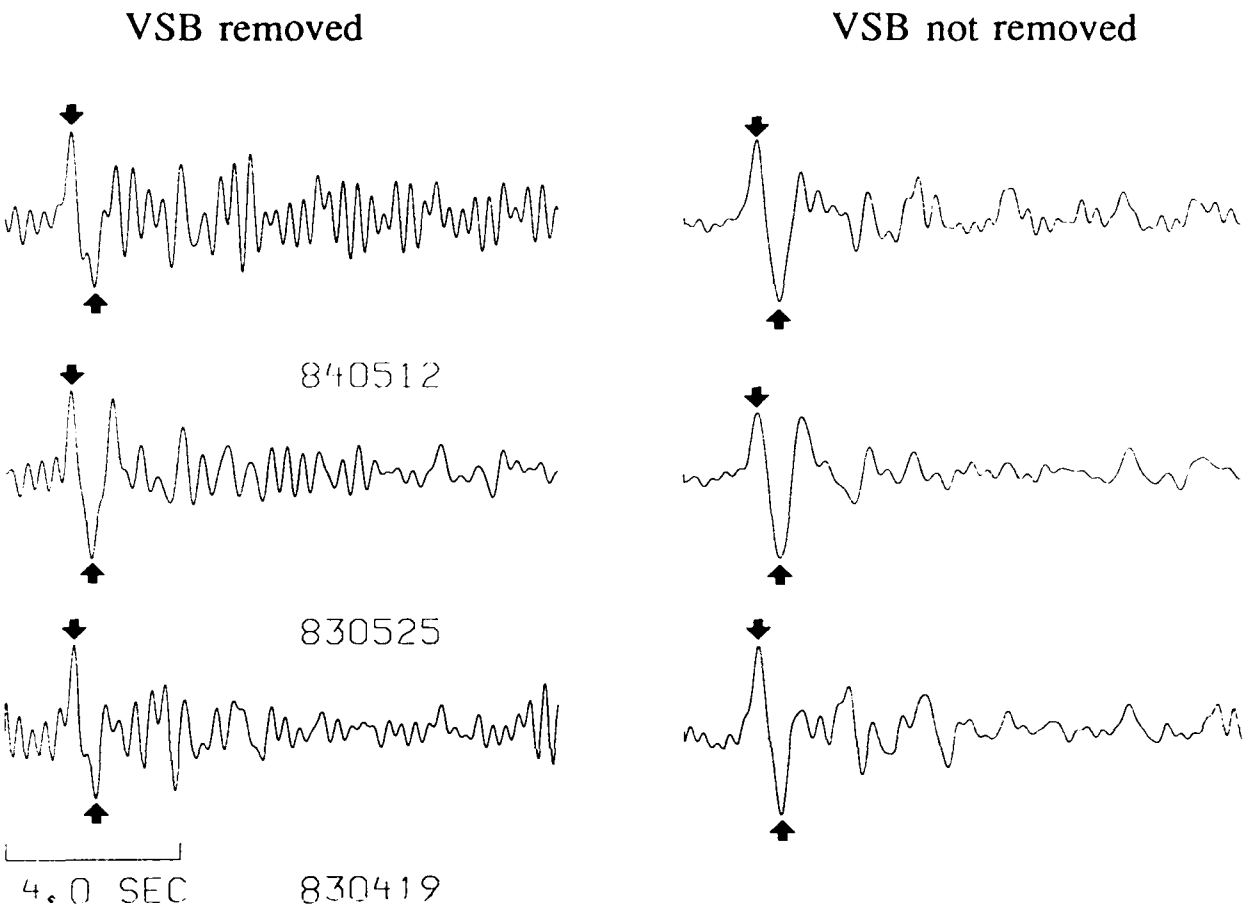

Figure 57. Deconvolved source functions for Tuamotu events recorded at the RSTN. To the left, the estimated VSB wavelet has been removed in the deconvolutions, while it has not been removed from the deconvolutions shown on the right.

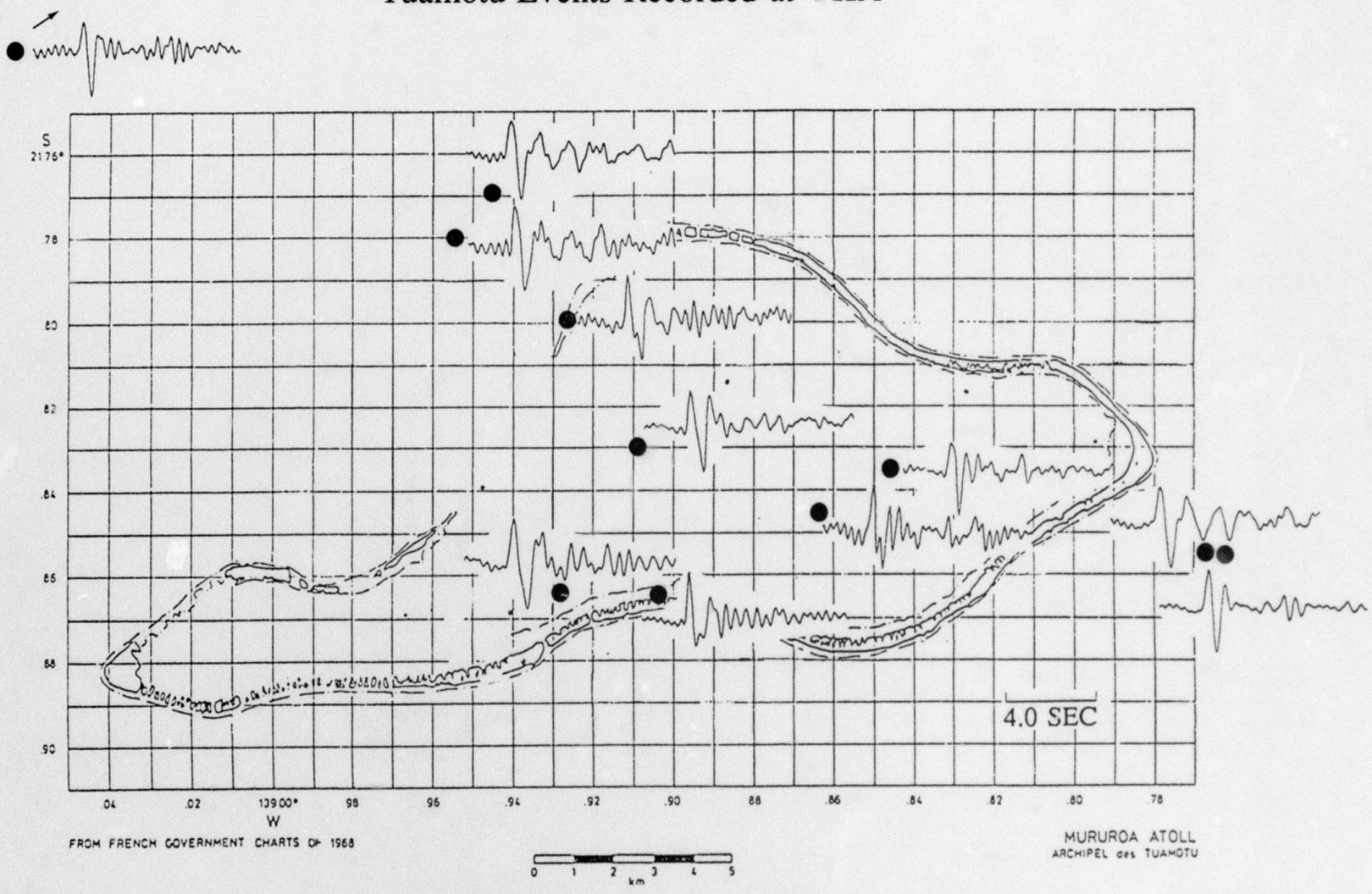

Figure 58. Deconvolved source functions for Tuamotu events recorded at YKA plotted on the map in Figure 53. The estimated VSB wavelet has been removed in the deconvolutions.

Deconvolved Source-Time Functions
Sinkiang Events recorded at the RSTN

3 Events and 2 Stations

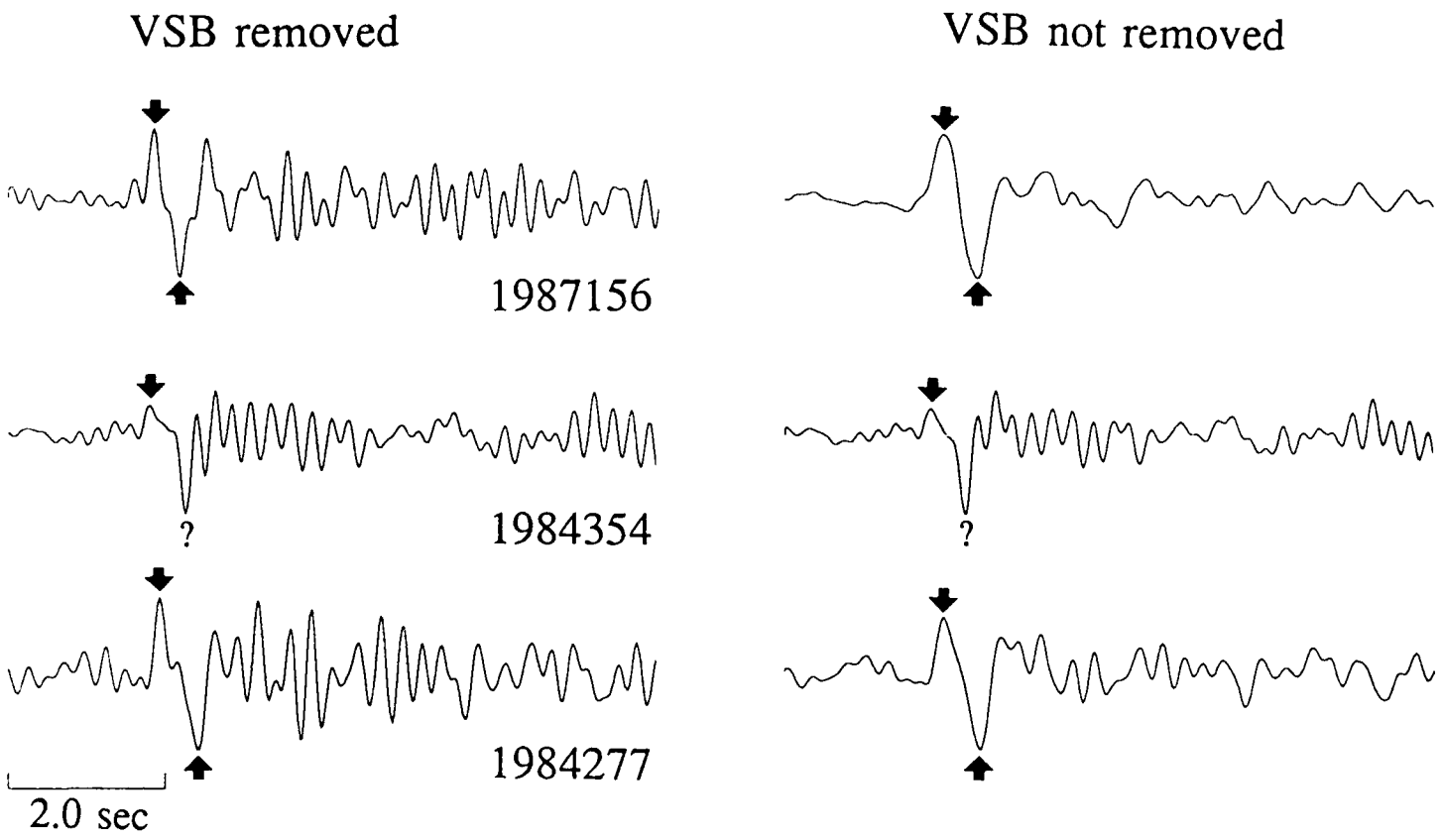

Figure 59. Deconvolved source functions for 3 Sinkiang events recorded at RSNT and RSSD. To the left, the VSB has been removed in the deconvolutions while it has not been removed in the deconvolutions on the right.

Deconvolved Source-Time Functions
Sinkiang Events recorded at the RSTN

2 Events and 3 Stations

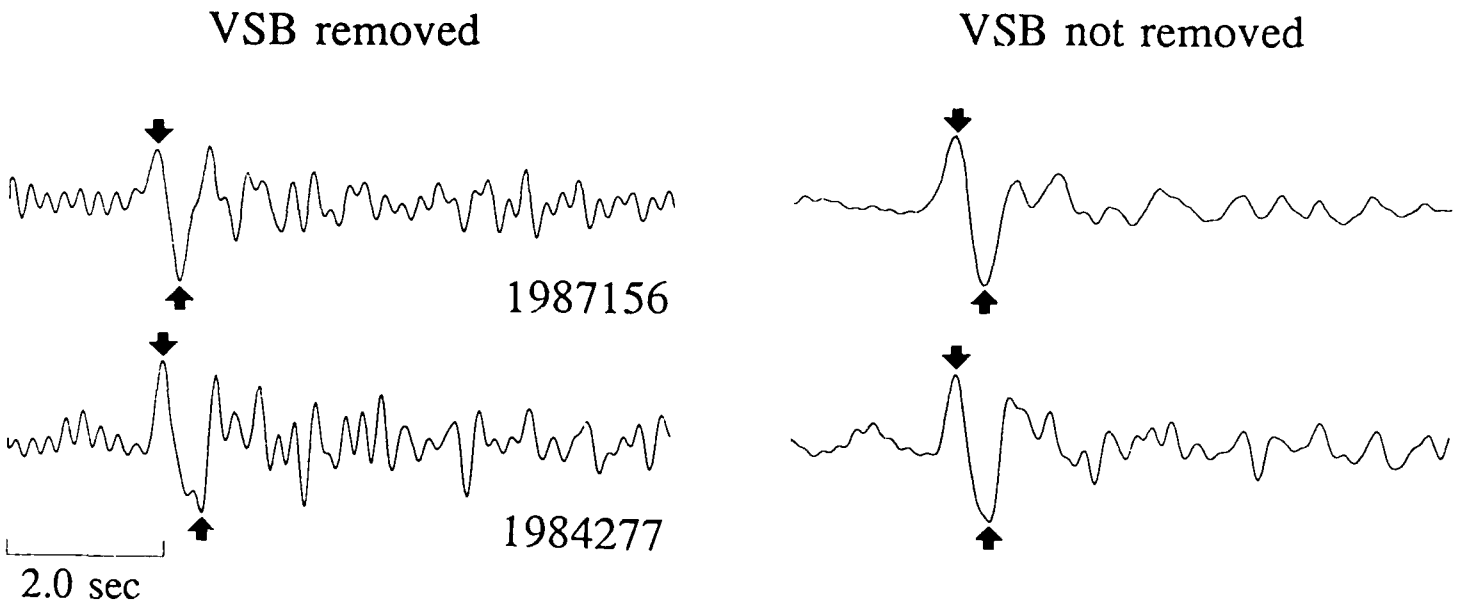

Figure 60. Deconvolved source functions for 2 Sinkiang events recorded at RSON, RSNT, and RSSD. To the left, the VSB has been removed in the deconvolutions while it has not been removed in the deconvolutions on the right.

determine), there are only minor changes in the waveforms, again indicating the robustness of the deconvolution procedure. All waveforms, whether or not the VSB is removed, appear to have a pP delay time of about 0.4 sec, which is somewhat curious given the variation in m_b between the events (4.7 to 6.3). Based on NEIS locations, the smallest of the three events (1984354) may have been detonated at a different test site than the other two events (McLaughlin *et al.* 1987c).

To assess the azimuthal source effects, we have included additional GDSN and SRO stations to perform joint deconvolutions. 2 SRO stations are available in addition to the 2 RSTN stations for the 3-event case as shown in Figure 61. The result of the joint deconvolution indicates very strong azimuthal source effects and scattering. The resolution of the source time for the smallest event 84354 is actually enhanced and worsen for the other two events. Better resemblance for the three source time functions is observed for the case when the vsb wavelet is not removed. For the 2-event case, in addition to the three RSTN stations, eight other GDSN and SRO stations are used to perform a joint deconvolution. The source-time functions are shown in Figure 62 and closely resemble those obtained earlier using 2 events and 3 stations indicating that the azimuthal source effects are not as strong in this case.

Pahute Mesa

Twelve Pahute Mesa events plus the shot Faultless were deconvolved at EKA, GBA, WRA, and YKA. A map of the relative locations of the events is shown in Figure 63 and deconvolved source functions, with the VSB source pulse removed, are shown in Figures 64 to 66. The deconvolutions of the Pahute Mesa events show a great deal of ringing and a relatively narrow bandwidth due to the low Q in the NTS region. Secondary arrivals are certainly present after the P arrival, but reliable pP phases cannot be picked for most of the events. The source function of Faultless deconvolved at EKA does not appear significantly different from

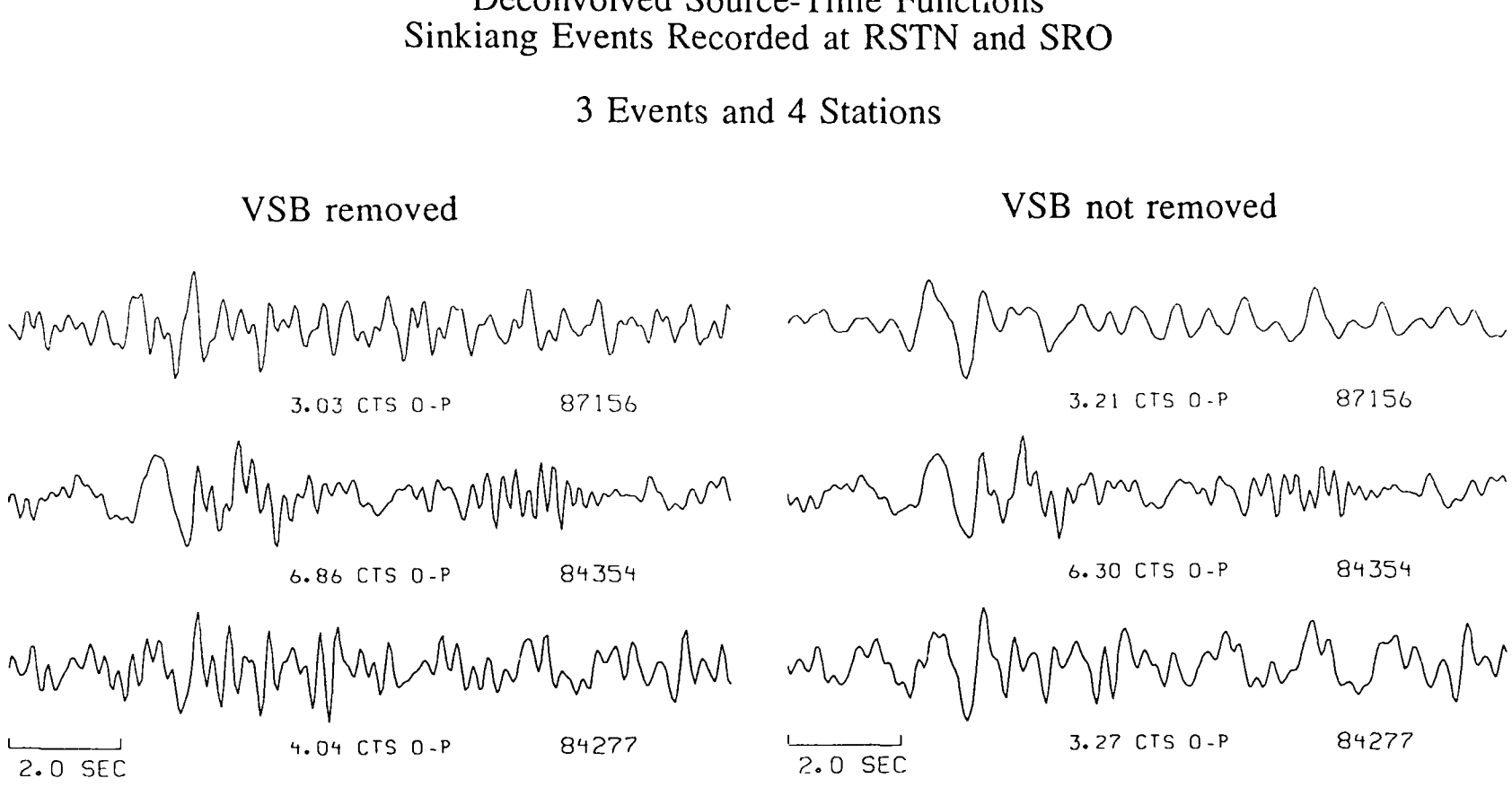

Figure 61. Deconvolved source functions for 3 Sinkiang events recorded at RSNT, RSSD, CHTO, and BCAO. To the left, the VSB has been removed in the deconvolutions while it has not been removed in the deconvolutions on the right.

Deconvolved Source-Time Functions
Sinkiang Events Recorded at RSTN and GDSN

2 Events and 11 Stations

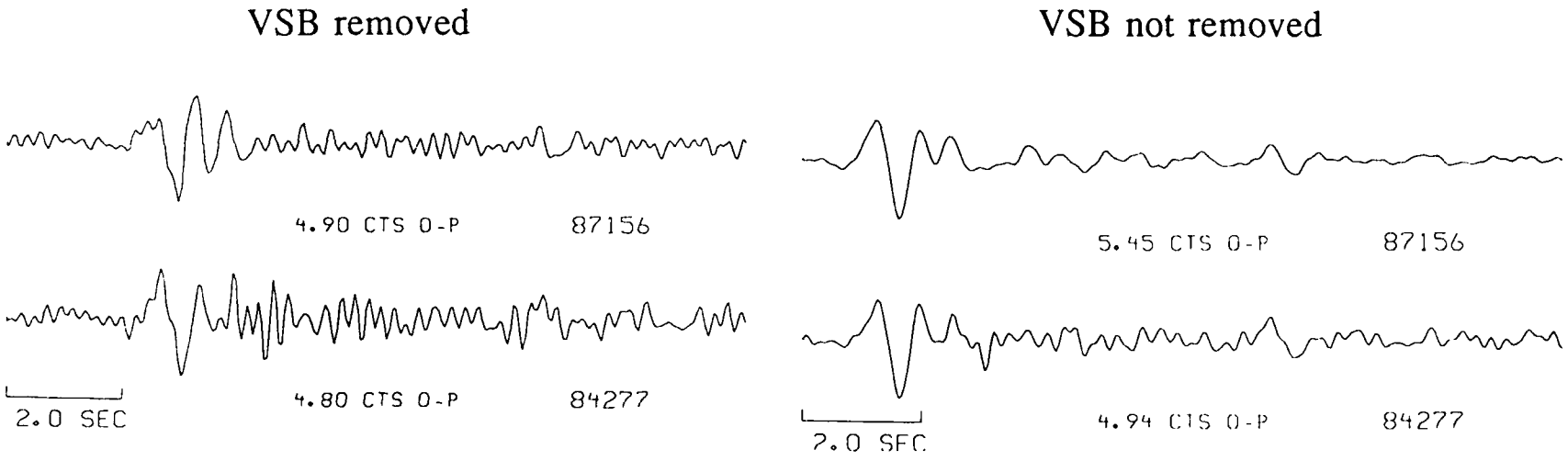

Figure 62. Deconvolved source functions for 2 Sinkiang events recorded at RSON, RSNT, RSSD, CTAO, COL, CHTO, BCAO, ANTO, KONO, KEV, and GRFO. To the left, the VSB has been removed in the deconvolutions while it has not been removed in the deconvolutions on the right.

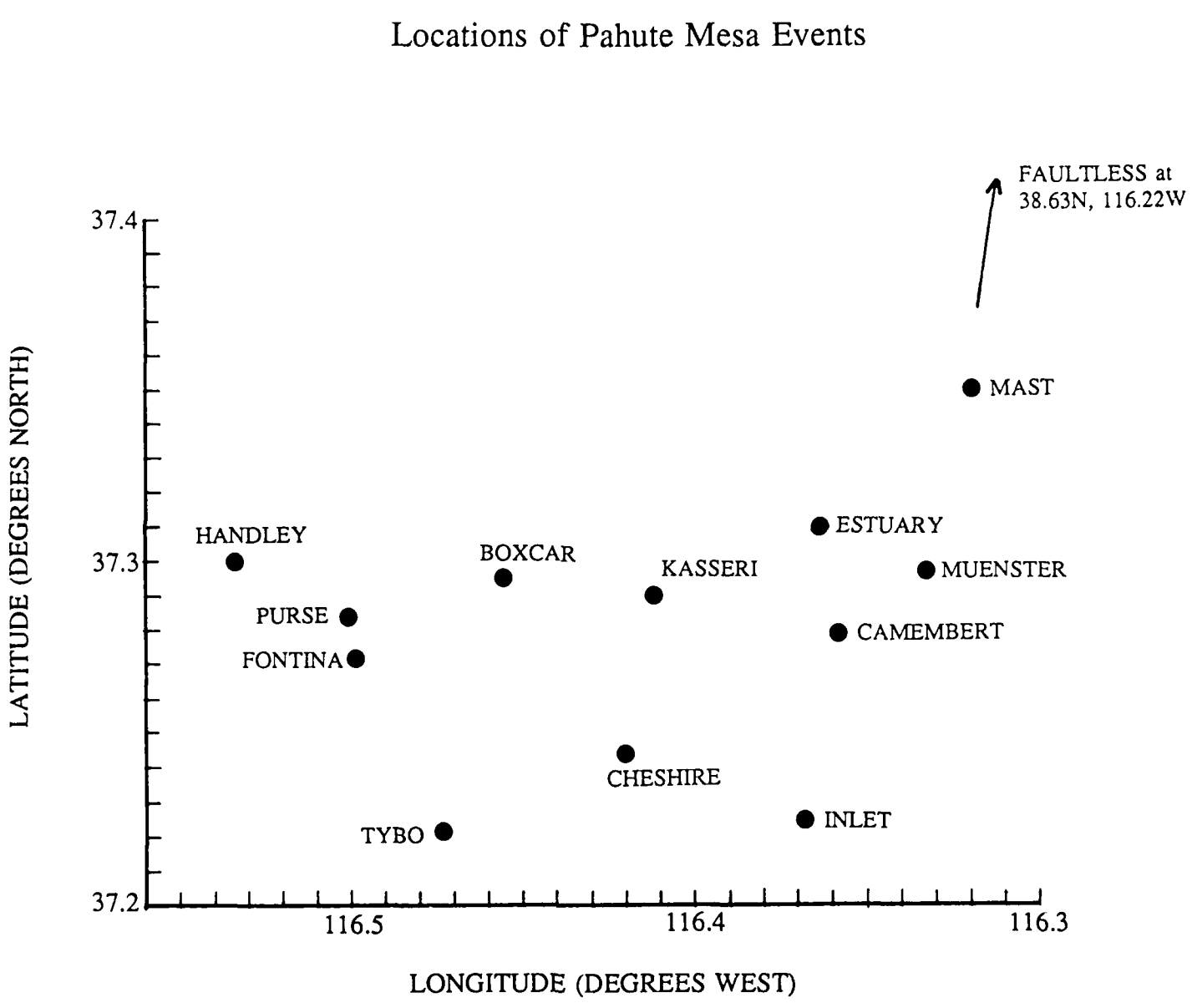

Figure 63. Locations of the Pahute Mesa events analyzed in this report.

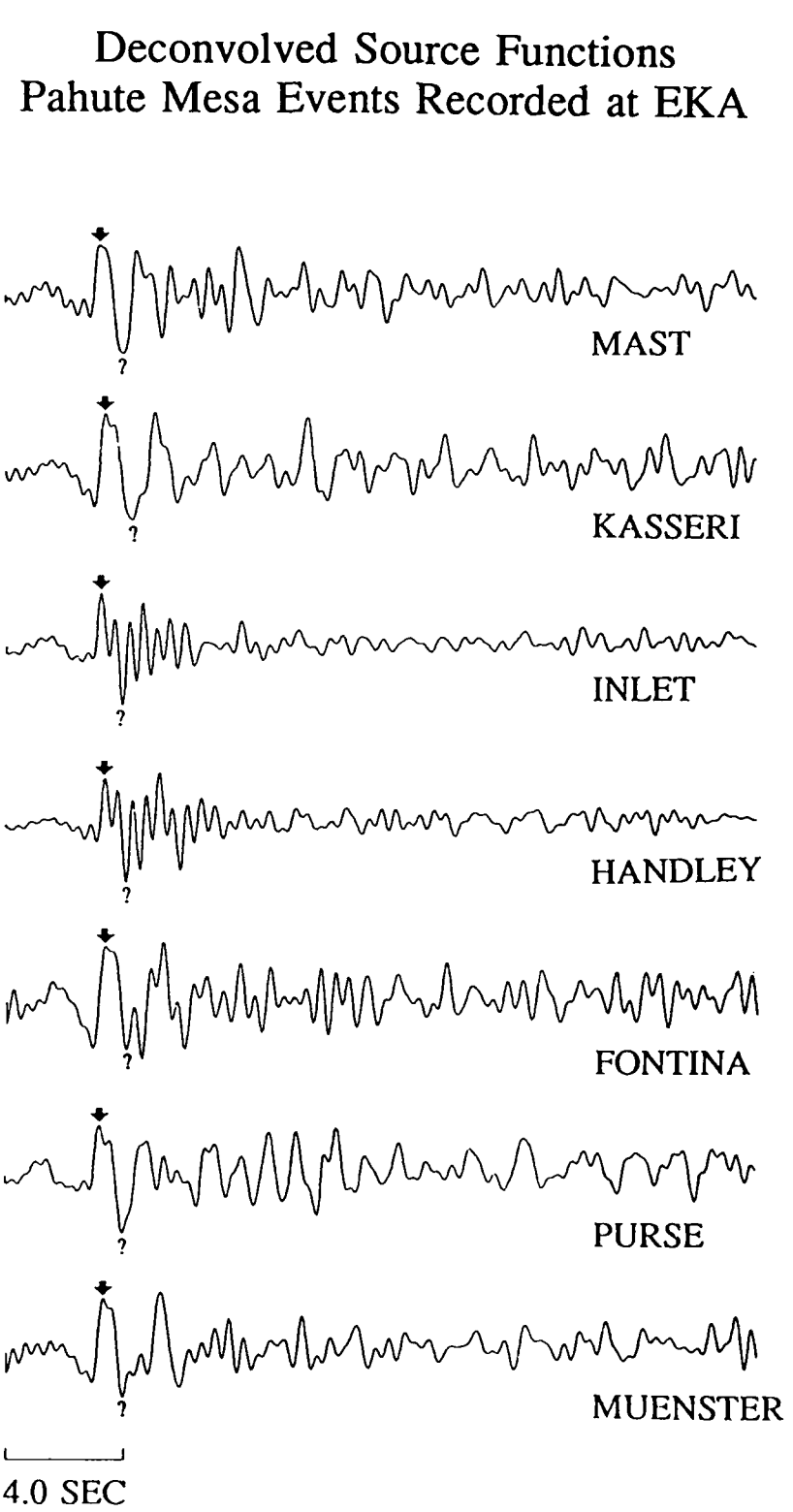

Figure 64. Source time function estimates for Pahute Mesa explosions recorded at EKA. VSB wavelets have been removed in these deconvolutions.

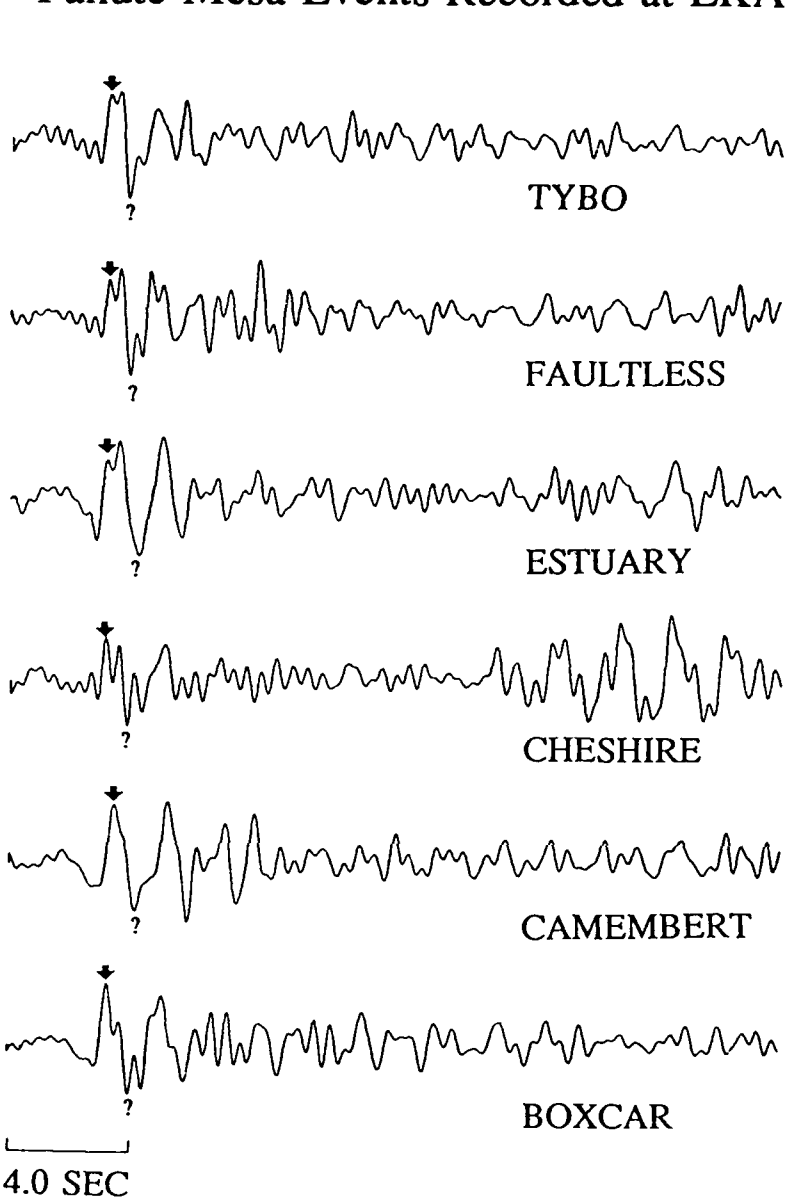

Figure 64 (cont'd)

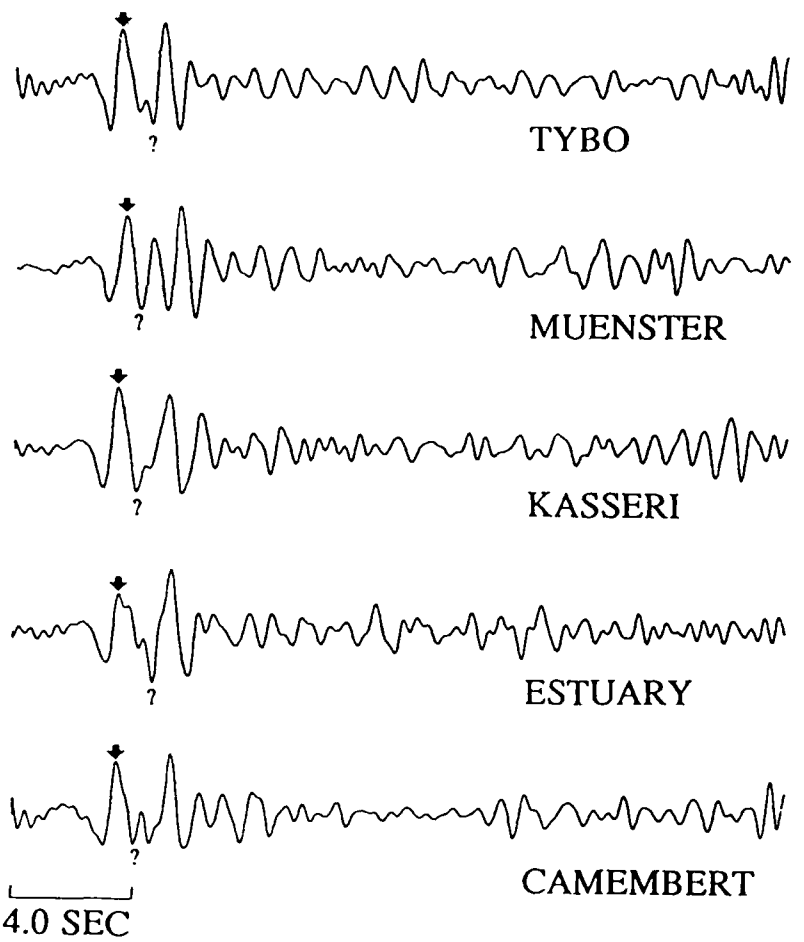

Figure 65. Source time function estimates for Pahute Mesa explosions recorded at GBA. VSB wavelets have been removed in these deconvolutions.

Deconvolved Source Functions
Pahute Mesa Events Recorded at WRA

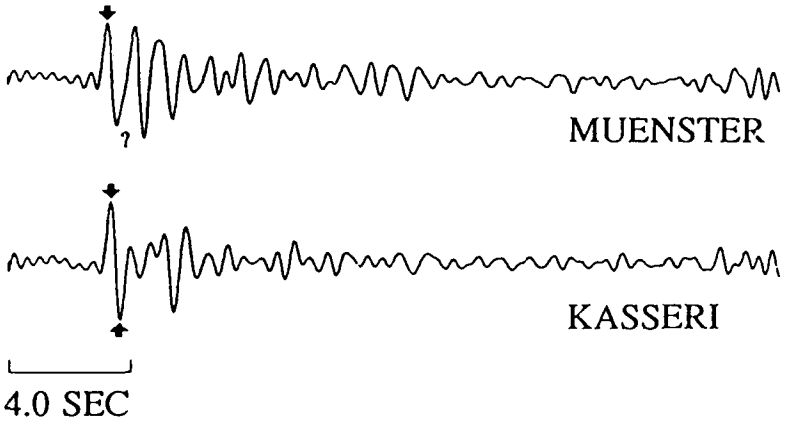

Figure 66. Source time function estimates for Pahute Mesa explosions recorded at WRA. VSB wavelets have been removed in these deconvolutions.

the deconvolved source functions of other large events at Pahute Mesa.

Figure 67 shows the deconvolved source time functions for events recorded at EKA plotted on a map of Pahute Mesa. As with the other test site, there are instances where events located near each other have similar source time functions. However, this is not always the case, and a peculiar pair of events is Handley and Inlet which are located at opposite sides of the test site yet have similar source time functions. With the possible exception of Cheshire, none of the other events have the high frequency content characteristic of Handley and Inlet.

Yucca Flats

Data for Yucca Flats events were available at three of the AWRE arrays: EKA, GBA, and YKA. The locations of the events are shown in Figure 68, and deconvolved source time functions with the VSB source pulse removed are shown in Figures 69 to 71. The recordings of Yucca Flats events exhibit complex waveforms and ringing at all arrays. This is commonly attributed to reverberations in the low velocity sediments at Yucca Flats (for finite difference simulations, see McLaughlin *et al.* 1987a). It appears that merely factoring out the instrument and t* operators is not sufficient and some deconvolution of the near source ringing would have to be introduced. The waveforms at YKA are also triplicated by upper mantle discontinuities. The late, ringing wavetrain about 12 seconds after the first arrival in many of the waveforms in Figure 71 is probably due to the forward branch associated with the 600 km discontinuity. Tentative picks for some "pP" arrivals for Yucca Flats show them to be quite late, but the ringing makes such picks doubtful. Since NTS is a low Q site (Der *et al.* 1982, 1985a) we have a very limited bandwidth to work with at teleseismic distances. The trace reconstructions for the Yucca Flats events are good reproductions of the original traces (Figure 72).

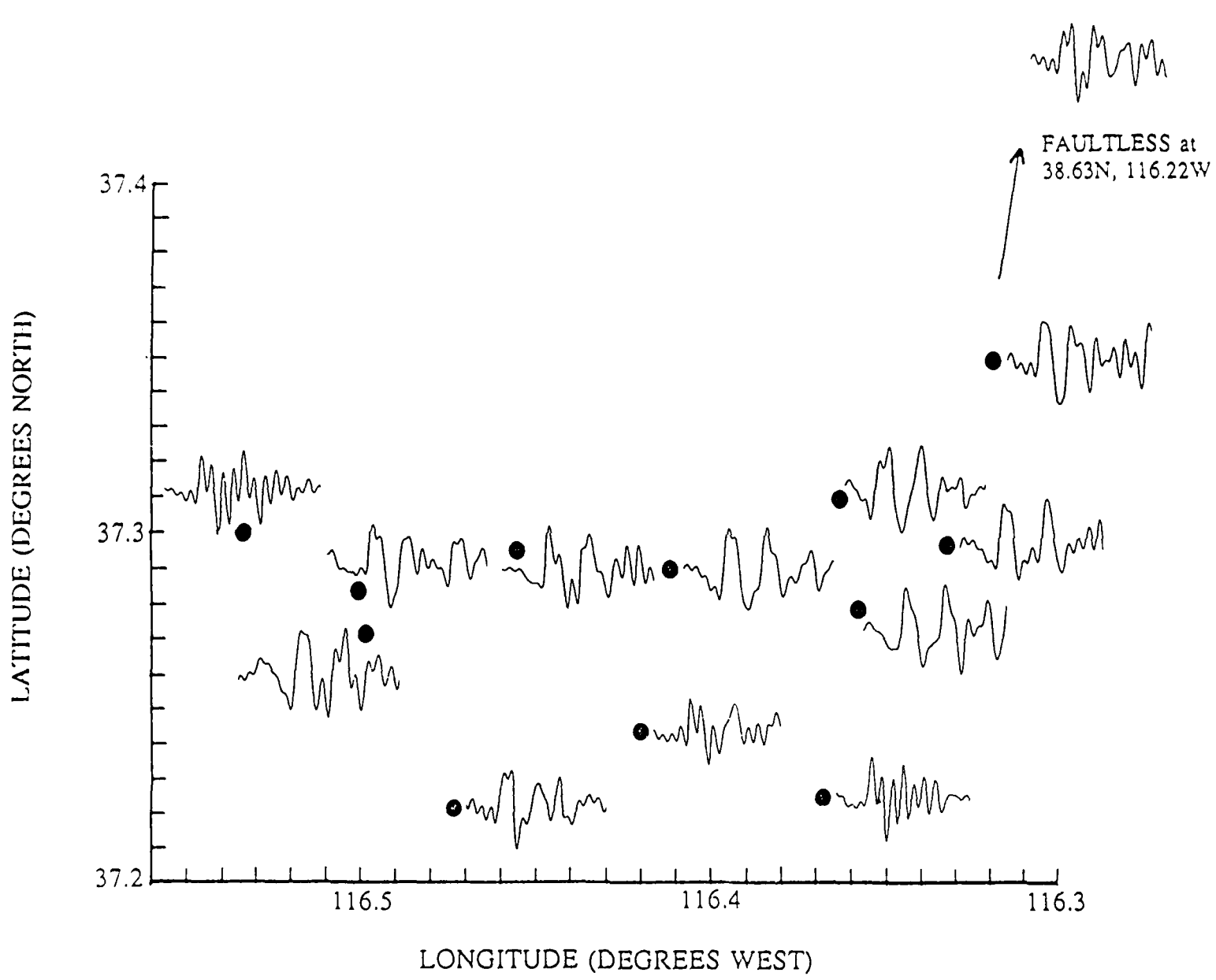

Figure 67. Deconvolved source functions for Pahute Mesa events recorded at EKA plotted on the map in Figure 63. The estimated VSB wavelet has been removed in the deconvolutions.

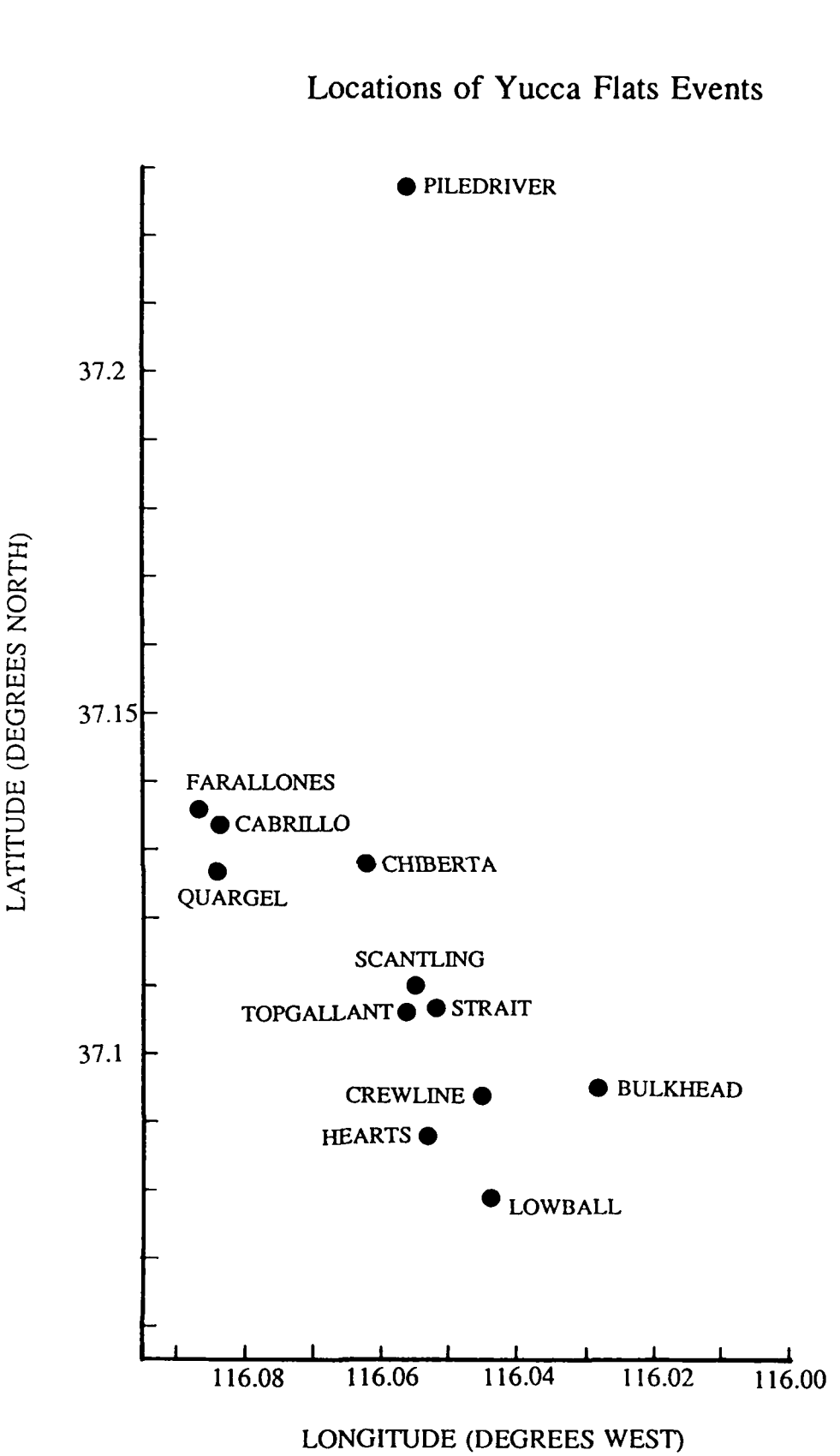

Figure 68. Locations of the Yucca Flats events analyzed in this report.

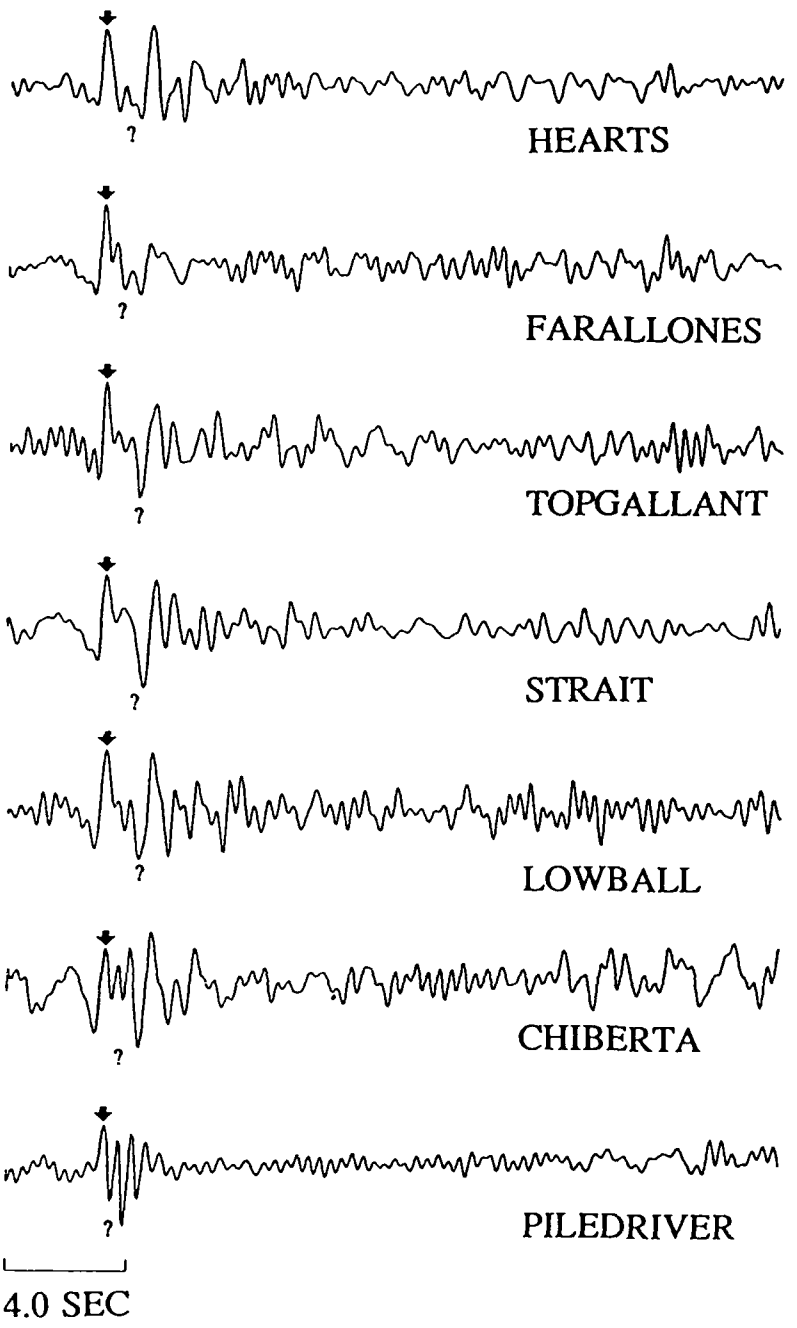

Figure 69. Source time function estimates for a set of Yucca Flats events recorded at EKA. VSB wavelets have been removed in these deconvolutions. The explosion Piledriver (north of Yucca Flats) shows a simpler waveform without the ringing associated with Yucca Flats events.

Deconvolved Source Functions
Yucca Flats Events Recorded at GBA

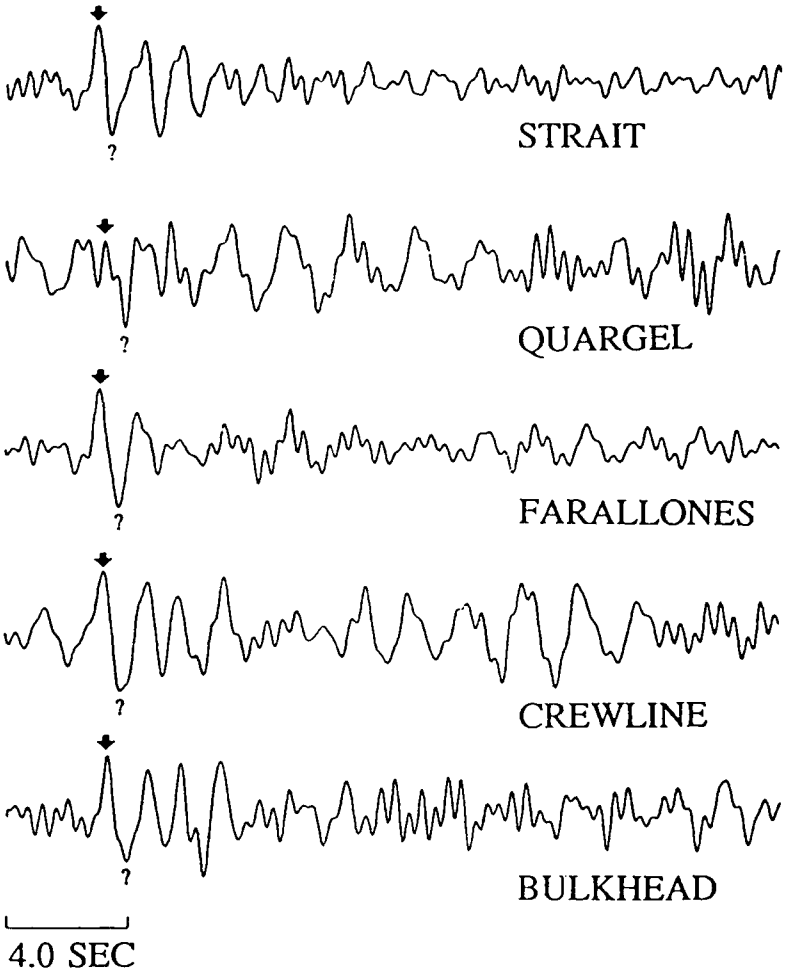

Figure 70. Source time function estimates for a set of Yucca Flats events recorded at GBA. VSB wavelets have been removed in these deconvolutions.

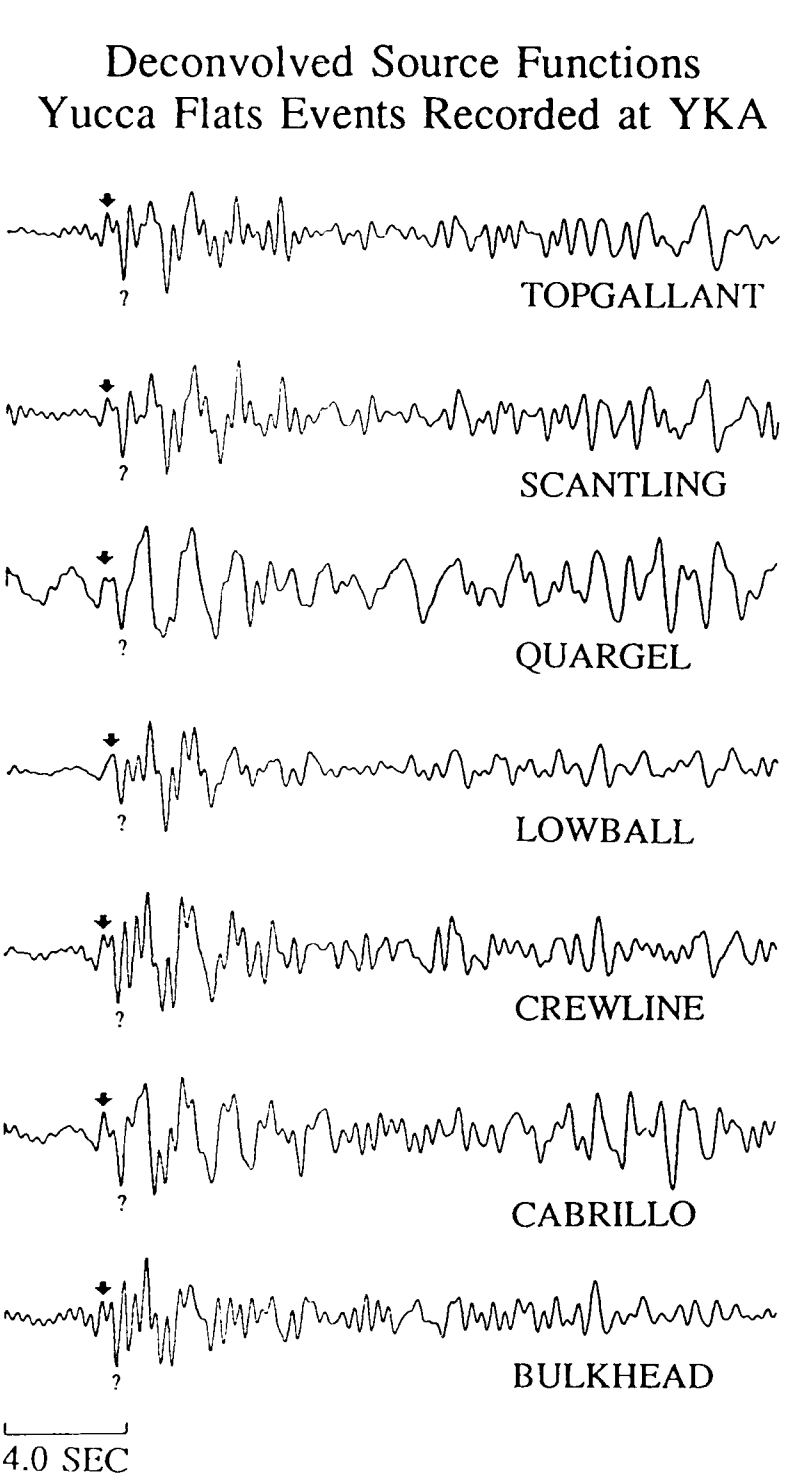

Figure 71. Source time function estimates for Yucca Flats events recorded at YKA. The second set of arrivals is an upper mantle triplication. VSB wavelets have been removed in these deconvolutions.

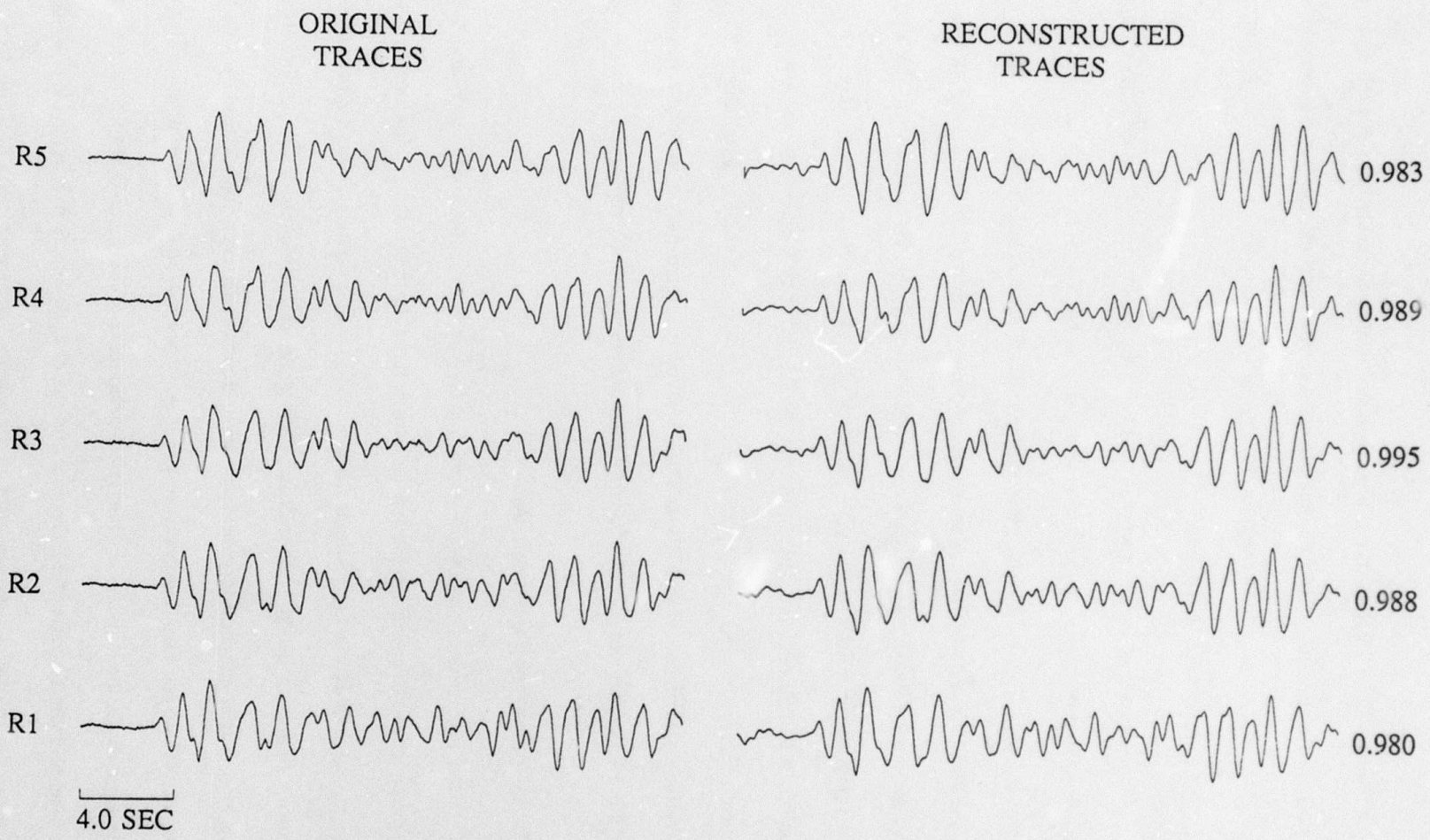

Figure 72. Examples of trace reconstructions (for event Cabrillo) at YKA as compared to original traces.

Figures 73 to 75 show the source time functions from recordings at each array plotted on a map of the test site. Even though there are much variation between the waveforms among each site, some similarities exist for some nearby events, for example, Topgallant and Strait recorded at both YKA and EKA.

The data set of events recorded at EKA (Figure 69) is particularly interesting in that it includes Piledriver, one of the few granite shots at NTS and an important calibration event in many studies. This event is not located at Yucca Flats but in a granite body north of it. Due to the short distance between Yucca Flats and the location of Piledriver, the recording site factors for Yucca Flats can also be expected to be applicable for Piledriver. The deconvolution for Piledriver is relatively simple compared to those for the Yucca Flats events. Piledriver exhibits a double negative peak following the first positive P-wave arrival. The first of these is timed appropriately for the expected pP, though it has a smaller amplitude than the second negative peak. Douglas and Rivers (1988) have interpreted the double negative peaks in terms of a non-isotropic component of energy release induced by the explosion.

Three-Component Teleseismic Data

The particle motions of teleseismic body waves are only linear for P and S in the first approximation. Even for simple layered structure of the crust, the motion becomes elliptical in the most complex manner (Su and Dorman 1965) with prograde and retrograde motions in the various frequency bands. For realistic, three dimensional models of the near-receiver geology, the motion becomes truly complex and three dimensional even for supposedly simple, linear P waves. While the first few cycles of the P wave are reasonably linear-elliptical in the plane of the azimuth of the arrival, the transverse component quickly builds up with time, approaching to a respectable fraction of the vertical and radial components in energy. It is a logical extension of the deconvolution work on multiple sites to approach the problem by treating each

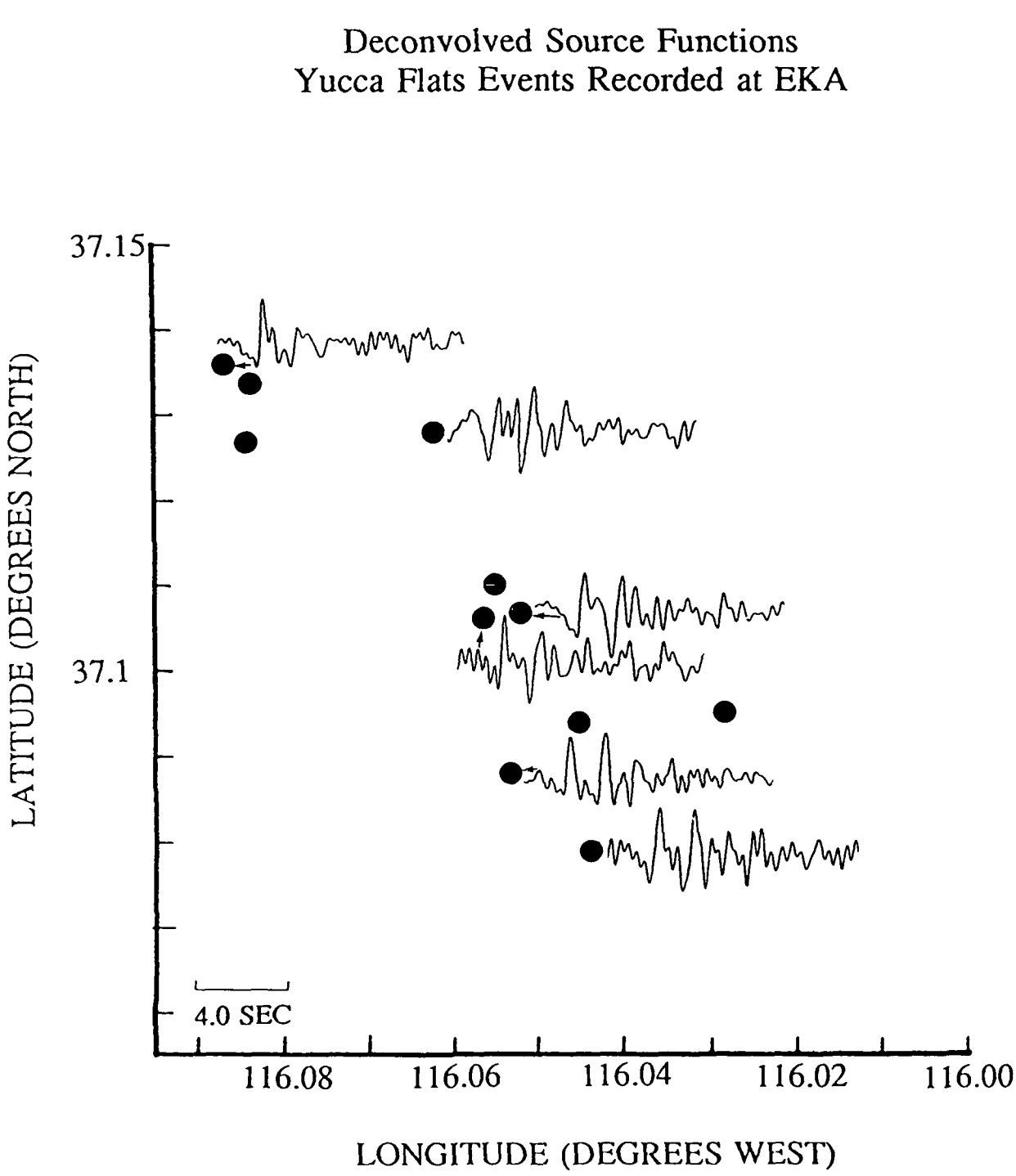

Figure 73. Deconvolved source functions for Yucca Flats events recorded at EKA plotted on the map in Figure 68. The estimated VSB wavelet has been removed in the deconvolutions.

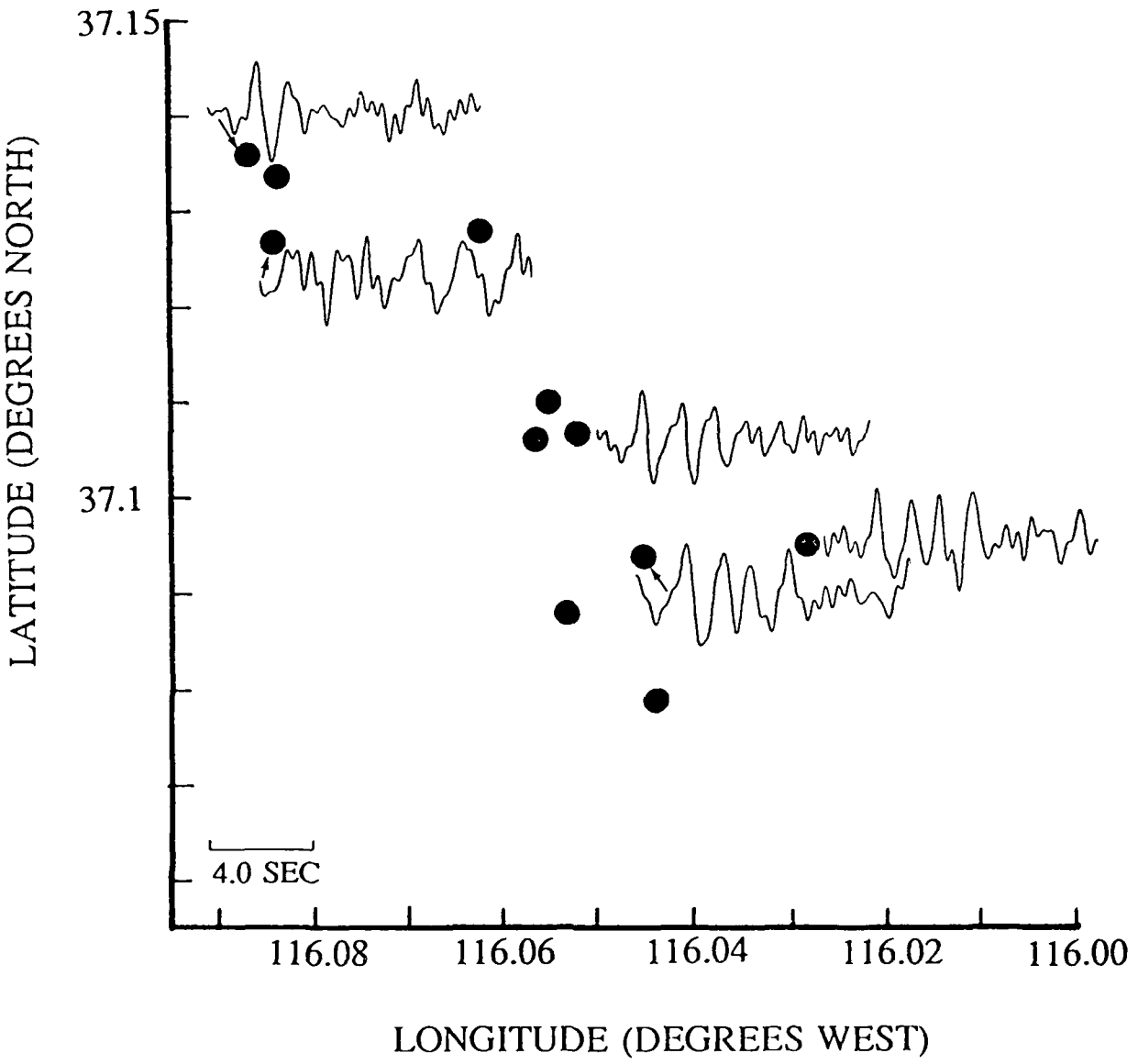

Figure 74. Deconvolved source functions for Yucca Flats events recorded at GBA plotted on the map in Figure 68. The estimated VSB wavelet has been removed in the deconvolutions.

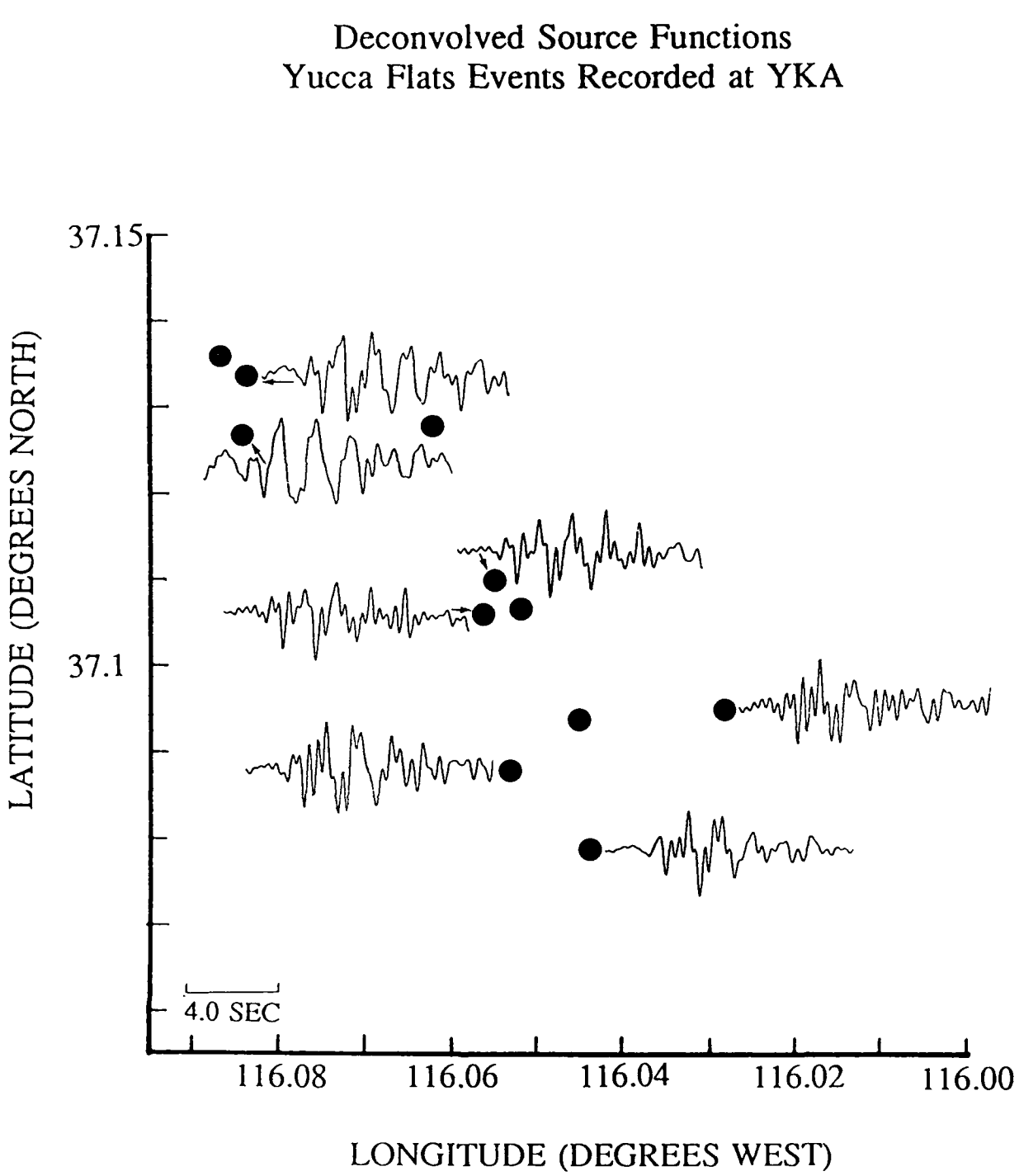

Figure 75. Deconvolved source functions for Yucca Flats events recorded at YKA plotted on the map in Figure 68. The estimated VSB wavelet has been removed in the deconvolutions.

component of motion as a separate "site" in the deconvolution process. Each component will have a "site factor" in the frequency domain which characterizes the transformation of the motion due to local geology, these factors will depend, of course, on the slowness vector (azimuth-distance) of the P arrivals and may thus be used to recognize or characterize source regions of P waves.

The approach developed here is fundamentally different from practically all of the 3-component processing work being done recently (Christofferson *et al.* 1986, Harris 1981). Instead of assuming a simply polarized wave appropriate to a halfspace, we plan to utilize the particle motion as it is, with all its complexities. A knowledge base of such characteristics may be accumulated observationally for a large number of source areas, without the need for understanding the detailed mechanism of the generation of complex particle motion. Although such an approach may be less practical presently, advances of computer technology will make it quite feasible to store such information. We believe that source regions may be identified quickly and automatically by recognizing patterns of 3-component site factors rather than computing back-azimuths based on simplistic assumptions about polarization patterns. Any systematic deviations between the true azimuths and the back azimuths can be automatically accounted for in such schemes, as long as the master events used to derive the 3-component "site" factors are accurately located (possibly independently).

To test such concepts we have assembled a data base of four master events at the Kazakh test site as recorded at the RSTN station network. The deconvolved source time functions appear to be quite simple for these, mainly consisting of P and (presumably) pP arrivals as marked (Figure 76). The site impulse responses tend to be the most complex on the transverse components building up gradually with time, as expected, but simpler and impulse-like on the vertical and radial components (Figure 77). Nevertheless, all the component "site" time func-

Deconvolved Source Functions

Shagan Events Recorded at 3-Component RSTN Stations

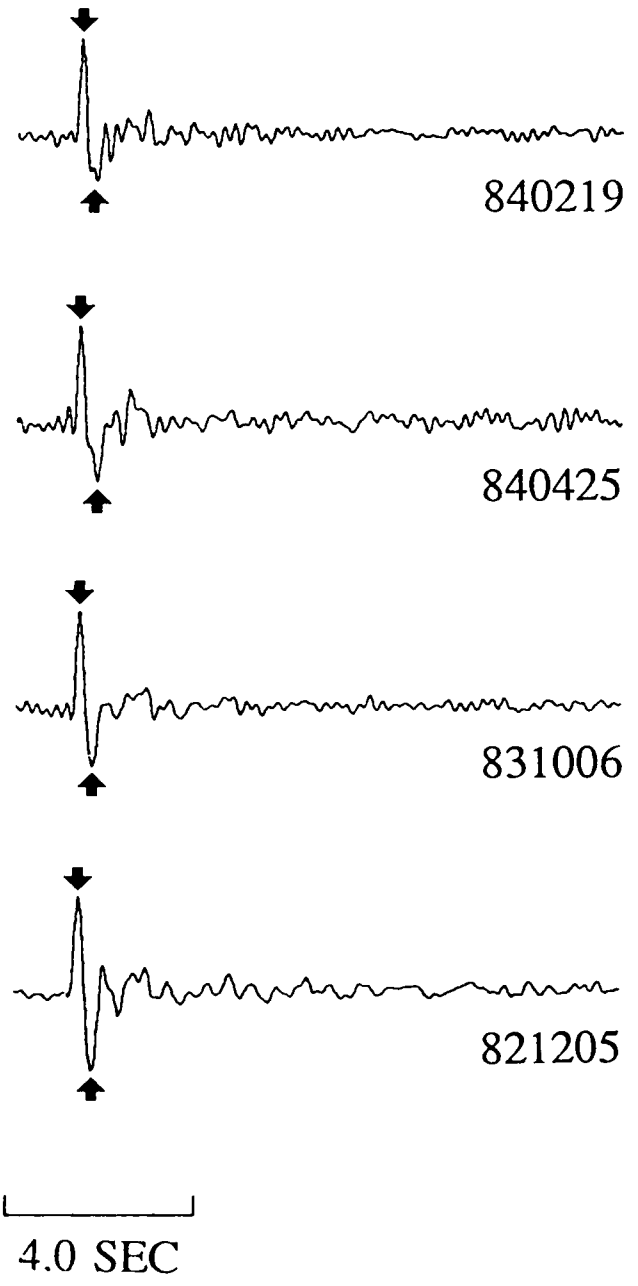

Figure 76. Source time function estimates for four Shagan events obtained from the total data set from RSTN three component recordings. VSB wavelets have been removed in these deconvolutions. All of these show the prominent "pP" arrival.

Deconvolved Site Functions

Shagan Events Recorded at 3-Component RSTN Stations

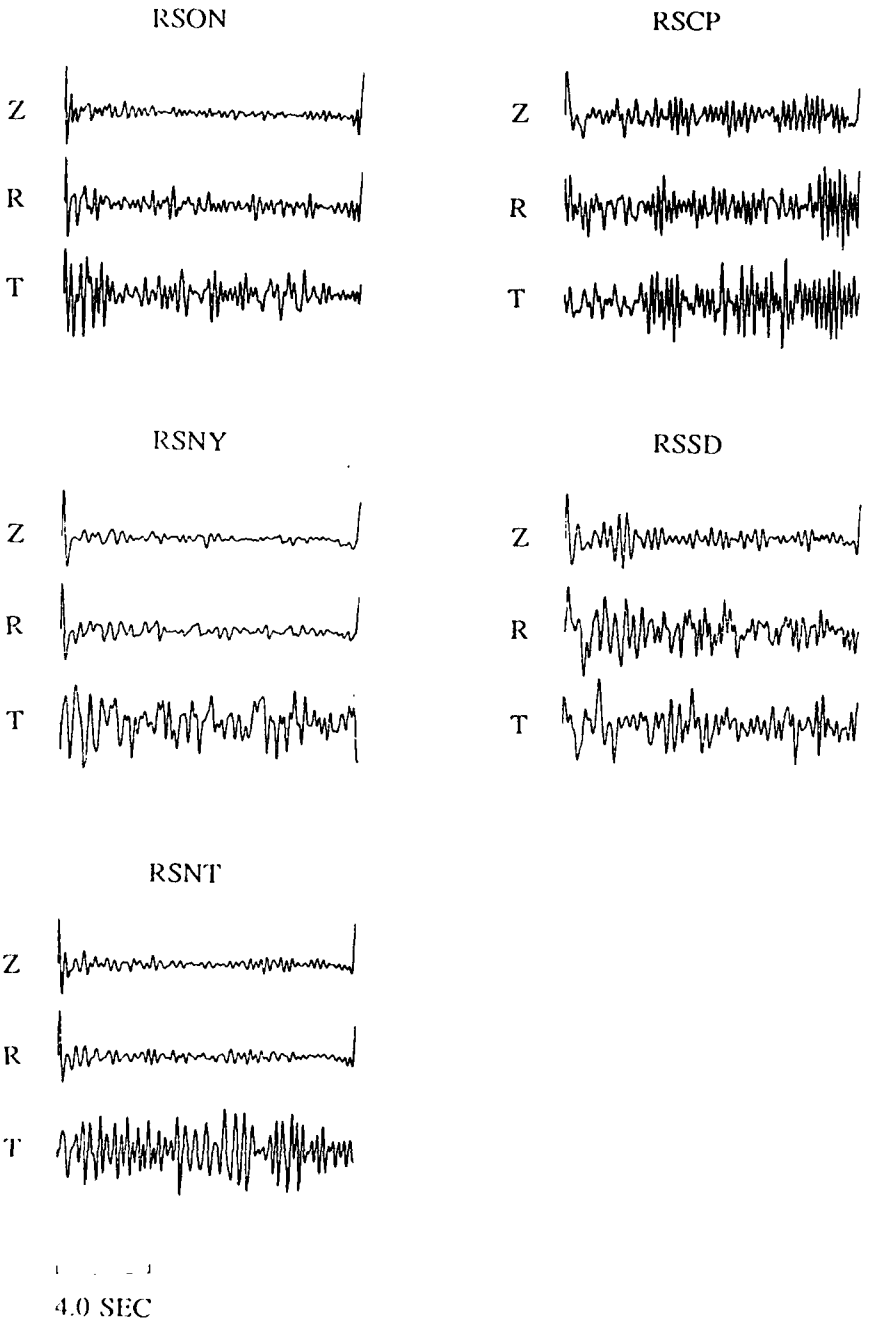

Figure 77. Site time function estimates for all components at the five RSTN stations from deconvolutions of Shagan events. The RSCP and RSSD site functions are considerably more complex than those for RSON, RSNY and RSNT. This may be due to more complex geological structures at the former stations.

tions seem to be much more complicated at RSCP and RSSD, two sites under which the geological structure have been shown to be complex by other studies (Owens *et al.* 1987). Some raw data traces of these events are shown in Figure 78, and opposing them, we show the trace reconstructions for easy comparison. The good similarity of the original and reconstructed traces show that the "site" approach works well for three component data despite the larger variation of the back azimuths from the source region compared to seismic arrays, and that the complexities in particle motion can be reliably characterized by "component-site" transfer functions.

Three-Component Regional Data

With the success of deconvolutions of three-component teleseismic data, we then attempted deconvolution of three-component regional data. The first example is a set of six Leningrad region mineblasts recorded at NORESS. Strictly speaking, at ~9°, these may not be regional events, but they are complex waveforms as seen in Figure 79 which shows original traces and reconstructions for one of the events. The excellent quality of the reconstructions shows that the deconvolution procedure is valid for regional signals. Figure 80 shows the deconvolved source time functions. Many of them exhibit a monochromatic ringing initial arrival which may be the result of a ripple fired sequence of events often used for mining explosions. For some of the events, the Pn is very emergent. Figure 81 shows a set of site terms for one of the three-component sensors at NORESS. These are quite similar to the three component site terms observed at the RSTN stations for the teleseismic Shagan events with impulsive vertical and radial components and a very noisy transverse component due to compressional wave scattering into the transverse component.

A set of earthquakes and mining explosions in southwestern Norway about 4° from NORESS were also deconvolved from arrivals recorded at NORESS. The source time

Original and Reconstructed Traces of

Shagan Event 1984050 Recorded at 3-Component RSTN Stations

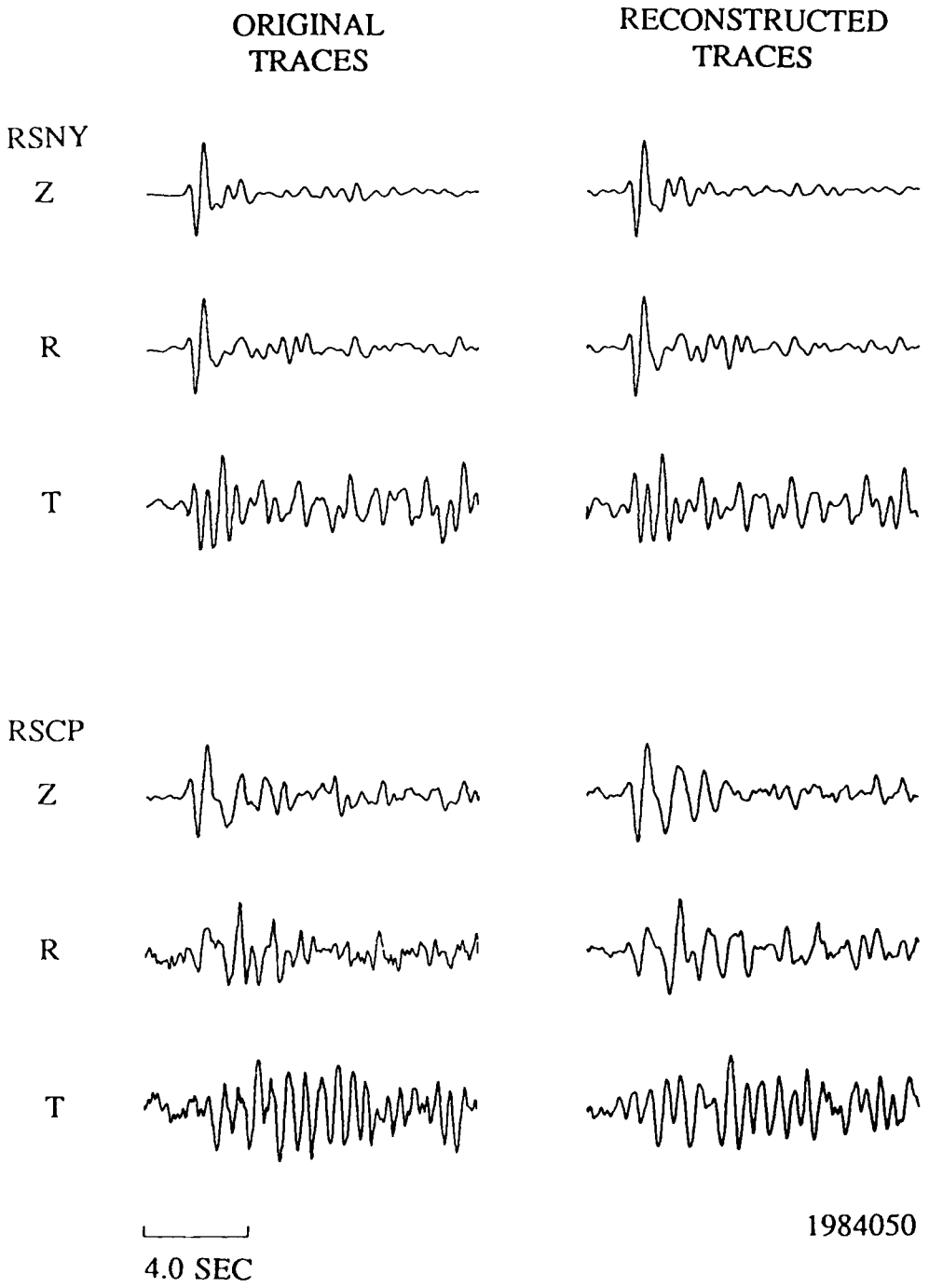

Figure 78. Original and reconstructed traces at three component RSTN stations for a Shagan event. These reconstructions are quite good considering the fact that the RSTN stations cover a wide area.

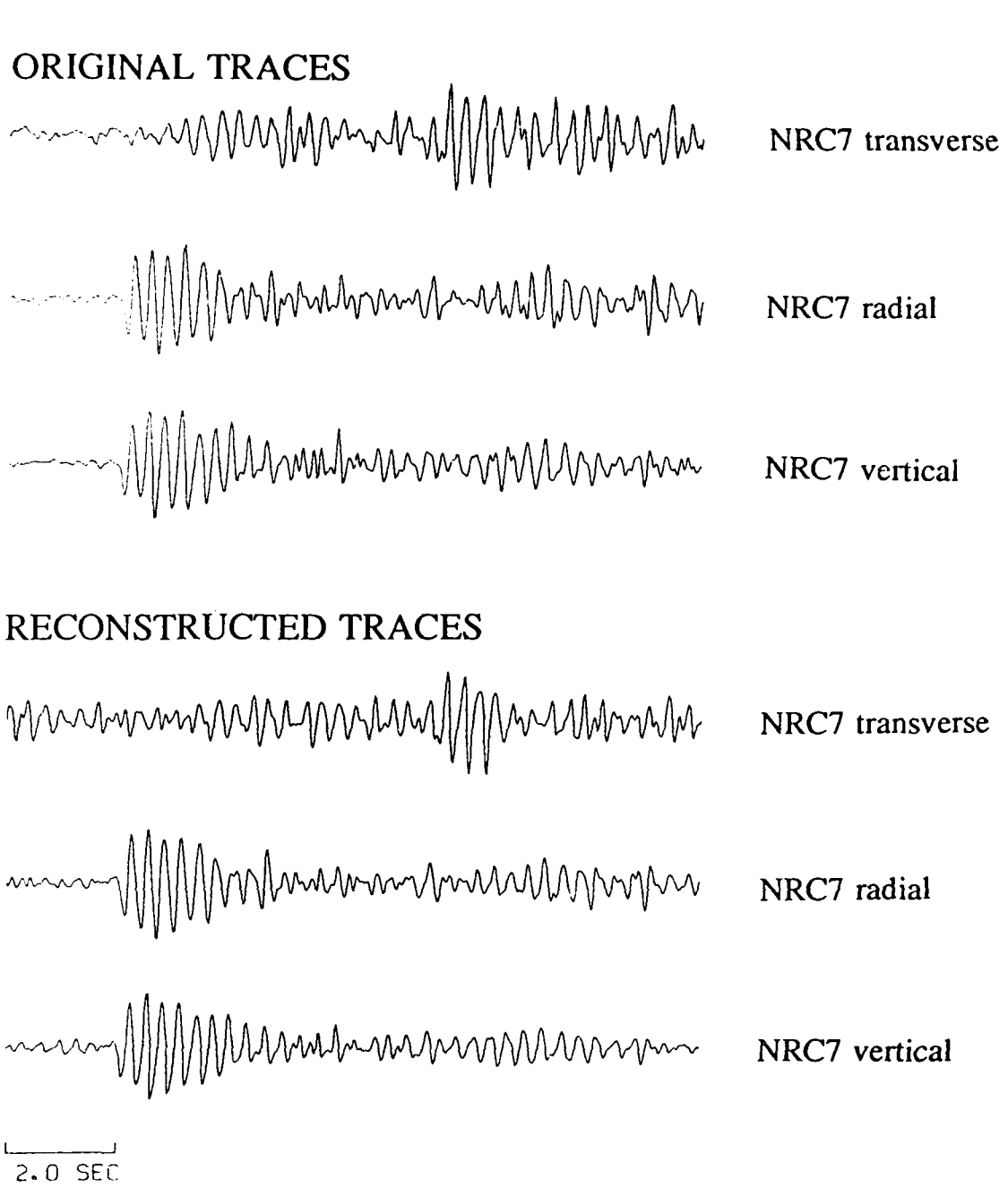

Figure 79. Examples of original and reconstructed three-component traces for the Leningrad region mineblast of 1986155 recorded at NORESS.

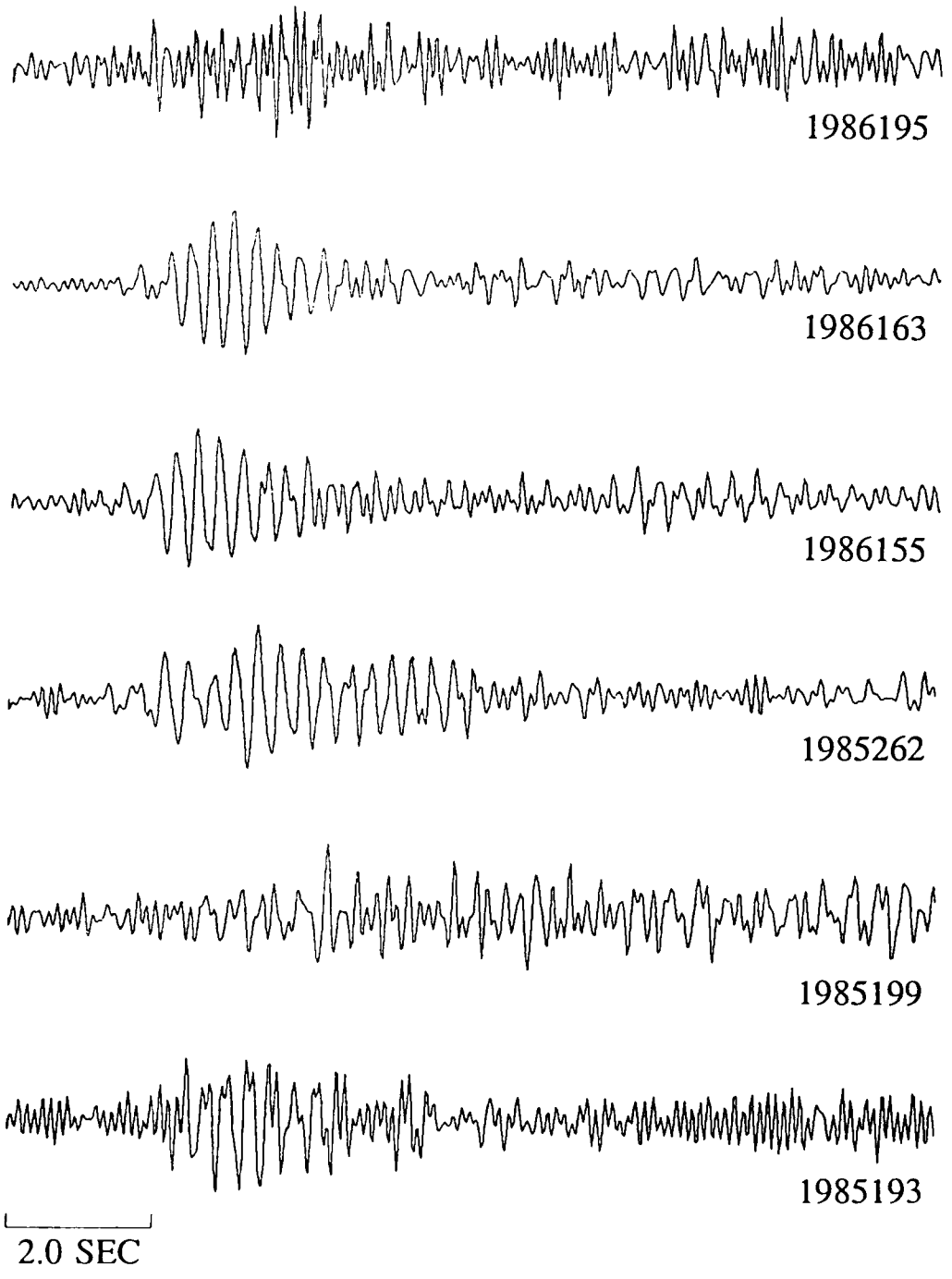

Figure 80. Deconvolved source time functions for six Leningrad region mineblasts recorded at NORESS. A VSB has not been removed in the deconvolution process.

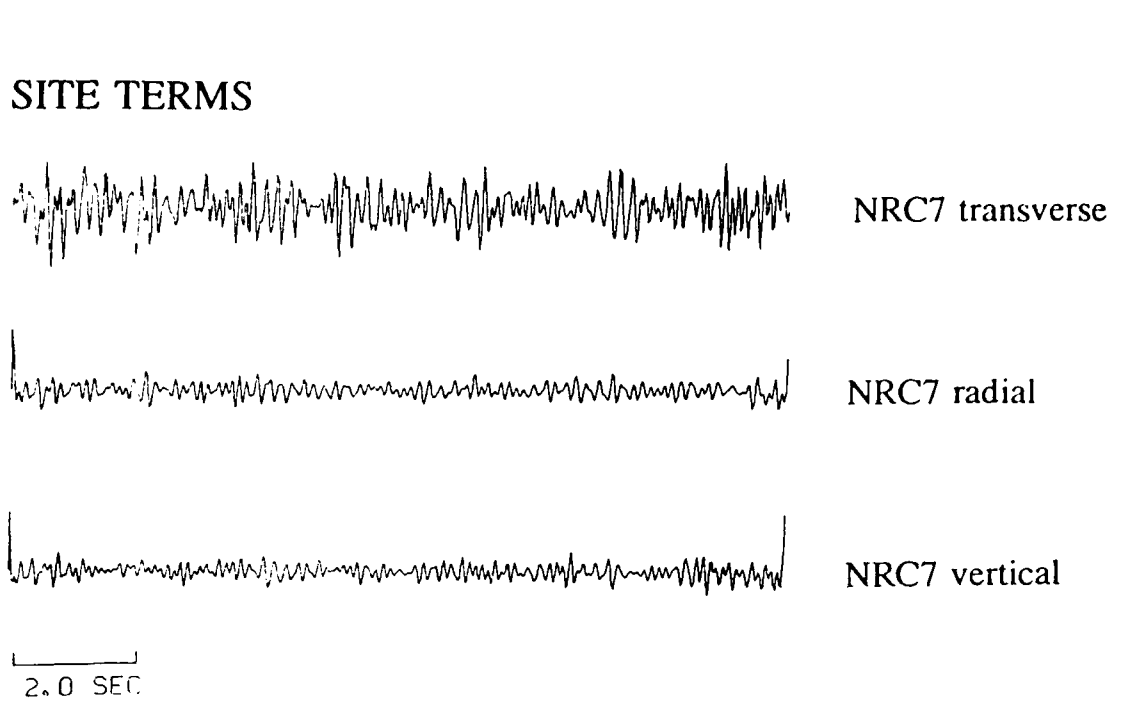

Figure 81. Examples of three-component site terms from deconvolutions of Leningrad region mineblasts recorded at NORESS.

functions are shown in Figure 82. Again, being regional arrivals, the initial P wave is much more complicated than in the teleseismic case. Two of the explosions in Figure 82 (1985317 and 1986017) have a higher frequency first arrival than do the earthquakes (1985324a-c). Some of the three-component NORESS site terms are shown in Figure 83 for these events. Again, the vertical and radial components have a large initial pulse followed by smaller arrivals which the transverse components are very noisy. Each site term has been normalized to its maximum amplitude so that the relative amplitudes between the site terms are not apparent in the figure.

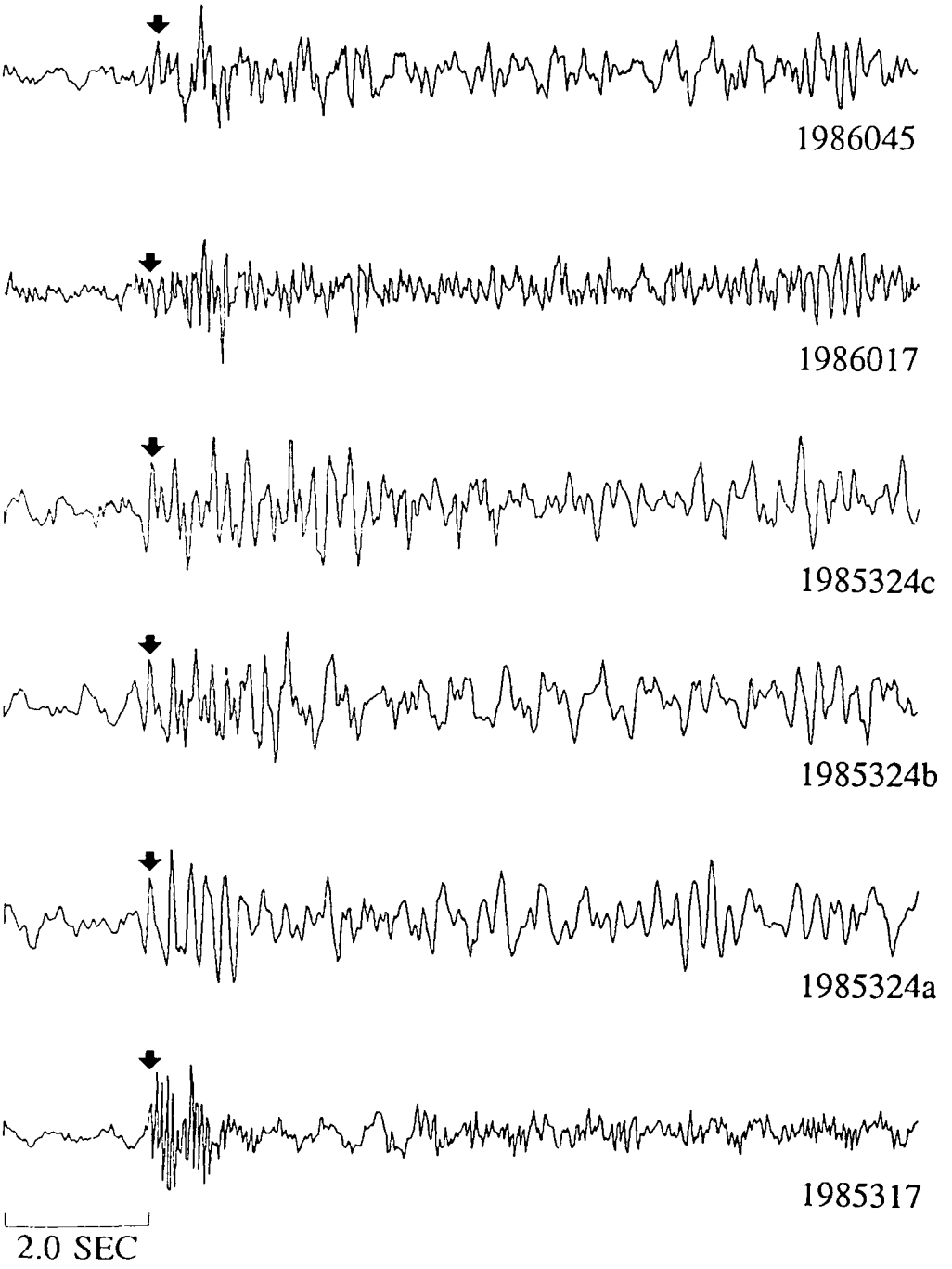

Figure 82. Deconvolved source time functions for six events from southwestern Norway recorded at NORESS. A VSB has not been removed in the deconvolution process. The three events of 1985324 are presumed earthquakes while the other three events are presumed explosions (mineblasts) (per Dysart 1986).

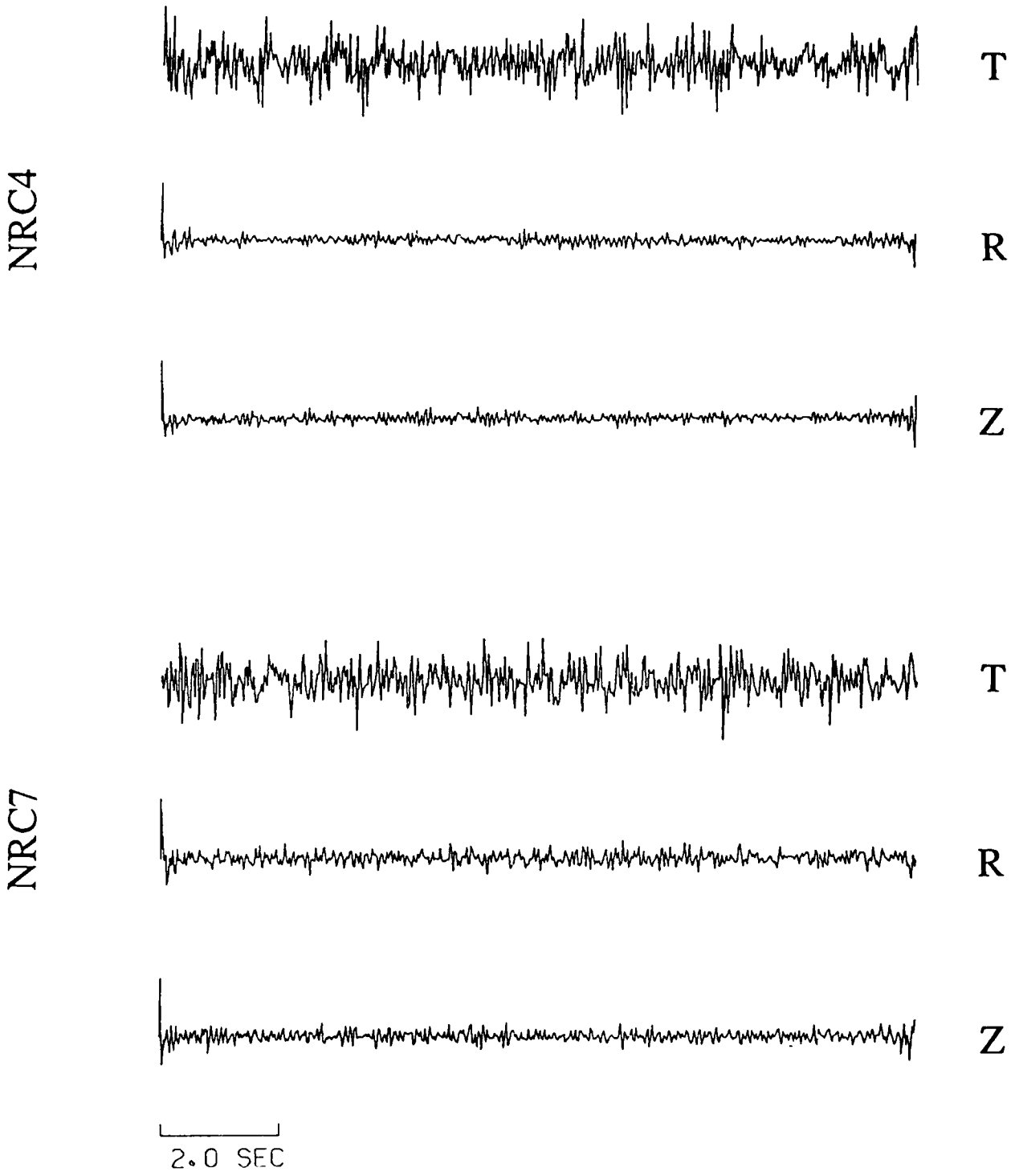

Figure 83. Deconvolved site terms at two fo the three-component sensors at NORESS, C4 and C7, for regional events ~4° to the southwest of NORESS. For each sensor, the site terms for the vertical (Z), radial (R), and transverse (T) components are shown.

DECONVOLUTIONS FOR DIFFERENT RECEIVER REGIONS

It is interesting to look briefly at the variations in site terms with azimuth. Figures 84 to 87 give some examples of site terms at various azimuths from deconvolutions of recordings at YKA, EKA, and NORESS. Generally, the differences in a given site terms with azimuth are much more apparent than any similarities. A more realistic way to look at these site terms would be to filter them with a wavelet consisting of a VSB, t*, and instrument response as was shown in Figure 2. This also gives a clearer pi ture of the contribution of the site terms to the observed seismic coda.

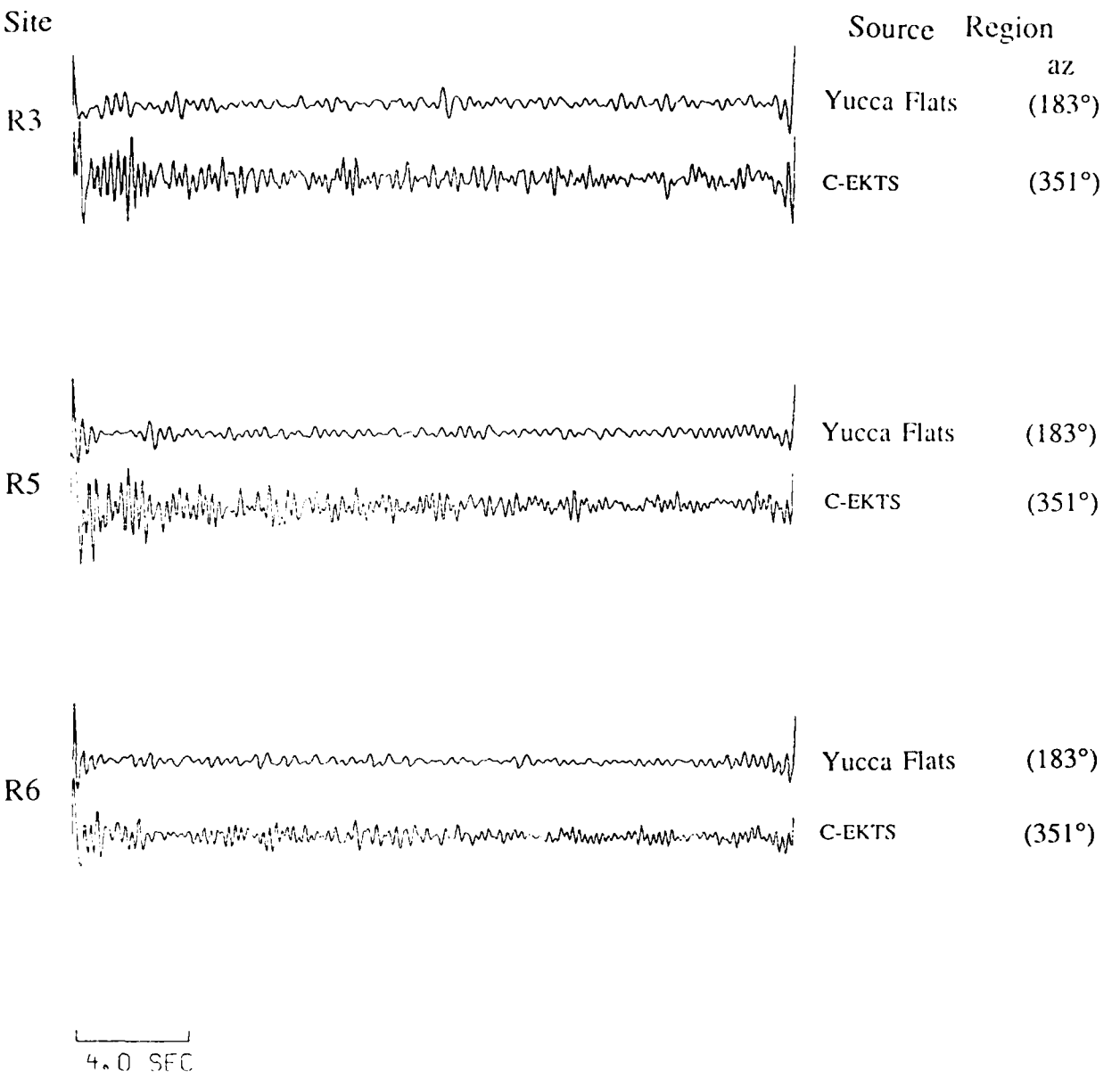

Figure 84. Deconvolved site time functions (wrapped around time zero) at three sensors of YKA for two test sites, Yucca Flats and Degelen (C-EKTS). The azimuth from YKA to each test site is shown to the right.

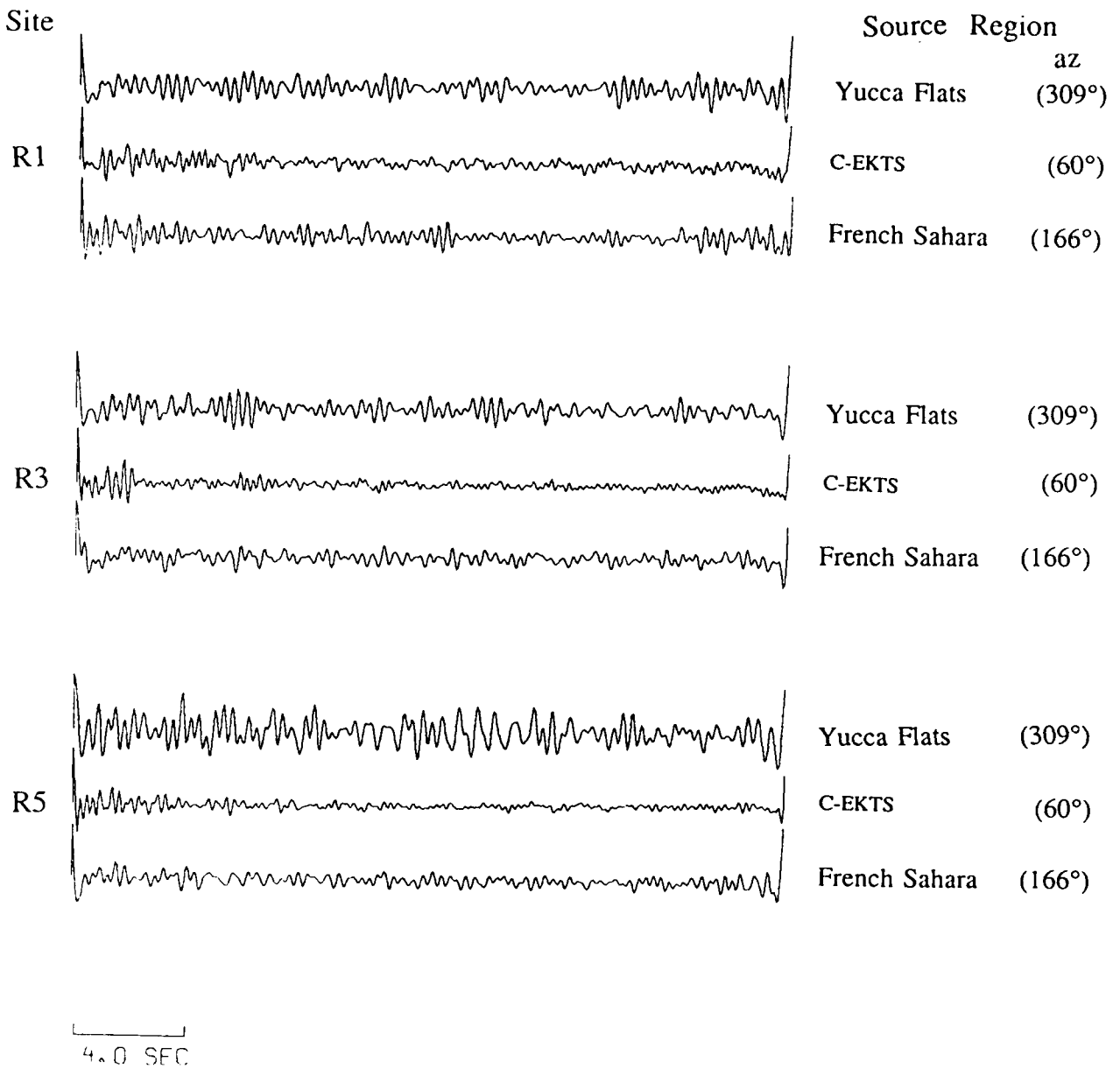

Figure 85. Deconvolved site time functions (wrapped around time zero) at three sensors of EKA for three test sites, Yucca Flats, Degelen (C-EKTS), and the French Sahara. The azimuth from EKA to each test site is shown to the right.

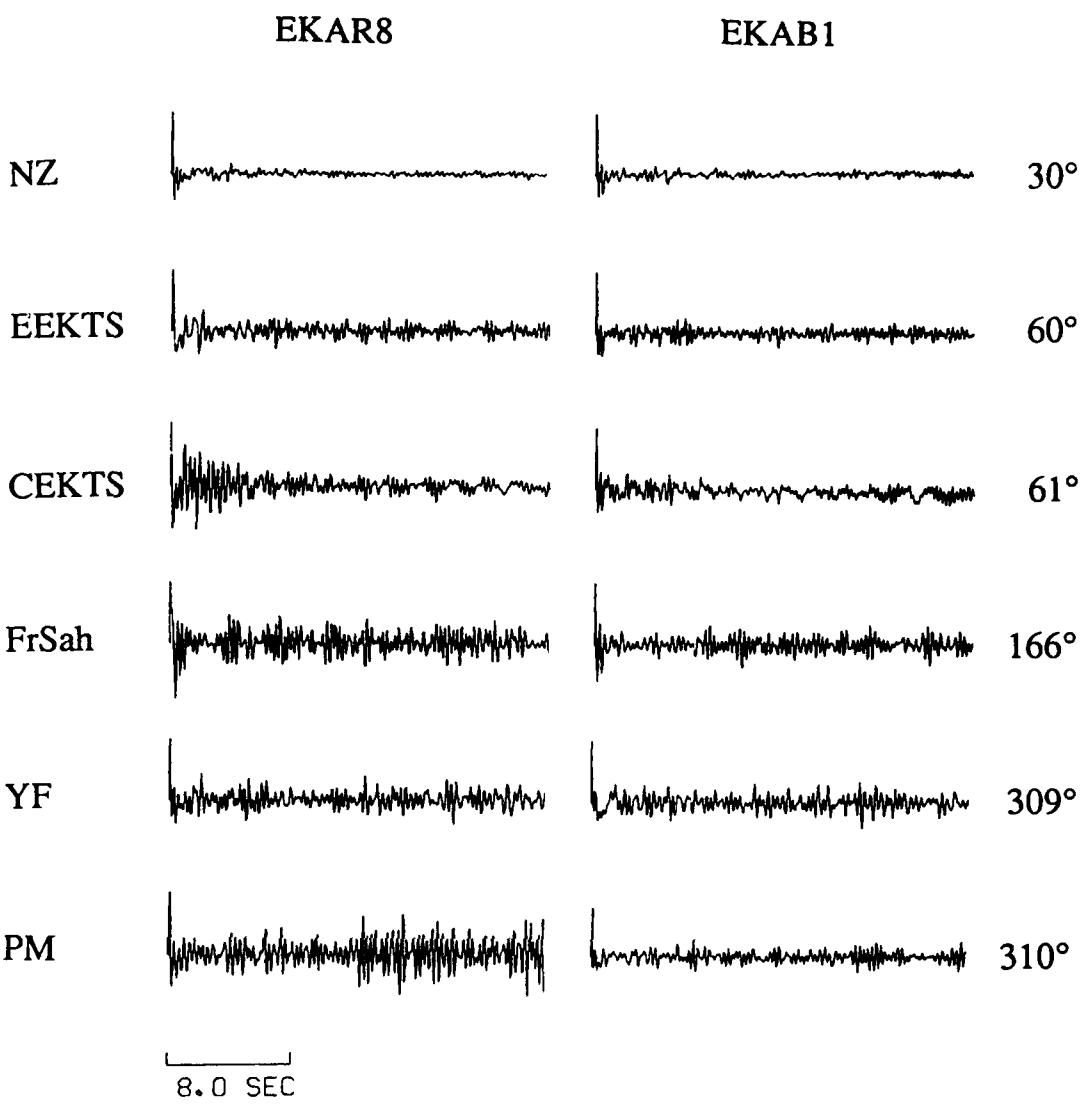

Figure 86. Deconvolved site terms for the EKA sensors R8 (left) and B1 (right) for events from different test sites: from top to bottom, Novaya Zemlya, Shagan, Degelen, French Sahara, Yucca Flats, and Pahute Mesa. The azimuth from EKA to each test site is shown to the right of each pair of traces.

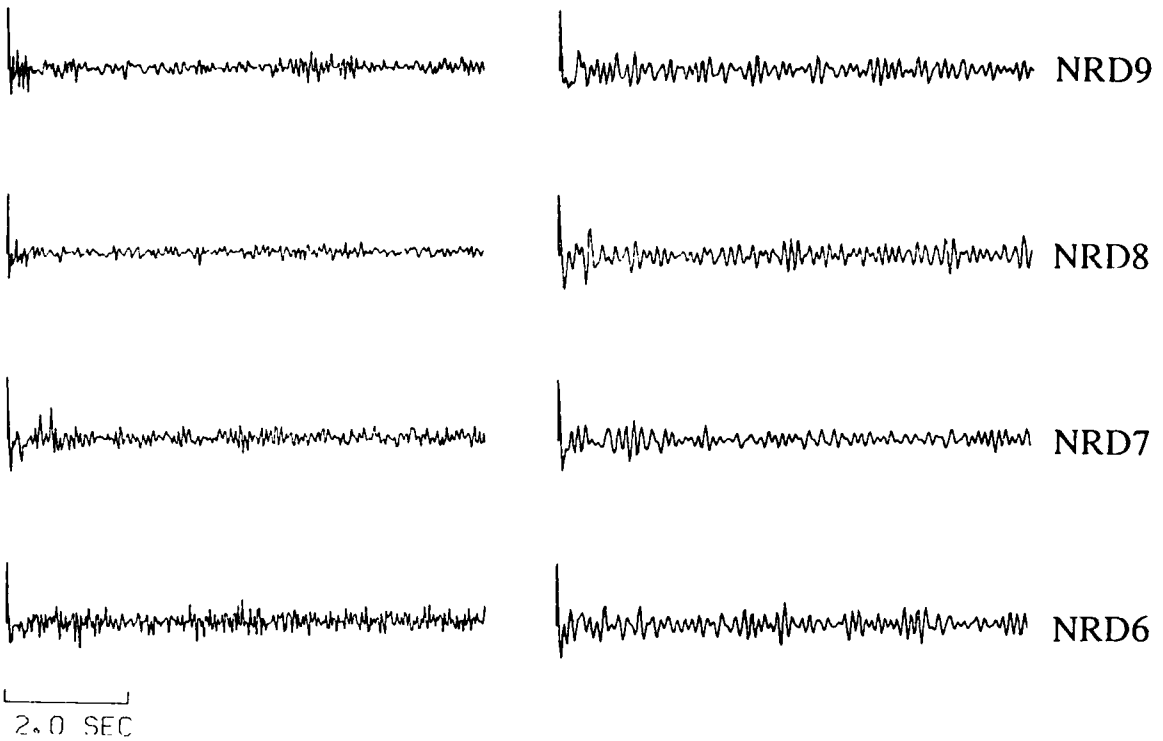

Figure 87. Deconvolved site terms for the NORESS sensors D9, D8, D7, and D6 for regional events from the southwest (left side, azimuth 247°) and from the Leningrad region (right side, azimuth 58°).

USE OF DECONVOLUTION RESULTS FOR YIELD ESTIMATION

From the above discussions it is apparent that the deconvolution method uses repeated averaging over sites and events in an iterative manner, while deconvolving the source and site factors as well as the assumed known parameters consisting of the instrument, t*, and source wavelet. The basic idea is to average *waveforms* such that all traces are given an equal weight. In order to ensure this, the whole process is started by equalizing all trace amplitudes by initial amplitude factors. Thus, the largest event does not dominate the site factor estimates and the site with the largest amplitude does not contaminate the source factor estimates. This way the traces with both the smallest and the largest absolute amplitudes can be reconstructed with about equal fidelity to the original waveforms. An inevitable consequence of this approach is that the absolute signal amplitudes become intractable through the process. The idea of waveform averaging, an essential ingredient of this deconvolution method, is in basic conflict with the preservation of the absolute signal amplitudes. To preserve the approximate equal weighting of the trace *waveforms* inside the program the t*, instrument, and source wavelet amplitudes are all normalized, rather than scaled. In order to go back to absolute amplitudes we must relate the signal amplitudes or m_b to the deconvolution results through the absolute amplitudes measured for the set of traces originally entering the procedure.

A better measure of the event size may be constructed the following way: by dividing the original seismograms by the appropriate source and site time functions, normalized instrument response, and a non-normalized t* operator, the result (properly limited in bandwidth to match the band used for the deconvolution) will be a simple impulsive waveform the log(amplitude) of which may be used as a new "m_b" parameter. The deconvolution of all these factors constitutes a set of corrections for site effects, pP, instrument, and t^* with the absolute amplitude information in the original wave amplitudes restored. The absolute amplification

factors due to sites will still have to be averaged out in the absence of any absolute site amplitude reference levels in the data. This method assumes that we know the forms of the attenuation operators and, if we wish to remove the explosion source time function as well, this time function too. We can assume that the instrument response to be removed poses no problems at all, since it can be determined with great accuracy by calibration measurements.

Simulations for Estimating m_b Bias

In this section we explore the consequences of pP interference as derived from the deconvolution results and combined with the present best estimates of attenuation variations. The m_b measurements are complex functions of yield, attenuation bias and the interaction of pP times with the wavelet shapes. Figure 88 shows an example of the effect of pP on m_b measurements. All of the waveforms are plotted on the same scale, and have been synthesized by assuming the same 100kt granite VSB, a shield-to-shield t*, and a WWSSN short-period instrument response. The only difference is in the delay time of the pP arrival. The presence of pP causes a positive interference which gives a larger amplitude and m_b measurement, with the exact effect depending on the particular pP delay time. A very short delay has only a small effect, an intermediate delay (~0.25 sec in this case) produces the maximum increase in amplitude, and a long delay has no effect since the pP is too late to cause produce any interference with the P wave. This is similar to the results presented in Figure 4.

Using pP amplitude and delay parameters measured from the deconvolved P waves from different test sites, we have synthesized wavelets and used the relative amplitudes to estimate the m_b bias between test sites for various yields. The "pP" delay times measured from the deconvolutions may be upper limits rather than actual values because of the limited time resolution of the deconvolution method. The simulations all assume a VSB-shaped source-time

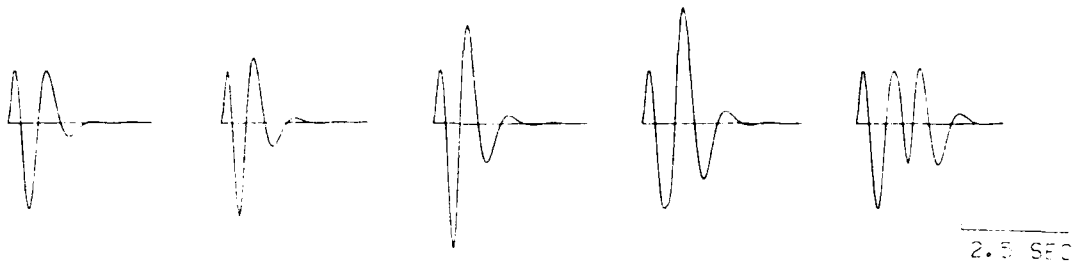

pP amp	0	-0.8	-0.8	-0.8	-0.8
pP delay (sec)	0	0.15	0.25	0.5	1.0
max 0→pk amp	26.3	29.0	39.0	36.1	26.3

All Wavelets: 100kT VSB, shield → shield t*,
WWSSN short period instrument

Figure 88. Effect of pP amplitude and delay time on m_b measurements. The wavelets across the top were synthesized with a pP of amplitude and delay as noted below each waveform. The wavelets are plotted on the same scale and the measured maximum zero to peak amplitude is also noted for each waveform in the figure. Constructive interference by the pP can cause amplitude variations of at least 30% as shown by the middle wavelet relative to the wavelets to the far left and far right which have no pP and a very long pP delay, respectively. All wavelets were synthesized with a 100kt granite VSB, a shield to shield t*, and a WWSSN short-period instrument response.

function, a constant t* appropriate to the source region, and a WWSSN short-period instrument response. All the simulations are based on the assumptions that the first "P" pulse is a cube-root scaled von Seggern-Blandford pulse and that the shapes of the wavelets can be described in terms of constant $\overline{t^*}$ operators consistent with spectra of the P waves observed (Der *et al.* 1985a). Moreover we assume that the t*(f) relationships are of the quasi-parallel type (Der and Lees 1985, Der *et al.* 1986). Table 18 gives the parameters used in these simplified simulations. m_b was measured from the maximum peak-to-peak amplitude and the amplitude was corrected for period as done in standard m_b measurements.

Figures 89 and 90 show the results for the conventional m_b vs yield. We see a bias of about 0.2 magnitude units between the Shagan and Degelen m_b values due to the constructive interference of pP at Shagan. The Degelen data includes the Shagan cratering explosion as expected. This bias was discussed by Der *et al.* (1985b, 1987) and McLaughlin *et al.* (1985). The NTS-to-Shagan bias in m_b is quite large, of the order of 0.5 magnitude units for the NTS explosions without pP, but less for those with a pP, because of the constructive interference of pP with P at the longer dominant wave periods due to larger attenuation despite the possibly larger pP time delay (this cannot be verified due to the limited resolution of NTS deconvolutions). In these simulations, Tuamotu and NTS have about the same bias relative to Degelen. We have estimated a much larger t* for Tuamotu than for NTS, but the south Pacific events have prominent pP arrivals unlike the NTS events, so at Tuamotu the positive interference from the pP compensates for the larger attenuation.

Yield Estimates from Deconvolved Waveforms

If the pP arrival can be resolved in the deconvolutions, the most logical approach is to use some measure of the energy in the first positive pulse of the deconvolved record to estimate yield without ever estimating m_b. This approach was followed by Douglas *et al.* (1987)

Table 18

Waveform Parameters used for Bias Estimates			
Test Site	t*	pP Amp	pP Delay
Degelen	0.15	0	-
Shagan	0.15	-0.8	0.25
NTS	0.45	0	-
Tuamotu	0.6	-0.8	0.5
Novaya Zemlya	0.15	-0.8	0.3

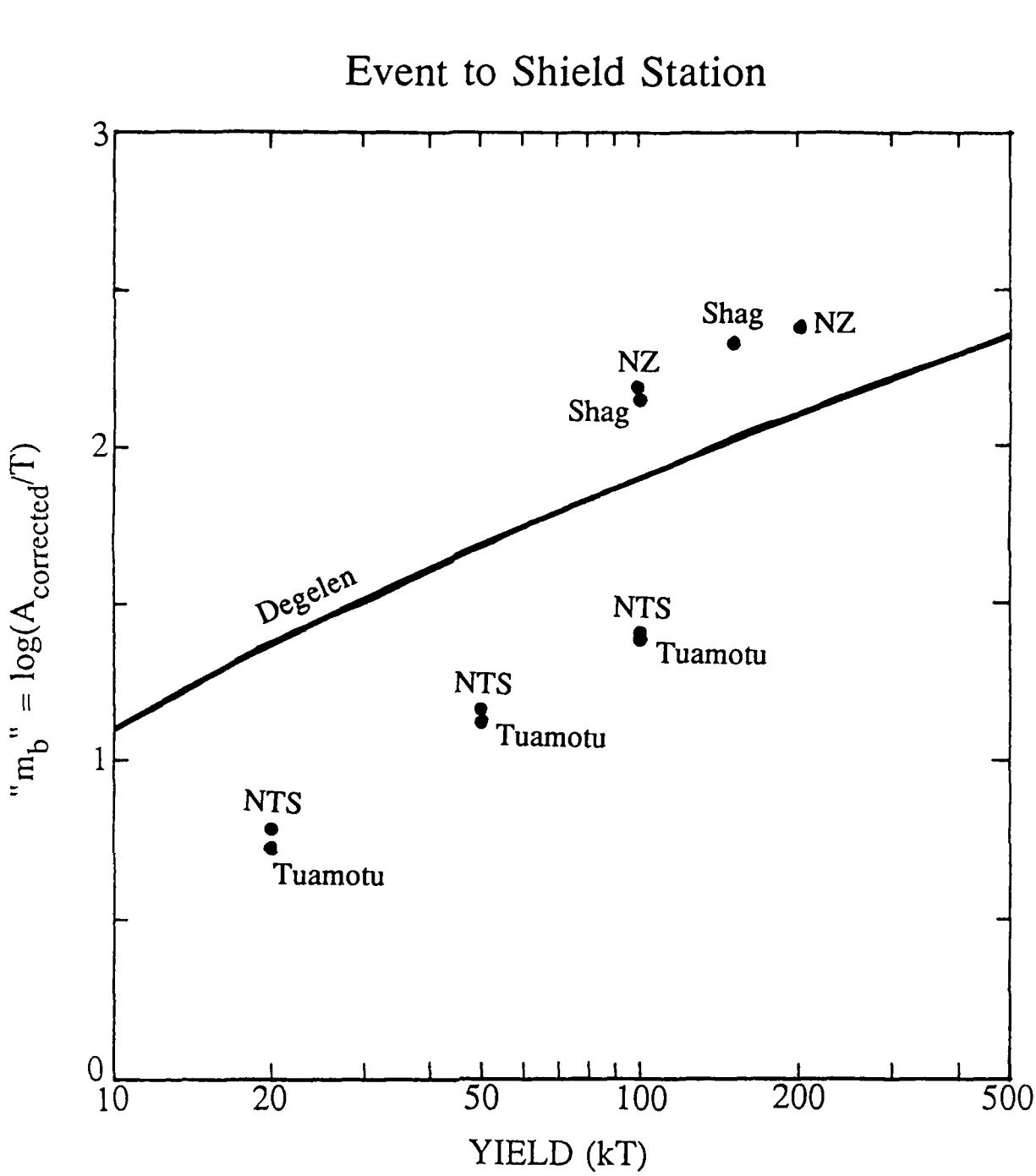

Figure 89. Estimates of m_b bias between nuclear test sites. The "m_b" estimates are made from synthetic wavelets like those in Figure 88, assuming pP amplitudes and delays estimated from the deconvolved source time functions (see Table 18). A shield is assumed for the station part of the t* and the yields for the VSB are as noted on the abscissa. The line label "Degelen" is the control case which assumes that no pP is present.

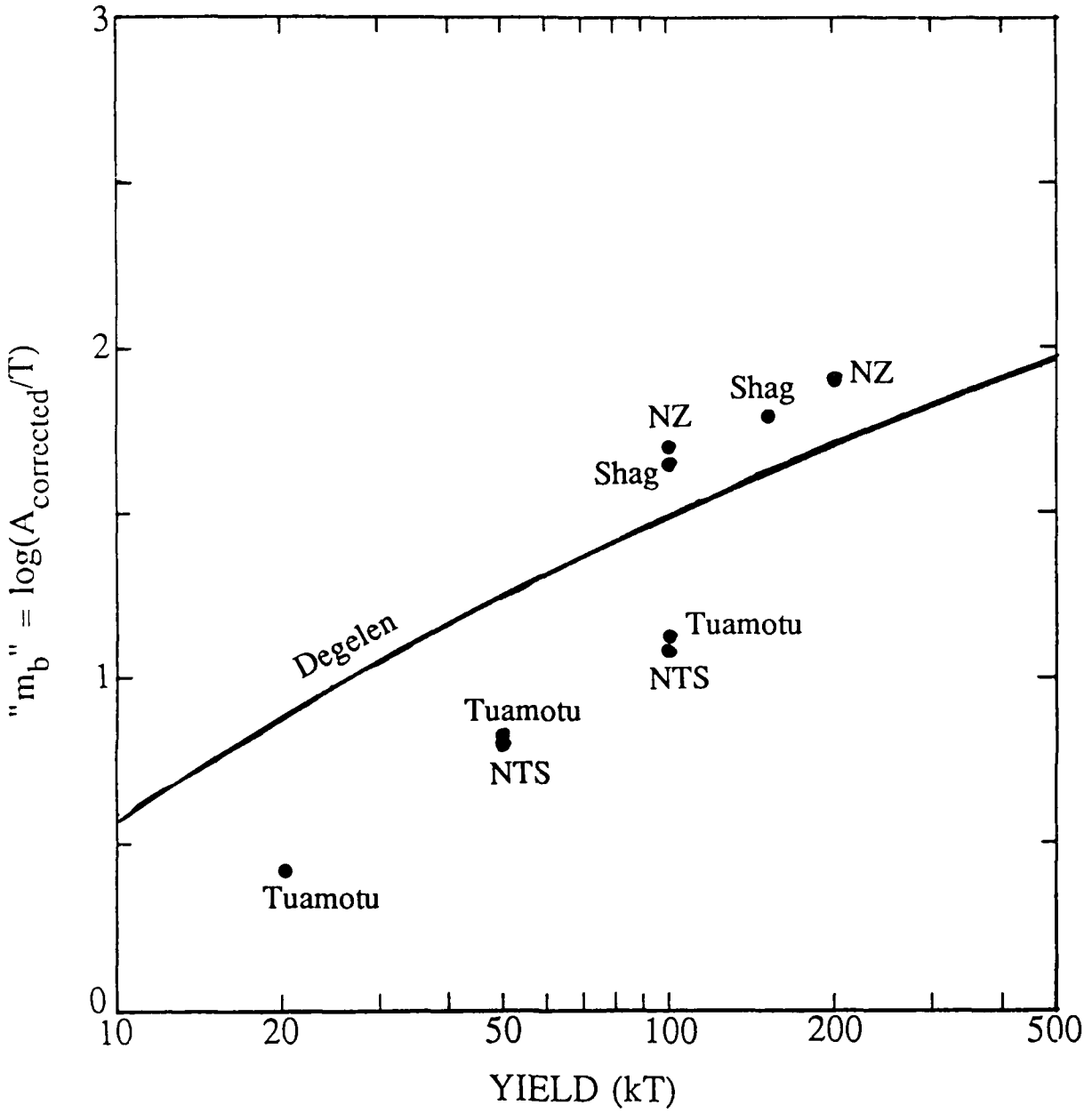

Figure 90. Like Figure 89 except that a tectonic t* is assumed for the station contribution to the total t*.

and should be preferable to estimating yields from m_b. McLaughlin *et al.* (1987b) have recently applied this approach to the source time functions from the multichannel deconvolutions to estimate the yields of some of the French Sahara nuclear tests at Ahaggar. Figure 91 shows the deconvolved source time functions for four of the French Sahara events from recordings at EKA and YKA. The area under the initial P wave pulse has been darkened in. Estimates of the integrated area of the positive pulses are shown in Figures 92 and 93. In Figure 92, the area was estimated within the pulse defined by the boxes on the figure. In the second case, Figure 93, the displacement far-field source was integrated, and the causal step was estimated as shown. For both cases, the resulting moment (after the appropriate distance, velocity, and density corrections, see McLaughlin *et al.* 1987b), was in reasonable agreement with moments obtained in other ways for the same events.

Estimation of Seismic P Wave Moment from Deconvolved Source-Time Functions for French Sahara Events Recorded at EKA (McLaughlin et al, 1987)

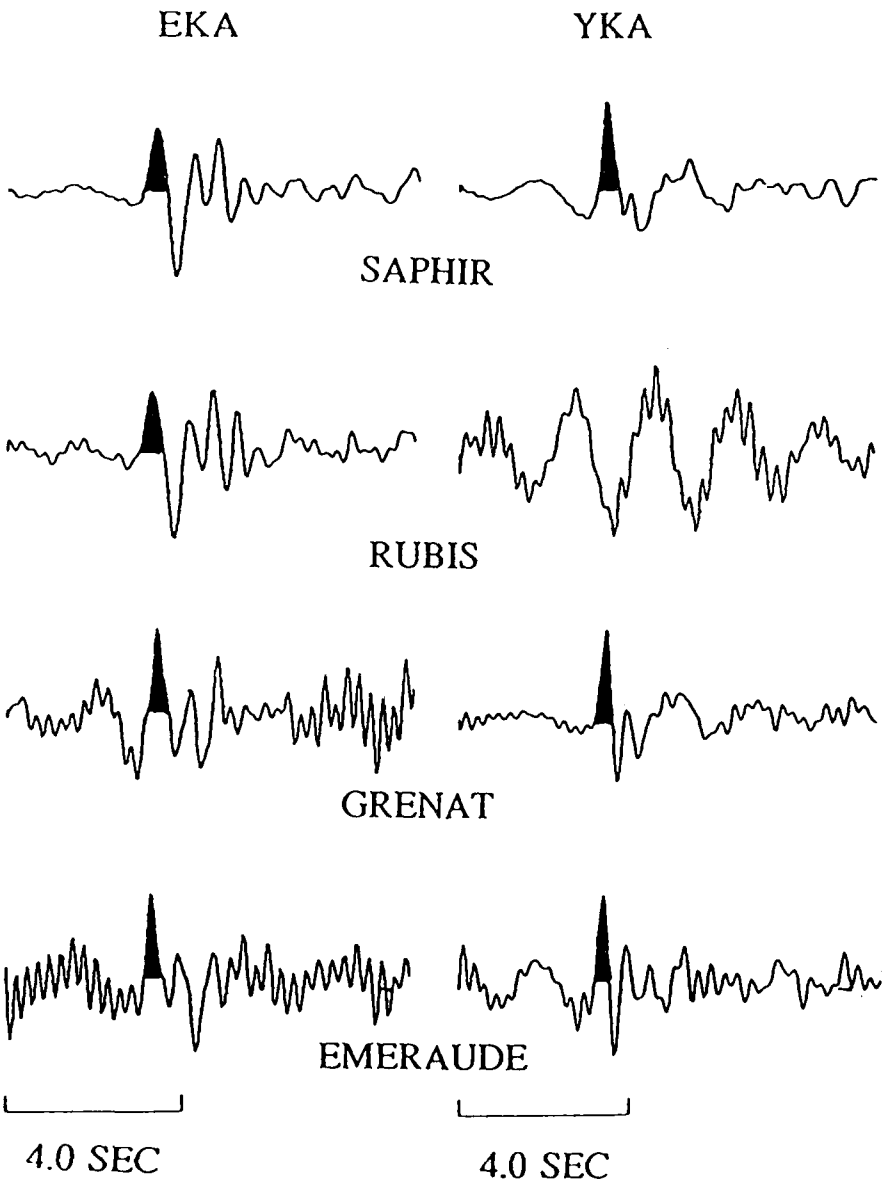

Figure 91. Estimation of seismic P wave moment from deconvolved source-time functions for French Sahara events recorded at EKA. As indicated by the shading, the moment is estimated from the area under the pulse of the deconvolved P wave. (After McLaughlin *et al.* 1987b.)

Estimation of Seismic P Wave Moment from Deconvolved Source-Time Functions for French Sahara Events Recorded at EKA (McLaughlin et al, 1987)

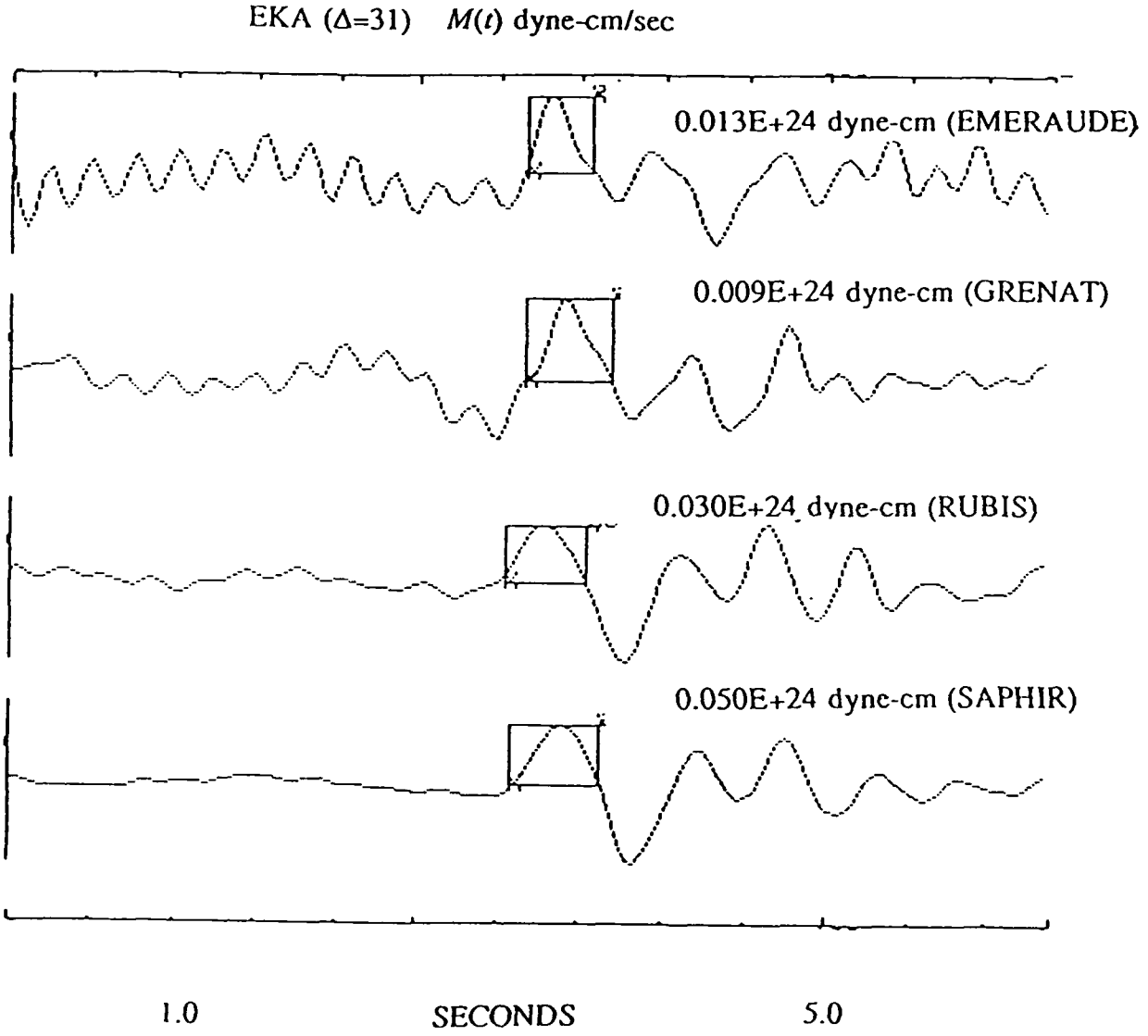

Figure 92. Equivalent seismic sources, M(t) for four French Sahara events recorded at EKA. The explosion moment inferred from the P pulse area is indicated. (After McLaughlin *et al.* 1987b.)

Estimation of Seismic P Wave Moment from Deconvolved Source-Time Functions for French Sahara Events Recorded at EKA (McLaughlin et al, 1987)

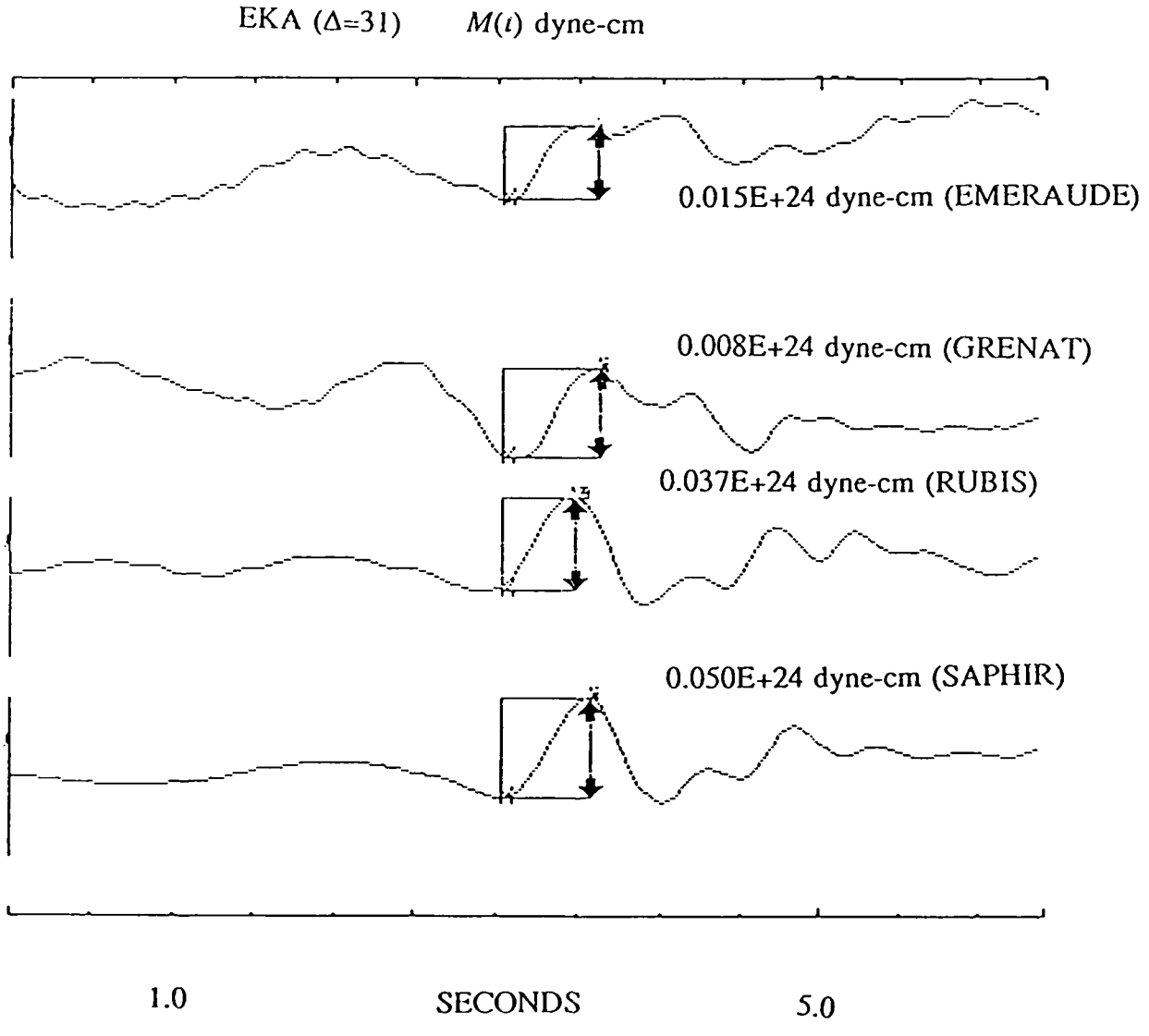

Figure 93. Equivalent seismic sources, M(t) for four French Sahara events recorded at EKA. The explosion moment inferred from the P pulse area is indicated. (After McLaughlin *et al.* 1987b.)

CONCLUSIONS

- Most of the ambiguities associated with the pP estimation methods proposed in the past are associated with the fact that, for most explosions, the simple P + pP model is not valid. This can be verified by analyses of inter-event spectral ratios and the results of our multichannel deconvolutions showing initial time sequences that are considerably more complicated than those of a simple P + pP model. A spall phase may be present in many of the deconvolutions. In addition, for single channel, the site effects will also disguise any pP arrivals even if they are present. Furthermore, at small delays the linear theory may not be applicable because the zone of nonlinear deformation may reach the free surface. The interpretation of the arrivals derived from the deconvolutions must be tied to the (possibly nonlinear) physical processes dominant near the explosions. Therefore, most results concerning pP using the P+pP model, narrow band synthetics, cross-equalization and spectral fitting, can be shown to be invalid by broad-band analyses.

- The deconvolved source-time functions vary substantially *between* test sites and oftentimes *within* test sites. Azimuthal variations are also significant in both source and receiver regions. These variations may correlate with local geology or testing practices.

    - Shagan explosion deconvolutions usually have a clear pP of delay ~0.3 sec although the cratering shot has a distinctly more complex source-time function without a clear pP. The source-time functions vary systematically across the test site consistent with the observations of Marshall *et al.* (1984).

    - Degelen explosion deconvolutions commonly show no or a poorly defined pP arrival. The radiation from the Degelen site seems to have strong azimuthal

asymmetries as evidenced by the poor reconstruction of the original traces following joint deconvolutions of data from four different azimuths. The variation in source time functions might be correlated with the mountainous topography of Degelen and the testing practices used in the region.

- Novaya Zemlya source time functions usually show a clear pP of ~0.35 sec delay. There are strong azimuthal variations in the source time functions, with particularly strong P coda observed at the azimuth of YKA. The P wave from a single southern Novaya Zemlya event deconvolves to give a simpler P wave source time function than do events from northern Novaya Zemlya. Variations in the P wave source time functions might be correlated with mountainous topography and the Soviet testing practices used in the region. Deconvolutions were also successfully performed for Novaya Zemlya event PcP recorded at EKA. This allowed examination of larger events for which the P waves are clipped at the AWRE stations. The PcP are simple with substantial pPcP arrivals, and the pPcP delay times are consistent with the pP delay times.

- Deconvolved source time functions of Astrakhan events show a clear pP with a delay of greater than 1 sec. Other distinct arrivals are also present in the first few seconds which may be due to reflections off of layers in this salt dome region.

- The French nuclear explosions in the Sahara give complex source functions with strong azimuthal variations. Again, mountainous topography and testing practices probably play a role in the observed source time function variations.

- French explosions at the Tuamotu archipelago deconvolve to show prominent pP arrivals with delay ~0.5 to ~0.6 sec. The relatively long delay may be consistent with the probable low velocity of the material in which the explosions are detonated.

- Deconvolutions of three Sinkiang explosions which range in m_b from 4.7 to 6.3 all show pP arrivals with a delay of ~ 0.4 sec.

- Deconvolutions of Yucca Flats events show no obvious pP arrival, though there are many secondary arrivals after the P arrival. Piledriver (granite) deconvolutions show a simpler, higher frequency source-time function. The complex nature of the waveforms may be due to local geology.

- Deconvolutions of Pahute Mesa events also show no obvious pP but many secondary arrivals. Again, the local geology may play an important role in the excitation of the source time functions.

- Deconvolutions of teleseismic and regional 3-component data are successful. Regional P_n source functions are very complex compared to the teleseismic source functions. For P waves, the vertical and radial site terms are fairly impulsive, while the transverse site term is more complex, building gradually with time as expected with energy being scattered into the transverse component.

- Deconvolved source-time functions can be used to estimate m_b bias and yield. Much of the observed m_b bias can be ascribed to the effects of pP interference, but not all, especially at NTS where other physical processes must be involved. Estimation of the

seismic moment from the area under the deconvolved source time function of French Sahara events gives a value consistent with those obtained using other techniques.

- Reconstructions from the site and source time series and the source wavelets show excellent agreement with the original traces including fine details in the coda. The coda is partially due to both near site and source scattering.

- The multichannel deconvolution procedure is a useful tool for a variety of projects related to source function determination and yield estimation.

REFERENCES

Bache, T.C. (1982). Estimating the yield of underground nuclear explosions. *Bull. Seism. Soc. Am., 72,* S131-S168.

Bache, T.C., P.D. Marshall, and L.B. Bache (1985). Q for teleseismic P waves from central Asia, *J. Geophys. Res., 90,* 3575-3587.

Bakun, W.H., and L.R. Johnson (1973). The deconvolution of teleseismic P waves from explosions MILROW and CANNIKIN, *Geophys. J. R. astr. Soc., 34,* 321-342.

Blandford, R.R., T.J. Cohen, and J.W. Woods (1973). An iterative approximation to the mixed-event processor. Technical Report *SDAC-TR-73-7,* Teledyne Geotech, Alexandria, Virginia.

Burdick, L.J., and D.V. Helmberger (1979), Time functions appropriate for nuclear explosions. *Bull. Seism. Soc. Am., 69,* 957-974.

Burdick, L.J., Wallace, T. and T. Lay, (1984), Modeling near-field and teleseismic observations from the Amchitka Test Site, *J. Geophys. Res., 89,* 4373-4388.

Christofferson, A., E.S. Husebye, and S.F. Ingate (1987). Wavefield decomposition using ML-probabilities in modeling single-site 3-component records, submitted to *Geophys. J. R. astr. Soc.*

Cohen, T.J. (1970). Source depth determinations using spectral estimation and cepstral analysis, *Geophys. J. R. astr. Soc., 20,* 223-231.

Cohen, T.J. (1975). Ps and pP phases from seven Pahute Mesa events, *Bull. Seism. Soc. Am., 65,* 1029-1032.

Cormier, V.F. (1982). The effect of attenuation on seismic body waves, *Bull. Seism. Soc. Am., 72,* S169-S200.

Der, Z.A., and A.C. Lees (1985). Methodologies for estimating t*(f) from short-period body waves and regional variations of t*(f) in the United States. *Geophys. J. R. A. S., 82,* 125-140.

Der, Z.A., T.W. McElfresh, and A. O'Donnell (1982). An investigation of the regional variations and frequency dependence of anelastic attenuation in the mantle under the United States in the .5-4 Hz band. *Geophys. J. R. A. S., 69,* 67-100.

Der, Z.A., R.H. Shumway, L.M. Anderson, T.W. McElfresh, and J.A. Burnetti (1983). Analysis of estimators for pP times and amplitudes, Technical Report *VSC-TR-83-17,* Teledyne Geotech, Alexandria, Virginia.

Der, Z.A., T.W. McElfresh, R. Wagner, and J. Burnetti (1985a). Spectral characteristics of P waves from nuclear explosions and yield estimation. *Bull. Seism. Soc. Am., 75,* 379-390, and Errata, *Bull. Seism. Soc. Am., 75,* 1222.

Der, Z.A., R.H. Shumway, A.C. Lees, and E. Smart (1985b). Multichannel deconvolution of P waves at seismic arrays, *TGAL-85-4,* Teledyne Geotech, Alexandria, Virginia.

Der, Z.A., W.W. Chan, A.C. Lees, and M.E. Marshall (1986). Models of the frequency dependence of Q in the mantle underlying tectonic areas of North America, Eurasia, and eastern Pacific, *TGAL-86-5*, Teledyne Geotech, Alexandria, Virginia.

Der, Z.A., R.H. Shumway, and A.C. Lees (1987). Multichannel deconvolution of P waves at seismic arrays, *Bull. Seism. Soc. Am., 77*, 195-211.

Douglas, A., and D.W. Rivers (1988). An explosion that looks like an earthquake, *Bull. Seism. Soc. Am., 78*, 1011-1019.

Douglas, A., J.A. Hudson, P.D. Marshall, and J.B. Young (1974). Earthquakes that look like explosions, *Geophys. J. R. astr. Soc., 36*, 227-233.

Douglas, A., P.D. Marshall, and J.B. Young (1987). The P waves from the Amchitka Island explosions, *Geophys. J. R. astr. Soc., 90*, 101-117.

Dysart, P. (1986). Autoregressive analysis of regional seismograms from earthquakes and explosions, Section 3.4, Technical Report *C86-07*, Center for Seismic Studies, Arlington, Virginia.

Filson, J., and C.W. Frasier (1972). Multisite estimation of explosive source parameters, *J. Geophys. Res., 77*, 2045-2061.

Goldman, S. (1953). *Information Theory*, Prentice Hall Inc., Englewood Cliffs, New Jersey.

Greenfield, R.J. (1971). Short period P wave generation by Rayleigh wave scattering at Novaya Zemlya, *J. Geophys. Res., 77*, 1988.

Gupta, I.N., K.L. McLaughlin, R. Wagner, T.W. McElfresh, M.E. Marshall, and R.-S. Jih (1987). Miscellaneous studies in decoupling, *TGAL-87-4*, Teledyne Geotech, Alexandria, Virginia.

Harris (1981). Recursive least squares with linear constraints, Proceedings of the IEEE Conference on Acoustics, Speech and Signal Processing, March 30,31 and April 1, 1981.

Hart, R.S., D.M. Hadley, G.R. Mellman, and R. Butler (1979). Seismic amplitude and waveform search, Technical Report *SGI-P-70-002*, Sierra Geophysics, Arcadia, California.

Israelson, H. (1983). Deconvolution based on source scaling applied to teleseismic signals, *FOA Rapport C 20514-T1*, Forsvarets Foskningsanstalt, Huvudavdelning 2, Stockholm, Sweden.

Jurkevics, A., and R. Wiggins (1984). A critique of seismic deconvolution methods, *Geophysics, 49*, 2109-2116.

Kemerait, R.C., and A.F. Sutton (1982). A multidimensional approach to seismic event depth estimation, in : *Seismic Analysis and Discrimination*, Elsevier Publishing Co.

King, D.W., and G. Calcagnile (1976). P-wave velocities in the upper mantle beneath Fennoscandia and western Russia, *Geophys. J. R. A. S., 46*, 407-432.

Lay, T., C.G. Arvesen, R.W. Burger, and L.J. Burdick (1984a). Estimating seismic yield and defining distinct test sites using complete waveform information, Technical Report *WCCP-R-84-04*, Woodward-Clyde Consultants, Pasadena, California.

Lay, T., L.J. Burdick, and D.V. Helmberger (1984b). Estimating yields of the Amchitka tests by waveform intercorrelation. *Geophys. J. R. Astr. Soc., 78,* 181-207.

Levy, S., and P.K. Fullagar (1981). Reconstruction of sparse spike train from a portion of its spectrum and application to high resolution deconvolution, *Geophysics, 46,* 1235-1243.

Lilwall, R.C., and P.D. Marshall (1986). Body wave magnitudes and locations of Soviet underground explosions at the Novaya Zemlya test site, AWRE Report No. O 17/86, AWRE, MOD(PE), Aldermaston, Berkshire, England.

Lundquist, G.M., G.R. Mellman, and D.M. Hadley (1980). Relative receiver functions for three different array concepts, Technical Report *SGI-R-80-021*, Sierra Geophysics, Inc., Arcadia, California.

Marshall, P.D. (1972). Some seismic results from a worldwide sample of large underground explosions, *AWRE Report O 49/72,* AWRE, MOD(PE), Aldermaston, Berkshire, England.

Marshall, P.D., T.C. Bache, and R.C. Lilwall (1984). Body wave magnitudes and locations of Soviet underground explosions at the Semipalatinsk test site, *AWRE Report No. O 16/84,* AWRE, MOD(PE), Aldermaston, Berkshire, England.

Marshall, P.D., R.C. Lilwall, and P.J. Warburton (1985). Body wave magnitudes and locations of French underground explosions at the Mururoa test site, *AWRE Report No. O 12/85,* AWRE, MOD(PE), Aldermaston, Berkshire, England.

McLaughlin, K.L., I.N. Gupta, and R. Wagner (1985). Magnitude determination of cratering and non-cratering nuclear explosions, *TGAL-85-3,* Teledyne Geotech, Alexandria, Virginia.

McLaughlin, K.L., R.O. Ahner, and M.E. Marshall (1986a). Maximum likelihood event magnitudes and log (max/a) at the Novaya Zemlya and Degelen test sites, *TGAL-86-02,* Teledyne Geotech, Alexandria, Virginia.

McLaughlin, K.L., R.H. Shumway, R.O. Ahner, M.E. Marshall, T.W. McElfresh, and R. Wagner (1986b). Determination of event magnitudes with correlated data and censoring: a maximum-likelihood approach, *TGAL-86-01,* Teledyne Geotech, Alexandria, Virginia.

McLaughlin, K.L., L.M. Anderson, and A.C. Lees (1987a). Effects of local geologic structure on Yucca Flats, NTS, explosion waveforms: 2-dimensional finite difference calculations, *Bull. Seism. Soc. Am., 77,* 1211-1222.

McLaughlin, K.L., A.C. Lees, and Z.A. Der (1987b). Teleseismic spectral and temporal M_0 and Ψ_∞ estimates for four French explosions in the southern Sahara, submitted to *Bull. Seism. Soc. Am.*

McLaughlin, K.L., M.E. Marshall, R. Wagner, W.W. Chan, A.C. Lees, and R.-S. Jih (1987c). A maximum-likelihood general linear model (GLM87) for inter-test site yield estimation and P-wave measures of yield at the Novaya Zemlya and Sinkiang test sites, *TGAL-87-5*, Teledyne Geotech, Alexandria, Virginia.

Mellman, G.R., and S.K. Kaufman (1981). Relative waveform inversion, *SGI-R-81-048*, Sierra Geophysics, Redmond, Washington.

Mellman, G.R., S.K. Kaufman, and W.C. Tucker (1984). Depth corrections for yield estimation of underground nuclear explosions, in : *Basic Research in the VELA Program*, AFOSR review meeting, Santa Fe, New Mexico, May 7-9, 1984.

Mowat, W.M.H., and R.F. Burch (1977). Handbook for the stations which provide seismograms to the Blacknest Seismological Centre United Kingdom, *REF No. 44/47/29, Issue 2*, AWRE, MOD(PE), Aldermaston, Berkshire, England.

Mueller, R.A., and J.R. Murphy (1971). Seismic characteristics of underground nuclear detonations, *Bull. Seism. Soc. Am., 61*, 1675-1692.

Oldenburg, D.W. (1981). A comprehensive solution of the linear deconvolution problem, *Geophys. J. R. astr. Soc., 65*, 331-358.

Oldenburg, D.W., S. Levy, and K.P. Whittal (1981). Wavelet estimation and deconvolution, *Geophysics, 46*, 1528-1542.

Owens, T.J., S.R. Taylor, and G. Zandt (1987). Crustal structures at Regional Seismic Test Network stations determined from inversion of broadband teleseismic P-waveforms, *Bull. Seism. Soc. Am., 77*, 631-662.

Robinson, E.A., and S. Treitel (1980). *Geophysical Signal Analysis*, Prentice Hall, Englewood Cliffs, New Jersey.

Rodean, H.C. (1979). ISC events from 1964 to 1976 at and near the nuclear testing ground in eastern Kazakhstan, *UCRL-52856*, Lawrence Livermore Laboratory, Livermore, California 94550.

Shumway, R.H. (1984). Deconvolution of multiple time series, in : *Statistical Analysis of Time Series*, Japan-U.S. joint seminar, Tokyo.

Shumway, R.H., and R.R. Blandford (1978). On detecting and estimating multiple arrivals from underground nuclear explosions, Technical Report *SDAC-TR-77-8*, Teledyne Geotech, Alexandria, Virginia.

Shumway, R.H., and Z.A. Der (1985). Deconvolution of multiple time series, *Technometrics, 27*, 385-393.

Su, S.S., and J. Dorman (1965). The use of leaking modes in seismogram interpretation and in studies of crust-mantle structure, *Bull. Seism. Soc. Am., 55*, 989-1021.

von Seggern, D.H., and R.K. Blandford (1972). Source time functions and spectra for underground nuclear explosions, *Geophys. J. R. astr. Soc., 31*, 83-97.

Wiggins, R.A. (1978). Minimum entropy deconvolution, *Geoexploration, 16*, 21-35.

DISTRIBUTION LIST
FOR UNCLASSIFIED REPORTS
DARPA-FUNDED PROJECTS
(Last Revised: 3 Mar 1988)

RECIPIENT	NO. OF COPIES
DEPARTMENT OF DEFENSE	
DARPA/GSD ATTN: Dr. R. Alewine and Dr. R. Blandford 1400 Wilson Boulevard Arlington, VA 22209-2308	2
DARPA/PM 1400 Wilson Boulevard Arlington, VA 22209-2308	1
Defense Intelligence Agency Directorate for Scientific and Technical Intelligence Washington, D.C. 20301	1
Defense Nuclear Agency Shock Physics Washington, D.C. 20305-1000	1
Defense Technical Information Center Cameron Station Alexandria, VA 22314	12
DEPARTMENT OF THE AIR FORCE	
AFGL/LWH ATTN: Dr. J. Cipar and Mr. J. Lewkowicz Terrestrial Sciences Division Hanscom AFB, MA 01731-5000	2
AFOSR/NPG ATTN: Director Bldg. 410, Room C222 Bolling AFB, Washington, D.C. 20332	1

AFTAC/DA 1
ATTN: STINFO Officer
Patrick AFB, FL 32925-6001

AFTAC/TT 3
Patrick AFB, FL 32925-6001

AFWL/NTESG 1
Kirtland AFB, NM 87171-6008

DEPARTMENT OF THE NAVY

NORDA 1
ATTN: Dr. J.A. Ballard
Code 543
NSTL Station, MS 39529

DEPARTMENT OF ENERGY

Department of Energy 1
ATTN: Mr. Max A. Koontz (DP-52)
International Security Affairs
1000 Independence Avenue
Washington, D.C. 20545

Lawrence Livermore National Laboratory 2
ATTN: Dr. J. Hannon and Dr. M. Nordyke
University of California
P.O. Box 808
Livermore, CA 94550

Los Alamos Scientific Laboratory 2
ATTN: Dr. K. Olsen and Dr. T. Weaver
P.O. Box 1663
Los Alamos, NM 87544

Sandia Laboratories 1
ATTN: Mr. P. Stokes
Geosciences Department 1255
Albuquerque, NM 87185

OTHER GOVERNMENT AGENCIES

Central Intelligence Agency 1
ATTN: Dr. L. Turnbull
OSI/NED, Room 5G48
Washington, D.C. 20505

U.S. Arms Control and Disarmament Agency 1
ATTN: Dr. M. Eimer
Verification and Intelligence Bureau, Rm 4953
Washington, D.C. 20451

U.S. Arms Control and Disarmament Agency 1
ATTN: Mrs. M. Hoinkes
Multilateral Affairs Bureau, Rm 5499
Washington, D.C. 20451

U.S. Geological Survey 1
ATTN: Dr. T. Hanks
National Earthquake Research Center
345 Middlefield Road
Menlo Park, CA 94025

U.S. Geological Survey 1
ATTN: Dr. R. Masse
Global Seismology Branch
Box 25046, Stop 967
Denver Federal Center
Denver, CO 80225

UNIVERSITIES

Boston College 1
ATTN: Dr. A. Kafka
Western Observatory
381 Concord Road
Weston, MA 02193

California Institute of Technology 1
ATTN: Dr. D. Harkrider
Seismological Laboratory
Pasadena, CA 91125

Columbia University 1
ATTN: Dr. L. Sykes
Lamont-Doherty Geological Observatory
Palisades, NY 10964

Cornell University 1
ATTN: Dr. M. Barazangi
INSTOC
Snee Hall
Ithaca, NY 14853

Harvard University 1
ATTN: Dr. J. Woodhouse
Hoffman Laboratory
20 Oxford Street
Cambridge, MA 02138

Massachusetts Institute of Technology 3
ATTN: Dr. S. Soloman, Dr. N. Toksoz, and Dr. T. Jordan
Department of Earth and Planetary Sciences
Cambridge, MA 02139

Southern Methodist University 1
ATTN: Dr. E. Herrin
Geophysical Laboratory
Dallas, TX 75275

State University of New York at Binghamton 1
ATTN: Dr. F. Wu
Department of Geological Sciences
Vestal, NY 13901

St. Louis University 2
ATTN: Dr. O. Nuttli and Dr. R. Herrmann
Department of Earth and Atmospheric Sciences
3507 Laclede
St. Louis, MO 63156

The Pennsylvania State University 1
ATTN: Dr. S. Alexander
Geosciences Department
403 Deike Building
University Park, PA 16802

University of Arizona 1
ATTN: Dr. T. Wallace
Department of Geosciences
Tucson, AZ 85721

University of California, Berkeley 1
ATTN: Dr. T. McEvilly
Department of Geology and Geophysics
Berkeley, CA 94720

University of California Los Angeles 1
ATTN: Dr. L. Knopoff
405 Hilgard Avenue
Los Angeles, CA 90024

University of California, San Diego 1
ATTN: Dr. J. Orcutt
Scripps Institute of Oceanography
La Jolla, CA 92093

University of Colorado 1
ATTN: Dr. C. Archambeau
CIRES
Boulder, CO 80309

University of Illinois 1
ATTN: Dr. S. Grand
Department of Geology
1301 West Green Street
Urbana, IL 61801

University of Michigan 1
ATTN: Dr. T. Lay
Department of Geological Sciences
Ann Arbor, MI 48109-1063

University of Nevada 1
ATTN: Dr. K. Priestley
Mackay School of Mines
Reno, NV 89557

University of Southern California 1
ATTN: Dr. K. Aki
Center for Earth Sciences
University Park
Los Angeles, CA 90089-0741

DEPARTMENT OF DEFENSE CONTRACTORS

Applied Theory, Inc. 1
ATTN: Dr. J. Trulio
930 South La Brea Avenue
Suite 2
Los Angeles, CA 90036

Center for Seismic Studies 2
ATTN: Dr. C. Romney and Mr. R. Perez
1300 N. 17th Street, Suite 1450
Arlington, VA 22209

ENSCO, Inc.
ATTN: Mr. G. Young 1
5400 Port Royal Road
Springfield, VA 22151

ENSCO, Inc. 1
ATTN: Dr. R. Kemerait
445 Pineda Court
Melbourne, FL 32940

Gould Inc. 1
ATTN: Mr. R. J. Woodard
Chesapeake Instrument Division
6711 Baymeado Drive
Glen Burnie, MD 21061

Pacific Sierra Research Corp. 1
ATTN: Mr. F. Thomas
12340 Santa Monica Boulevard
Los Angeles, CA 90025

Rockwell International 1
ATTN: B. Tittmann
1049 Camino Dos Rios
Thousand Oaks, CA 91360

Rondout Associates, Inc. 1
ATTN: Dr. P. Pomeroy
P.O. Box 224
Stone Ridge, NY 12484

Science Applications, Inc. 1
ATTN: Dr. T. Bache, Jr.
P.O. Box 2351
La Jolla, CA 92038

Science Horizons 2
ATTN: Dr. T. Cherry and Dr. J. Minster
710 Encinitas Blvd.
Suite 101
Encinitas, CA 92024

Sierra Geophysics, Inc. 2
ATTN: Dr. R. Hart and Dr. G. Mellman
11255 Kirkland Way
Kirkland, WA 98124

SRI International 1
ATTN: Dr. A. Florence
333 Ravensworth Avenue
Menlo Park, CA 94025

S-Cubed, A Division of 1
Maxwell Laboratories Inc.
ATTN: Dr. S. Day
P.O. Box 1620
La Jolla, CA 92038-1620

S-Cubed, A Division of
Maxwell Laboratories Inc.
ATTN: Mr. J. Murphy
11800 Sunrise Valley Drive
Suite 1212
Reston, VA 22091 — 1

Teledyne Geotech
ATTN: Dr. Z. Der and Mr. W. Rivers
314 Montgomery Street
Alexandria, VA 22314 — 2

Woodward-Clyde Consultants
ATTN: Dr. L. Burdick and Dr. J. Barker
556 El Dorado St.
Pasadena, CA 91105 — 2

NON-U.S. RECIPIENTS

National Defense Research Institute FOA 290
ATTN: Dr. O. Dahlman
Box 27322
S-10254 Stockholm, Sweden — 1

Blacknest Seismological Center
ATTN: Mr. P. Marshall
Atomic Weapons Research Establishment
UK Ministry of Defence
Brimpton, Reading, Berks. RG7-4RS
United Kingdom — 1

NTNF NORSAR
ATTN: Dr. F. Ringdal
P.O. Box 51
N-2007 Kjeller
Norway — 1

OTHER DISTRIBUTION

To be determined by the project office — 9